

Electronic Thesis and Dissertation Repository

2-21-2020 2:30 PM

Extracellular Matrix-Derived Modular Bioscaffolds for Soft Connective Tissue Regeneration

Pascal Morissette Martin, *The University of Western Ontario*

Supervisor: Flynn, Lauren E., *The University of Western Ontario*

A thesis submitted in partial fulfillment of the requirements for the Doctor of Philosophy degree in Anatomy and Cell Biology

© Pascal Morissette Martin 2020

Follow this and additional works at: <https://ir.lib.uwo.ca/etd>



Part of the [Biomaterials Commons](#), [Cell Biology Commons](#), and the [Molecular, Cellular, and Tissue Engineering Commons](#)

Recommended Citation

Morissette Martin, Pascal, "Extracellular Matrix-Derived Modular Bioscaffolds for Soft Connective Tissue Regeneration" (2020). *Electronic Thesis and Dissertation Repository*. 6840.
<https://ir.lib.uwo.ca/etd/6840>

This Dissertation/Thesis is brought to you for free and open access by Scholarship@Western. It has been accepted for inclusion in Electronic Thesis and Dissertation Repository by an authorized administrator of Scholarship@Western. For more information, please contact wlsadmin@uwo.ca.

Abstract

Human decellularized adipose tissue (DAT) represents a promising extracellular matrix (ECM) source for the development of biomaterials, with its properties conducive of angiogenesis, adipogenesis, and scaffold remodelling. This thesis sought to provide new fundamental insight into the design of ECM-derived bioscaffolds by developing novel modular biomaterials for soft connective tissue regeneration and by studying the effects of ECM composition on cell function and fate.

Initial studies explored the effects of ECM composition of pre-assembled bead foams derived from DAT or commercially-sourced bovine collagen (COL) on human wound edge dermal fibroblasts (weDFs) sourced from chronic wounds. *In vitro* testing under conditions simulating chronic wound stresses and *in vivo* investigation in a murine subcutaneous implantation model indicated that weDF survival and angiogenic marker expression were significantly enhanced in the DAT bead foams as compared to the COL bead foams. These results confirmed DAT as an ECM source with pro-regenerative properties.

Building from this work, a novel scaffold format comprised of fused networks of ECM-derived beads was generated through a “cell-assembly” approach using human adipose-derived stromal cells (ASCs) seeded on DAT beads. The cell-assembled bead foams, stabilized by the synthesis of new ECM, were structurally robust, easily handled, and contained a high density of viable ASCs distributed throughout the scaffold. Within a murine subcutaneous implantation model, the cell-assembled DAT bead foams showed enhanced early cell retention using a non-invasive *in vivo* cell tracking approach, along with increased detection of CD31⁺ endothelial cells within the implant at day 28, relative to ASC-seeded pre-assembled DAT bead foams. Overall, it was found that the novel cell-assembled DAT bead foams represented a promising pro-regenerative cell-delivery system.

The novel cell-assembly methods were extended to produce tissue-specific cell-assembled bead foams derived from decellularized trabecular bone (DTB) and COL. Preliminary findings indicated that the DAT and COL scaffold groups provided a highly supportive microenvironment for adipogenic differentiation in culture. Results also suggested that the DTB group may have inhibitory effects on ASC adipogenesis. Overall, this work established

that the cell-assembly approach can be used to generate platforms for exploring the effects of ECM composition on stem cell differentiation.

Keywords

Extracellular matrix; decellularized adipose tissue; collagen; microenvironment; tissue engineering; adipose-derived stromal cells; fibroblasts; cell delivery; wound healing.

Summary for Lay Audience

Soft connective tissues have a limited healing capacity following traumatic injuries or when subjected to chronic disease conditions, such as peripheral vascular disease and chronic wounds. To drive the repair and regeneration of these tissues, cellular therapies and biomaterials have both been independently investigated. However, a growing body of evidence is now showing that approaches combining the use of biomaterials and pro-regenerative cell populations may augment the efficacy of these new strategies.

Recognizing the need for new regenerative therapies, human decellularized adipose tissue (DAT) represents a promising source for the development of new biomaterials that can facilitate the localized delivery of therapeutic cells, such as adipose-derived stromal cells (ASCs). From this perspective, this thesis aimed to develop novel modular biomaterials for soft connective tissue regeneration using DAT and ASCs, and to study the effects of ECM composition within DAT-based biomaterials.

Initial studies explored the effects of ECM composition of “pre-assembled” bead foams on human wound edge dermal fibroblasts (weDFs) sourced from chronic wounds. Using pre-assembled bead foams derived from DAT and commercially-sourced bovine collagen (COL), it was found that the survival and capacity of the weDFs to stimulate blood vessel formation were significantly enhanced on the DAT bead foams. Building from these findings, a next-generation scaffold format was developed through a new cell-assembly approach using DAT beads seeded with ASCs. The novel “cell-assembled” DAT bead foams were structurally robust, easily handled, and contained a high density of viable ASCs homogeneously distributed throughout the biomaterial. Results from animal experiments showed that the new cell-assembled bead foams had a greater pro-angiogenic capacity than the previously-established pre-assembled bead foams, confirming their pro-regenerative potential. Lastly, the effects of ECM composition in this new biomaterial format were investigated by comparing cell-assembled bead foams produced from distinct ECM sources, including DAT, COL, and decellularized trabecular bone (DTB). Preliminary data suggested the DAT and COL bead foams promoted ASC differentiation into fat cells, while the DTB bead foams inhibited differentiation. Overall, the work completed in this thesis supports the rationale that DAT-

derived bioscaffolds are promising pro-regenerative biomaterials and cell delivery platforms for applications in soft tissue regeneration.

Co-Authorship Statement

Chapter 2 was published in *Acta Biomaterialia* in 2019: “*Morissette Martin P, Grant A, Hamilton DW, Flynn LE (2019). Matrix composition in 3-D collagenous bioscaffolds modulates the survival and angiogenic phenotype of human chronic wound dermal fibroblasts. Acta Biomaterialia, 83(2019): 199-210*”. I conceptualized this study in collaboration with Dr. Douglas Hamilton and Dr. Lauren Flynn. Aside from the human wound edge dermal fibroblast isolations, which were performed by Dr. Hamilton and his team, I personally designed and conducted all of the *in vitro* and *in vivo* experiments. Dr. Grant is the clinical collaborator that provided the human adipose tissue samples. I analyzed the data in collaboration with Dr. Flynn and I produced all the Figures. The manuscript was written in collaboration with Dr. Lauren Flynn.

The work presented in Chapter 3 forms the basis of a manuscript that is currently in preparation for submission. I conceptualized the study in collaboration with Dr. Lauren Flynn. I personally designed and performed all of the experimental studies described in the Chapter, with technical support from: Ms. Kellie Kim with bioscaffold production, Dr. Laura Juignet with the flow cytometry, and Dr. Amanda Hamilton with the lentiviral vector production and transduction. In addition, Dr. John Ronald provided scientific guidance with the lentiviral transduction and granted me access to the *in vivo* imaging system (IVIS) platform. I analyzed the data in collaboration with Dr. Flynn and I produced all the Figures. The manuscript was written in collaboration with Dr. Lauren Flynn.

The work presented in Chapter 4 was conceptualized in collaboration with Dr. Lauren Flynn. I personally designed and performed all of the experiments, with technical support from Ms. Courtney Brooks with the RT-qPCR. I analyzed the data in collaboration with Dr. Flynn and I produced all the Figures. The manuscript was written in collaboration with Dr. Lauren Flynn.

Acknowledgments

I would first like to thank my supervisor, Dr. Lauren Flynn. Thank you for your support, your patience, your meticulousness, your incredible availability, and above all, for the trust you have placed in me. Your passion for research is contagious and I am truly honored to have worked in the outstanding collaborative work environment you have put in place. The professional and personal skills you taught me during my years in the lab will be invaluable lifelong resources.

I would also like to extend my gratitude towards my advisory committee members, Dr. Douglas Hamilton, Dr. Dale Laird, Dr. Alison Allan, and Dr. Peter Merrifield. Thank you for your time and feedback. I would also like to acknowledge Dr. John Ronald, Dr. Amanda Hamilton, and Dr. David Hess for their assistance and guidance in our collaborative work.

I would also like to thank my Flynn lab colleagues, past and present, for your encouragement, your energy, and your wisdom. Warmest thanks to Dr. Claire Yu, Cody Brown, and Dr. JT Walker for showing me the ropes and coaching me at the beginning of my grand adventure in the world of decellularized-based biomaterials. All of you have helped me tremendously in so many ways. Special thanks to Dr. Laura Juignet for your refreshing presence and for the scientific guidance, to Dr. Arthi Shridhar for your kindness and positivity, to soon-to-be Dr. Tim Han for the laughs, to Courtney Brooks for your technical help, to Kellie Kim for your thoroughness, and last but not least, to Hisham Kamoun and Nadia Sharma for being crazy in the best of ways. To all the Flynn lab members, thank you all for the countless enriching conversations and fond memories that I made along the way.

Je voudrais également remercier mes parents et ma famille. Merci à vous tous pour votre aide, votre support inconditionnel et votre compréhension. Merci d'avoir accepté mon départ et pour votre indulgence lors de mes nombreuses absences... Merci à mes parents, et tout particulièrement à ma petite maman, pour votre amour et pour les sacrifices que vous avez effectués pour moi. Je ne vous remercierai jamais assez.

Finally, I would like to thank my partner, Eric, you have been amongst my biggest supporter throughout my degree. Your presence, empathy, encouragement, and emotional support has helped me in ways I can't even describe.

Table of Contents

Abstract.....	ii
Summary for Lay Audience.....	iv
Co-Authorship Statement.....	vi
Acknowledgments.....	vii
Table of Contents.....	viii
List of Tables.....	xiv
List of Figures.....	xv
List of Appendices.....	xvii
List of Abbreviations.....	xviii
Chapter 1.....	1
1 Literature review.....	1
1.1 Roles of cell-instructive bioscaffolds in regenerative medicine.....	1
1.2 The extracellular matrix.....	1
1.2.1 ECM Composition.....	3
1.2.2 ECM signal transduction.....	7
1.2.3 Tissue-specific ECM.....	9
1.3 ECM-derived scaffolds.....	10
1.3.1 Biomaterials and general considerations.....	10
1.3.2 Properties of the ECM that can modulate cell behaviour.....	11
1.3.3 Decellularization.....	13
1.3.4 Decellularized adipose tissue.....	15
1.3.5 Processing of decellularized tissues for the fabrication of bioscaffolds...	17
1.4 Angiogenesis and wound healing.....	21
1.4.1 Phases of wound healing.....	21
1.4.2 Physiology and mechanisms of angiogenesis.....	24

1.4.3	Pathologies with insufficient angiogenesis.....	26
1.4.4	Bioscaffold-derived and cell-derived regeneration strategies.....	28
1.4.5	<i>In vivo</i> preclinical animal models for assessing angiogenesis	29
1.5	Mesenchymal cells.....	30
1.5.1	Dermal fibroblasts.....	30
1.5.2	Mesenchymal stromal cells.....	30
1.5.3	Adipose-derived stromal cells.....	31
1.5.4	ASC-based tissue-engineering strategies and considerations	33
1.6	Objectives and specific aims.....	35
1.7	Project overview	35
Chapter 2.....		38
2	Matrix composition in 3-D collagenous bioscaffolds modulates the survival and angiogenic phenotype of human chronic wound dermal fibroblasts	38
2.1	Co-authorship statement	38
2.2	Abstract.....	39
2.3	INTRODUCTION	39
2.4	Materials and methods	41
2.4.1	Materials	41
2.4.2	Adipose tissue collection and decellularization.....	41
2.4.3	DAT and COL bead fabrication.....	42
2.4.4	Characterization of DAT and COL beads.....	43
2.4.5	DAT and COL bead foam fabrication	43
2.4.6	Characterization of the DAT and COL bead foams.....	44
2.4.7	Chronic wound fibroblast isolation, culture and characterization	45
2.4.8	DAT and COL bead foam seeding.....	46
2.4.9	Analysis of cell distribution.....	47
2.4.10	<i>In vivo</i> analysis of seeded DAT and COL bead foams	48

2.4.11	Statistical Analyses	49
2.5	Results.....	50
2.5.1	Beads and bead foams fabricated from DAT and COL are structurally similar	50
2.5.2	DAT and COL bead foams are compositionally distinct.....	51
2.5.3	weDF cell abundance and survival is enhanced on the DAT bead foams <i>in vitro</i>	52
2.5.4	Angiogenic gene expression is enhanced in the weDFs cultured on the DAT bead foams	55
2.5.5	Angiogenic factor secretion is enhanced in the weDFs cultured on the DAT bead foams prior to implantation	55
2.5.6	Human weDF abundance is enhanced <i>in vivo</i> in the DAT bead foams....	55
2.5.7	CD31 ⁺ cell recruitment is enhanced in the weDF-seeded DAT bead foams	56
2.6	Discussion.....	60
2.7	Conclusions.....	63
Chapter 3	64
3	Modular cell-assembled matrix-derived bead foams as a pro-angiogenic mesenchymal stromal cell delivery platform	64
3.1	Co-authorship statement	64
3.2	Abstract.....	65
3.3	INTRODUCTION	66
3.4	Materials and methods	68
3.4.1	Decellularization of adipose tissue and DAT bead synthesis	68
3.4.2	Human ASC isolation, expansion, and characterization.....	69
3.4.3	Production of cell-assembled DAT bead foams	70
3.4.4	Cell viability and abundance on DAT beads and within the cell-assembled DAT bead foams	71
3.4.5	Physical and biochemical characterization of the DAT beads and DAT bead foams.....	72

3.4.6	Gene expression analysis measured using RT-qPCR.....	75
3.4.7	Protein expression analysis measured using multiplex assay.....	76
3.4.8	Lentiviral transduction of ASCs and trilineage differentiation studies	76
3.4.9	Subcutaneous implantation of cell-assembled and pre-assembled DAT bead foams in an athymic mouse model.....	79
3.4.10	Statistical Analyses.....	81
3.5	Results.....	81
3.5.1	DAT beads support attachment and survival of ASCs following dynamic seeding	81
3.5.2	The use of a chemically-defined media allows for the production of scaffolds with high cell viability.....	83
3.5.3	The cell-assembled DAT bead foams remodel over the course of the 8-day fabrication process	85
3.5.4	The cell-assembly process is mediated by new ECM synthesis.....	87
3.5.5	The culture conditions modulated ASC gene and protein expression within the cell-assembled bead foams.....	87
3.5.6	Human ASCs co-expressing Fluc2 and tdT maintain their trilineage differentiation capacity	88
3.5.7	The cell-assembled bead foams show enhanced detection of viable ASCs at early timepoints and greater murine CD31 ⁺ cell recruitment at 28 days..	92
3.6	Discussion.....	94
3.7	Conclusions.....	99
Chapter 4	100
4	The effects of matrix composition on the adipogenic differentiation of human adipose-derived stromal cells in cell-assembled matrix-derived bead foams	100
4.1	Co-authorship statement	100
4.2	Abstract.....	101
4.3	Introduction.....	102
4.4	Materials and methods	104
4.4.1	Decellularization of human adipose tissue	104

4.4.2	Decellularization of bovine trabecular bone	104
4.4.3	Electrospraying of ECM suspensions	105
4.4.4	Human ASC isolation, expansion, and characterization.....	105
4.4.5	Physical and biochemical characterization of the individual ECM-derived beads	106
4.4.6	Production of cell-assembled DAT, COL, and DTB bead foams.....	107
4.4.7	<i>In vitro</i> adipogenic assessment	107
4.4.8	Statistical Analyses	109
4.5	Results.....	109
4.5.1	Beads derived from the three ECM sources have similar physical characteristics.....	109
4.5.2	DAT-, COL-, and DTB-derived beads similarly support ASC seeding and cell-assembled bead foam formation	112
4.5.3	DAT and COL scaffolds are adipo-conductive, while DTB scaffolds are adipo-repressive	112
4.6	Discussion.....	115
4.7	Conclusions.....	118
Chapter 5	119
5	General discussion and conclusions.....	119
5.1	General discussion	119
5.2	Future work.....	125
5.3	Summary and significance.....	128
References	129
Appendix A: Supplementary data	152
A.1	Supplementary data of Chapter 2.....	152
A.2	Supplementary data of Chapter 3.....	157
Appendix B: Research ethics board approval	161
Appendix C: Animal protocol approval	162

Curriculum Vitae 164

List of Tables

Table 1.1 List of naturally-derived biomaterials fabricated using DAT.....	18
Table 1.2 List of paracrine factors secreted by human ASCs.....	31

List of Figures

Figure 0.1 The soft-connective tissue microenvironment.....	2
Figure 0.2 Correlation between mechano-transduction, growth, and differentiation in mesenchymal stromal cells (MSCs) and fibroblasts.....	13
Figure 0.3 Overview of adipose decellularization and further processing steps for DAT-derived bioscaffold production	20
Figure 0.4 Schematic representation of cutaneous healing processes	21
Figure 0.5 Schematic representation of sprouting angiogenesis.....	25
Figure 2.1: DAT and collagen bead foams are structurally similar	51
Figure 2.2: DAT and COL bead foams are biochemically distinct	53
Figure 2.3: weDF cell abundance and survival is enhanced in vitro on the DAT bead foams as compared to the COL bead foams under conditions simulating stresses in the chronic wound microenvironment.....	54
Figure 2.4: Pro-angiogenic gene expression is enhanced in vitro in weDFs cultured on DAT bead foams relative to COL bead foams under conditions simulating stresses in the chronic wound microenvironment.....	56
Figure 2.5: Pro-angiogenic factor secretion is enhanced in weDFs cultured on DAT bead foams relative to COL bead foams prior to implantation in the in vivo model.....	57
Figure 2.6: Human weDF abundance is enhanced on the DAT bead foams relative to the COL bead foams at 14 days after subcutaneous implantation in an athymic mouse model.....	58
Figure 2.7: CD31+ cell recruitment is enhanced in the DAT bead foams seeded with human weDFs relative to seeded COL bead foams and unseeded controls at 14 days after subcutaneous implantation in an athymic mouse model	59
Figure 3.1: Soft and compliant DAT beads support the attachment and survival of seeded human ASCs in a spinner culture flask system at 24 h after seeding	82

Figure 3.2: Cells are proliferating and highly viable within the cell-assembled bead foams.	84
Figure 3.3: The cell-assembled DAT bead foams remodel over the course of the 8-day fabrication process	86
Figure 3.4: Cell-assembly is mediated through ECM synthesis	89
Figure 3.5: ECM-associated gene expression in ASCs within the cell-assembled bead foams is modulated by growth factor preconditioning.....	90
Figure 3.6: The ASCs within the cell-assembled bead foams produced pro-angiogenic proteins	91
Figure 3.7: Early human ASC retention, as well as murine CD31+ cell recruitment at 28 days, is enhanced within the cell-assembled (CA) DAT bead foams as compared to ASCs seeded and delivered on pre-assembled (PA) DAT bead foams	93
Figure 4.1: Qualitative microscopic analysis of DAT, COL, and DTB beads showed that the bead micro-architecture was similar across all ECM sources	110
Figure 4.2: DAT, COL, and DTB beads have similar starting physical properties	111
Figure 4.3: Representative microscopic and macroscopic images of ECM-derived beads and bead foams at 24 h post-seeding and 8-days post-moulding, respectively	113
Figure 4.4: Adipogenic differentiation was enhanced in the DAT and COL bead foams, compared to the DTB bead foams and TCPS controls, after 14 days of induction	114

List of Appendices

Appendix A: Supplementary data	161
Appendix B: Research ethics board approval	162
Appendix C: Animal protocol approval	164

List of Abbreviations

2-D	two-dimensional
3-D	three-dimensional
A2P	L-ascorbic acid 2-phosphate
ALP	alkaline phosphatase
ANGPT1	angiopoietin 1
ASC	adipose-derived stromal cell
ADAM	a disintegrin and metalloproteinase
ADAMTS	ADAM with thrombospondin motifs
BGLAP	bone gamma-carboxyglutamic acid-containing protein
BLI	bioluminescence imaging
BMP	bone morphogenic protein
BMSC	bone marrow-derived mesenchymal stromal cell
CA	cell-assembled
CAM	cell adhesion molecule
CCAC	Canadian Council on Animal Care
CCL22	C-C motif chemokine 22
CCL5	C-C motif chemokine 5
CCN2	connective tissue growth factor
CDC42	cell division control protein 42 homolog
CLI	critical limb ischemia
COL	bovine collagen
CPC	cardiac progenitor cells
CSF-1	colony stimulating factor-1
CSF-2	colony stimulating factor-2
CXC	C-X-C motif chemokine

CXCL1	CXC ligand 1
CXCL14	CXC ligand 14
CXCR4	CXC receptor 4
DAT	decellularized adipose tissue
DLL4	delta-like-4 ligand
DMMB	dimethylmethylene blue
DNase	deoxyribonuclease
GPDH	glycerol-3-phosphate dehydrogenase
DMEM/F12	Dulbecco's Modified Eagle Medium: Nutrient Mixture F-12
DTB	decellularized trabecular bone
dsDNA	double-stranded DNA
ECM	extracellular matrix
EDTA	ethylenediaminetetraacetic acid
ERK	extracellular signal-related kinase
FBS	fetal bovine serum
Fluc2	codon optimized firefly luciferase
FGF	fibroblast growth factor
FGF-2	fibroblast growth factor-2
GAG	glycosaminoglycan
HGF	hepatocyte growth factor
IBMX	isobutylmethylxanthine
IGF	insulin-like growth factor
IGF-1	insulin-like growth factor-1
IGF-2	insulin-like growth factor-2
IHC	immunohistochemical
IL-1	interleukin-1

IL-1RA	interleukin-1 receptor antagonist
IL-6	interleukin-6
IL-8	interleukin-8
iPSC	induced pluripotent stem cell
KGF	keratinocyte growth factor
LTBP	latent transforming growth factor- β binding protein
MAPK	mitogen-activated protein kinase
MOI	multiplicity of infection
MCP-1	monocyte chemoattractant protein-1
MMP	matrix metalloproteinase
NGF	nerve growth factor
OSX	osterix
P4	passage 4
PA	pre-assembled
PAD	peripheral artery disease
PAI-1	plasminogen activator inhibitor-1
PDGF	platelet-derived growth factor
PEG	polyethylene glycol
PI3K	phosphoinositide 3-kinase
PKB	protein kinase B
PlGF	placental growth factor
PPAR γ	peroxisome proliferator-activated receptor γ
RAC1	ras-related C3 botulinum toxin substrate 1
RNases	ribonucleases
RUNX2	Runt-related transcription factor 2
SCF	stem cell factor

SD	standard deviation
SDS	sodium dodecyl sulfate
SEM	scanning electron microscopy
SPARC	secreted protein acidic and rich in cysteine
SFK	Src-family protein tyrosine kinase
SSP1	secreted phosphoprotein 1
TCPS	tissue culture polystyrene
tdT	tdTomato
TGF- β	transforming growth factor- β
TIMP	tissue inhibitors of metalloproteinase
TNF- α	tumor necrosis factor- α
VEGF	vascular endothelial growth factor
VEGFR	VEGF receptor
weDF	wound edge dermal fibroblast
XFCD	xenogenic-free chemically-defined media

Chapter 1

1 Literature review

1.1 Roles of cell-instructive bioscaffolds in regenerative medicine

Regenerative medicine, the branch of biomedical engineering and medicine that aims to regenerate and restore normal tissue function, holds tremendous therapeutic potential to treat a wide variety of both acute and chronic diseases [1, 2]. Research in this field aims to develop therapeutic approaches for the treatment of traumatic injuries and the healing of chronic conditions, such as peripheral vascular disease, critical limb ischemia and chronic wounds. Previously, both cellular therapies and biomaterial scaffolds have been investigated in isolation for these conditions [1, 3]; however, a growing body of evidence suggests that the combination of these two approaches may augment host tissue regeneration, compared to either approach alone [2, 4, 5].

For this purpose, a wide range of synthetic, naturally-derived, and composite biomaterials have been developed as instructive cell-delivery vehicles designed to increase cell survival and to stimulate pro-regenerative functions, both *in vitro* and *in vivo* [5-8]. While the biochemical and mechanical properties of synthetic polymers can be more easily tuned, it remains challenging to fully replicate the intricate native tissue microenvironment using these materials [5-8]. With growing evidence of the critical importance of the extracellular matrix (ECM) of tissues in directing major cellular processes [9-15], bioscaffolds derived from the ECM of tissues have emerged as promising cell-instructive culture and delivery platforms [5, 16]. Consequently, particular attention will be given to the ECM and to ECM-derived biomaterials in the current chapter.

1.2 The extracellular matrix

Mammalian cells are subjected to intricate biochemical and biophysical signals through interactions with the ECM, a complex extracellular network of proteins and polysaccharides with tissue-specific composition and structure [16]. This complex milieu plays a pivotal role in mediating cellular phenotypes and functions [16]. Broadly, the ECM

can be classified into two categories: interstitial matrix and basement membrane [16]. The interstitial matrix is more abundant and surrounds the cells of all connective tissues, with the exception of blood [16]. The basement membrane, also known as the basal lamina, is comprised of flexible 40- to 120-nm thick specialized ECM sheets that separate specialized compartments within tissues [17]. In connective tissues, basement membranes can be found surrounding endothelial cells, Schwann cells, and adipocytes [17, 18]. Basement membranes can also be found separating epithelial tissues from connective tissues, as in the case of the epidermis and dermis in the skin [17].

Figure 1.1 provides a simplified visual representation of the soft connective tissue microenvironment, including both the cells and ECM components. These elements will be further discussed in subsequent sections.

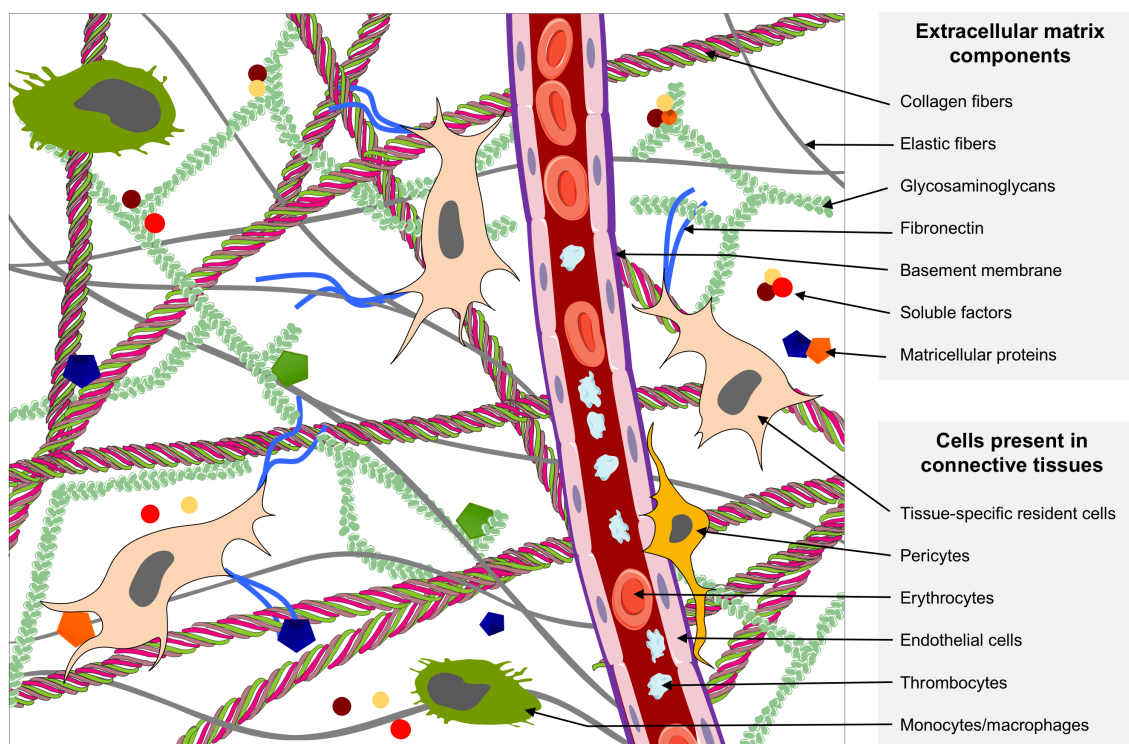


Figure 1.1 The soft-connective tissue microenvironment. Figure built from free of rights images from the cell biology collection of Servicer medical art (September 2019).

1.2.1 ECM Composition

1.2.1.1 Collagens

Collagen is the main component of the extracellular matrix and the most abundant protein present in the body [19]. Collagens play an important structural role within tissues, contributing to the integrity and tensile strength of the ECM. To date, more than 26 different types of collagen have been identified and can be classified into two main groups: fibrillar and non-fibrillar collagens. Fibrillar collagens (including type I, II, III, V, and XI collagens among others) are found within all connective tissues and are generally present in larger quantities [19, 20]. These collagens are mainly present in the interstitial matrix and type I collagen is its most ubiquitous member [16]. Type V collagen, another fibrillar collagen, interacts with other collagens of the interstitial matrix conferring structural integrity to soft connective tissues, such as the skin and subcutaneous adipose tissue [21]. In contrast, non-fibrillar collagens (type IV, VI, VIII, IX, X, and XII among others) are present in smaller quantities and play important roles in bridging and connecting elements of the fibrillar collagen network, in addition to being major components of basement membranes [19, 20]. More specifically, the network-forming collagen type IV assembles into a mesh-like structure that forms the main template for the basement membrane. The microfibrils of type VI collagen, another collagen found in the basement membrane of several tissues including skeletal muscle and adipose tissue, localize close to cells and helps stabilizing their membranes [22].

In addition to their structural roles, collagens are bioactive molecules that are able to interact with cell surfaces directly through integrin-binding interactions [19, 20]. For example, type I collagen was shown to modulate the response of dermal fibroblasts to mitogenic factors, as shown through increased human dermal fibroblast proliferation and migration when the cells were cultured on type I collagen coatings as compared to tissue culture polystyrene (TCPS) controls [23]. Increasing gradients of collagen type I alone were also shown to promote human dermal fibroblast migration *in vitro* [23]. Genetic diseases and murine knockout models resulting in collagen deficiencies have shown severe phenotypes, demonstrating the importance of collagens at the cellular, tissue, and organ levels. Examples include defects in collagen type III leading to cardiac deformities [24],

defects in collagen type V leading to impaired wound healing and joint pain [21], and defects in collagen type VII leading to severe skin blistering [25].

1.2.1.2 Elastic fibers

In addition to the collagen network, which gives connective tissues their tensile strength, soft connective tissues contain a network of fibrous elastic proteins comprised of elastin [26]. The role of elastin is to allow tissues to deform following mechanical stimulation and then return to their original shape. Elastin forms elastic fibers through interaction with fibrillin-1 [26]. The elastic fiber network is mainly synthesized early in life and tends to degrade slowly over time. This degradation, paired with the limited capacity for elastic fiber repair within adult tissues, explains the loss of elasticity often observed with aging, such as in skin [27].

1.2.1.3 Glycoproteins

Glycoproteins are proteins that contain saccharide chains following post-translational modifications. They are abundantly found in the ECM, where they play important roles in cell adhesion and ECM assembly. Well-characterized glycoproteins present in the ECM include fibronectin and laminins.

Fibronectin is a non-collagenous fibrous glycoprotein abundantly found in the ECM of most tissues [28]. Comprised of two monomers bound at their end through disulfide bonds, fibronectin contains several adhesion subunits that allow it to bind to various other proteins including collagens, fibrin, proteoglycans, and integrins [28]. Interactions between integrins and fibronectin can modulate multiple cell functions, including adhesion, migration, proliferation, and in some cases, differentiation [28-30]. Two main forms of fibronectin exist within the body: plasma and cellular fibronectin [31]. Plasma fibronectin is produced by hepatocytes in the liver and is soluble in the blood. Upon tissue injury, plasma fibronectin is incorporated into fibrin clots, where it helps to regulate platelet activity and mediates hemostasis within the repairing tissue [31]. Cellular fibronectin is non-soluble and produced in all connective tissues by several cell types, including fibroblasts, endothelial cells, adipocytes, osteoblasts, and mesenchymal stromal cells (MSCs) [29, 31]. Cellular fibronectin assembles into a fibril network that is tightly connected to collagen fibers and tissue resident cells [31, 32].

Laminins are a family of heteromeric glycoproteins that are major constituents of basement membranes. Laminin molecules are comprised of three interwoven chains and each member of the family contains a single α -chain, β -chain, and γ -chain [33]. Laminins provide cell-anchoring signals, along with strong survival and differentiation cues that are mediated through integrin binding interactions [33]. As major players of the basement membrane, laminins can greatly impact cell polarity, proliferation and migration; for example, laminins were shown to promote endothelial cell migration and proliferation, even in the presence of pharmacological inhibitors [34]. In addition to laminins, other important components of basement membranes include collagen type IV, nidogens (formerly known as entactins), and proteoglycans [18, 33].

1.2.1.4 Proteoglycans and glycosaminoglycans

Proteoglycans are a type of specialized glycoprotein with large sulphated glycosaminoglycan (GAG) chains [17]. These GAGs are linear and unbranched polysaccharides, typically ~ 80 sugars long and made from disaccharide building blocks [17]. The most common GAGs are chondroitin sulphate, heparin and heparan sulphate, and dermatan sulphate [35]. By definition, proteoglycans can have one or more polysaccharide chain, but at least one of their sugar side chains must be a GAG [17]. The main proteoglycans expressed in connective tissues are biglycan, decorin, and versican [35, 36].

The unique structure of the GAG bound to the peptide core gives proteoglycans strong water-binding and gel-like properties [35]. More specifically, the negative charges of the GAGs attract and trap water molecules within the interstitial space of the tissue [35]. The highly hydrated nature of the ECM is important for metabolite diffusion and tissue compression [35]. GAGs can interact directly with growth factors and cytokines through charge interactions between the negatively-charged GAGs and positively-charged soluble factors [17, 35]. By binding, stabilizing, and sequestering growth factors and cytokines, GAGs can act as a reservoir that can become available following tissue injury [35, 36]. Examples of pro-angiogenic molecules that can be sequestered within GAGs include vascular endothelial growth factor (VEGF), fibroblast growth factor-2 (FGF-2), hepatocyte growth factor, (HGF), and platelet-derived growth factor (PDGF) [35, 36].

1.2.1.5 ECM-bound soluble proteins

In addition to the soluble factor-GAG interaction previously described, growth factors, cytokines, matricellular proteins, enzymes, and other soluble molecules have the ability to bind to other ECM proteins [35, 36]. Their presence in the matrix is important for tissue homeostasis and function. For example, VEGF [37], HGF [38], and PDGF [39] were shown to have specific binding affinity for fibronectin. Follistatin domains found in many ECM glycoproteins and proteoglycans were also shown to be binding sites for bone morphogenic proteins (BMPs) and transforming growth factor- β (TGF- β) [36, 40]. TGF- β itself can be found in latent forms bound to several ECM proteins, with a particular affinity for latent transforming growth factor- β binding proteins (LTBPs), which in turn bind to fibrillin and fibronectin [36, 41]. These TGF- β /LTBP complexes act as a readily available TGF- β reservoir and can release active TGF- β following tissue injury [41].

The matricellular protein family is another class of important ECM-bound soluble proteins. Matricellular proteins are small, soluble, non-structural proteins that can modulate resident cell behaviours including ECM secretion and deposition, along with cell proliferation, migration, and recruitment [42, 43]. Unlike growth factors, which function through enzyme-linked or G protein-coupled cell surface receptors, matricellular proteins predominantly interact with cells through integrins [43, 44]. While most matricellular proteins contain at least one ECM-binding domain (e.g. fibronectin-binding, heparin-binding, etc.), all matricellular proteins have integrin-binding domains [42]. Examples of matricellular proteins include thrombospondins, tenascins, osteonectin, connective tissue growth factor (CCN2), galectins, and periostin [43]. Matricellular proteins have been shown to participate in a number of processes related to tissue repair, which have been demonstrated through the use of knockout mouse models [43, 44].

Other proteins found in the extracellular space include the matrix metalloproteinase (MMP) family of enzymes and their inhibitors, tissue inhibitors of metalloproteinases (TIMPs). As endopeptidases, MMPs have the ability to cleave multiple substrates and are involved in ECM degradation and remodelling [45]. Most MMP members are secreted in a latent form, called pro-enzymes or pro-MMPs, which can be activated by cleavage of pro-peptides blocking the catalytic site of the peptidase domains [45]. MMPs are part of the metzincin-superfamily of zinc-peptidases, with distinct members associated to either the ECM or

cytoplasmic membranes. The ECM-associated members include MMP-1, MMP-2, MMP-3, and MMP-9, which can all be found in latent forms within the ECM of connective tissues [46]. The cytoplasmic membrane-associated members are not classically considered as part of the ECM, and include three main subfamilies: the a disintegrin and metalloproteinases (ADAMs), the ADAM with thrombospondin motifs (ADAMTSs), and the membrane-type MMPs (MT-MMPs) subfamilies [45, 47]. The enzymatic activity of these zinc-peptidases can be inhibited by TIMPs, which are a family of four protease inhibitors (TIMP-1 to TIMP-4). Due to their ECM remodeling abilities, MMPs and TIMPs play central roles in tissue development and morphogenesis, along with tissue repair and wound healing [45].

1.2.2 ECM signal transduction

1.2.2.1 Integrin-mediated responses

Cells adhere to the ECM through small transmembrane proteins called integrins. Integrins are heterodimers made up of one α and one β subunit. The 18 known α and 8 known β subunits are known to assemble into a total of 24 different integrin heterodimers [48]. Classically seen as adhesion molecules, integrins can bind to ligands including structural proteins, glycoproteins, proteoglycans, matricellular proteins, and MMPs. The 24 integrin heterodimers have affinities to a variety of ECM components, and the nature of the heterodimers dictate the nature of the ligands to which they can bind [48].

It is now acknowledged that integrins function as more than adhesion proteins, and through their interaction with their surrounding ECM ligands, integrins allow cells to sense their microenvironment [48]. Depending on the nature of the integrins that are activated, intricate integrin-mediated signals can be transduced to the interior of cells. Transduction through these pathways is initiated by integrins at cell adhesion complexes, or focal adhesion complexes, which are integrin-containing protein complexes localized at the cytoplasmic membrane [41, 49]. These transmembrane focal adhesion complexes bridge the ECM to the intracellular space and actin cytoskeleton [41, 49]. Cross-talk between intracellular domains of integrins and intracellular kinases mediate several intracellular signalling pathways [41, 49]. For example, integrins regulate the formation of adhesion complexes through focal adhesion kinase (FAK) and Src-family protein tyrosine kinase (SFK), as well as cell growth through the mitogen-activated protein kinase (MAPK)

pathway, cell migration through the PI 3-kinase pathway, and actin cytoskeleton changes through pathways involving the Ras superfamily of GTPases [49, 50].

1.2.2.2 Transmembrane receptor-mediated responses

Cells can also interact with the extracellular space through a variety of specialized transmembrane receptors. Usually specific to a family of ligands, some transmembrane receptors are specialized in binding small soluble molecules, such as cytokines, growth factors, and hormones, while other transmembrane proteins specialise in direct cell-cell interactions [51].

Transmembrane receptors that bind to small molecules are classified based on their tertiary folding structures and are separated into three broad groups: G-protein coupled receptors, enzyme-linked receptors, and ionotropic receptors [51-53]. The G-protein receptor group encompasses several receptor superfamilies, including but not limited to: C-X-C motif chemokine (CXC) receptors; olfactory, taste, and photo sensory receptors; and several neurotransmitter receptors [51]. The enzyme-linked receptor group also includes two superfamilies: (i) the receptor tyrosine kinase family, with more than 20 different classes of receptors that can bind to FGFs, HGF, PDGFs, VEGFs, and angiopoietins, and (ii) the receptor serine/threonine-specific protein kinase family that interacts with TGFs and BMPs [52]. Lastly, the ionotropic receptors are a group of ion-channel-associated receptors that plays important roles in neuron polarization following neurotransmitter binding [53].

Cells also have the ability to interact directly with one another using transmembrane proteins. Direct cell-cell contacts are very common in tissues with a high cell density, such as epithelial tissues [54]. In connective tissues however, cells tend to be more sparse and spread-out than cells within epithelial tissues, reducing direct cell-cell contacts and increasing paracrine and endocrine signaling [55, 56]. Paracrine and endocrine signaling rely on small secreted factors to transduce signals between cells, either locally using growth factors and cytokines (paracrine signaling) or through the vasculature over greater distances using hormones (endocrine signaling) [55, 56].

1.2.3 Tissue-specific ECM

1.2.3.1 Adipose ECM

Adipose tissue ECM shares a lot of similarities with that of other soft connective tissues in the body, such as dermis, tendons and ligaments, fibrous connective tissues and fascias. Adipose ECM is comprised of a dense network of collagen, enriched with components associated with peripheral nerves and the vasculature [55, 57]. A unique feature of the adipose ECM is that the mature cell population, termed adipocytes, are individually surrounded by basement membranes and further assembled into groups called lobules [58, 59].

It was shown through immunohistochemistry that adipose tissue is an abundant source of collagen types I through VI (with the exception of type II), with collagens types I and IV being the most prevalent [60, 61]. In addition to collagens, the ECM of adipose tissue is rich in fibronectin, laminin, GAGs and proteoglycans such as biglycan and decorin [58, 62]. The presence of basement membrane around the individual adipocytes, comprised of laminins, collagen type IV, V and VI, is key to maintaining the structure, integrity, and shape of the tissue [58].

Other proteomic techniques have successfully identified numerous growth factors, matricellular proteins and other soluble factors sequestered within the complex ECM [55, 62]. These proteins include angiopoietin-like proteins, FGFs, galectins, HGF, and VEGF [62]. In addition to the soluble factors actively secreted by the resident cells, these sequestered factors are thought to play roles in mediating adipocyte differentiation, angiogenesis, and overall adipose tissue homeostasis [55, 63].

1.2.3.2 Bone ECM

Bones are comprised of mineralized tissues, also called osseous tissues, and semi-solid gelatinous tissues referred to as bone marrow [64]. Osseous tissues are comprised of two main subtypes of mineralized tissues: (i) cortical bone, which is the compact and dense exterior of the bone, and (ii) the more porous trabecular bone that is mainly found inside of long bones and vertebrae. Trabecular bone is comprised of a sponge-like network interspersed with the soft bone marrow [64, 65].

The ECM of osseous tissues is made up of approximately 70% inorganic compounds [66, 67]. These inorganic compounds are comprised of a calcium- and phosphate-containing mineral called hydroxyapatite, which provides the bone with its characteristic hardness that allows it to resist mechanical loading forces [66, 67]. The other part of the ECM is comprised of organic material, primarily collagen types I, III, IV, V, and XII, as well as fibronectin, proteoglycans, and matricellular proteins including osteocalcin (also known as bone gamma-carboxyglutamic acid-containing protein; BGLAP), osteonectin (also known as secreted protein acidic and rich in cysteine; SPARC), osteopontin (also known as secreted phosphoprotein 1; SSP1), and bone sialoproteins [65, 68, 69]. The roles of these matricellular proteins are to facilitate adhesion between the cells and the inorganic compounds, and to stabilise the interactions between the organic and inorganic components of the ECM [70]. Proteomic analyses have also shown the presence of sequestered soluble factors within the ECM, such as BMPs, insulin-like growth factors (IGFs), LTBP, stromal cell-derived factor-1 (SDF-1/CXCL12), and TGF- β [62].

1.3 ECM-derived scaffolds

1.3.1 Biomaterials and general considerations

Aiming to promote constructive tissue regeneration, naturally-derived biomaterials are designed to provide structural and biological cues that can positively regulate pro-regenerative cellular responses [71].

Two main strategies exist to produce ECM-derived biomaterials: bottom-up or top-down approaches. Bottom-up approaches start with a basic template of purified ECM components to produce a homogeneous bioscaffold, to which other components can be subsequently added to tune the composition and potentially modulate other scaffold properties [72, 73]. In contrast, top-down approaches apply decellularized tissues as complex ECM sources to produce bioscaffolds [73-76]. Further described in Section 1.3.3, decellularization is the process of removing immunogenic components from native tissues (e.g. cells, intracellular organelles, and DNA), while preserving the structure and composition of the native ECM as much as possible. Although they represent powerful tools to systematically probe the effects of various ECM-derived factors on cellular responses, materials fabricated using bottom-up approaches often fail to recapitulate the

complexity of the native ECM [73, 77, 78]. Advantages of using decellularized tissues over purified ECM sources, such as gelatin or purified collagen type I, include enhanced retention of physical and biochemical properties that are specific to the complex extracellular microenvironment of the native tissue source [74, 79]. Given that different tissues have varying functions, physical properties, and biochemical composition, there is a clear rationale for using a tissue-specific approach when designing biomaterials tailored for specific applications [71, 74, 79]. For these reasons, decellularized tissues have emerged as a promising ECM source for the production of ECM-derived bioscaffolds [73, 75, 76].

There are several important design considerations when developing bioscaffolds from decellularized tissues [80, 81]. First, the final scaffolds must be capable of supporting relevant cell populations for the target application with high cell viability. For example, utilization of cytotoxic reagents such as cross-linkers (formaldehyde, paraformaldehyde, and glutaraldehyde) should be avoided whenever possible, as traces of these reagents in the scaffolds have been associated with decreased cell growth and viability *in vitro* and undesired calcification *in vivo* [82, 83]. In addition, the biomaterial should allow the delivery of predictable doses of cells, while ideally promoting long-term retention and viability, as well as directing the function of the delivered cells in animal models [84]. Second, the ECM architecture and composition should be preserved as much as possible during the decellularization and fabrication processes [85]. Third, the development of reproducible and successful therapies is dependent on the ability of the ECM-derived biomaterials to promote a favourable host response, integrate into the surrounding tissues, and help to coordinate constructive tissue remodelling and repair following implantation *in vivo* [71, 84]. Lastly, the resulting formats of the ECM-derived biomaterials should be stable and have appropriate mechanical properties for handling and for the targeted applications [74].

1.3.2 Properties of the ECM that can modulate cell behaviour

The biochemical, structural, and biomechanical properties of the ECM can have a profound impact on seeded and/or infiltrating cells and can modulate their behavior [71]. *In vitro* studies investigating the response of cells seeded on ECM-based coatings have shown the importance of biochemical composition on cell monolayers. In particular, a study focusing

on tissue-specific ECM composition from decellularized cardiac tissues demonstrated that tissue-specific myocardial matrix supported murine cardiac progenitor cell (CPC) survival under stress in response to H₂O₂ treatment, when compared to purified type I collagen coating controls [86]. Another study using high throughput screening approaches investigated the impact of combined ECM components on the phenotype of induced human pluripotent stem cells (iPSC)-derived endothelial cells [87]. More specifically, the findings indicated that two specific ECM combinations: (i) collagen, gelatin, heparan sulfate, and laminin, and (ii) collagen, fibronectin, gelatin, heparan sulfate, and laminin, significantly increased the survival of the iPSC-derived endothelial cells under hypoxia (1% O₂) and a reduced serum condition (1% fetal bovine serum; FBS) [87]. Similar high throughput screening approaches have also demonstrated that ECM composition could improve hepatocyte function of murine hepatocytes and increase the hepatogenic differentiation of murine embryonic stem cells [88].

In addition to biochemical composition, physical properties of cell substrates are also important mediators of cell function. For example, substrate stiffness was shown to mediate cell fate and differentiation *in vitro*, using bone marrow-derived MSCs [89, 90]. In this context, a stiffer matrix was shown to stimulate differentiation towards the chondrogenic and osteogenic lineages, while softer substrates promoted differentiation towards the adipogenic lineage [89, 90]. Similar effects of matrix stiffness were noted in dermal fibroblasts [89, 90]. The intracellular pathways involved in this adipogenic-proliferative-osteogenic balance within MSCs and fibroblasts is briefly detailed in Figure 1.2. Further studies comparing the role of matrix stiffness also demonstrated that fibroblast proliferation, stress fiber formation, and fibrotic marker expression is enhanced on stiffer substrates [89, 90]. In contrast, softer substrates and increased matrix compliance were associated with increased angiogenic potential [91, 92]. Thus, these observations suggest the important role of matrix stiffness in governing cell survival, cell function, and cell fate, illustrating the importance of designing biomaterials with appropriate mechanical properties for targeted applications.

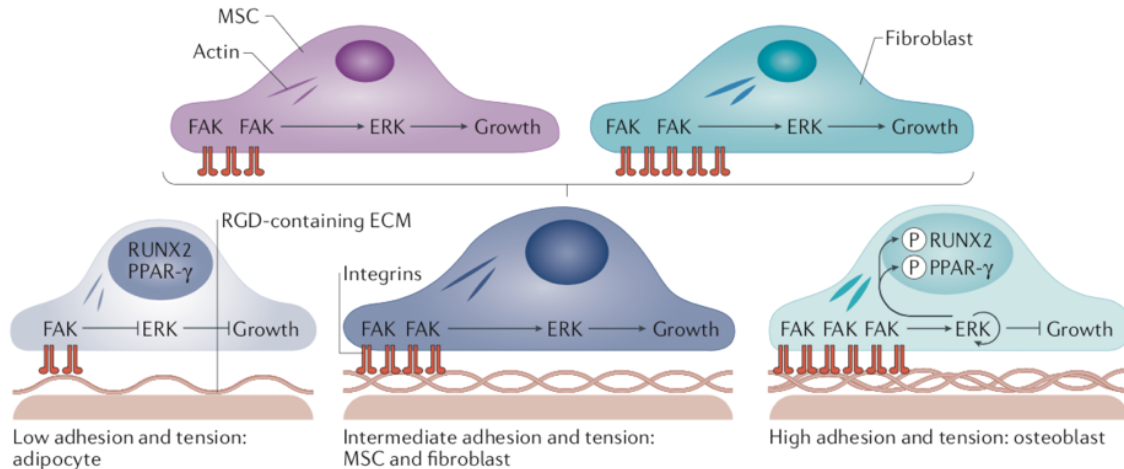


Figure 1.2 Correlation between mechano-transduction, growth, and differentiation in mesenchymal stromal cells (MSCs) and fibroblasts. The lack of strong focal adhesion complexes on low-adhesion and tension substrates tends to reduce the activation of focal adhesion kinase (FAK) within MSCs and fibroblasts, which in turn inhibits mitogen-activated protein kinase (MAPK) and extracellular signal-related kinase (ERK) mediated cell growth. This cell growth inhibition is associated with limited phosphorylation of the master adipogenic and osteogenic transcription factors, which keeps them in their active and inactive states respectively (master adipogenic factor = peroxisome proliferator-activated receptor- γ (PPAR γ); master osteogenic transcription factor = Runt-related transcription factor 2 (RUNX2)), thereby promoting adipogenesis. At the other end of the spectrum, high ECM tension and stiffness promotes adhesion, stimulating the formation of high levels of focal adhesion complexes resulting in strong FAK signaling. Strong FAK signaling strongly activates the MAPK/ERK pathway, which causes the phosphorylation of both PPAR γ and RUNX2, inactivating the former and activating the latter, to promote osteogenesis. The presence of a negative feedback loop of ERK, following the strong FAK activation, allows for limited cell growth. On substrates with intermediate stiffness, FAK signaling induces the MAPK/ERK pathway, but below the threshold of the negative feedback loop, which allows for cell growth. Adapted with permission from [89].

1.3.3 Decellularization

As previously mentioned, decellularization is the process of removing cells and their components from tissues, while minimizing ECM alterations as much as possible [93]. Extraction of cells and other potentially antigenic components is dependent on the intrinsic nature of the tissue, including its specific physical and biochemical characteristics, and results in the reduction in immunogenic properties of the decellularized tissue [93]. To

maximize cell removal, most decellularization protocols utilize a combination of physical, chemical, and enzymatic treatments, either concomitantly or in succession [93-95]. Each of these treatments can affect the ultrastructure and biochemical composition of the resulting decellularized ECM, which in turn has the potential to impact the host response to the material and the overall ability of decellularized-based biomaterial to mediate desired cell functions for targeted applications [94].

1.3.3.1 Physical methods for tissue decellularization

Physical processing of the tissue, such as freeze-thaw cycles, pressure, sonication, and agitation, can be employed to mechanically remove cellular components from native tissues [93, 95]. Considered one of the most gentle physical methods for tissue decellularization, freeze-thawing of tissues can help disrupt cell membranes through ice crystal formation [96]. Mechanical agitation and application of pressure on the tissue are also widely used methods to facilitate the extraction of cellular components from the ECM, functioning in part by increasing the exposure of the tissues to the reagents [93, 97]. Excessive physical manipulation can disrupt the ECM structure; however, these methods can be easily controlled and are often used conjointly with other methods described in the next sections [93, 98].

1.3.3.2 Chemical methods for tissue decellularization

Chemical methods for decellularizing tissue include the use of hypertonic or hypotonic solutions, alkaline or acid treatment, polar solvents, and detergents. The use of hypertonic and hypotonic solutions prepared with chelating agents, such as ethylenediaminetetraacetic acid (EDTA), is a very common cell-lysing and integrin cofactor sequestering method [93, 99, 100]. Alkaline and acid treatments can facilitate the solubilization of cellular components by altering the pH of the tissue [101]. Acid treatments are also used to demineralize hard connective tissues such as bones [102, 103]. Alcohols and other polar solvents are effective for dissolving and extracting lipids from tissues [104-108]. With their ability to solubilize cell debris and aid in dissociating DNA from the ECM, detergents are also widely employed in decellularization protocols [109-111].

The limitations of osmotic cell lysis buffers and divalent ion chelating solutions in decellularization protocols are attributed to their gentle nature. In particular, these

treatments must typically be performed in conjunction with other methods as they are not effective at fully extracting cellular components from the tissues [93]. Adverse effects of using alkaline and acid treatments for decellularization include the hydrolytic degradation of biomolecules, such as collagens and GAGs, and the extraction of soluble factors found within the ECM [112]. Polar solvent extraction can lead to protein dehydration [112] and matrix stiffening [105], although matrix stiffness was reported to be unchanged in the case of some tissues, such as adipose tissue [113]. Finally, the use of detergents has been associated with several adverse effects, including the reported loss of non-structural proteins including growth factors and GAGs in treatments with non-ionic detergents, as well as the disruption of structural proteins with the use of ionic detergents [110, 114]. There is also concern about residual detergent remaining within the decellularized tissues, as this has been associated with cytotoxic effects and impaired cell growth *in vitro* [85, 115].

1.3.3.3 Enzymatic methods for tissue decellularization

The catalytic activity of certain enzymes can be harnessed in the decellularization of tissues and organs. Proteases (e.g. trypsin and collagenases), nucleases (e.g. deoxyribonucleases and ribonucleases; respectively DNases and RNases), and lipases have all been explored in various decellularization protocols [93]. Proteolytic enzymes such as trypsin can disrupt integrins, releasing the cells from the ECM, while partially digesting dense ECM to allow for better penetration and exposure to other reagents [94]. DNase and RNase can successfully digest residual nucleic acids within the ECM, which helps to prevent adverse host immunogenic responses following implantation of decellularized tissues [94, 116]. Adverse effects of proteolytic enzymes include over-digesting the ECM leading to the loss of ECM components and architecture [117]. Enzymes, including proteases and nucleases, have also been reported to have immunogenic properties themselves, emphasizing the need for extensive wash procedures following treatments [94, 116].

1.3.4 Decellularized adipose tissue

Human adipose tissue is routinely discarded as surgical waste from cosmetic surgeries, either as lipoaspirates or resected fat from cosmetic surgeries. Advantages of surgically-discarded adipose tissue over other ECM sources include the abundance of adipose tissue

compared to other soft connective tissues (e.g. dermis) and its human origin. Both resected adipose tissue and lipoaspirates can be processed into decellularized adipose tissue (DAT) following published protocols [104, 118-125]. The resulting DAT is comprised of collagen types I, III, and IV, laminin, fibronectin, vitronectin, elastin, and GAGs, and also contains other soluble growth factors and matricellular proteins, such as FGF-2, VEGF, and galectins [62, 104, 118, 119, 124].

The Flynn laboratory has pioneered adipose tissue decellularization, being the first research group to develop a detergent-free method to produce DAT in 2010 [104]. The 5-day decellularization protocol uses a combination of physical, chemical, and enzymatic decellularization methods. Briefly, the approach involves freeze-thaw cell-lysis cycles combined with washes in a hypotonic solution containing EDTA to enhance cell extraction, digestion with trypsin-EDTA to disrupt cell-cell interactions, isopropanol extraction of lipids, and combined DNase-RNase-lipase digestion. Interestingly, the resulting DAT has biomechanical properties similar to native adipose tissue [113]. The DAT was also shown to have *in vitro* cell-instructive (i) “adipo-inductive” and (ii) “adipo-conductive” properties on tissue-specific human adipose-derived stromal cells (ASCs), which can be respectively described as (i) promoting adipogenesis in a microenvironment not typically supportive of adipocyte differentiation and (ii) enhancing adipogenesis under adipogenic differentiation conditions [14]. In addition, the resulting DAT displayed pro-regenerative properties *in vivo*, as demonstrated through its remodelling into healthy host-derived fat following subcutaneous implantation [14]. This remodelling demonstrated the pro-angiogenic and pro-adipogenic capacities of the DAT, with the scaffolds promoting the recruitment of host endothelial cells, macrophages, and adipogenic progenitors [126].

A proteomic study performed by Thomas-Porch *et al.* in 2018 compared the biochemical composition of the DAT produced from the Flynn laboratory protocol, along with two other methods [124], respectively based on the use of detergents [123] or the use of urea and chloroform treatments [127]. The study findings demonstrated that the Flynn laboratory approach was the only method amongst the three that could achieve proper delipidation and nucleic content removal, while maintaining structural integrity of the tissue [124]. The trypsinization-based mass spectrometry analyses revealed a significant decrease in the detection of proteins from intracellular, membrane, and blood origins in the Flynn

laboratory protocol, demonstrating that the two other approaches led to incomplete removal of cell debris from the tissues [124]. Of note, a multi-enzyme-based digestion approach using collagenase to deplete collagen in samples prior to mass spectrometry analysis was developed by Kuljanin *et al.* (2017) using DAT produced using the Flynn laboratory protocol [62]. This study directly compared traditional sample preparation methods using trypsin digestion to a new approach using collagenase digestion to selectively deplete collagens found in high abundance in the samples. Collagenase digestion increased the number of proteins identified in the DAT by ~2.2 fold, to a total of 804 identified proteins[62]. When compared to bovine collagen and human decellularized bone tissue, this study revealed that DAT was enriched in factors associated with adipogenesis, including FGFs, CXCL14, and protein Wnt-11; along with factors associated with angiogenesis, including angiopoietin-like proteins, FGFs, HGF, and VEGF [62].

1.3.5 Processing of decellularized tissues for the fabrication of bioscaffolds

In addition to being applied in their intact form as three-dimensional (3-D) scaffolds, decellularized tissues can be further processed into other formats [74]. This strategy allows for the fabrication of new biomaterials that incorporate the complex ECM composition within platforms that offer greater flexibility in terms of other scaffold properties, including enhanced porosity or more tuneable mechanical properties. This processing often starts with the fragmentation of the intact ECM, which can include methods such as mincing and/or cryo-milling, followed by homogenization of the ECM into a suspension or a solution, with or without the use of enzymatic digestion [128-130]. Once an ECM suspension or solution is obtained, it can either be used directly or mixed with other compounds to produce naturally-derived or composite bioscaffolds, respectively. Table 1.1 list naturally-derived biomaterials that have been explored using DAT as an ECM source.

Table 1.1 List of naturally-derived biomaterials fabricated using DAT

Scaffold format	DAT processing method	Solvent for DAT suspension	Year and reference
Hydrogel	Thermo-sensitive gelation of pepsin digested-DAT solution following neutralization	0.1 M hydrochloric acid (neutralized)	2011 [119]
Mesh	Electrospinning of homogenized DAT suspension in organic solvent	hexafluoro-2-propanol or trifluoroacetic acid	2012 [131]
Cross-linked DAT micro-carriers	Pepsin-digested DAT was solubilized in a sodium alginate solution, sprayed into a CaCl ₂ solution using an air-jet droplet system, cross-linked using rose Bengal, glutaraldehyde, or riboflavin, followed by an alginate extraction step using a sodium citrate buffer	0.5 M acetic acid with sodium alginate	2012* [132]
Foams	Lyophilization of α -amylase digested DAT homogenized into a suspension	0.2 M acetic acid (lyophilized)	2013* [14]
Bead foams	Lyophilization of electrosprayed beads inside of a mould, made from α -amylase digested DAT homogenized into a suspension	0.2 M acetic acid (lyophilized)	2013* [14]
Micro-particles	DAT particles were directly resuspended in neutral buffer following cryo-milling	Saline	2013 [125]
Enzymatic cross-linked hydrogel	Thermo-sensitive gelation of pepsin digested-DAT solution following neutralization, supplemented with transglutaminase for <i>in situ</i> enzymatic cross-linking	0.1 M hydro-chloric acid (neutralized)	2014 [133]
Extrusion based bio-printed lattices	Bio-printed lattice of a single-phase hydrogel, produced by thermo-sensitive gelation of pepsin-digested DAT solution following neutralization	0.1 M hydro-chloric acid (neutralized)	2014 [134]
Porous micro-carriers	Lyophilization of electrosprayed microcarriers, made from α -amylase digested DAT homogenized into a suspension	0.2 M acetic acid (lyophilized)	2017* [135]
Coatings	Homogenized α -amylase-DAT and neutralized pepsin digested-DAT suspensions were coated in cell culture dish and air-dry.	0.2 M acetic acid (lyophilized)	2019* [136]

Note: references labelled with (*) are from the Flynn research group

As seen in Table 1.1, several porous and non-cross-linked DAT bioscaffold formats were pioneered by the Flynn lab. These formats include the intact DAT itself [104], as well as an array of other scaffold formats derived from processed DAT, including DAT-derived microcarriers, foams, and bead foams [14, 132, 135, 136]. The key steps to achieving the production of these bioscaffolds formats, from the adipose tissue itself to the resulting materials, are illustrated in Figure 1.3.

Notably, *in vivo* studies directly comparing the regenerative potential of intact DAT scaffolds and DAT bead foams after subcutaneous implantation in a Wistar rat model

showed differences in the host response [14]. While both formats integrated into the host tissues and remodelled over time, the DAT bead foams induced greater cell infiltration, noted by the increased presence of blood vessels and inflammatory cell migration at earlier time points relative to the intact DAT [14]. Adipogenic differentiation was observed in both groups, with an increased presence in the intact DAT group as compared to the DAT bead foam group [14]. This study also displayed full integration of the DAT bead foams within the host tissues after 12 weeks, whereas the intact DAT implants macroscopically maintained their volume over this time course [14]. These results revealed the intrinsic potential of the DAT bead foams for therapeutic angiogenesis and the inherent potential of intact DAT for adipose tissue engineering. It was postulated that the different outcomes may have been linked to the matrix processing, resulting in more homogeneous and porous DAT bead foams as compared to more heterogeneous and denser intact DAT scaffolds.

In addition to their pro-angiogenic capacity and potential for host integration, the DAT bead foams have other advantages over other bioscaffold formats. Based on their modular nature, the bead foam technology is highly adaptable and allows for the fabrication of scaffolds with well-defined geometries. The resulting scaffolds have both a microporous architecture within individual spheres, along with a macroporous architecture of channels between the spheres [14]. In contrast with some other approaches described in Table 1.1, the production of the DAT bead foams was designed to exclude the use of any detergents, cross-linking agents, and synthetic materials, in an attempt to preserve the complex composition of the adipose ECM and to circumvent cytotoxicity concerns associated with residual chemicals.

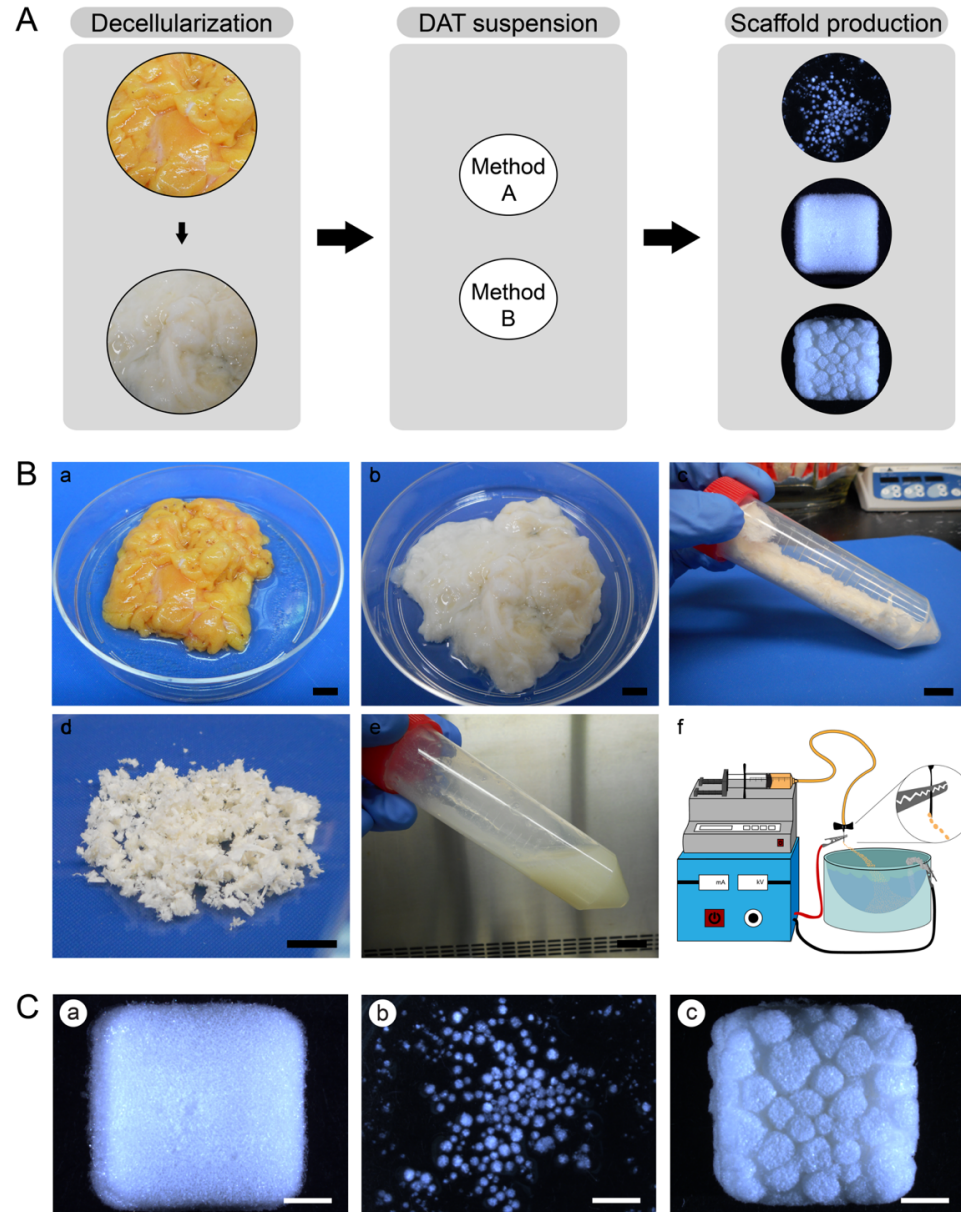


Figure 1.3 Overview of adipose decellularization and further processing steps for DAT-derived bioscaffold production. (A) Flow chart highlighting the key stages for the production of the various DAT scaffold formats. (B) Macroscopic appearance during the main decellularization and processing steps. (a) Excised adipose, (b) Fresh DAT, (c) Lyophilized DAT, (d) Lyophilized minced DAT, (e) Homogenized DAT suspension in acetic acid. (f) Diagram of the electro spraying apparatus used for the production of DAT microcarriers/beads used to make bead foams. A syringe pump is used to control the flow rate of the DAT suspension into liquid nitrogen. Scale bars = 1 cm. (C) Representative macroscopic images of (a) DAT foams, (b) DAT microcarriers, and (c) DAT bead foams. Scale bars = 2 mm. Modified with permission from a book chapter published by Morissette Martin *et al.* in 2018 [130].

1.4 Angiogenesis and wound healing

All biomaterials invoke an initial inflammatory response following implantation [75]. The description of the classic host response is generally broken into several stages, beginning with the traumatic tissue injury during implantation surgeries and continuing throughout the wound-healing period [75]. This body response following implantation is similar to physiological wound healing [137]. For these reasons, the phases of normal wound healing and the mechanisms of angiogenesis elicited following ECM-derived biomaterial implantation will be described in Sections 1.4.1 and 1.4.2.

1.4.1 Phases of wound healing

Following tissue injury, cascades of complex cellular mechanisms are initiated at the wound site. These mechanisms are classically grouped into four major overlapping phases: hemostasis, inflammation, proliferation, and remodeling [138, 139]. The phases of cutaneous wound healing are illustrated in Figure 1.4.

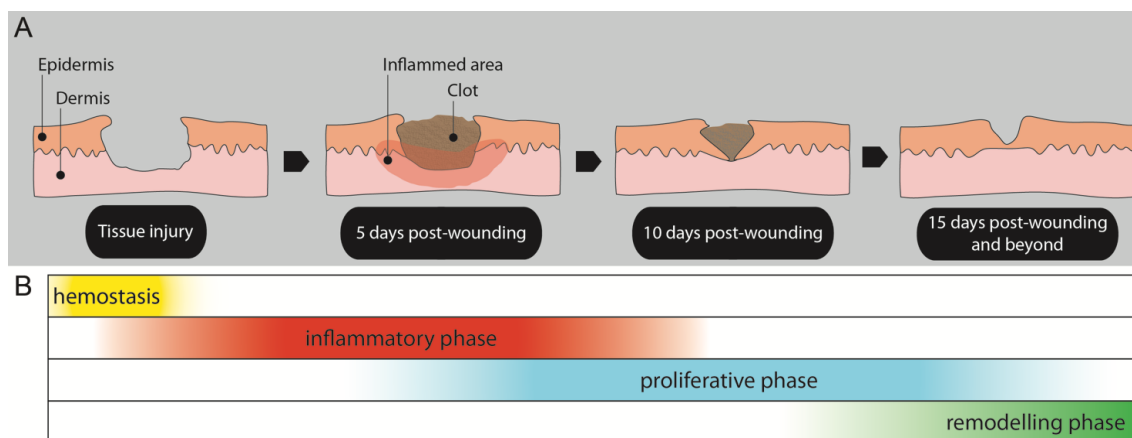


Figure 1.4 Schematic representation of cutaneous healing processes. (A) Wound cross-sectional representation at various time points. (B) Temporal representation of the four overlapping phases of healing. Modified with permission from a book chapter published by Morissette Martin *et al.* in 2016 [140].

1.4.1.1 Hemostasis

Hemostasis includes a set of cellular and molecular processes to stop bleeding following wounding. This process is highly regulated by thrombocytes, also known as platelets, which will start to agglomerate at the site of injury to limit blood loss [138]. In parallel, enzymatic cascades are initiated by the thrombocytes, which will lead to the polymerization of plasma soluble fibrinogen into insoluble fibrin at the wounded site. This coagulation step completes the hemostatic plug, also known as a thrombus. These processes occur rapidly, on the order of minutes, to limit blood loss [138, 141].

1.4.1.2 Inflammatory phase

The inflammatory phase begins following the release of pro-inflammatory molecules from the resident cells of the wounded tissues and from the hemostatic plug. Early mediators of inflammation include interleukins-1, -6 and -8 (IL-1, IL-6 and IL-8), and TGF- β [138, 141]. These factors will stimulate the recruitment of neutrophils, as well as leukocytes specialized in phagocytosis of foreign particles and bacteria. During the 24-to-48-hour period when they are present in high abundance in the wound, neutrophils have a strong pro-inflammatory action [138, 141]. In particular, neutrophils secrete cytokines including monocyte chemoattractant protein-1 (MCP-1), TNF- α , and IL-1 β , concomitantly with proteases and reactive oxygen species [142]. This assortment of factors initiates the recruitment and infiltration of circulating monocytes, which then differentiate into macrophages at the wound site [143].

Macrophages are key effectors involved in a plethora of immune processes, ranging from phagocytosis, lymphocyte chemo-attraction, antigen presentation to lymphocytes, and initiation of the proliferative phase [143]. Macrophages can accomplish these various functions through a process called macrophage polarization, where macrophages specialize their phenotypes in response to dynamic signals from the microenvironment [143]. Classic definitions comprise two main subtypes of macrophages: M1 pro-inflammatory macrophages, specialized in phagocytosis and sustaining a strong pro-inflammatory response, and M2 pro-regenerative macrophages, specialized in resolving the inflammatory response and initiating tissue repair [143]. However, it is now understood that *in vivo* macrophage polarization is a dynamic continuum, with few cells at both ends

of the M1/M2 spectrum [143]. The activity of M1-like macrophages is mediated through the secretion of pro-inflammatory factors, such as TNF- α , IL-1 β , and IL-6, while the activity of the M2-like macrophages is mediated through the secretion of pro-regenerative and pro-proliferative factors TGF- β , interleukin 4 (IL-4), interleukin-1 receptor antagonist (IL-1RA), and VEGF, among others [143].

1.4.1.3 Proliferative phase

The proliferative phase is characterized by the migration and proliferation of several cell types, ultimately resulting in the formation of scar tissue [138, 141]. Depending on the afflicted tissue and the anatomical localization of the wound, different cell types are involved; however, three main processes are usually defined within the proliferative phase of skin healing: re-epithelialisation (keratinocyte migration), granulation tissue formation (fibroblast and immune cell migration, paired with ECM secretion), and angiogenesis (migration of endothelial cells to re-vascularize the newly formed granulation tissue, described in section 1.4.2) [138, 141].

The formation of granulation tissue, the temporary and fast-remodelling connective tissue secreted at the wounded site, is first initiated by neighboring fibroblasts in response to the cytokines released by the thrombocytes and neutrophils [144]. The arrival of macrophages sustains the fibroblast activation through the action of several cytokines, including FGF-2, EGF, PDGF, and TGF- β , and will induce fibroblast proliferation and migration into the fibrin-fibronectin provisional matrix formed during hemostasis [144, 145]. Cells within the granulation tissue start remodelling this matrix through MMP-mediated degradation and ECM deposition, including the weaker but rapidly-assembled collagen type III, fibronectin, GAG and proteoglycans, along with small amounts of collagen type I [145].

1.4.1.4 Remodelling phase

The remodelling phase is characterized by both a degradation and deposition of ECM by myofibroblasts [145]. Originating from different precursor cells, primarily local connective tissue fibroblasts, along with local pericytes, local and circulating MSCs, myofibroblasts differentiate in the wound microenvironment through the action of sustained TGF- β -mediated signaling and matrix stiffening [146, 147]. Temporal secretion substrate-specific MMPs and TIMPs by the myofibroblast populations orchestrate ECM degradation [144].

This degradation is concomitant with ECM deposition of more mature components by the myofibroblasts, primarily collagen type I, but also other glycoproteins including matricellular proteins and proteoglycans [43, 144]. In normal non-pathologic wound healing, myofibroblast numbers will then decrease through apoptosis, with few cells present in the mature scar tissue [144].

1.4.2 Physiology and mechanisms of angiogenesis

Angiogenesis is a highly regulated physiological process associated with the extension of the blood vessel network from previously-existing blood vessels and capillaries. Two different types of angiogenesis can be defined: sprouting angiogenesis (Figure 1.5) and intussusceptive angiogenesis [148]. While being an important vascular network extension strategy in the body, intussusception is usually recognized as much less prominent than sprouting angiogenesis in the context of tissue repair and neo-vascularization of soft biomaterials [149]. For these reasons, particular attention will be given to sprouting angiogenesis in this chapter.

Several steps are required to drive the maturation of the endothelial sprouts into functional vessels and capillaries. The first stage of sprouting angiogenesis is associated with endothelial cell activation and budding within neighbouring tissues, including wound granulation tissues and ECM-derived implants (Figure 1.5A). Paracrine growth factor gradients, such as VEGF, along with EGF, FGF-2, HGF, and IGF, can activate endothelial cells [150, 151]. Strongly activated endothelial cells then inhibit lateral endothelial cells through Notch signaling and the sprouting “tip” endothelial cells begin to degrade their surrounding basement membrane. Neighbouring pericytes also become activated by the mitogen gradients, which results in a reduction of their cell-cell stabilizing interaction with the endothelial cells [148].

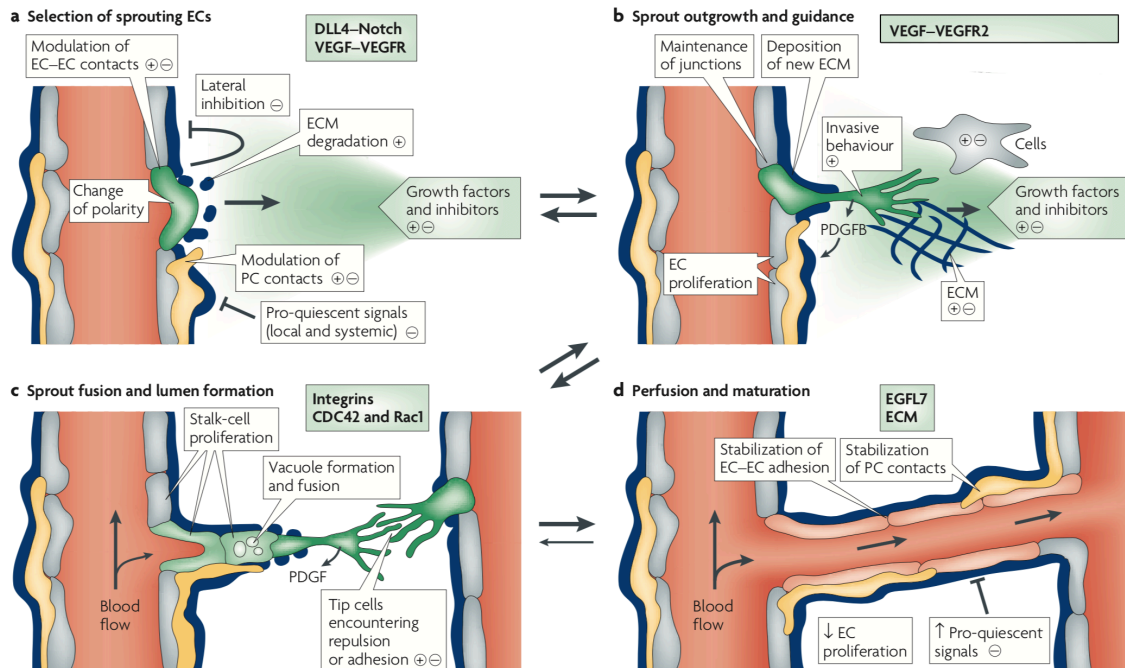


Figure 1.5 Schematic representation of sprouting angiogenesis. A) Sprouting is controlled by the balance between pro-angiogenic and pro-quiescent signals. Strongly activated endothelial cells start sprouting (in green), whereas other endothelial cells remain quiescent (in gray). Pericytes (in yellow) modulate their cell-cell interactions with the endothelial cells. (B) Endothelial cell sprouts are growing and are guided by the growth factor gradient and surrounding microenvironment. (C) Interactions between tip cells regulate the fusion of sprouts and vessels. Lumen formation in stalk endothelial cells involves the fusion of vacuoles and other tube-forming mechanisms. (D) Perfusion of the vessels with blood promotes maturation processes, including the stabilization of cell junctions, matrix deposition, and pericyte-endothelial cell interactions. Abbreviations: Cell division control protein 42 homolog: CDC42, DLL4: delta-like-4 ligand, EC: endothelial cells, ECM: extracellular matrix, PC: pericytes, PDGF: platelet-derived growth factor, Ras-related C3 botulinum toxin substrate 1: Rac1, VEGF: vascular endothelial growth factor, VEGFR: VEGF receptor. Adapted with permission from [148].

The second stage of sprouting angiogenesis, sprout outgrowth and guidance (Figure 1.5B), is characterized by the invasive phenotype of the endothelial tip cells [148]. More specifically, activated tip cells show highly proliferative and migratory behavior towards the gradient of growth factors. In contrast to fibroblasts, this migration occurs sequentially, with the endothelial cells first aligning with each other to form proto-capillaries [148]. Pericytes are then recruited at the base of the new sprouts through paracrine secretion of

PDGF by the tip cells. This process ensures sufficient stabilization to support the growing endothelium [148].

Sprout fusion and lumen formation, the third stage of sprouting angiogenesis, is then self-initiated by the tip cells when they encounter other sprouts or existing vasculature (Figure 1.5C). To form new vascular connections, tip cells downregulate their invasive motile and explorative phenotype upon interacting with target endothelial cells. These interactions with endothelial cells from other sprouts or vessels initiate the assembly of cell-cell junctions [152]. This step is also characterized by stalk endothelial cell proliferation and basement membrane formation, stabilizing the base of the proto-capillary. Proto-capillaries can be converted into tubes in various ways, including pinocytosis and vacuole formation within the stalk endothelial cells [148]. These processes are dependent on the activity of small GTPases (Cell division control protein 42 homolog and Ras-related C3 botulinum toxin substrate 1; CDC42 and RAC1, respectively) and only occur in stalk cells forming strong integrin-basement membrane adhesions [148].

The proto-capillaries may be called capillaries once they are able to transport blood following the formation of a lumen, at the end of the fourth stage of the sprouting angiogenesis process (Figure 1.5D). Following perfusion of the newly formed capillaries, the presence of shear flow will inhibit endothelial cell proliferation and strengthen endothelial cell-cell interactions [148]. Mural cells, including pericytes in the case of capillaries and smooth muscle cells in larger diameter blood vessels, will migrate around the endothelial cell tubes and initiate stabilizing cell contacts [148]. Secretion of angiostatic molecules, such as angiopoietin-1, vascular endothelial statin (also known as EGF-like domain-7; EGFL7), TGF- β , and thrombospondins, also helps to stabilize the capillaries by inhibiting endothelial cell proliferation and stabilizing cell-cell interactions [150, 153].

1.4.3 Pathologies with insufficient angiogenesis

1.4.3.1 Cutaneous chronic wounds

Also known as skin ulcers, cutaneous chronic wounds are wounds that fail to go through normal wound healing processes and a large proportion of these wounds never resolve and will deteriorate over time [154]. These wounds are especially prevalent in the diabetic population, where 15 to 25% of diabetic patients will develop at least one lower limb ulcer

in their lifetime [155]. In the context of an aging population, with an estimated population of 415 million diabetics worldwide in 2015, chronic wounds are expected to steadily increase [156]. Chronic wound complications include pain, claudication, peripheral neuropathy, tissue necrosis (gangrene), and amputations in the most severe cases [155]. Indeed, amputations are required in 15 to 27% of non-healing wound cases, when all other conventional treatments have been unsuccessful [157]. Care associated with wounds and their complications represents a burden for healthcare systems and is estimated to cost more than 25 billion dollars annually in the United-States alone [158].

While a variety of effectors have been postulated as possible co-factors that modify the wound bed to create a microenvironment that is non-permissive for healing, the causes leading to the chronicity of impaired wound healing are diverse and are currently not well understood [154]. Possible effectors include insufficient oxygen and nutrient delivery, improper cellular waste removal, ischemia-reperfusion injuries, along with the hyperglycemic microenvironment and altered immune cell functions in diabetic patients [154, 159-162].

1.4.3.2 Peripheral artery disease

Peripheral artery disease (PAD), also known as peripheral vascular disease or lower extremity arterial disease, is characterized by atherosclerotic lesions in arteries that supply blood to the limbs, with the lower extremities being the most commonly affected. The build-up of occlusive atherosclerosis plaques, comprised of fibrous tissue and lipid deposition in the lumen of blood vessels, reduces blood flow in the extremities [163]. Between 2000 and 2010, the prevalence of PAD increased by 23.5% worldwide, impacting approximately 202 million people in 2010 [163]. The chronicity of PAD can lead to its more severe form, critical limb ischemia (CLI), which is associated with a chronic lack of oxygen delivery in the limbs. CLI is considered as the end stage of PAD and can lead to complications that are similar to the ones associated with chronic ulcers, ranging from pain to tissue necrosis, and can often require amputations [164]. PAD is usually diagnosed in half of all cases of chronic ulcers, and together, PAD and CLI accounts for 2-4% of the healthcare budgets of industrialised countries [165]. Percutaneous or open surgical revascularization is considered as the best therapy to eliminate pain and to trigger wound healing of PAD-associated lesions [164].

1.4.3.3 Clinical need to promote angiogenesis

Gold standard treatments in the field of chronic wounds include classical wound care (debridement, moist wound environment, selection of proper wound dressings, etc.), resolution of infections, offloading of wounded areas when possible, and medication to reduce the effect of contributing factors (e.g. diabetes, atherosclerosis, or high blood pressure) [165]. Current clinical treatments for PAD and CLI include medications targeted to prevent atherosclerotic plaque deposition (including but not limited to anti-low-density lipoprotein, anti-platelet, and anti-coagulant medications), compression stockings that can help venous drainage when appropriate, and revascularization surgery to re-establish proper blood flow when possible [165, 166].

The previously-discussed complications associated with CLI and chronic wounds remain severe and illustrate the frequent failure of the aforementioned conventional treatment approaches to enable adequate revascularization and healing. Both CLI and chronic wounds are highly hypoxic environments characterized by a lack of nutrient and oxygen diffusion to the affected areas [166, 167]. In this context, pro-angiogenic therapies hold tremendous potential for the treatment of CLI and chronic wounds [168].

1.4.4 Bioscaffold-derived and cell-derived regeneration strategies

While biomaterials alone have shown some success in promoting wound healing and therapeutic angiogenesis [169, 170], the clinical efficacy of these approaches is unclear. The current commercially-available bioscaffolds approved for wound healing applications are only accredited for limited subset of wound etiologies [170, 171]. Possible reasons for the mixed success of biomaterials-based approaches are still ambiguous, but recent findings suggest that poor host cell infiltration and scaffold remodelling caused by low scaffold porosity may be factors that affect the therapeutic potential of these biomaterials [172, 173]. Cell therapy-based approaches have also been reported to have some success in triggering therapeutic angiogenesis, with some ongoing human clinical trials; however, none of these therapies have been currently approved for clinical use due to the limited functional effects observed [174]. Postulated reasons for the poor translation of cell-only approaches from preclinical to clinical studies may include the loss of the injected cell populations at the ischemic site after treatment, potentially due to cell death in the harsh

low-nutrient and hypoxic environment of the wounds or to a host immune system response following injection [174, 175]. Notably, studies investigating combined biomaterial and cell approaches within biomaterials-based cell-delivery systems have reported increased treatment efficiency in preclinical models, compared to biomaterials alone or cell alone controls [126, 176-179].

1.4.5 *In vivo* preclinical animal models for assessing angiogenesis

Due to the limited opportunities to carry out controlled studies assessing tissue repair processes in humans, *in vivo* preclinical models for assessing tissue repair in animals are frequently performed on rodents (mice and rats), lagomorphs (rabbits), and pigs [180, 181]. Due to lower cost, ease of use, and the availability of small animal facilities, murine models are often preferred to other animal models [180, 181]. The availability of various transgenic mouse strains also provides powerful tools to better understand the biological mechanisms associated with tissue repair. For example, immuno-compromised rodent models are of great interest for preclinical testing of cell-based products or biomaterials of human origin [182]. The preclinical animal models used for assessing tissue repair can be classified in several categories, including cutaneous wound healing models, ischemic models, and implantation models. Given their broad use in the biomaterials field, this section will focus will be on the subcutaneous implantation models.

Subcutaneous implantation models in rodents are often used to evaluate host cell infiltration, immunogenic reactivity, and neo-vascularization of new biomaterials subjected to *in vivo* settings. In this model system, the implants are positioned within a subcutaneous pocket, into which host plasma can infuse if the material is porous [180]. Cells from the host can then migrate and infiltrate the non-vascularized and hypoxic implants, forming a granulation-like tissue. Depending on the implant material, further tissue remodelling may occur over time [180]. Additionally, murine subcutaneous implantation models have been extensively used in the field of adipose tissue engineering due to the close proximity of the subcutaneous compartment with native adipose tissue. Several implant locations have been studied, with the dorsum being the most common implantation site due to the ability to reduce animal numbers by implanting two or four scaffolds per animal [183]. Surgical techniques include free implantation into a subcutaneous pocket [14], suturing of implants to secure it in place [184], implantation of

a pre-fixed material onto a frame [185], and injection of liquid phase materials or particles [119, 125]. Interestingly, neo-vascularization has been reported in all surgical iterations [14, 125, 184, 185], which confirms the utilization of the dorsal subcutaneous implantation as a valid strategy to study angiogenesis and tissue repair mechanisms.

1.5 Mesenchymal cells

1.5.1 Dermal fibroblasts

Dermal fibroblasts are the major resident cells within the dermis, which is the vascularized skin connective tissue that supports the outermost layer of the skin, the non-vascularized epidermis. These cells can be found interspersed in the dermal matrix, mostly isolated from one another. Dermal fibroblasts play constitutive roles in tissue homeostasis and participate in tissue repair following injuries as detailed in Section 1.4.1.

When subjected to chronic wound microenvironments, the phenotype of dermal fibroblasts is altered, compared to fibroblasts from non-involved tissues [186-189]. For example, human wound edge dermal fibroblasts (weDFs) sourced from chronic wound tissues were shown to express significantly lower levels of pro-fibrotic markers in the presence of TNF- α , compared to dermal fibroblasts from non-involved tissues (niDF) [186]. Reduction in proliferation rates [187, 188] and impaired responses to pro-regenerative growth factors [189] in weDF were also observed. These phenotypic differences could be partially explained by epigenetic differences observed in the weDF and niDF populations, denoted by different genome-wide DNA methylation patterns between the two populations [190].

1.5.2 Mesenchymal stromal cells

Adult MSCs were first identified in the bone marrow by Friedenstein and colleagues in 1976 [191]. It is now known that MSCs can be found in nearly all tissues of the body, with the three main sources currently identified as bone marrow, adipose tissue, and peripheral blood [192]. While their name varies from author-to-author, these cells are generally termed bone marrow-derived mesenchymal stromal cells (BMSCs), adipose-derived stromal cells (ASCs), and peripheral blood-derived mesenchymal stromal cells (PBMSCs), respectively. Originating from different tissues, these MSC populations are fibroblastic in nature and are closely related, playing similar roles in tissue homeostasis through their

migratory and paracrine abilities during inflammation, tissue injuries and repair [192, 193]. In the context of the current thesis, MSCs from the adipose niche, or ASCs, will be discussed in detail in the following sections.

1.5.3 Adipose-derived stromal cells

The stromal vascular fraction of adipose tissue is rich in mesenchymal cell types, including fibroblasts, pericytes, mesenchymal progenitors, preadipocytes, and ASCs [194]. Approximately 2% of the resident stromal cells of adipose tissue are multipotent ASCs [194]. In single cell clonal experiments, ASCs were shown to have the ability to differentiate *in vitro* towards the three classic mesenchymal lineages (e.g. adipogenic, osteogenic, and chondrogenic) [195-198]. The scientific community has given three main guidelines to identify cell populations as ASCs. First, the cells must be isolated from adipose tissue and must be able to adhere to TCPS. Second, their immunophenotype must be more than 80% positive for CD105, CD90, CD73, CD29, and CD44, concomitant with less than 2% positive for CD31 and CD45 [199]. Finally, the cells should be able to differentiate towards the three main mesenchymal lineages (e. g. adipogenic, osteogenic, and chondrogenic), as demonstrated with a combination of methods. These methods can include histological staining, gene expression, or enzyme activity assays [199].

While ASCs and MSCs have the ability to differentiate *in vitro*, a growing body of evidence suggests that the main mediator of their pro-regenerative effects *in vivo* is their secretion of beneficial paracrine factors [191, 200, 201]. Indeed, the ASC secretome was shown to include numerous factors involved in mediating angiogenic and inflammatory processes, as highlighted in Table 1.2.

Table 1.2 List of paracrine factors secreted by human ASCs

Soluble factor	Main function in tissue repair processes	Reference
angiopoietin-1	Acts as a vascular growth factor participating in endothelial cell-cell interactions, tube formation, and capillary stability.	[202]
angiopoietin-2	Antagonist of angiopoietin-1. Plays important roles in capillary destabilization required for earlier stages of angiogenesis.	[203]
colony stimulating factor 1(CSF-1)	Also known as monocyte colony-stimulating factor (M-CSF). Involved in macrophage recruitment and polarization into an M1 phenotype.	[201]

colony stimulating factor 2 (CSF-2)	Also known as granulocyte-macrophage colony-stimulating factor (GM-CSF). Involved in neutrophil, eosinophil, monocyte, and macrophage recruitment.	[201]
CXC ligand 1 (CXCL1)	Cytokine with mitogenic properties on multiple cell types and a potent neutrophil and monocyte chemoattractant.	[203]
C-C motif chemokine 22 (CCL22)	Cytokine with chemotactic activity for monocytes, dendritic cells, natural killer cells and activated T lymphocytes.	[203]
C-C motif chemokine 5 (CCL5)	Cytokine with chemotactic and activating activity for blood monocytes, memory T helper cells and eosinophils.	[203]
FGF-2	Pleiotropic mitogenic agent involved in several biological processes, with particularly potent paracrine effects on mesenchymal and endothelial cells in the context of wound healing.	[201]
HGF	Pleiotropic mitogenic agent involved in several biological processes, with particularly potent paracrine effects on epithelial, mesenchymal, and endothelial cells in the context of wound healing.	[201]
IGF-1	Pleiotropic mitogenic agent secreted by the liver with important endocrine effects. Produced by several cell types during tissue repair, with important mitogenic activity on dividing cells.	[204]
IL6	Pro-inflammatory cytokine involved in several inflammatory processes. Involved in regulating the balance between M1 and M2 macrophage polarization.	[205]
IL8	Cytokine with mitogenic properties on several cell types and a potent neutrophil, monocyte, and endothelial cell chemoattractant.	[204]
Keratinocyte growth factor (KGF)	Common mitogenic agent involved in several biological processes, with particularly potent paracrine effects on epithelial cells.	[204]
MCP-1	Cytokine involved in monocyte, T cell, and dendritic cell recruitment.	[206]
Nerve growth factor (NGF)	Mitogenic agent involved in the growth and maintenance of peripheral neurons. Chemoattractant agent for tip endothelial cells.	[207]
Placental growth factor (PlGF)	Member of the VEGF sub-family. Strong mitogenic and chemoattractant effects for endothelial cells.	[175]
PDGF	Pleiotropic mitogenic agent involved in several biological processes, with particularly potent paracrine effects on mesenchymal and endothelial cells in the context of wound healing.	[204]
Plasminogen activator inhibitor-1 (PAI-1)	Principal inhibitor of tissue plasminogen activator and urokinase, and hence an inhibitor of fibrinolysis. Its enzymatic activity plays pro-angiogenic roles in the context of wound healing.	[208]
stem cell factor (SCF)	Pleiotropic agent associated with several hematopoietic processes. Plays roles in mast cell regulation in the context of wound healing.	[203]
SDF1/CXCL12	Potent homing factor for circulating stem cells, including endothelial progenitor cells. Plays roles in inflammation and angiogenesis.	[209]
TGF- β	Pleiotropic mitogenic agent regulating cell proliferation, differentiation and growth. Its expression is strongly associated with pro-fibrotic cell phenotypes in the context of wound healing.	[201]
VEGF	Strong mitogenic and chemoattractant agent for endothelial cells. Plays important roles in destabilizing and increasing the permeability of blood vessels, allowing endothelial cell activation and sprouting.	[201]

1.5.4 ASC-based tissue-engineering strategies and considerations

1.5.4.1 Therapeutic advantages of using ASCs

The use of ASCs as a pro-regenerative cell population has several advantages as compared to other MSC populations from other tissues. Inherent advantages of ASCs include their availability and accessibility through minimally-invasive harvesting methods. ASCs can be isolated from lipoaspirated adipose tissue under local anesthesia, as compared to the invasive hipbone aspiration of bone marrow under general anaesthesia required to isolate BMSCs. In addition, larger quantities of adipose tissue can be extracted from a single intervention, compared to hipbones aspirates. Moreover, the harvesting yield of ASCs is greater than for BMSCs [210, 211], with a gram of adipose tissue yielding more stem cells than a gram of bone marrow, with approximately 5×10^3 ASCs per gram of adipose tissue and between 1×10^2 to 1×10^3 BMSCs per gram of bone-marrow [211].

When looking at the presence of 22 surface markers, the immunophenotype of human ASCs is similar to that of human BMSC and human dermal fibroblasts [212]. However, recent evidence indicates that ASCs, BMSCs, and fibroblasts show differences in their secretory profiles. More specifically, ASCs were reported to secrete higher levels of immunomodulatory factors compared to BMSCs, such as CXCL1, CCL22, CSF-1, and IL-6 [209]. ASCs were also shown to secrete higher levels of pro-angiogenic factors, including angiopoietin-1, HGF, and VEGF, and lower levels of pro-inflammatory factors as compared to dermal fibroblasts, including MCP-1 and CCL5 [203]. These observed differences may play important roles in mediating tissue regeneration [203, 209]. ASC-conditioned media has also been shown to better stimulate endothelial cell proliferation and tube formation, compared to BMSC- and dermal fibroblast-conditioned media [203, 209].

The delivery of high doses of ASCs was shown to be an important factor for the development of approaches for therapeutic angiogenesis. Dose-response experiments demonstrated that injecting higher doses of adult stem cells positively correlated with tissue repair and reperfusion in a hindlimb ischemia model [175]. Findings of this study showed that the lowest doses of 1×10^5 ASCs injected intramuscularly induced a modest increase

in blood reperfusion in hindlimbs compared to saline controls, while the highest tested dose of 1×10^6 cells stimulated robust reperfusion as compared to lower doses of cells [175]. Similar dose-response results were seen following injection of BMSCs in a hamster heart failure model, where higher doses correlated with lower cardiac fibrosis [213].

1.5.4.2 MSC preconditioning strategies

While biomaterial-based strategies have shown promise to enhance localized cell retention and viability, other strategies have been shown to increase MSC resilience and survival following implantation [214]. Such strategies include *in vitro* preconditioning prior to delivery, including hypoxic culture [215, 216], soluble factor treatments [217-219], and dynamic culture [220, 221].

Hypoxic preconditioning can enhance the therapeutic potential of several MSC populations, including ASCs [215, 216]. Previous studies have demonstrated that oxygen tension below 5% increased the secretion of pro-angiogenic soluble factors [215, 216, 222]. Conditioned media from MSC treated in oxygen tension below 5% was also shown to stimulate endothelial cell tube formation [215, 216, 222]. These effects were shown to be mediated through the activation of the alpha subunit of the transcription factor hypoxia-inducible factor 1 (HIF1 α), the master regulator of the hypoxia signalling cascade [222, 223].

Effective preconditioning of MSCs was also demonstrated through the addition of small soluble mitogenic agents to culture media. Soluble molecules investigated to date include growth factors such as epithelial growth factor (EGF) [217, 224], basic fibroblast growth factor (FGF-2) [218, 225], and insulin-like growth factor-1 (IGF-1) [219, 226]. In particular, it was shown that EGF treatments promoted cell growth, without compromising stem cell multipotency, and stimulated the secretion of pro-angiogenic molecules including HGF and VEGF over untreated control groups through the activation of the ERK1/2 signalling pathway [217, 224]. Other studies focusing on FGF-2 preconditioning demonstrated that FGF-2 could mediate the activation of protein kinase B (PKB; also known as Akt)/ERK1/2, Smad2, and Stat3 signaling pathways, which resulted in decreased oxidative stress, cellular senescence and apoptosis, concomitant with increased expression of α -smooth muscle actin and enhanced secretion of TGF- β and VEGF [218, 225]. Finally,

IGF-1 treatments were shown to enhance MMP activity, to promote PDGF and VEGF secretion, and to stimulate cell resistance to hypoxia through apoptosis-resistant mechanisms through activation of the phosphoinositide 3-kinase (PI3K)/Akt signalling pathway [219, 226].

Emerging literature has also identified dynamic culture conditions as a potential preconditioning strategy to modulate the phenotype of MSCs within biomaterial scaffolds. Several types of 3-D systems have shown promising results, including spinner flasks and rotating wall vessel bioreactors that increased the adipogenic and osteogenic differentiation potential of the BMSCs compared to TCPS controls [220], and orbital-shaker culture that enhanced ECM synthesis and adipogenic differentiation by ASCs [221].

1.6 Objectives and specific aims

The overarching hypothesis for this project is that 3-D DAT-derived bead foams will promote the retention and paracrine function of seeded cell populations both *in vitro* and *in vivo*, and will enhance the adipogenic differentiation of seeded human ASCs relative to bead foams fabricated from other ECM sources.

To test this hypothesis, the three specific aims of this thesis are:

1. To investigate the effects of ECM composition within the bead foams on the survival, pro-fibrotic, and pro-angiogenic function of human weDFs.
2. To establish a new fabrication approach for generating “cell-assembled bead foams” incorporating a high density of human ASCs and investigate their potential to support localized cell retention and function for applications in therapeutic angiogenesis.
3. To explore the role of ECM composition on the lineage-specific differentiation of human ASCs towards the adipogenic lineage within cell-assembled bead foams made from DAT, decellularized trabecular bone (DTB), or purified type I collagen.

1.7 Project overview

Recognizing the need for a better understanding of the mechanisms of regeneration associated with DAT-based biomaterial strategies for tissue repair, the first aim of the current project (Chapter 2) focused on studying the effects of the biochemical composition

of modular biomaterials termed bead foams, comprised of porous beads synthesized exclusively of ECM and assembled into cohesive 3-D networks, on the phenotype of human weDFs sourced from chronic wound tissues. To compare the effects of ECM composition, the bead foams were fabricated from human DAT or commercially-sourced bovine tendon collagen (COL) as a control. Compared to COL bead foams, the structurally similar but compositionally distinct DAT bead foams were shown to enhance weDF survival and angiogenic marker expression *in vitro*, when tested under conditions simulating stresses within the chronic wound microenvironment, and *in vivo* within a subcutaneous athymic mouse model. Taken together, the results demonstrated the enhanced potential of DAT as a pro-regenerative cell-instructive ECM source on weDF as compared to COL.

Aiming to overcome limitations associated with the relatively low cell infiltration observed in the bead foams applied in the first aim, the second aim of the current project (Chapter 3) established new methods to generate novel modular bioscaffolds through a “cell-assembly” approach using human ASCs. *In vitro*, these cell-assembled bead foams supported human ASC survival and growth. Histological and biochemical characterization confirmed that there was a high density of ASCs that were well distributed throughout the scaffolds and showed that the assembly process was mediated by matrix remodeling and the synthesis of new ECM. Subcutaneous implantation of the cell-assembled scaffolds in an immune-compromised mouse model showed enhanced ASC retention and neo-vascularization as compared to the previous bead foam technology, supporting the potential of this new format for soft tissue regeneration and therapeutic angiogenesis.

The third aim of the current project (Chapter 4) expanded on the new cell-assembly methods towards establishing a platform technology for exploring the effects of tissue-specific ECM on ASC differentiation. More specifically, the effects of ECM composition on the adipogenic differentiation of human ASCs were explored using cell-assembled bead foams fabricated with DAT, COL, and decellularized trabecular bone (DTB). Initial studies focused on modifying the methods to generate structurally comparable and stable scaffolds using the 3 distinct ECM sources. Next, pilot studies were performed to compare the adipogenic response of human ASCs within the various cell-assembled bead foams. The preliminary data suggested that adipogenic differentiation was enhanced in the cell-

assembled bead foams fabricated from DAT and COL as compared to DTB, supporting that the ECM composition within the platforms can modulate ASC differentiation.

Chapter 2

2 Matrix composition in 3-D collagenous bioscaffolds modulates the survival and angiogenic phenotype of human chronic wound dermal fibroblasts

2.1 Co-authorship statement

A version of this chapter was published in *Acta Biomaterialia* in 2019: “*Morissette Martin P, Grant A, Hamilton DW, Flynn LE (2019). Matrix composition in 3-D collagenous bioscaffolds modulates the survival and angiogenic phenotype of human chronic wound dermal fibroblasts. Acta Biomaterialia, 83(2019): 199-210*”.

I conceptualized this study in collaboration with Dr. Douglas Hamilton and Dr. Lauren Flynn. I personally designed and performed all of the experimental studies described in the Chapter, with support from the remaining authors. More specifically:

- Dr. Hamilton and his team isolated and banked the human wound edge dermal fibroblasts used for the study.
- Dr. Grant is the clinical collaborator that provided the human adipose tissue samples.

I analyzed all the data in collaboration with Dr. Flynn. I made all the figures and supplementary content (table and figures). The manuscript was written in collaboration with Dr. Lauren Flynn.

2.2 Abstract

There is a substantial need for new strategies to stimulate cutaneous tissue repair in the treatment of chronic wounds. To address this challenge, our team is developing modular biomaterials termed “bead foams”, comprised of porous beads synthesized exclusively of extracellular matrix (ECM) and assembled into a cohesive three-dimensional (3-D) network. In the current study, bead foams were fabricated from human decellularized adipose tissue (DAT) or commercially-sourced bovine tendon collagen (COL) to explore the effects of ECM composition on human wound edge dermal fibroblasts (weDFs) sourced from chronic wound tissues. The DAT and COL bead foams were shown to be structurally similar, but compositionally distinct, containing different levels of glycosaminoglycan content and collagen types IV, V, and VI. *In vitro* testing under conditions simulating stresses within the chronic wound microenvironment indicated that weDF survival and angiogenic marker expression were significantly enhanced in the DAT bead foams as compared to the COL bead foams. These findings were corroborated through *in vivo* assessment in a subcutaneous athymic mouse model. Taken together, the results demonstrate that weDF survival and paracrine function can be modulated by the matrix source applied in the design of ECM-derived scaffolds and that the DAT bead foams hold promise as cell-instructive biological wound dressings.

2.3 INTRODUCTION

The treatment of chronic or non-healing skin wounds, including diabetic, pressure, and venous ulcers, places a substantial burden on healthcare systems around the globe [154]. Moreover, it is expected that the prevalence of these conditions will continue to rise, given the increasing frequency of risk factors including diabetes, peripheral vascular disease, obesity, and the aging of the population [227, 228]. Treating these patients is resource intensive, with annual costs approaching \$25B USD in North America [158, 229]. Responses to current therapies are highly variable and chronic wounds remain a leading cause of lower limb amputation, which is associated with high rates of mortality [230].

Although the pathophysiology of chronic skin wounds is not well understood [154], deleterious effects on healing have been attributed to an imbalance in extracellular matrix (ECM) turnover [231, 232] and the aberrant expression of bioactive factors including matricellular proteins, cytokines, and growth factors [43, 233]. Resident and infiltrating cells are subjected to a complex dysfunctional milieu within the chronic wound, which can alter their phenotypes and contribute to a pro-inflammatory state that is non-permissive for healing [43, 234, 235]. From this perspective, complex bioscaffolds incorporating pro-regenerative ECM components have the potential to disrupt this cycle and shift the balance in the wound microenvironment to stimulate healthy tissue regeneration [236-238].

Our laboratory has pioneered the development of pro-regenerative bioscaffolds derived from human fat for applications in soft tissue regeneration and cell delivery [14, 104, 126]. Abundantly discarded as surgical waste, human adipose tissue is an accessible matrix source that can be extracted through detergent-free decellularization to obtain scaffolds incorporating a diverse range of structural collagens, matricellular proteins, proteoglycans, adhesion glycoproteins, growth factors, and cytokines [62]. In addition to using decellularized adipose tissue (DAT) in its intact form, the ECM can be further processed to generate alternative scaffold formats with properties tuned to specific applications. In previous work, methods were established to fabricate novel porous scaffolds termed “DAT bead foams”, comprised of fused networks of ECM-derived beads that were stable without the need for chemical crosslinking [14].

While tissue-specific ECM has been postulated to be a mediator of cell function, relatively few studies to date have focused on systematically comparing the effects of different matrix sources on cellular function within three-dimensional (3-D) engineered microenvironments. The bead foam technology provides a versatile platform for exploring the influence of ECM composition on the cellular response for applications in wound healing. Expanding on our previous work, the novel processing methods were adapted to fabricate bead foams from human DAT and commercially-sourced bovine tendon collagen (COL). Based on our recent proteomics characterization of these matrix sources [62], it was postulated that DAT and COL bead foams could be generated that were structurally similar, but biochemically distinct. The initial studies focused on characterizing the physical properties and composition of the resultant scaffolds to validate this hypothesis.

Subsequent analyses probed the response of primary human dermal fibroblasts isolated from chronic wound tissues on the DAT and COL bead foams both *in vitro* and *in vivo*. As key players involved in multiple processes in wound repair, dermal fibroblasts have the potential to influence the behaviour of resident and transient wound cells through the secretion of soluble factors including growth factors, cytokines, and matricellular proteins [203, 239, 240]. Relative to fibroblasts sourced from healthy tissues, dermal fibroblasts from chronic wounds have been reported to have altered functionality, including an impaired response to TNF- α [239], a decreased ability to withstand oxidative stress [241] and reduced pro-angiogenic functions [242], which may impact their capacity to stimulate healing [241, 242]. Based on this, our studies focused on exploring whether the ECM composition in the bead foams could modulate the response of human wound edge dermal fibroblasts (weDFs) under stresses simulating features of the chronic wound microenvironment. *In vitro* testing was performed under serum-free conditions to create a non-permissive environment for proliferation, as would be expected when healing does not progress from the inflammatory phase [188]. Further, the media was supplemented with pathophysiological levels of tumor necrosis factor- α (TNF- α) (1 ng/mL) [243, 244], and all testing was performed under 2% oxygen tension [166, 167], to simulate the harsh conditions within human chronic wounds. *In vivo* testing was conducted using a subcutaneous implant model in athymic mice to provide a complementary analysis of the effects of the human cells delivered in the engineered scaffolds within a complex living system. Using both models, weDF survival and angiogenic function were explored on the DAT and COL bead foams to assess whether the matrix source could impact the regenerative potential of the cells.

2.4 Materials and methods

2.4.1 Materials

Unless otherwise stated, all chemicals used were purchased from Sigma Aldrich Canada Ltd. (Oakville, ON, Canada).

2.4.2 Adipose tissue collection and decellularization

Subcutaneous adipose tissue samples were collected with informed consent from female patients undergoing elective lipo-reduction surgeries at the London Health Sciences

Centre (London, ON, Canada) with human research ethics board approval (REB# 105426). The samples were transported to the lab on ice in sterile phosphate buffered saline (PBS) with 2% bovine serum albumin (BSA), transferred into a hypotonic cell lysis buffer (Solution A: 10 mM Tris base and 5 mM ethylenediaminetetraacetic acid (EDTA), pH 8.0), and frozen at -80°C.

After thawing, the adipose tissue was processed with a 3-day detergent-free decellularization protocol. All decellularization solutions were supplemented with 1% antibiotic-antimycotic solution (Gibco, Burlington, ON, Canada) and 1% phenylmethylsulphonyl fluoride (PMSF), with the exception of the enzymatic treatment steps where the PMSF was excluded. All incubation steps were performed with 3-4 adipose tissue segments (starting volume ~3 cm x 3 cm x 3 cm) in 100 mL of solution under agitation at 150 rpm and 37°C. In brief, the freshly-thawed adipose tissue was rinsed in Solution A and then incubated in fresh Solution A for 2 h. Each tissue segment was then centrifuged in 30 mL of fresh Solution A at 1500 xg for 30 min, transferred into fresh Solution A, and incubated for an additional 2 h. After rinsing in fresh Solution A, the samples were incubated overnight in 0.25% trypsin-0.1% EDTA (Gibco). On the second day, the samples were incubated twice in fresh absolute isopropanol for 3 h, with gentle mechanical pressing and centrifugation at 1500 xg for 30 min in 30 mL of fresh isopropanol between solution changes to promote lipid extraction. The samples were then incubated overnight in fresh absolute isopropanol. On the third day, the samples were mechanically compressed and transferred into fresh isopropanol for a final 4 h extraction prior to rehydration by three 30 min incubations in a rinsing buffer comprised of 8 g/L NaCl, 200 mg/L KCl, 1 g/L Na₂HPO₄, and 200 mg/L KH₂PO₄, at pH 8.0 (BioShop Canada Inc, Burlington, ON, Canada). Finally, the individual DAT segments were mechanically compressed, rinsed in deionized water, and transferred into 50 mL conical tubes, prior to freezing at -80°C and lyophilization.

2.4.3 DAT and COL bead fabrication

Lyophilized DAT samples (pooled from 5 donors) or commercially-sourced collagen from bovine Achilles tendon (Cat# C9879, Sigma) were finely minced and digested with α -amylase from *Aspergillus oryzae* to prepare ECM suspensions (25 mg/mL) following published methods [14]. To synthesize the individual spherical subunits for the bead foams,

the DAT and COL suspensions were electrosprayed into liquid nitrogen as previously described [14], using plastic syringes fitted with 25G butterfly needles (BD Medical, Mississauga, ON, Canada) positioned 3 cm from the surface of the liquid nitrogen with an applied voltage of 16-17 kV and infusion at 35 mL/h. Following synthesis, the DAT and COL beads were collected and transferred into absolute ethanol prior to gradual rehydration in an ethanol series (100%, 98%, 95%, 90%, 75%, 50%, 25%, and 12.5% (v/v) diluted with sterile PBS), followed by three washes in sterile PBS.

2.4.4 Characterization of DAT and COL beads

Feret's diameters of hydrated DAT and COL beads were measured ($n = 25-35$ beads/trial, $N = 3$ trials with different ECM suspensions) under brightfield microscopy using ImageJ. The mechanical properties of the hydrated DAT and COL beads were assessed using a CellScale MicroSquisher system (Waterloo, ON, Canada) and the Young's moduli were calculated using nonlinear least squares curve fitting with a published extended mechanics model for large elastic deformations of spherical microparticles [245]. In brief, the micro-scale parallel-plate compression system was equipped with a 203 μm diameter cantilever attached to a square platen (2 mm x 2 mm), and testing of individual beads was performed in a PBS bath at 37°C. The beads were compressed to 50% deformation for 3 preconditioning cycles at a strain rate of 0.01 s^{-1} , and then data was collected from 3 consecutive cycles and analyzed ($n=6$ beads/trial, $N=3$ trials with different ECM suspensions).

2.4.5 DAT and COL bead foam fabrication

To fabricate the bead foams, the DAT and COL beads were collected immediately following electrospraying, allowed to thaw, and gently transferred without excess fluid into cylindrical moulds (diameter = 8 mm, height = 5 mm), which were frozen at -80°C overnight and lyophilized. The resultant bead foams were decontaminated and gradually rehydrated through an ethanol series (100%, 90%, 75%, 50%, 25%, and 12.5% (v/v) diluted with sterile PBS), followed by three washes in sterile PBS. The rehydrated scaffolds were stored at 4°C for up to 1 week.

2.4.6 Characterization of the DAT and COL bead foams

2.4.6.1 Scanning electron microscopy

The ultrastructure of the DAT and COL bead foams was visualized by scanning electron microscopy (SEM) using published protocols [135]. Briefly, the scaffolds were lyophilized, coated with osmium, and imaged with a LEO 1530 scanning electron microscope at an accelerating voltage of 1 kV and working distance of 4 to 5 mm.

2.4.6.2 Porosity measurement

A modified Archimedes' method [246] was used to estimate the porosity of the bead foams (n=3 scaffolds/trial, N=5 trials with different ECM suspensions) using isopropanol as the solvent and assuming the scaffolds were comprised primarily of collagen with a density of 1.343 g/mL [247].

2.4.6.3 Hydroxyproline and dimethylmethylene blue assays

The scaffolds were digested with 60 mU/mL of proteinase K (Promega, Madison, WI, USA) in Tris-EDTA buffer (200 nM Tris-HCl, 200 nM EDTA, pH 7.5) under agitation at 300 rpm and 65°C for 1 h, followed by a 10 min incubation at 95°C to inactivate the enzyme (n=3 scaffolds/trial, N=3 trials with different ECM suspensions).

For the hydroxyproline assay, digested samples were hydrolyzed in 12 N hydrochloric acid at 110°C for 24 h, neutralized with 6 N sodium hydroxide, and filtered using activated charcoal. Equal volumes of 0.05 N chloramine-T/20% 2-methoxyethanol (20 min incubation), 3.15 N perchloric acid (5 min incubation) and Ehrlich's reagent (20 min incubation at 60°C) were sequentially added to the digested scaffolds (1:80 in deionized water) inside a 96-well plate. After a 5 min incubation at 4°C and a 20 min incubation at room temperature, the absorbance was measured at 560 nm using a CLARIOstar® spectrophotometer (BMG LABTECH Inc., Cary, NC, USA), including a hydroxyproline standard curve.

For the DMMB assay, 10 µL aliquots of the digested scaffolds were transferred in technical triplicate into a 96-well plate and 200 µL of a 1.6% solution of DMMB in deionized water supplemented with 1% ethanol and 0.2% formic acid was added. The absorbance at 525

nm was recorded using a CLARIOstar® spectrophotometer (BMG LABTECH Inc.), including a chondroitin sulphate standard curve.

2.4.6.4 Immunohistochemical analysis of ECM constituents in the DAT and COL bead foams

DAT and COL bead foams (n=2 – 6 scaffolds/trial, N=3 trials with different ECM suspensions) were fixed for 24 h in 10% formalin, embedded in Tissue-Tek OCT compound (Sakura Finetek, Torrance, CA, USA), and snap frozen in liquid nitrogen prior to cryosectioning (7- μ m transverse sections). Following fixation in acetone and blocking (in 10% goat serum in Tris buffered saline; TBS) sections were stained overnight at 4°C with primary antibodies against collagen type I (dilution 1:100 in TBS with 1% BSA, ab90395, Abcam, Toronto, ON, Canada), collagen type IV (dilution 1:100, ab6586, Abcam), collagen type V (dilution 1:300, ab7046, Abcam), collagen type VI (dilution 1:300, ab6588, Abcam), fibronectin (dilution 1:150, ab23750, Abcam), or laminin (dilution 1:200, ab11575, Abcam). Detection was carried out using an anti-rabbit secondary conjugated to Alexa Fluor 594 (dilution 1:200, ab150080, Abcam) or an anti-mouse secondary conjugated to Dylight 650 (dilution 1:200, ab96882, Abcam). No primary and tissue positive controls (Supplementary Fig. 1) were included in all trials. Images were acquired with a Zeiss Imager M2 microscope (Zeiss Canada, Toronto, ON, Canada). Semi-quantitative analysis of the relative expression levels was performed using ImageJ. Results were reported as a percentage of the positive signal area normalized to the total scaffold area.

2.4.7 Chronic wound fibroblast isolation, culture and characterization

Chronic wound tissues were harvested from the amputated lower limbs of patients with non-healing skin wounds at the London Health Sciences Centre, with human research ethics board approval (REB# 16245E). Human fibroblasts were isolated from the tissues following published explant isolation methods [147] and stored in liquid nitrogen at passage 1 (P1). Primary cell populations from three donors (Supplementary Table 2.1) were included in the studies.

All subsequent cell culture was performed in a hypoxic chamber (Whitley H35 Hypoxystation, Don Whitley Scientific Limited, West Yorkshire, UK) with 2% O₂ and 5% CO₂ at 37°C. Prior to scaffold seeding, the cells were thawed and expanded to passage 4 (P4) in complete medium comprised of Dulbecco's Modified Eagle's medium (DMEM; Gibco) supplemented with 10% fetal bovine serum (FBS; cat# 12483020; Gibco), 100 U/mL penicillin and 0.1 mg/mL streptomycin (1% pen-strep; Gibco). Media was changed every 2-3 days and the cells were passaged at 90% confluence.

Immunophenotyping was performed on P4 fibroblasts using a Guava easyCyte 8HT flow cytometer (Millipore, Billerica, MA, USA) as described previously [248]. Single marker staining was performed with monoclonal, fluorochrome-conjugated antibodies from eBioscience (San Diego, CA, USA), as follows: CD90-FITC, CD-105-PE, CD73-FITC, CD44-PE-Cy7, CD29-PE, CD34-APC, CD31-PE, CD146-FITC (Supplementary Table 2.2). All samples were stained for 30 min at 4°C and then fixed in 0.5% paraformaldehyde for 10 min at 4°C. Unstained controls were included in every trial.

2.4.8 DAT and COL bead foam seeding

Prior to seeding, the rehydrated bead foams were incubated overnight in complete medium. Each DAT or COL bead foam was seeded with 2×10^5 P4 chronic wound fibroblasts in 20 μ L of complete medium. Following 2 h incubation, the complete medium was topped up to 1.5 mL and the scaffolds were incubated for an additional 24 h (2% O₂ and 5% CO₂, 37°C).

2.4.8.1 Comparison of seeded DAT and COL bead foams *in vitro*

For the *in vitro* assessments, the scaffolds were transferred into serum-free DMEM supplemented with 1% pen-strep for 24 h (2% O₂ and 5% CO₂, 37°C), and then cultured in serum-free DMEM supplemented with 1 ng/mL TNF- α (R&D System Inc., Minneapolis, MT, USA) and 1% pen-strep for an additional 1 or 7 days (2% O₂ and 5% CO₂, 37°C). The media was changed daily, with fresh TNF- α added.

2.4.9 Analysis of cell distribution

Immunostaining for vimentin (dilution 1:200, ab92547, Abcam) was performed to assess cell distribution within scaffold cryo-sections at 3 days post-seeding, following similar methods to Section 2.5.4.

2.4.9.1 Cell abundance and cytotoxicity assays

weDF abundance was measured at 1, 3 and 9 days post-seeding using the Quant-iT™ PicoGreen® dsDNA kit (Molecular Probes, Burlington, ON, Canada) (n=3 scaffolds/trial, N=3 trials with different cell donors). The scaffolds were rinsed in PBS, snap frozen, and stored at -80°. After thawing, the scaffolds were digested using proteinase K as described in Section 2.6.3, and total double-stranded DNA (dsDNA) was quantified according to the manufacturer's instructions. Cell lysates prepared from 2×10^5 P4 dissociated weDFs were included in the assay and used to normalize the data to the initial seeding levels. The conditioned media from the 3 and 9 day samples was also collected and stored at -80°C, and analyzed using the Toxilight™ non-destructive cytotoxicity assay (Lonza, Walkersville, MD, USA) according to the manufacturer's instructions. A standard curve was prepared using serial dilutions of lysed weDFs, and the results were normalized to the total dsDNA content in the corresponding sample.

2.4.9.2 Gene expression (RT-qPCR)

At day 9 post-seeding, the DAT and COL bead foams (n=3 scaffolds/trial, N=3 trials with different cell donors) were finely minced and RNA was extracted in TRIzol® (Thermo Fisher Scientific, Burlington, ON, Canada) and purified using RNeasy® mini kits (Qiagen, Valencia, CA, USA). Taqman™ real-time RT-qPCR was performed using qSCRIPT® XLT one-step real-time quantitative PCR ToughMix (Quanta Biosciences, Gaithersburg, MD, USA) following the manufacturer's instructions. Taqman™ probes targeted against the angiogenic markers *CXCL12* (Hs03676656_mH), *HGF* (Hs0030159_m1), and *VEGFA* (Hs00900055_m1) were used, with 18S rRNA (4352655) as the housekeeping gene. Calculations were based on relative standard curves made from serial dilutions of pooled template mRNA for each probe set. After confirming that amplification efficiencies were between 90%-110% for all probe sets, C_t values for each of the samples were converted into mRNA quantities using linear regression, and the technical triplicate values were

averaged. These quantities were then normalized to the housekeeping gene for each sample, and reported relative to the COL bead foam group.

2.4.10 *In vivo* analysis of seeded DAT and COL bead foams

All studies followed the Canadian Council on Animal Care (CCAC) guidelines and were reviewed and approved by the Animal Care Committee at The University of Western Ontario (Protocol #2015-049). To facilitate identification of the scaffolds in tissue sections under fluorescence microscopy, the DAT and COL bead foams (cylindrical moulds; diameter = 8 mm, height = 5 mm) were pre-labeled prior to cell seeding with an Alexa Fluor 350 Succinimidyl Ester (A10168, Thermo Fisher Scientific) following the manufacturer's instructions. Scaffolds were then seeded with human weDFs and cultured for 24 h as described in Section 2.8.

2.4.10.1 Analysis of weDF angiogenic factor secretion on DAT and COL bead foams

To provide a baseline for the *in vivo* model, angiogenic factor secretion was assessed in the conditioned media collected 24 h after scaffold seeding (n=3 scaffolds/trial, N=3 trials with different cell donors) using a Luminex® multiplex assay directed against angiopoietin-1, CXCL12, HGF, PDGF-BB, and VEGFA, according to the manufacturer's instructions (R&D Systems). The samples were analyzed on a Bio-Plex® MAGPIX™ Multiplex Reader (Bio-Rad, Mississauga, ON), and the levels were normalized to the total dsDNA content in the corresponding scaffolds measured using the Picogreen® assay.

2.4.10.2 Subcutaneous implantation of DAT and COL bead foams in an athymic mouse model

Seeded DAT and COL bead foams (n=4-6 scaffolds/trial, N=3 trials with different cell donors), along with unseeded controls, were implanted subcutaneously in female Crl:NU-Foxn1nu mice (nu/nu nude mice; Strain Code 088, Charles River, Wilmington, MA, U.S.A.) [14]. Briefly, the mice were anesthetised with isoflurane and given subcutaneous injections of meloxicam (2 mg/kg loading dose; 1 mg/kg follow up dose at 24 h; Boehringer Ingelheim, Burlington, ON, Canada) and bupivacaine (2 mg/kg; Hospira, Saint-Laurent, QC, Canada). Bilateral paraspinal incisions (~1 cm) were made on the dorsa and subcutaneous pockets were created on each flank, below the panniculus carnosus. Each

mouse received one DAT and one COL bead foam and the incisions were closed with surgical staples. The animals were sacrificed by CO₂ overdose at 2 weeks post-implantation and the scaffolds were carefully excised within their surrounding tissues, embedded in OCT and stored at -20°C.

2.4.10.3 Immunohistochemical analysis of scaffold explants

After acetone fixation and blocking (5% goat serum, 5% BSA, and 0.2% tween diluted in TBS), immunostaining was performed to identify human cells (antigen: human-specific Ku80, CST-2180, Cell Signaling Technologies, Danvers, MA, USA) and murine endothelial cells (antigen: CD31, ab28364, Abcam) on scaffold cryo-sections (7 µm) at 3 different depths. Ku80 staining was performed as described by Allard *et al.* [249] and CD31 staining was performed overnight at 4°C (dilution 1:200 in blocking solution, ab28364, Abcam). A secondary anti-rabbit antibody conjugated to Alexa Fluor 594 (dilution 1:100, ab150080, Abcam) was used for detection and nuclei were counterstained with PicoGreen Reagent® (dilution 1:600, Thermo Fisher Scientific). The fluorescently-labeled scaffold cross-sections were imaged using an EVOS FL Cell Imaging System (Thermo Fisher Scientific). Ku80⁺ human cells were counted in up to 5 non-overlapping fields of view within the scaffold region using ImageJ analysis software. CD31 expression was quantitatively assessed through positive pixel counting within the entire scaffold cross-section using ImageJ, normalized to the total scaffold area. For comparative purposes, the results were reported as a fold change relative to the unseeded DAT control group.

2.4.11 Statistical Analyses

All data were expressed as the mean ± standard deviation (SD) and analyzed by t-test or two-way ANOVA with Tukey's post-hoc comparison of the means. The Kolmogorov–Smirnov non-parametric test was used to compare the size distribution of the DAT and COL beads. Statistical analyses were performed using GraphPad Prism 7 (GraphPad, La Jolla, CA, USA) and differences were considered statistically significant at $P < 0.05$.

2.5 Results

2.5.1 Beads and bead foams fabricated from DAT and COL are structurally similar

The DAT and COL beads and bead foams were characterized to confirm that varying the ECM source did not substantially alter the physical properties of the scaffolds. Macroscopically, the DAT and COL beads and bead foams (Figure 2.1A) had a similar appearance, with the COL scaffolds having a whiter colouration consistent with the starting materials. Analysis of the hydrated bead diameter revealed similar bimodal size distributions for the electrosprayed DAT and COL beads (Figure 2.1B). The DAT and COL beads were soft and compressible, showing similar viscoelastic behaviour (Figure 2.1C). Further, there was no significant difference in the Young's modulus (DAT = 0.49 ± 0.06 kPa, COL = 0.36 ± 0.09 kPa) between the two formulations (Figure 2.1D). SEM analysis of the bead foams (Figure 2.1A) revealed that the scaffolds had a similar ultrastructure comprised of spherical subunits with void spaces between the beads. Both types of scaffolds were highly porous, with values of $96.7 \pm 0.8\%$ and $96.2 \pm 0.5\%$ estimated for the DAT and COL bead foams respectively using a modified Archimedes' test (Figure 2.1E).

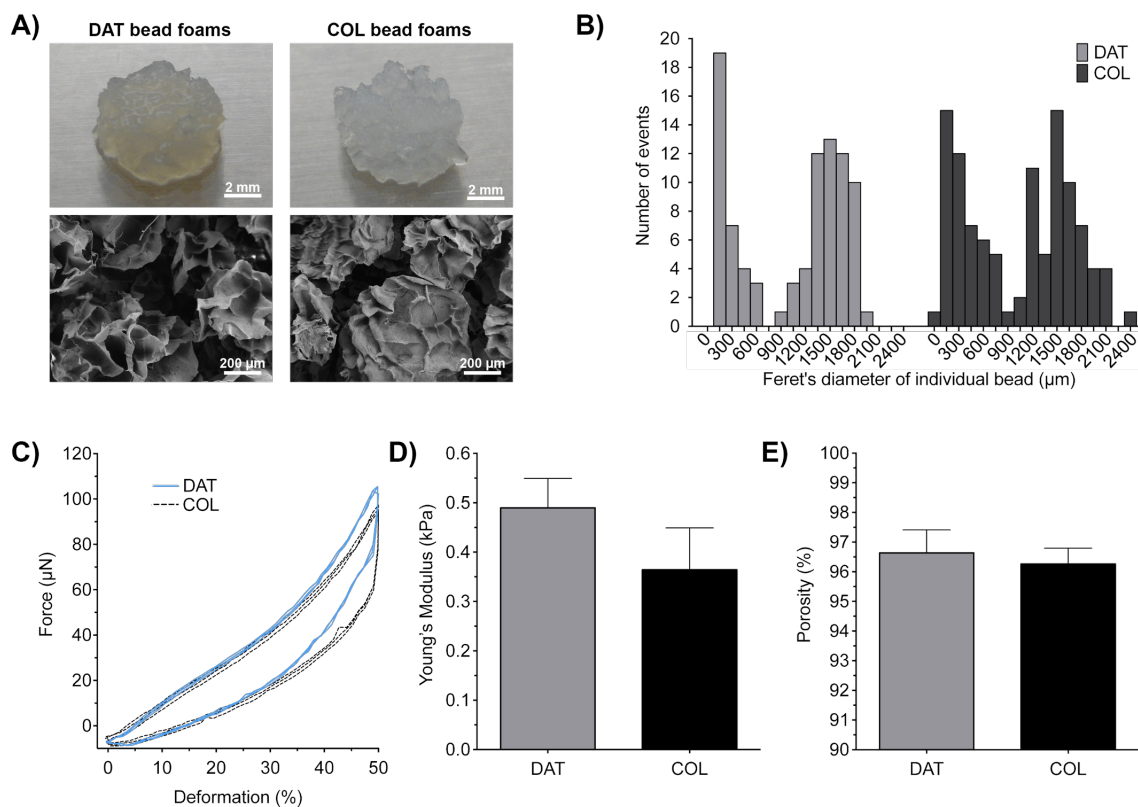


Figure 2.1: DAT and collagen bead foams are structurally similar. (A) Representative macroscopic and SEM images of DAT and COL bead foams, showing that both are comprised of a network of spherical beads with qualitatively similar morphology. (B) Feret's diameter of the individual beads used to fabricate the foams ($n=25-35$ beads/trial, $N=3$ trials with different ECM suspensions). There was no significant difference in the size distributions when analysed with the Kolmogorov-Smirnov test. (C) Representative force versus deformation curves for individual DAT and collagen beads. Data from 3 cycles are shown with compression at a strain rate of 0.01 s^{-1} . (D) Young's modulus of the individual DAT and collagen beads, with no significant difference measured between the two groups ($n=6$ beads/trial, $N=3$ trials with different ECM suspensions). (E) Porosity of the bead foams measured with a modified Archimedes' method, showing that both scaffold groups had a similar high level of porosity ($n=3$ bead foams/trial, $N=5$ trials with different ECM suspensions).

2.5.2 DAT and COL bead foams are compositionally distinct

Following confirmation that the scaffolds had similar structural properties, the biochemical composition of the DAT and COL bead foams was assessed. Analysis of total collagen content with the hydroxyproline assay demonstrated that both types of scaffolds were

enriched in collagen, with $91.5 \pm 4.1 \mu\text{g}$ and $85.3 \pm 8.3 \mu\text{g}$ of hydroxyproline per mg dry mass for the DAT and COL bead foams respectively (Figure 2.2A). In contrast, the DMMB assay revealed that the total sulphated GAG content was significantly higher in the DAT bead foams, at ~ 4.5 times the levels observed in the COL bead foams (Figure 2.2B). Semi-quantitative immunohistochemical analyses indicated that both scaffold types contained a similar distribution of collagen type I and fibronectin, with no laminin detected in either group (Supplementary Figure 2.2). However, the DAT bead foams were shown to contain higher levels of collagen type IV, V, and VI, distributed throughout the scaffolds with some regional variability (Figure 2.2C). Taken together with the total collagen content data, the immunofluorescence staining results suggested that the DAT and COL bead foams contained similar amounts of collagen, but that the relative abundance and distribution of collagen subtypes varied between the groups.

2.5.3 weDF cell abundance and survival is enhanced on the DAT bead foams *in vitro*

Initial cell culture studies focused on exploring whether the ECM source could mediate the *in vitro* survival of human weDFs under stresses simulating features of the chronic wound microenvironment (Figure 2.3A). Immunostaining for vimentin indicated that there were qualitatively more weDF on the DAT bead foams at 3 days post-seeding, with a higher cell density observed in proximity to the seeded scaffold surface in both groups (Figure 2.3B). While cell abundance was similar on both platforms at 24 h post-seeding, quantification of total dsDNA supported that there were significantly more cells on the DAT bead foams at both 3 and 9 days (Figure 2.3C). Measurement of adenylate kinase release via the ToxilightTM assay further corroborated these findings, indicating there were significantly higher levels of compromised or dying cells on the COL bead foams at 9 days post-seeding (Figure 2.3D).

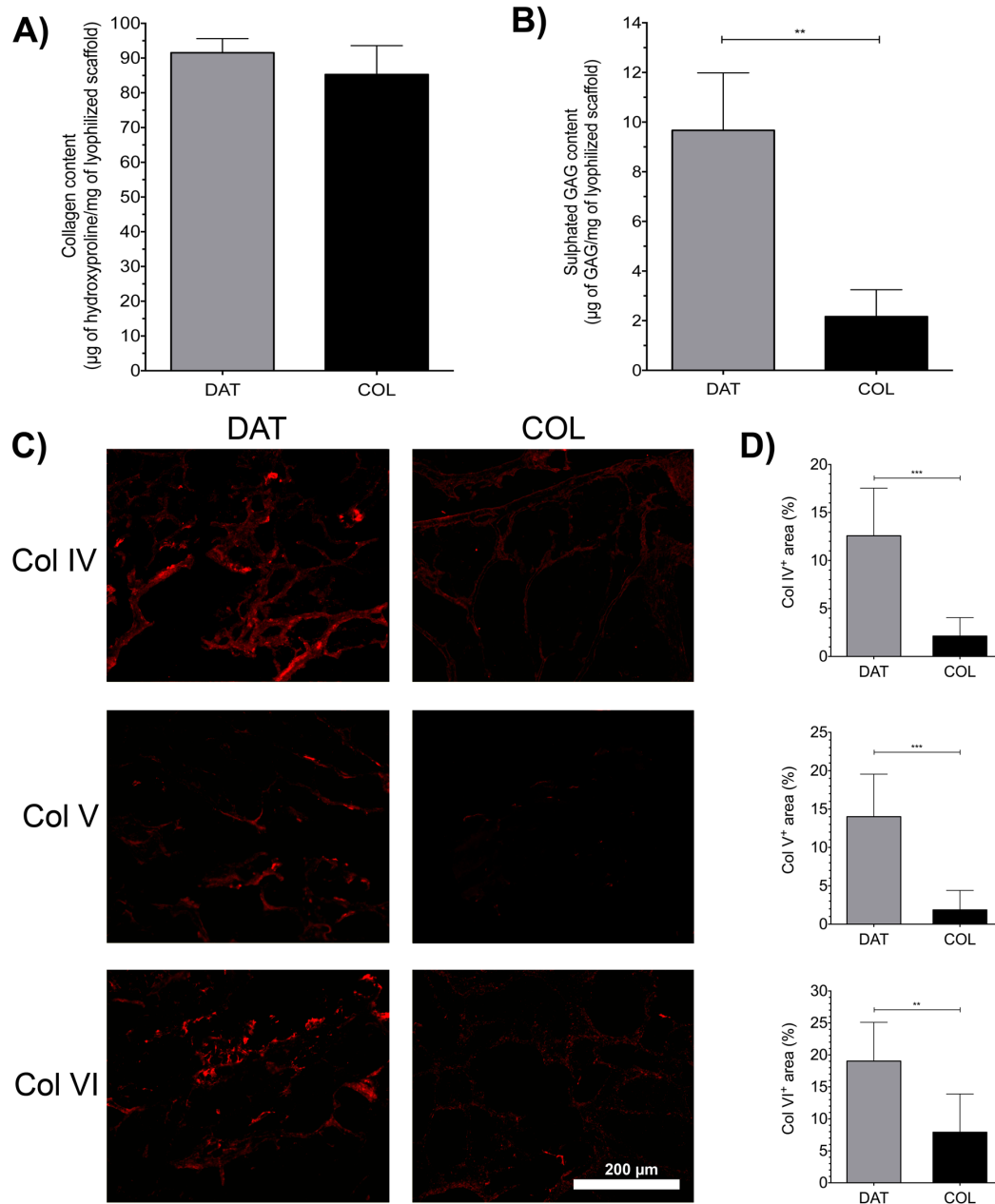


Figure 2.2: DAT and COL bead foams are biochemically distinct. (A) Quantitative analysis of total collagen content with the hydroxyproline assay, demonstrating that both scaffold groups contained similar levels of total collagen (n=3 scaffolds/trial, N=3 trials with different ECM suspensions). (B) Sulphated glycosaminoglycan (GAG) content measured with the DMMB assay, showing that the DAT bead foams contained significantly more sulphated GAG (n=3 scaffolds/trial, N=3 trials with different scaffolds). (C) Representative immunohistochemical staining for collagen types IV, V, and VI in cryo-sections of the DAT and COL bead foams. (D) Quantification of relative collagen type IV, V and VI levels, showing significantly higher levels in the DAT bead foam group (n=2-6 scaffolds/trial, N=3 trials with different ECM suspensions). *** = $P < 0.001$, ** = $P < 0.01$.

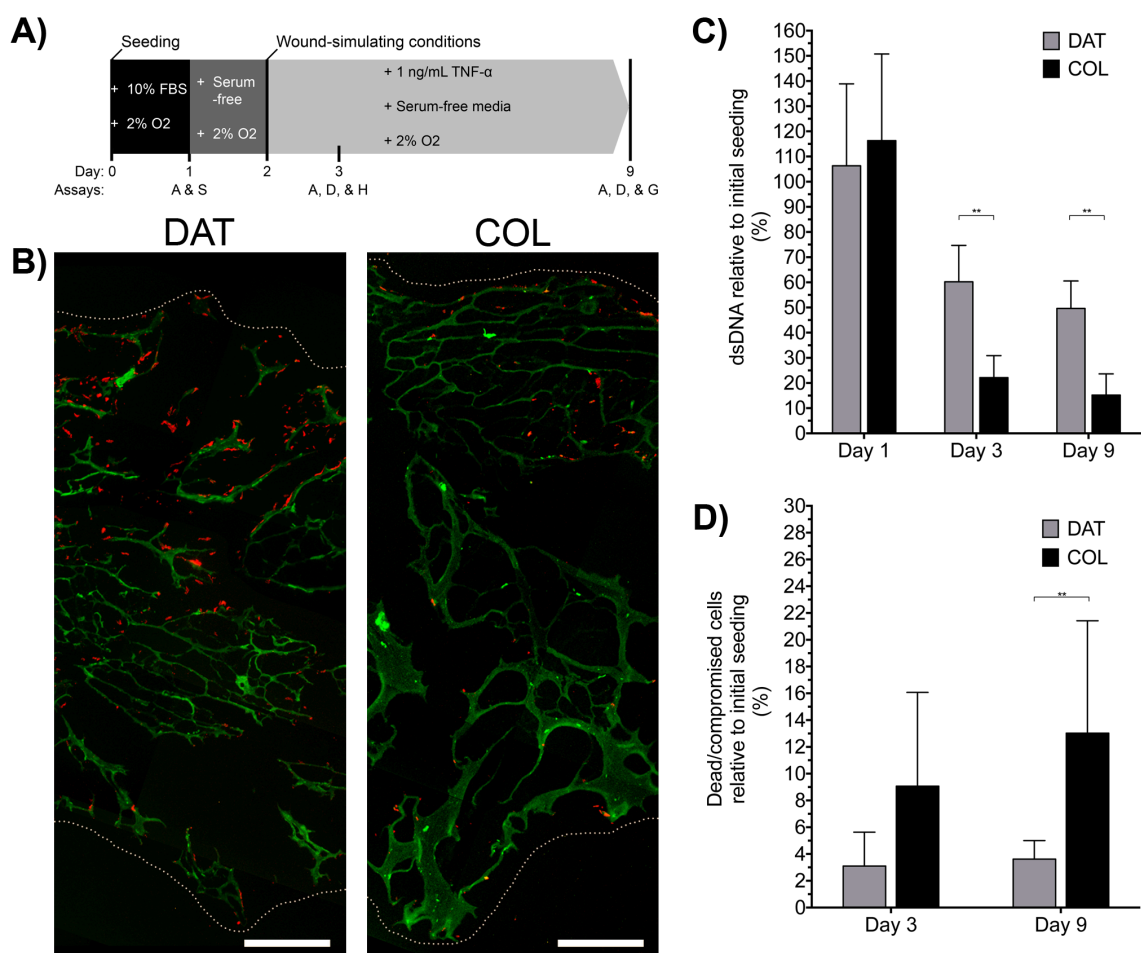


Figure 2.3: weDF cell abundance and survival is enhanced *in vitro* on the DAT bead foams as compared to the COL bead foams under conditions simulating stresses in the chronic wound microenvironment. (A) Overview of the cell culture conditions and experimental endpoints. A = cell abundance assay; S = secretome analysis; D = cell death assay; H = histological assessment; G = gene expression analysis. (B) Representative vimentin immunostaining (red) showing qualitatively enhanced weDF abundance on the DAT bead foams at 3 days post-seeding. Scaffold autofluorescence shown in green, and white lines denote the scaffold boundary, with the seeded surface oriented at the top of the images. Scale bars = 200 μ m. (C) Picogreen® dsDNA assay results showing enhanced cell abundance on the DAT bead foams at 3 and 9 days post-seeding. (D) Quantification of cell death as measured by the Toxilight™ assay indicating that there were higher levels of dead/dying cells on the COL bead foams at 9 days post-seeding. (n=3 scaffolds/trial, N=3 cell donors); ** = $P < 0.01$.

2.5.4 Angiogenic gene expression is enhanced in the weDFs cultured on the DAT bead foams

RT-qPCR analysis of angiogenic gene expression was performed to probe weDF function on the DAT and COL bead foams after 9 days of culture *in vitro* (Figure 2.4) under the stress-inducing conditions in the current study (Figure 2.3A). *VEGFA* and *HGF* expression levels were significantly higher in the weDFs cultured on the DAT bead foams, with consistent trends across all cell donors studied (Supplementary Figure 2.3). While the pooled data indicated that *CXCL12* expression was also significantly enhanced in the DAT bead foam group, this trend only held for 2 of the 3 cell donors, with similar levels of expression observed on the DAT and COL bead foams for cell donor 1 (Supplementary Figure 2.3C).

2.5.5 Angiogenic factor secretion is enhanced in the weDFs cultured on the DAT bead foams prior to implantation

Building from the *in vitro* findings, the subsequent studies focused on further probing the effects of bead foam composition on weDF survival and function through testing in an *in vivo* model. Prior to implantation, the weDFs were cultured on the DAT or COL bead foams under hypoxic conditions (2% O₂) for 24 h. As previously indicated, quantification of total dsDNA content indicated there was no significant difference in cell attachment at 24 h between the groups (Figure 2.3B). Screening of the supernatant media revealed that the weDFs on the DAT bead foams secreted significantly higher levels of VEGFa, HGF, CXCL12/SDF-1 α , angiopoietin-1, and PDGF-BB (Figure 2.5). In contrast to the gene expression results, CXCL12 protein secretion was enhanced in the DAT bead foam group for all cell donors. Notably, PDGF-BB was only detected in the DAT bead foams seeded with cell donors 2 and 3, with no measurable levels observed in the COL bead foam group for any of the cell donors.

2.5.6 Human weDF abundance is enhanced *in vivo* in the DAT bead foams

At two weeks post-implantation in the athymic mouse model, immunohistochemical analysis of human-specific Ku80 expression [249] identified the weDFs within the seeded DAT and COL bead foams (Figure 2.6). Similar to the *in vitro* results, quantification of the

Ku80⁺ human cells demonstrated that there were more weDF detected within the DAT bead foams as compared to the COL bead foams at 14 days post-implantation, suggestive of enhanced survival.

2.5.7 CD31⁺ cell recruitment is enhanced in the weDF-seeded DAT bead foams

Immunohistochemical analysis revealed that there were murine CD31⁺ cells distributed heterogeneously at the scaffold-tissue interface in all of the implant groups (Figure 2.7A). While there were no differences in total cell infiltration between the groups based on analysis of nuclear staining, endothelial cell density and infiltration appeared to be qualitatively enhanced in the seeded scaffolds as compared to the unseeded controls (Supplementary Figure 2.4). Quantitative analysis of the CD31 staining suggested that early angiogenesis was enhanced in the weDF-seeded DAT bead foams as compared to the seeded COL bead foams and both unseeded controls (Figure 2.7B).

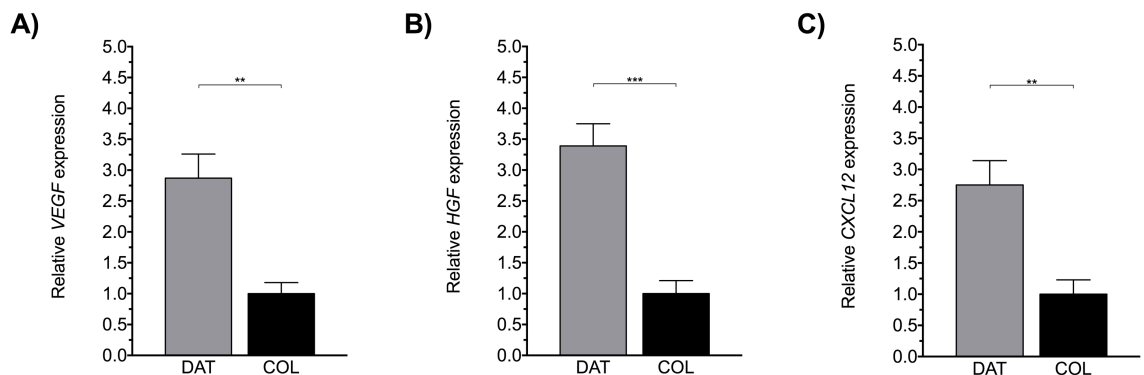


Figure 2.4: Pro-angiogenic gene expression is enhanced *in vitro* in weDFs cultured on DAT bead foams relative to COL bead foams under conditions simulating stresses in the chronic wound microenvironment. Pooled data from the three cell donors showing relative mRNA expression levels at 9 days post-seeding of the pro-angiogenic markers (A) *VEGFA*, (B) *HGF*, and (C) *CXCL12*, with significantly increased expression in the weDFs cultured on the DAT bead foams. Gene expression levels were normalized to the COL bead foam group for each cell donor, with 18S as the housekeeping gene. (n=3 scaffolds/trial, N=3 cell donors); *** = $P < 0.001$, ** = $P < 0.01$, * = $P < 0.05$.

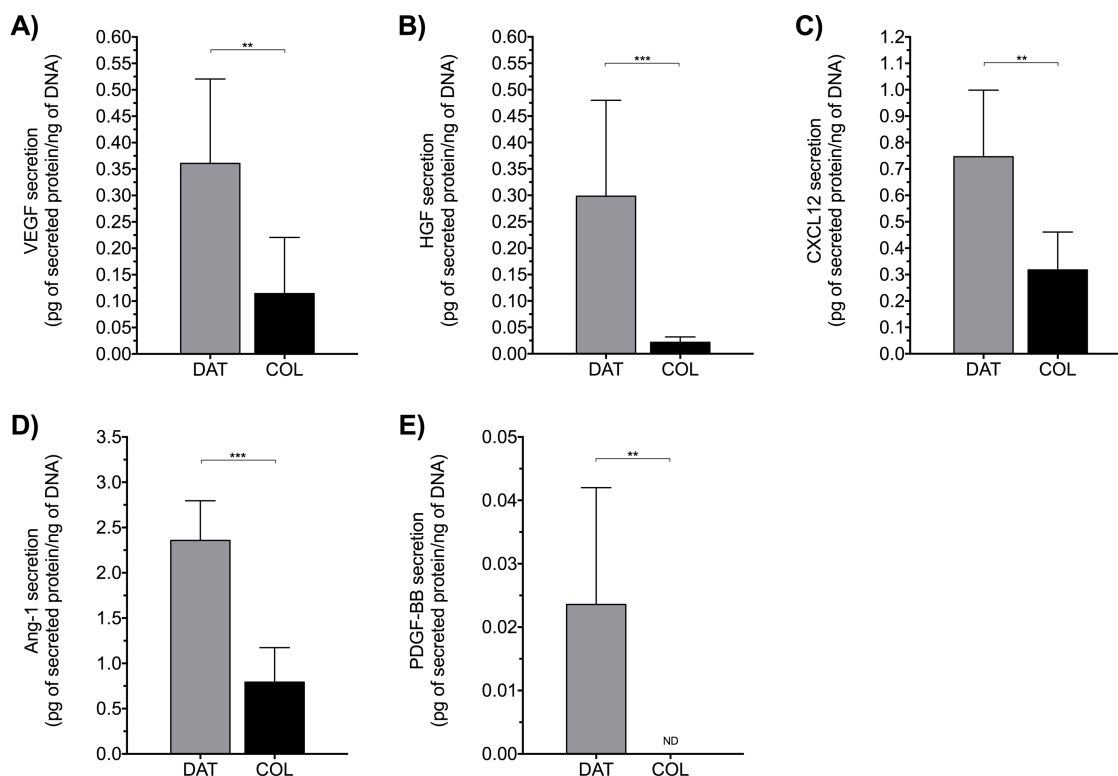


Figure 2.5: Pro-angiogenic factor secretion is enhanced in weDFs cultured on DAT bead foams relative to COL bead foams prior to implantation in the *in vivo* model. Quantification of secreted proteins in cell culture supernatants at 24 h post-seeding, normalized to total dsDNA content, showing that weDFs secreted significantly higher levels of (A) VEGFa, (B) HGF, (C) CXCL12, (D) Ang-1, and (E) PDGF-BB on the DAT bead foams. (n=3 scaffolds /trial, N=3 cell donors) *** = $P < 0.001$, ** = $P < 0.01$, * = $P < 0.05$. ND = not detected.

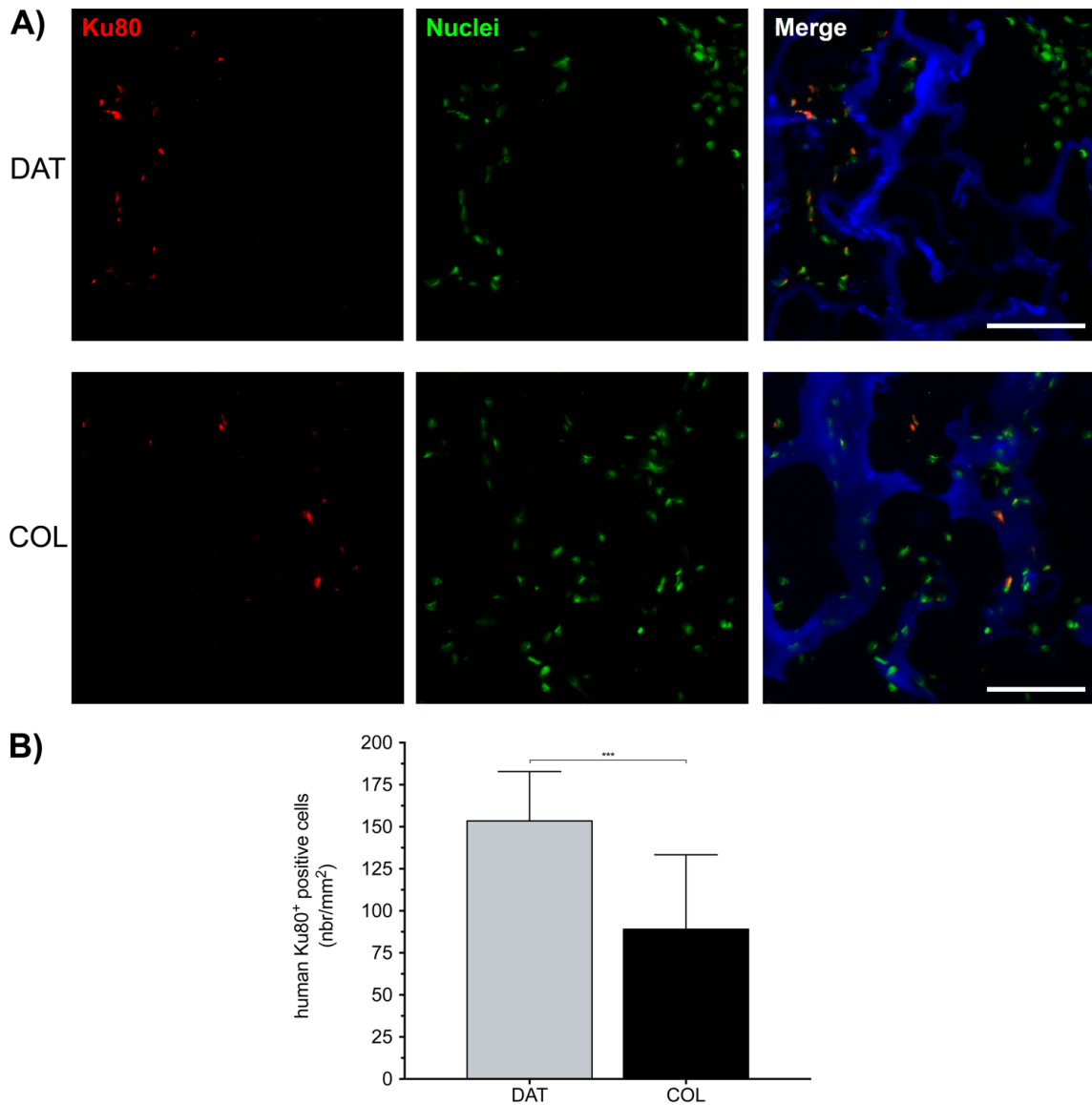


Figure 2.6: Human weDF abundance is enhanced on the DAT bead foams relative to the COL bead foams at 14 days after subcutaneous implantation in an athymic mouse model. (A) Representative human Ku80 immunostaining (red) showing qualitatively enhanced weDF abundance within the DAT bead foams. Nuclei were counter-stained with PicoGreen Reagent® (green) and the scaffolds were pre-labeled with an Alexa Fluor 350 succinimidyl ester (blue). Scale bars = 100 μ m. (B) Human Ku80⁺ cell density quantified using ImageJ showing significantly increased numbers of human cells in the DAT bead foams. (n=4-6 scaffolds /trial, N=3 cell donors) *** = $P < 0.001$.

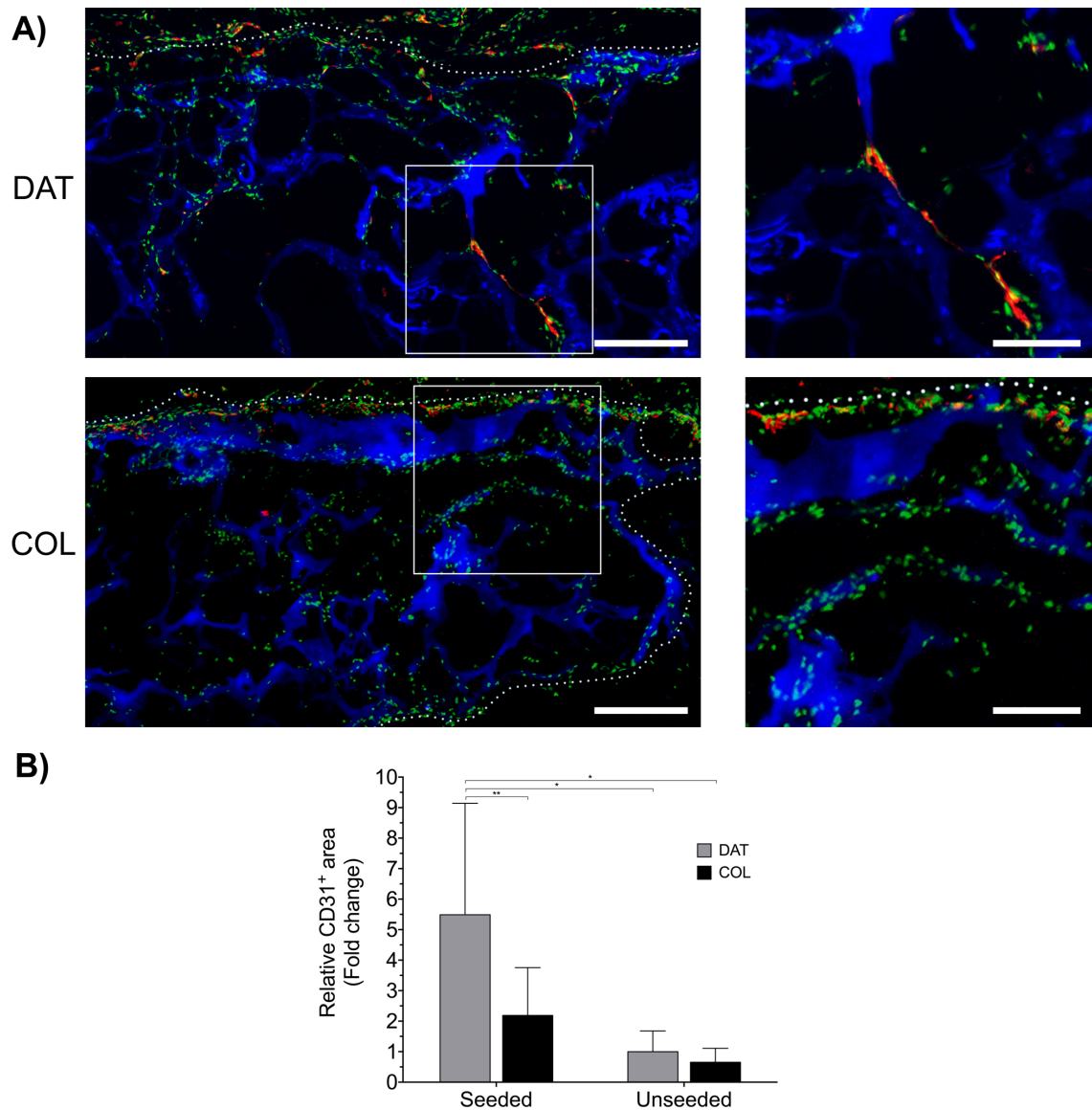


Figure 2.7: CD31⁺ cell recruitment is enhanced in the DAT bead foams seeded with human weDFs relative to seeded COL bead foams and unseeded controls at 14 days after subcutaneous implantation in an athymic mouse model. (A) Representative CD31 immunostaining (red) showing qualitatively enhanced cell infiltration in the seeded DAT bead foams relative to the seeded COL bead foams at 14 days post-implantation. Nuclei were counter-stained with PicoGreen Reagent® (green) and the scaffolds were pre-labeled with an Alexa Fluor 350 succinimidyl ester (blue). White dotted lines denote the scaffold periphery. Scale bars = 200 μ m (left panel) and 100 μ m (right panel). (B) Relative CD31⁺ expression levels, normalized to the unseeded DAT control group, suggesting that early angiogenesis was enhanced in the seeded DAT bead foams relative to all other groups. ** = $P < 0.01$, * = $P < 0.05$.

2.6 Discussion

Numerous collagenous wound dressings have been explored for the treatment of chronic wounds [169, 170]. However, the clinical efficacy of these approaches is unclear and the existing collagen-based bioengineered products available for skin healing are approved for only a limited subset of wound etiologies [170, 171, 250]. Possible reasons for the mixed success of these biological dressings are not well understood, but pre-clinical studies suggest that poor host cell infiltration and scaffold remodeling may be important factors limiting the therapeutic potential of these biomaterials [172, 173].

In the present study, human DAT was compared as a complex matrix source for the production of bioscaffolds to commercially-sourced bovine collagen, similar to the bovine collagen incorporated in numerous commercially-available skin substitutes including INTEGRA™, Apligraf®, PermaDerm™, Matriderm®, and OrCel® [169]. Previously, DAT bead foams were shown to stimulate regeneration in a subcutaneous implant model in immunocompetent rats, with increased cell infiltration and more rapid remodelling relative to intact DAT [14], supporting the selection of this more highly processed scaffolding format for wound healing applications.

While the bead foam technology was developed using DAT [14], any collagen-rich tissue could theoretically be applied as a matrix source to generate tissue-specific scaffolds, as demonstrated in the present study using commercially-available collagen. Advantages of the bead foams include their modular approach that allows for tunability in the design of both the spherical subunits and the larger assembled scaffolds. Further, the highly-porous DAT and COL bead foams were soft and compliant, with the modulus of the individual beads being within the range reported for normal human skin (0.1 kPa - 10 kPa, as measured by atomic force microscopy) [251], which may help to promote implant integration.

The DAT and COL bead foams were stable without synthetic additives or chemical cross-linking, which may be favourable from biocompatibility and bioactivity perspectives [85, 252]. In general, bead foam stability is enhanced when there is greater contact between adjacent beads, as well as more ECM present within the overall structure. As such, in our experience it is easier to synthesize larger scaffolds appropriate for clinical applications, as

compared to smaller constructs for use in pre-clinical studies. While DAT- and collagen-based bioscaffolds are biodegradable and will be remodelled over time, previous studies in our lab have demonstrated that non-chemically crosslinked DAT microcarriers, foams, and bead foams can be designed to remain stable for extended periods of time *in vitro*. In particular, these platforms have been successfully applied in culture studies with human adipose-derived stem/stromal cells (ASCs) extending from 14 to 28 days [14, 135]. Under the conditions in the current study, the DAT and COL bead foams did not macroscopically contract but remained intact over the 9-day culture period. However, in applying these platforms, it is important to note that cell types that express high levels of matrix metalloproteinases (MMPs) may interfere with scaffold integrity over time.

Manipulating ECM-derived scaffolds is challenging, as changes in composition can cause alterations in the biophysical and biomechanical properties of the constructs [236], and few studies have systematically investigated the effects of complex ECM composition on cell function within 3-D engineered microenvironments. Frequently, studies using tissue-derived scaffolds lack appropriate 3-D controls to be able to fully interpret the effects of scaffold composition on the cellular response. Recognizing this limitation, the bead foam fabrication methods were successfully applied to generate DAT and COL bead foams that were structurally similar. While the substrates were designed to have comparable initial properties, it is acknowledged that there may be subtle differences in scaffold architecture and/or biomechanics, and that the scaffold properties may have changed over time as the cells interacted with their environment. Regardless, the DAT bead foams reproducibly enhanced the survival and angiogenic function of the human weDFs relative to bead foams derived from bovine collagen, suggesting that human adipose tissue may be a promising cell-instructive matrix source for wound healing applications.

The current findings suggest that the complex ECM composition within the scaffolds modulated the response of dermal fibroblasts isolated from the chronic wounds of patients undergoing limb amputation. The xenogeneic sourcing of the bovine COL bead foams may be a factor impacting the cellular response. However, the ECM is highly conserved between species [253, 254] and human fibroblasts and keratinocytes have been previously shown to be responsive to matrices produced from bovine collagen [169, 255]. The higher levels of sulphated GAGs and collagen types IV, V, and VI in the DAT bead foams may

be advantageous for wound healing, as these ECM components are known to play important roles in angiogenesis. More specifically, sulphated GAGs can act as a depot for pro-angiogenic factors and can modulate endothelial cell attachment and migration directly through α_5 and α_V integrin interactions [256]. Endothelial cell recruitment can also be stimulated through interactions with collagen type IV [257], which has been shown to have dose-dependent effects on vessel elongation and stabilization [258]. Recent studies have also identified collagen type VI as an emerging pro-angiogenic factor through its role in macrophage and endothelial cell recruitment in the context of tumour angiogenesis [22]. Lastly, collagen type V has been positively associated with newly-developing blood vessels in granulation tissue, as well as wound healing [259].

Fibroblasts sourced from non-healing wounds, such as those used in the present study, have been reported to have innate impaired functions [241, 242]. To the authors' knowledge, the current study is the first to directly compare the effects of ECM composition on the pro-regenerative phenotype of human weDFs. The findings suggest that weDFs can contribute to tissue repair through the secretion of pro-angiogenic factors, and that cell survival and functional capacity can be modulated by the matrix source applied in the design of cell-instructive ECM-derived scaffolds. In terms of complex ECM promoting cell survival under stress, the *in vitro* findings are consistent with previous work demonstrating enhanced survival in response to H₂O₂ treatment when murine cardiac progenitor cells (CPCs) were cultured in decellularized myocardial matrix hydrogels as compared to collagen gel controls [86].

The design of cell-instructive microenvironments that harness the pro-regenerative paracrine capacity of stromal cell populations is an area of emerging research interest. To date, the influence of complex ECM composition on cellular secretomes has been more extensively explored in the context of cancer biology [260, 261]. For example, using a 3-D culture model with Matrigel supplemented with collagen type I, Biondani *et al.* recently reported that human cancer stem cells secreted lower levels of a range of pro-angiogenic factors in matrices that contained higher amounts of collagen type I [260]. These findings, along with the results of the current study, suggest that the incorporation of complex ECM components within collagenous wound dressings could enhance regeneration by inducing cells within the wound bed to adopt a more pro-angiogenic phenotype.

2.7 Conclusions

Relative to the bead foams fabricated from bovine collagen, the survival and pro-angiogenic capacity of human dermal fibroblasts sourced from chronic wounds were enhanced on the DAT bead foams both *in vitro* and *in vivo*. The assembled data supports that the complex ECM composition within engineered bioscaffolds can be harnessed to establish a more pro-regenerative microenvironment for cells involved in the process of wound repair. Future work could assess the pro-regenerative effects of the scaffolds in pre-clinical models of impaired wound healing, as well as exploring the DAT bead foams as cell-instructive platforms for regenerative cell populations, such as mesenchymal stem/stromal cells (MSCs). Overall, decellularized adipose tissue represents a promising and clinically-relevant human matrix source for the design of novel pro-angiogenic wound dressings.

Chapter 3

3 Modular cell-assembled matrix-derived bead foams as a pro-angiogenic mesenchymal stromal cell delivery platform

3.1 Co-authorship statement

The work presented in Chapter 3 forms the basis of a manuscript that is currently in preparation for submission, entitled: “*Modular cell-assembled matrix-derived bead foams as a pro-angiogenic mesenchymal stromal cell delivery platform*”, with the following list of authors: “*Morissette Martin P, Kim KJ, Juignet L, Hamilton AM, Ronald JA, Flynn LE*”.

I conceptualized the study in collaboration with Dr. Lauren Flynn. I personally designed and performed all of the experimental studies described in the Chapter, with support from the remaining authors. More specifically:

- Ms. Kellie J. Kim helped with the production of the cell-assembled bead foams for Figures 3.2, 3.3, and 3.4.
- Dr. Laura Juignet operated the flow cytometer and performed flow cytometry data analysis (Figure 3.2D and E).
- Dr. Amanda Hamilton produced the lentiviral vectors and transduced the cells that were used for the animal experiments.
- Dr. John Ronald provided scientific guidance with the lentiviral transduction and granted access to the *in vivo* imaging system (IVIS) platform.

I analyzed all the data in collaboration with Dr. Flynn. I made all the figures and supplementary content (tables and figures). The manuscript was written in collaboration with Dr. Lauren Flynn.

3.2 Abstract

There is a need for new approaches for bioscaffold fabrication that enable the localized delivery of a high density of pro-regenerative cells for applications in soft tissue regeneration. Towards this goal, novel scaffolds comprised of fused networks of extracellular matrix (ECM)-derived beads were developed and generated through a “cell-assembly” approach using human adipose-derived stromal cells (ASCs) seeded on spherical decellularized adipose tissue (DAT) beads. Our novel fabrication protocol successfully produced robust 3-D cell-assembled bead foams that were easy to handle and contained a high density of viable ASCs. Histological, biochemical and gene expression assays demonstrated that the cell-assembly process was mediated through the synthesis of new ECM, including collagen, fibronectin and glycosaminoglycans (GAGs), combined with enhanced ECM remodelling. Further, the ASCs within the cell-assembled bead foams were shown to express a variety of pro-angiogenic proteins. *In vivo* assessment in a subcutaneous implant model in athymic nude mice was performed to probe ASC retention and angiogenesis using the new cell-assembled bead foam platform relative to ASCs seeded on pre-assembled DAT foams. To enable *in vivo* cell tracking, all scaffolds were prepared with transduced human ASCs that were engineered to express codon optimized firefly luciferase (Fluc2) and tdTomato (tdT). Bioluminescence imaging (BLI) results indicated that there were significantly more viable ASCs present in the cell-assembled bead foams at 2 days post-implantation, with the enhanced signal in this group diminishing over time. BLI and histological analysis of the tdT⁺ cell population within the scaffolds confirmed that both platforms contained similar levels of ASCs at 28 days post-implantation. Further, the cell-assembled bead foam implants were shown to contain a higher density of CD31⁺ cells at 28 days, suggesting that this platform was favorable for stimulating localized angiogenesis. Overall, the novel cell-assembled DAT bead foams represent a promising pro-regenerative cell delivery system that supports the localized *in vivo* retention of delivered ASCs with pro-angiogenic functionality.

3.3 INTRODUCTION

There is growing interest in the development of new approaches to stimulate soft tissue regeneration for applications in plastic and reconstructive surgery, including the restoration of soft tissue defects caused by post-oncologic resection, trauma, and congenital abnormalities [74, 84]. While the implantation of pro-regenerative biomaterials may be sufficient for the treatment of small defects or voids, more complex strategies would likely be required for stable mid-to-large volume soft tissue augmentation [74, 79]. In particular, there remains a significant need for new strategies that can help to augment angiogenesis within engineered tissue replacements, to avoid eventual failure due to the lack of a supporting vascular network within the implant [74, 79]. From this perspective, cell-based therapies harnessing the pro-regenerative paracrine functionality of mesenchymal stromal cells (MSCs) have shown promise in stimulating angiogenesis within implanted biomaterials [126, 175, 262, 263].

Towards the goal of designing innovative strategies for soft tissue repair, our lab has pioneered the development of bioscaffolds derived from human decellularized adipose tissue (DAT) [14, 104, 126, 264]. From a translational perspective, adipose tissue is abundantly discarded as surgical waste and is a uniquely accessible source of human extracellular matrix (ECM) that can be decellularized using our detergent-free decellularization process [104]. The resulting DAT incorporates a diverse range of biomacromolecules, such as collagens, proteoglycans, glycosaminoglycans, adhesion glycoproteins, growth factors, cytokines, and matricellular proteins, which may be favourable for cell survival and angiogenesis [264]. Recent studies from our group and others have also shown that DAT can be further processed into a variety of bioscaffold formats, including foams [14, 264], microcarriers [13, 135], coatings [136], hydrogels [119], meshes [131], and bioinks for 3-D printing applications [134]. These alternative scaffold formats have properties, such as porosity, stiffness, and architecture, that can be tuned depending on the target application [13, 14, 119, 131, 134-136, 264].

In previous studies, we developed a DAT “bead foam” platform that was fabricated by subjecting spherical porous DAT beads combined within a mould to a controlled freezing

and lyophilization procedure that resulted in fusion of the beads to generate 3-D constructs stabilized through physical interactions [135, 265]. Using this pre-assembled bead foam format, DAT was shown to have cell-instructive properties in terms of enhancing the survival and pro-angiogenic functionality of human dermal fibroblasts isolated from chronic wounds relative to similar foams derived from purified collagen both *in vitro* and *in vivo* [264]. While the cell-supportive and pro-angiogenic properties of the previous DAT bead foam technology were promising, a limitation was that the foams tended to be fragile and could only be seeded and cultured using static approaches, which resulted in limited cellular infiltration and distribution. Having a core devoid of cells is not ideal for strategies striving to apply MSCs to promote scaffold integration and implant vascularization [74, 84].

To address these limitations, the overall objective of the current study was to establish new fabrication techniques to generate robust three-dimensional (3-D) DAT bioscaffolds containing a high density of viable cells that were well distributed throughout the scaffolds. More specifically, we sought to harness the innate capacity of human adipose-derived stromal cells (ASCs) to synthesize and remodel ECM [221, 266] in order to produce novel “cell-assembled” bead foams. ASCs are a logical cell source for soft tissue regeneration strategies, given their relative abundance and accessibility [267], as well as their capacity to promote regeneration through the secretion of pro-angiogenic and immunomodulatory paracrine factors [201, 203, 209].

To generate the cell-assembled foams, the ASCs were first seeded onto porous DAT beads under dynamic conditions within a spinner culture system [135]. Following a 24 h cell attachment period, the seeded beads were then transferred into moulds and cultured for 8 days to promote scaffold assembly. In developing the new fabrication protocols, the effects of varying the culture conditions were explored, with the goal of improving the handling properties of the scaffolds, while ensuring the ASCs retained high viability and pro-angiogenic paracrine functionality. In previous studies with MSCs, preconditioning with soluble factors including epidermal growth factor (EGF) [224], basic fibroblast growth factor (FGF-2) [225], and insulin-like growth factor-1 (IGF-1) [226] has been shown to have positive effects in terms of stimulating cell growth, decreasing apoptosis, and enhancing the secretion of a variety of factors including pro-angiogenic and pro-fibrotic

molecules, as well as matrix metalloproteinases (MMPs) that regulate ECM remodelling [218, 219, 224-226, 268]. In addition, dynamic culture was employed throughout all stages of the process, as previous literature has identified that dynamic preconditioning can enhance ECM synthesis by human ASCs [221], and promoting media exchange within the scaffolds may also help to augment cell viability and paracrine factor production [269].

Following the establishment of the fabrication methods, detailed *in vitro* characterization studies were performed with a focus on assessing ASC number, distribution, proliferation, and viability, as well as probing for pro-angiogenic markers along with ECM synthesis and remodelling. Subsequently, the capacity of the scaffolds to support viable human ASC retention *in vivo* was investigated within a subcutaneous implant model in athymic nude mice relative to ASCs delivered on our previous pre-assembled DAT bead foam platform. To enable *in vivo* cell tracking, the scaffolds were prepared with human ASCs that had been transduced to constitutively express codon optimized firefly luciferase (Fluc2) and tdTomato (tdT), a red fluorescent protein [270]. Bioluminescence imaging (BLI) was performed over 28 days, and the implants were collected within their surrounding tissues at day 28, for histological analysis of tdTomato⁺ cell retention and immunohistochemical staining for CD31 as a marker of angiogenesis within the scaffolds.

3.4 Materials and methods

3.4.1 Decellularization of adipose tissue and DAT bead synthesis

Human subcutaneous adipose tissue was obtained with informed consent from elective lipo-reduction procedures at the London Health Sciences Centre in London, Canada (HREB #105426) and transferred within 2 h of collection into a hypotonic cell lysis buffer (Solution A: 10 mM Tris base and 5 mM ethylenediaminetetraacetic acid (EDTA), pH 8.0) and frozen at -80°C. All decellularization solutions were supplemented with 1% antibiotic-antimycotic solution (Gibco, Burlington, ON, Canada) and 1% phenylmethylsulphonyl fluoride (PMSF), with the exception of the enzymatic treatment steps where the PMSF was excluded. After thawing, the tissues were processed following a published five-day decellularization protocol [104].

Lyophilized DAT samples from five patients were pooled and finely minced, suspended into 0.2 M acetic acid, and homogenized (PowerGen Model 125 homogenizer, Fisher

Scientific, Ottawa, ON, Canada). The homogenized DAT suspension was diluted with deionized water to obtain a final ECM concentration of 20 mg ECM/mL (dry weight), and then electrosprayed to synthesize DAT beads following published methods [264]. In brief, the beads were produced by electrospraying the suspension directly into a Dewar flask filled with liquid nitrogen with an applied voltage of 16-18 kV, an extrusion speed of 35 mL/h, and the needle positioned 3 cm from the surface of the liquid nitrogen. Immediately following synthesis, the frozen beads were collected into conical tubes, lyophilized, and stored under vacuum at room temperature.

Following synthesis, DAT beads were decontaminated and rehydrated through an ethanol series (100%, 99%, 98%, 95%, 90%, 80%, 70%, 50, 25%, and 12.5% (v/v) diluted with sterile PBS), followed by three washes in sterile PBS. The rehydrated beads were stored at 4°C before being used in characterization and cell culture studies.

3.4.2 Human ASC isolation, expansion, and characterization

Collected human adipose tissue was processed within 2 h for ASC isolation following published protocols [12]. Isolated ASCs were cultured on tissue culture polystyrene (TCPS; Corning, NY, USA) at 37°C, 5% CO₂ in proliferation medium comprised of DMEM:Ham's F12 (Wisent Bio Products, Montreal, QC) supplemented with 10% fetal bovine serum (FBS; Wisent Bio Products), 100 U/mL penicillin and 0.1 mg/mL streptomycin (Wisent Bio Products). Media was changed every 2-3 days. Cells were frozen at passage 0, stored in liquid nitrogen, and thawed when needed. Primary cell populations from three donors (Supplementary Table 3.1) were included in the studies.

Immunophenotyping (Supplementary Figure 3.1) was performed on P4 ASCs using a Guava easyCyte 8HT flow cytometer (Millipore, Billerica, MA, USA) as previously described [248]. Single marker staining was performed with monoclonal, fluorochrome-conjugated antibodies from eBioscience (San Diego, CA, USA), as follows: CD90-FITC, CD-105-PE, CD73-FITC, CD44-PE-Cy7, CD29-PE, CD34-APC, CD31-PE, CD146-FITC. All samples were stained for 30 min at 4°C in 5% FBS diluted in PBS. Unstained controls were included in every trial.

3.4.3 Production of cell-assembled DAT bead foams

3.4.3.1 Cell seeding regimen on DAT beads

Rehydrated DAT beads were resuspended in proliferation medium and incubated overnight at 4°C. The next day, the beads were transferred into 250 mL CELLSPIN® spinner flasks (INTEGRA Biosciences, AG, Switzerland) with 100 mL of proliferation media. Passage 4 or 5 ASCs were trypsinized and seeded into the spinner flasks at a ratio of 1.25×10^6 cells/mg of DAT beads (wet weight in 100% ethanol). Immediately after the addition of the cells into the spinner flasks, a 12-h stirring regimen was performed (37°C, 5% CO₂) [135]. In brief, (i) the cultures were stirred for 2 min at 25 rpm, followed by 30 min of static culture repeated over a period of 3 h, (ii) the cultures were then maintained under static conditions for 6 h, and (iii) the intermittent stirring conditions described in stage (i) were repeated for the final 3 h. After the seeding period, the spinner flasks were stirred continuously at 25 rpm for 12 h.

Cell attachment was assessed by counting the number of unadhered cells in the spinner flask system at 24 h after seeding. More specifically, the media was collected and centrifuged to pellet the cells (1200 xg, 5 min), which were counted using a hemocytometer with a 1:1 ratio of cell suspension with trypan blue. Cell numbers were reported as a percentage of unadherent cells relative to the initial number of cells inoculated into each flask (n = 3 replicate samples/cell donor, N = 3 cell donors).

3.4.3.2 Cell assembly of the DAT beads into DAT bead foams

Following cell seeding, ASC-seeded DAT beads were transferred into circular moulds comprised of 12-well transwell inserts lined with medical-grade silicone rings (inner diameter: 8 mm; outer diameter: 12 mm; height: 3 mm). Prime-XV® MSC EXPANSION XSFM Medium (cat#91149, Irvine Scientific, CA, USA), a xenogenic-free chemically-defined (XFCD) media, was supplemented with 50 µg/mL of L-ascorbic acid 2-phosphate (A2P) to promote ECM deposition [271, 272], as well as 100 U/mL penicillin and 0.1 mg/mL streptomycin. In addition, in one set of samples supplementation of the media with 5 ng/mL of recombinant human EGF, 10 ng/mL of recombinant human FGF-2, and 20 ng/mL of recombinant LONG® R3 human IGF-1 (+GF) was also investigated as a possible

strategy to enhance cell proliferation and matrix production. All three growth factor stock solutions were reconstituted with 1 mg/mL of human serum albumin.

For both groups, media was changed every two days with freshly-supplemented A2P. After three days of static culture, 12-well plates containing the scaffolds were transferred onto an orbital-shaker for dynamic culturing until harvesting (75 rpm, 37°C, 5% CO₂).

3.4.4 Cell viability and abundance on DAT beads and within the cell-assembled DAT bead foams

3.4.4.1 Cell viability and distribution analysis using confocal microscopy

To qualitatively analyse ASC viability and distribution on the surface of the DAT beads, cell-seeded beads were stained at 24 h after seeding with a Live/Dead® assay kit (Cat. # L-3224; Life Technologies, Burlington, ON, Canada) and imaged with a Zeiss LSM800 confocal microscope (Zeiss Canada, Toronto, ON, Canada) (N = 3 cell donors).

3.4.4.2 Cell viability analysis using flow cytometry

After 7 days of transwell culture, the cell-assembled DAT bead foams were rinsed in PBS and incubated in trypsin to dissociate the cells (1 h, 37°C, 75 rpm). The samples were then neutralized using complete proliferation media, filtered through 100-µm and 40-µm nylon meshes, pelleted, and rinsed in ice-cold PBS supplemented with 5% FBS. Isolated cells were then stained for annexin-V and propidium iodide using an Apoptosis Detection Kit I (cat. # 556547; BD bioscience, Mississauga, ON, Canada) according to the manufacturer's instructions, and analyzed using an LSR II/FACSCanto flow cytometer (BD bioscience; n = 3 scaffolds/cell donor, N = 3 cell donors). Controls included unstained cell-assembled bead foams, along with propidium iodide and Annexin-V single and double-stained ASCs cultured on TCPS. In addition, ASCs cultured on TCPS were treated with staurosporine (1 µM staurosporine, 16 hrs, 37°C, 5% CO₂) as a positive control for apoptosis.

3.4.4.3 Cell abundance and total double-stranded DNA content measurements

Cell-assembled bead foam samples were rinsed in PBS, snap frozen, weighed, and lyophilized. Samples were then digested with 60 mU/mL of proteinase K (Promega,

Madison, WI, USA) in Tris-EDTA buffer (200 nM Tris- HCl, 200 nM EDTA, pH 7.5) under agitation at 500 rpm and 56°C overnight, followed by a 10 min incubation at 95°C to inactivate the enzyme (n = 3 scaffolds/cell donors, N = 3 cell donors).

To estimate the number of cells incorporated within the bead foams, DNA extraction from the proteinase K-digested lyophilized samples was performed using a DNeasy® Blood and Tissue kit (cat# 69504; Qiagen, Valencia, CA, USA) according to the manufacturer's instructions. Total double-stranded DNA (dsDNA) was quantified from the column-purified DNA samples using the Quant-iT™ PicoGreen® dsDNA assay (Molecular Probes, Burlington, ON, Canada) according to the manufacturer's instructions, with analysis using a CLARIOstar® spectrophotometer (BMG LABTECH Inc., Cary, NC, USA). Cell lysates prepared from ASCs cultured on TCPS were included to generate standard curves to report the data in terms of cell numbers (n = 3 scaffolds/cell donors, N = 3 cell donors).

3.4.5 Physical and biochemical characterization of the DAT beads and DAT bead foams

3.4.5.1 Bead diameter

Hydrated DAT beads were imaged under a light microscope at low magnification. The Feret's diameter function on ImageJ (NIH, <http://imagej.nih.gov/>) was used to measure the largest diameter of the beads (N= 3 donors, n= 25 to 35 biological replicates per donor).

3.4.5.2 Mechanical Testing

The mechanical properties of individual DAT beads were assessed using a CellScale MicroTester system (Waterloo, ON, Canada). Testing of individual beads was performed in a PBS bath at 37°C, using a 203 µm diameter cantilever attached to a square platen (2 mm x 2 mm), and the beads were compressed to 50% deformation for 3 preconditioning cycles at a strain rate of 0.01 s⁻¹ (1 cycle = 45 s compression, 1 s hold, 45 s recovery). The data was collected from 3 consecutive cycles and the Young's moduli were calculated using nonlinear least squares curve fitting with a published extended mechanics model for large elastic deformations of spherical microparticles [245] (n=6 beads/batch; N=3 batches from 3 different ECM donors).

3.4.5.3 Contraction Measurement of Cell-Assembled DAT Bead Foams

Macroscopic images were acquired after 8 days of transwell culture. Using the inner diameter of the silicone ring to represent the initial area at day 0, contraction measurements were performed using ImageJ and were reported as a percentage compared to the initial day of moulding (n=15-18 replicates per donor, N=3 cell donors).

3.4.5.4 Porosity measurement

Rehydrated DAT beads and DAT bead foams were lyophilized and weighed. After recording their dry mass, the scaffolds were immersed in 100% isopropanol overnight under light vacuum with gentle agitation to minimize the formation of air bubbles. Excess isopropanol was then removed through gentle blotting and the wet mass of the scaffold was recorded. Porosity was calculated using a modified Archimedes' method [246].

3.4.5.5 Hydroxyproline and dimethylmethylene blue assays

Total collagen and total sulphated glycosaminoglycan (GAG) contents were quantified using the hydroxyproline and dimethylmethylene blue (DMMB) assays respectively. Unseeded DAT beads, seeded DAT beads, and cell-assembled DAT bead foams were digested with 60 mAnson units of proteinase K/mL (Promega, Madison, WI, USA) in Tris-EDTA buffer (200 nM Tris-HCl, 200 nM EDTA, pH 7.5) under agitation at 500 rpm and 65°C for 2 h. Following digestion, the proteinase K was inactivated by a 10 min incubation at 95°C. Both DMMB and hydroxyproline assays were run using the same set of digested samples.

The DMMB assay was performed by mixing 10 μ L aliquots of the digested samples and 200 μ L of a 1.6% DMMB solution (solvent: 1% ethanol and 0.2% formic acid) into a 96-well plate. The absorbance at 525 nm was recorded using a CLARIOstar® spectrophotometer (BMG LABTECH Inc.) and the GAG concentration was determined by comparison to a chondroitin sulphate standard curve.

The hydroxyproline assay was performed following further processing of the proteinase K-digested samples. More specifically, sample aliquots were hydrolyzed (24 h incubation in 12 N hydrochloric acid at 110°C), neutralized (with 6 N sodium hydroxide), diluted (1:80

with water), and transferred in duplicate into a 96-well plate. Next, 0.05 N chloramine-T/20% 2-methoxyethanol solution was added to each well (incubated for 20 min at room temperature), followed by the addition of 3.15 N perchloric acid (incubated 5 min at room temperature), and Ehrlich's reagent (incubated 20 min at 60°C). After the stabilization of the colour (5 min incubation at 4°C followed by a 20 min incubation at room temperature), absorbance was measured at 560 nm using a CLARIOstar® spectrophotometer (BMG LABTECH Inc.). The hydroxyproline content was determined by comparison to a hydroxyproline standard curve.

3.4.5.6 Zymography

To determine the relative amounts of MMP activity within the experimental groups, conditioned media from the cell-assembled DAT bead foams was analysed using gelatin zymography. Media that had been conditioned for 48 h was collected at day 8 and stored at -80°C. Samples were thawed on ice, diluted in a 1:1 ratio with 4X Laemmli buffer (without β -mercaptoethanol) and loaded on 7.5% SDS-polyacrylamide gels containing 1 mg/mL gelatin (10 μ L of diluted conditioned media per gel well). To allow for protein size analysis and gel-to-gel normalization, BLUelf Prestained Protein ladder (FroggaBio) and 10 ng recombinant human MMP-2 standards (Biolegend; cat#554302) activated with 4-aminophenylmercuric acetate (Sigma; Cat#A9563) were loaded on all gels [273]. Media only controls (incubated 48 hours without scaffolds, 37°C, 5% CO₂) were also included.

Following electrophoresis, SDS was removed by incubating the gels in washing buffer (2.5% Triton X-100, 50 mM Tris HCl, 5 mM CaCl₂, 1 μ M ZnCl₂; two 30 min washes, 100 rpm, room temperature). Gels were then rinsed once in digestion buffer (1% Triton X-100, 50 mM Tris HCl, 5 mM CaCl₂, 1 μ M ZnCl₂; 10 min at 37°C) and incubated 24 h at 37°C in fresh digestion buffer. Gels were then stained with Coomassie blue (0.05% Coomassie blue, 10% acetic acid, 40% methanol, dissolved in water), destained (10% acetic acid, 40% methanol), imaged, and analyzed for densitometry using ImageJ. Results were normalized to the MMP-2 standard bands at ~60 kDa.

3.4.5.7 Immunohistochemical and histological analysis of DAT bead foams

To distinguish newly-synthesized ECM from the pre-existing DAT beads in the cryo-sections, DAT beads were pre-labeled with an Alexa Fluor 350 Succinimidyl Ester (A10168, Thermo Fisher Scientific, Oakville, ON, Canada) following the manufacturer's instructions. DAT beads were then seeded in the spinner flask system as described in section 3.3.1 and cultured as described in section 3.3.3.1 with protection from light exposure. After 8 days of transwell culture, the DAT bead foams (n = 3 scaffolds/cell donors, N = 3 cell donors) were rinsed in PBS, embedded in Tissue-Tek OCT compound (Sakura Finetek, Torrance, CA, USA), and snap frozen in liquid nitrogen prior to cryo-sectioning (7 µm transverse sections). Following fixation in acetone and blocking in 10% goat serum in PBS, the sections were stained overnight at 4°C with primary antibodies against collagen type I (1:200 in 5% goat serum in PBS, ab34710, Abcam, Toronto, ON, Canada), fibronectin (1:200, ab23750, Abcam), or Ki67 (1:200, ab16667, Abcam). Detection was carried out using an anti-rabbit secondary conjugated to Alexa Fluor 594 (dilution 1:200, ab150080, Abcam) and Picogreen® reagent to identify cell nuclei (dilution 1:400). No primary controls were included in all trials. Images were acquired with an EVOS FL Cell Imaging System (Thermo Fisher Scientific, Burlington, ON, Canada). In order to assess the collagen fiber network within the scaffolds, picrosirius red staining was also conducted (7 µm cryo-sections), with visualization under circularly polarized light using a Nikon Optiphot microscope (Nikon, Mississauga, ON, Canada) and an Infinity 2-3 CCD camera (Lumenera, Ottawa, Canada).

3.4.6 Gene expression analysis measured using RT-qPCR

Total cellular RNA was isolated from the cell-assembled bead foams using PureZOL™ RNA Isolation Reagent (Bio-Rad; cat# 7326880) and the Aurum™ Total RNA Fatty and Fibrous Tissue Kit (Bio-Rad; cat# 7326870). cDNA was then synthesized from 400 ng of input RNA using the iScript™ Reverse Transcription Supermix kit (Bio-Rad; Cat. # 1708840) according to the manufacturer's protocol.

Custom-made qPCR arrays (Bio-Rad; PrimePCR™ arrays) were designed to probe for 23 genes gene of interest (see Supplementary Table 3.2 for a list of gene symbols and gene names), along with the housekeeping genes ribosomal protein S18 (*RPS18*) and ubiquitin

C (*UBC*). Three cDNA samples from each experimental condition were pooled (3 ng of cDNA each/well, for a total of 9 ng of pooled cDNA per well) and run in technical duplicates for all genes. Samples from three cell donors were analyzed independently. Several technical controls were included in the plate design for each set of pooled samples, including a gDNA control, a RT control, a positive PCR control, and two RNA quality controls (cat# qHsaCtID0001004, qHsaCtD0001001, qHsaCtID0001003, qHsaCtID0001002, respectively; PrimePCR™ arrays; Bio-Rad).

Amplification was carried out using a CFX384 Touch™ Real-Time PCR Detection System (Bio-Rad) using SsoAdvanced Universal SYBR Green Supermix (Bio-Rad) in all wells as follows: initial incubation at 95°C for 2 min, followed by 40 cycles of 95°C for 5 s and 60°C for 30 s. The data was analyzed using the comparative Ct method with normalization to the geometric mean of two stable housekeeping genes (*RPS18* and *UBC*).

3.4.7 Protein expression analysis measured using multiplex assay

The expression of angiogenic factors was further investigated at the protein level using a Luminex® multiplex assay for angiopoietin-1, CXCL12, HGF, and VEGFa, according to the manufacturer's instructions (R&D Systems). Scaffold lysates were produced by rinsing the 8-day cell-assembled bead foams in PBS, snap freezing, and grinding them in liquid nitrogen using a mortar and pestle. Proteins were extracted using a TNGT buffer (50 mM Tris-HCl pH 7.4; 100 mM NaCl; 5% Glycerol; 1% Triton X), followed by a series of centrifugation steps to remove ECM debris. The samples were analyzed on a Bio-Plex® MAGPIX™ Multiplex Reader (Bio-Rad, Mississauga, ON), and the analyte levels were normalized to the total protein content in the corresponding scaffolds measured using the Pierce 660 nm protein assay (Thermo Fisher Scientific) with a CLARIOstar plate reader (BMG Labtech).

3.4.8 Lentiviral transduction of ASCs and trilineage differentiation studies

3.4.8.1 Lentiviral transduction of ASCs

To enable BLI and fluorescence tracking of the ASCs within the *in vivo* model, ASCs from 3 donors were transduced using lentiviral vectors co-expressing FLuc2 under the human

elongation factor 1-alpha promoter for constitutive expression (pEF1-alpha-tdT-FLuc2 reporter) [270]. Vector production and lentiviral transductions were performed on ASCs at passage 1 following previously published methods [270]. Briefly, integrating lentiviral vectors with pEF1-alpha-tdT-FLuc2 reporters were generated by cotransfecting packaging, envelope, and transfer plasmids into 293T cells. Vector supernatants were harvested 24 and 48 h after transfection and filtered through a 0.45 µm filter, aliquoted and frozen at -80°C until use. Functional viral titers were determined by transducing 1×10^5 H1299 cells with various volumes of vector supernatants and using an LSR II/FACSCanto flow cytometer (BD bioscience) for analysis. ASCs were then thawed, cultured 2-3 days, and transduced using a viral multiplicity of infection (MOI) of 75 and 100 µg/mL of protamine sulphate. ASC underwent a medium change 24 h post-transduction and were rinsed with PBS three times 48 h post-transduction, prior to passaging. Quantification of the percentage of transduced cells based on tdT expression was performed at passages 3 and 4 using a Guava easyCyte 8HT Benchtop flow cytometer (EMD Millipore, Billerica, MA, USA). Three ASC populations were used for the trilineage differentiation studies (Section 3.4.8.2) and two populations were used for the *in vivo* experimentations (Section 3.4.9).

3.4.8.2 Trilineage differentiation studies

Trilineage differentiation studies were performed to confirm maintenance of the multilineage differentiation capacity of the ASCs following transduction. Transduced and non-transduced ASCs at passage 4 from three donors were included.

ASCs were differentiated towards the adipogenic lineage using an adipogenic differentiation medium comprised of DMEM:Ham's F12 supplemented with 33 mM biotin, 17 mM pantothenate, 10 mg/mL transferrin, 100 nM hydrocortisone, 66 nM human insulin, 1 nM triiodothyronine, and 1% pen-strep, with 0.25 mM isobutylmethylxanthine (IBMX) and 1 mg/mL troglitazone supplemented for the first 3 days. Non-induced controls were also included by culturing the ASCs in proliferation media. After 14 days of culture, perilipin immunofluorescence and oil red O staining were performed to visualize intracellular lipid accumulation within the induced and non-induced groups ($n = 3$ wells/cell donor; $N = 3$ donors) following published methods [13]. In order to quantitatively analyze the levels of intracellular lipid accumulation, dye extraction on the oil red O-stained samples was performed after imaging. For extraction, the samples were

rinsed with deionized water twice, and once with 70% ethanol (quickly, 1 well at a time) to remove non-specific background, prior to the addition of 100% isopropanol to extract the dye (15 min incubation, 150 rpm, room temperature). Supernatants were then transferred from each replicate sample into triplicate wells of a 96-well plate, and absorbance was read at 492 nm using a CLARIOstar® spectrophotometer (BMG LabTech, Ortenberg, Germany). Data was expressed as a fold change relative to the non-transduced, non-induced conditions.

Osteogenic differentiation was induced using an osteogenic differentiation medium comprised of DMEM with 1 g/L of glucose supplemented with 10% FBS, 150 μ M A2P, 10 mM β -glycerophosphate, 10 nM dexamethasone, 10 nM 1,25-dihydroxyvitamin D₃, and 1% pen-strep. In addition to the osteogenic induced group, a group cultured in DMEM with 1 g/L of glucose supplemented with 10% FBS and 1% pen-strep was included as a non-induced control. Media was changed every 2-3 days for all groups and the cells were cultured for an additional 28 days. Osteogenic differentiation was assessed in terms of matrix mineralization performed by von Kossa staining and Osteoimage® fluorescent staining following published methods [135] and the manufacturer's instructions respectively. An alkaline phosphatase (ALP) activity assay was also performed to quantify the osteogenic differentiation response [135]. Cell lysate aliquots were combined with nitrophenyl phosphate substrate within a 96-well plate. Following a 30 min incubation at 37°C quenched with 3 N sodium hydroxide, the absorbance of each well was measured at 405 nm using a CLARIOstar® spectrophotometer (BMG LABTECH Inc.). Quantification of enzyme activity was performed using p-nitrophenol standards, and the data was normalized to total protein content using the Pierce 660 nm protein assay (Thermo Fisher Scientific).

Induction towards the chondrogenic lineage was performed in 3-D aggregate cultures of the ASCs at a density of 250,000 ASCs/aggregate. To form the aggregates, the cells were centrifuged at 300 xg for 5 min in 15 mL vented cap conical tubes and cultured for 48 h in proliferation medium. The cells were then transferred into chondrogenic differentiation medium comprised of DMEM:Ham's F12 supplemented with 10% FBS, 50 μ g/mL ascorbic acid, 6.25 mg/mL human insulin, 100 nM dexamethasone, 10 ng/mL transforming growth factor β 1 (TGF- β 1) and 1% pen-strep for an additional 28 days. Non-induced

aggregates cultured in proliferation media were included as a negative control. Chondrogenic differentiation was assessed through immunohistochemical (IHC) staining for collagen II. For this analysis, the cell aggregates were embedded in Tissue-Tek OCT compound (Sakura Finetek), cryo-sectioned (7 μm sections), and stained with collagen II anti-rabbit primary (1:200; cat. # ab34712; Abcam) following the methods described in section 3.4.5.7. The samples were mounted in DAPI fluoroshield mounting medium and imaged with an EVOS® FL Imaging microscope. No primary antibody controls were included to confirm staining specificity.

3.4.9 Subcutaneous implantation of cell-assembled and pre-assembled DAT bead foams in an athymic mouse model

All studies followed the Canadian Council on Animal Care (CCAC) guidelines and were reviewed and approved by the Animal Care Committee at The University of Western Ontario (Protocol #2015-049).

3.4.9.1 DAT bead foam fabrication

Cell-assembled bead foams were fabricated as described in Sections 3.3.1 and 3.3.3.1, using the transduced ASCs as described in section 3.3.8. To fabricate the pre-assembled bead foams, DAT beads were produced as described in section 3.3.1 and allowed to thaw immediately following electrospraying. Excess water was then removed, and the thawed beads were gently transferred into cylindrical moulds (diameter = 8 mm, height = 5 mm), frozen at -80°C , and lyophilized. The resulting pre-assembled bead foams were decontaminated and gradually rehydrated through an ethanol series (100%, 90%, 75%, 50%, 25%, and 12.5% (v/v) diluted with sterile PBS), followed by three washes in sterile PBS. The rehydrated scaffolds were stored at 4°C for up to 1 week. Prior to seeding, the rehydrated bead foams were incubated overnight in complete proliferation media (DMEM:F12 with 10% FBS, 100 U/mL penicillin and 0.1 mg/mL streptomycin). Each DAT bead foam was seeded with 3×10^5 P4 transduced ASCs in 20 μL of complete medium, to match the cell density within the cell-assembled bead foams. Following 1 h incubation, the complete medium was topped up to 1.5 mL and the scaffolds were incubated for an additional 24 h (2% O_2 and 5% CO_2 , 37°C).

To confirm that similar cell numbers were present on both types of scaffold prior to implantation, scaffolds were rinsed in PBS (twice; 2 min), submerged into a solution of D-luciferin dissolved in PBS (1.2 mg/mL; Syd Labs Inc., Natick, MA, USA), and an IVIS Lumina XRMS with optical-X-ray system (Perkin Elmer, Hopkinton, MA, USA) was used to image Fluc2 enzymatic activity. BLI images were captured until a peak BLI signal was obtained, up to 5 minutes after the start of the incubation and measured as an average radiance (photons/second/cm²/steradian).

3.4.9.2 Subcutaneous implantation surgery

Cell-assembled and pre-assembled DAT bead foams were implanted subcutaneously in female Crl:NU-Foxn1nu mice (nu/nu mice; Strain Code 088, Charles River, Wilmington, MA, USA) as described in previous work [264]. Briefly, the mice were anaesthetised with isoflurane and given subcutaneous injections of metacam (2 mg/kg loading dose; 1 mg/kg follow up dose at 24 h; Boehringer Ingelheim, Burlington, ON, Canada) and bupivacaine (2 mg/kg; Aspen Pharmacare, Toronto, On, Canada). Bilateral paraspinal incisions (~1 cm) were made on the dorsum and subcutaneous pockets were created on each flank, below the panniculus carnosus. Two bioscaffolds were implanted per animal (one per flank; positioning of experimental groups was randomized) and the incisions were closed with surgical staples.

3.4.9.3 Cell tracking

BLI was performed using an IVIS Lumina XRMS *In Vivo* Imaging System (PerkinElmer, Waltham, MA, USA). At postoperative days 0, 2, 4, 7, 14, 21, and 28, mice were anesthetized with isoflurane and received a 100 µL intraperitoneal injection of D-luciferin (30 mg/mL; Syd Labs Inc.). BLI images were captured for up to 90 minutes after injection, measured as an average radiance and reported as a percentage normalized on data at day 0 (photons/second/cm²/steradian).

3.4.9.4 Immunohistochemical analysis of scaffold explants

The animals were sacrificed by CO₂ overdose at 28 days post-implantation. The scaffolds were carefully excised within their surrounding tissues and fixed in 10% buffered formalin overnight at 4°C. The next morning, the explants were rinsed three times in PBS (20 min

each) and then subjected to a sucrose gradient (10%, 20%, 30% sucrose in PBS; incubated 8 to 16 hours in each solution). Explants were then embedded in OCT and stored at -20°C until cryo-sectioning ($7\ \mu\text{m}$ transverse sections).

After PBS incubation and blocking (10% goat serum and 0.2% tween diluted in TBS), immunostaining was performed to identify murine endothelial cells (antigen: CD31, ab28364, Abcam) in combination with localization of the transduced human ASCs using the endogenous tdT signal. CD31 staining was performed overnight at 4°C (1:200 in blocking solution, ab28364, Abcam). A secondary anti-rabbit antibody conjugated to Alexa Fluor 650 (dilution 1:100, ab96902, Abcam) was used for detection and nuclei were counter-stained using Fluoroshield mounting medium with DAPI (ab104139; Abcam). Cross-sections at 3 different depths were imaged per sample using an EVOS FL Cell Imaging System (Thermo Fisher Scientific). CD31 and tdT expression was quantitatively assessed through positive pixel counting within the entire scaffold cross-section using ImageJ, normalized to the total scaffold area ($n = 2\text{-}3$ scaffolds/trial, $N = 2$ trials with different donors).

3.4.10 Statistical Analyses

All data were expressed as the mean \pm standard deviation (SD) and analyzed by t-test or two-way ANOVA with Tukey's post-hoc comparison of the means. For the qPCR array analysis, a multiple t-test analysis with a false discovery rate correction of 5% was performed. Statistical analyses were performed using GraphPad Prism 7 (GraphPad, La Jolla, CA, USA) and differences were considered statistically significant at $P < 0.05$.

3.5 Results

3.5.1 DAT beads support attachment and survival of ASCs following dynamic seeding

The electrospraying process generated beads of varying diameter, with an average diameter of $819 \pm 265\ \mu\text{m}$ (Figure 3.1A). The beads were soft and compliant, with a Young's modulus of $0.35 \pm 0.14\ \text{kPa}$ (Figure 3.1B).

Using the established dynamic seeding regime in the spinner culture flasks, qualitative confocal imaging showed that viable ASCs were well distributed on the surface of the DAT

beads at 24 h after seeding (Figure 3.1C). The percentage of unadhered cells at 24 h was low, with ~2% living and ~3% dead cells detected in the media based on the initial seeding density (Fig. 3.1D).

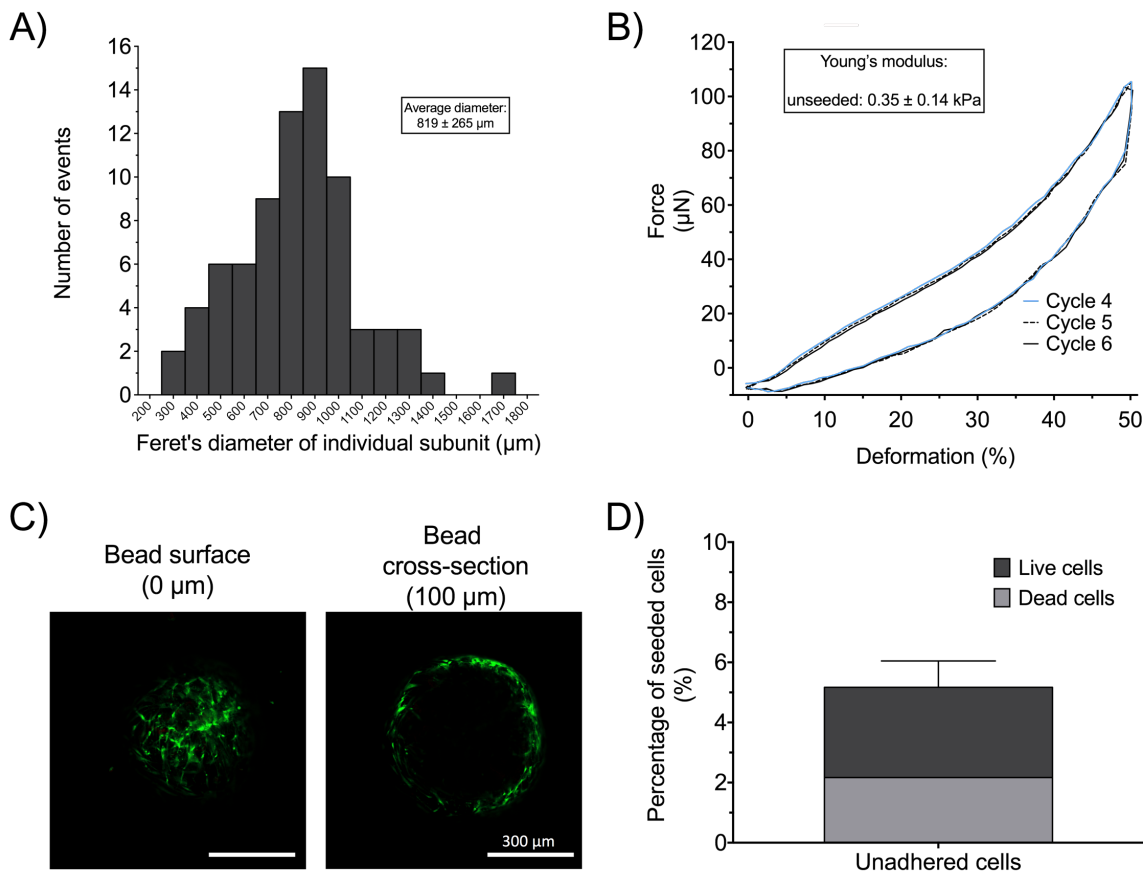


Figure 3.1: Soft and compliant DAT beads supported the attachment and survival of seeded human ASCs in a spinner culture flask system at 24 h after seeding. (A) Feret's diameter of the individual beads used to fabricate the foams prior to seeding (Pooled results: $n=25-28$ beads/trial, $N = 3$ trials with different ECM suspensions). (B) Representative force versus deformation curves for individual DAT beads prior to seeding. Data from 3 cycles are shown with compression at a strain rate of 0.01 s^{-1} . Young's moduli were calculated using nonlinear least squares curve fitting ($n=6$ beads/trial, $N=3$ trials with different ECM suspensions). Modulus represented as mean \pm SD. (C) Representative Live/Dead[®] staining at 24 h after seeding showed living cells in green, with no dead cells (red) visualized on the beads. Scale bars: 300 μm . (D) Percentage of unadhered cells at 24 h after seeding, based on the initial seeding density. (C-D) $n=3$ biological replicates/trial, $N=3$ trials.

3.5.2 The use of a chemically-defined media allows for the production of scaffolds with high cell viability

Following cell seeding, novel methods were established to synthesize robust and cohesive cell-assembled DAT bead foams. More specifically, the process involved 3 days of static culture within a mould, followed by 5 additional days of dynamic culture on an orbital shaker using Prime-XV base media freshly supplemented with A2P (Prime-XV+A2P), both with and without additional supplementation with recombinant human EGF, FGF-2, and IGF-1 (+GF). Representative macroscopic images of the resulting cell-assembled bead foams at day 8 are shown in Figure 3.2A. In general, the cell-assembled foams maintained the geometry defined by the cylindrical moulds. Scaffolds produced in both media formulations displayed excellent handling properties; however, the scaffolds generated in the +GF condition were macroscopically more cohesive and uniform.

The number of ASCs initially seeded into the moulds (day 0) and in the final cell-assembled bead foams (day 8) was estimated using a Picogreen® dsDNA assay (Figure 3.2B). In general, there were significantly more cells present in the cell-assembled foams at day 8 as compared to day 0, suggestive of cell proliferation. Further, there were significantly greater numbers of cells in the +GF cell-assembled foams as compared to the basal Prime-XV+A2P condition. Complementary Ki-67 staining showed the presence of proliferative cells within the constructs, with qualitatively higher densities of proliferative cells visualized closer to the scaffold boundaries in both groups. Figure 3.2C shows the staining patterns for the +GF condition at day 8, which was qualitatively similar to the basal Prime-XV+A2P media condition. While the cell density was qualitatively higher in the scaffold periphery, DAPI⁺ cells were well-distributed throughout the cell-assembled foams.

The viable, apoptotic, and primary necrotic ASC populations within the cell-assembled bead foams were quantified through flow cytometry analysis of annexin V and PI stained cells isolated from the scaffolds (Figure 3.2D-E; controls available in supplemental Figure 3.1). The cells were more than 95% viable in both media formulations, and higher viability in the basal media condition (Figure 3.2E). Although the expression of apoptotic and primary necrotic cell markers was low under all conditions studied, the frequency of apoptotic cell populations (as measured through positive annexin V staining) and primary necrotic cell populations (as measured through single propidium iodide staining) quantified

by flow cytometry was significantly higher in the +GF group, as compared to the basal media condition (Figure 3.2E).

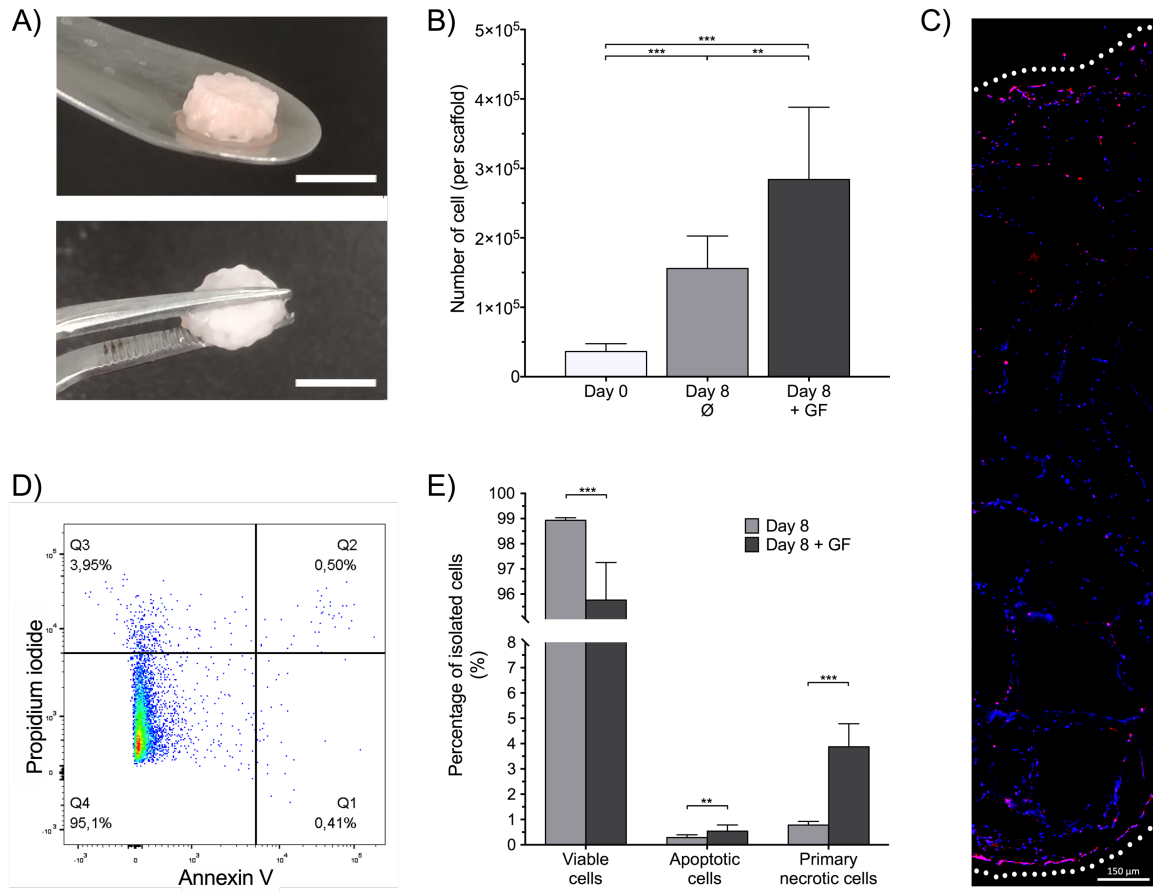


Figure 3.2: Cells were proliferating and were more than 95% viable within the cell-assembled bead foams. (A) The cell-assembled DAT bead foams were cohesive, structurally robust, and easy to handle, with geometries defined by the cylindrical moulds. (B) Picogreen® dsDNA assay results showed increased cell numbers within the cell-assembled bead foams from the + GF group at day 8 as compared to the basal Prime-XV+A2P medium condition at day 8 and the initial number of ASCs seeded into the moulds at day 0. (C) Representative Ki-67 immunostaining (red) showed a qualitatively higher distribution of proliferative cells close to the scaffold boundaries (white lines) after 8 days of culture. Nuclei are counterstained with DAPI (blue). Scale bar: 150 μ m. (D) Representative flow cytometry plot following cell isolation and staining for annexin V and propidium iodide at 7 days. (E) Analyzed flow cytometry results revealed high viability (>95%) in both groups, with significantly higher viability in the basal Prime-XV+A2P medium condition compared to the +GF group. (A-E) $n=3$ scaffold/trial, $N=3$ trials with different cell donors; ANOVA (B) with Tukey's post-hoc test or t-test (E); ** $P<0.01$, *** $P<0.001$.

3.5.3 The cell-assembled DAT bead foams remodel over the course of the 8-day fabrication process

The macroscopically-enhanced stability in the cell-assembled foams fabricated in the +GF conditions was consistent with the contraction data measurements (Figure 3.3A and B), which showed that contraction was significantly higher in the +GF conditions as compared to the basal Prime-XV+A2P medium. As expected, an inverse relationship was observed between scaffold contraction and porosity, with significantly lower porosity in the +GF condition (Figure 3.3C).

The physical differences observed between the two groups also suggested that the cell culture conditions had an impact on scaffold remodelling. To further characterize this remodelling, quantification of total sulphated GAG content revealed higher levels of GAG in the cell-assembled bead foams at day 8 relative to the seeded and unseeded beads at day 0. Significant differences were also observed between the day 8 + GF and basal media conditions, with significantly higher GAG levels in the + GF group (Figure 3.3D). Total hydroxyproline content, indicative of the total collagen content, was similar in all of the groups investigated (Figure 3.3E). Zymographic analysis of the proteolytic enzymatic activity of gelatinases was also performed as an indicator of matrix remodelling (Figure 3.3F). When normalized to an MMP-2 standard, increased gelatin degradation and protease activity was noted in the + GF condition at day 8 as compared to the basal media condition.

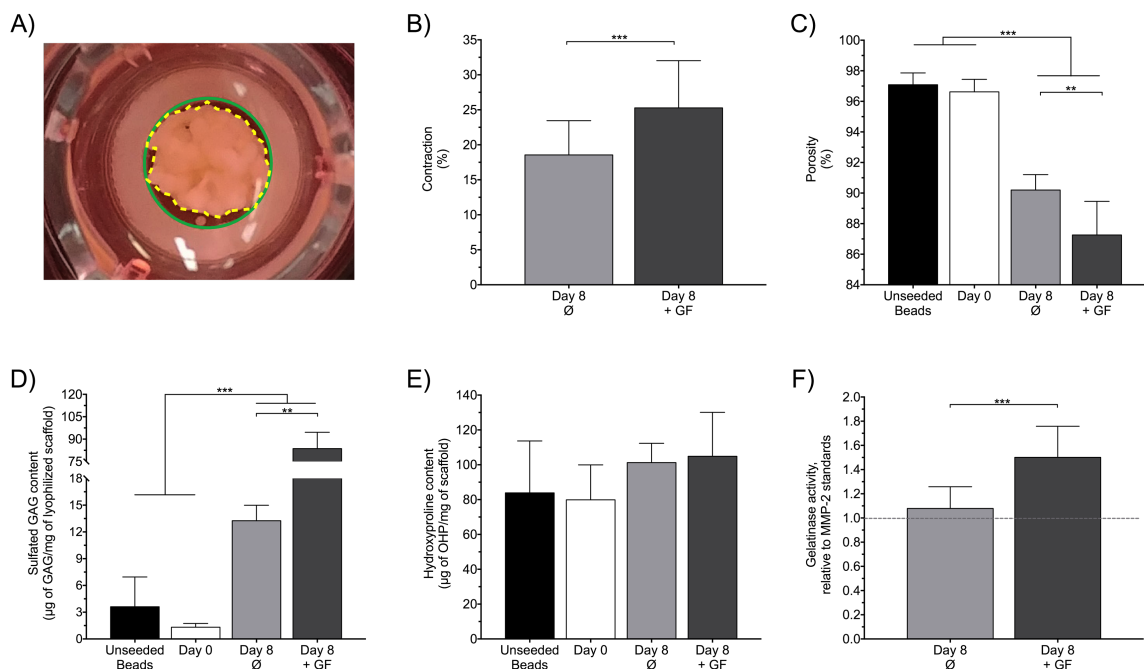


Figure 3.3: The cell-assembled DAT bead foams remodelled over the course of the 8-day fabrication process. (A) Representative macroscopic image of a contracted scaffold. The green line represents the original area occupied by the beads in the mould at day 0, while the yellow dotted line represents the contracted scaffolds after 8 days of culture. The inner diameter of the silicone ring forming the mould measures 8 mm. (B) Contraction measurements at day 8 showed enhanced contraction in the + GF culture condition (n=15-18 replicates per donor, N=3 donor). (C) Porosity results obtained using a modified Archimedes' method showed a significant reduction in porosity in the day 8 + GF condition compared to all other conditions (n=3 replicates per donor, N=3 donor). (D) DMMB assay showing significantly higher levels of sulphated glycosaminoglycans in the day 8 + GF condition as compared to all other groups. (E) Total hydroxyproline content as a measure of the total collagen content showing no significant differences between the groups. (F) Densitometry analysis of gelatinase enzymatic activity, relative to MMP-2 standards, displayed increased activity in the day 8 +GF group. (B-F) n=3 scaffolds/trial, N=3 trials with different cell donors; t-test (B-F) or ANOVA (C-D-E) with Tukey's post-hoc test; ** $P < 0.01$, *** $P < 0.001$.

3.5.4 The cell-assembly process is mediated by new ECM synthesis

To gain insight into the mechanisms of the cell-assembly process, immunohistochemical staining for type I collagen and fibronectin were performed on scaffold cross-sections. As shown in Figure 3.4, newly synthesized type I collagen and fibronectin (both in red; Figure 3.4) were localized in the cell-dense regions between the beads (blue, pre-labelled with Alexa Fluor 350® succinimidyl ester; Figure 3.4), suggesting that the ASCs were actively secreting ECM that functioned to fuse the beads together.

3.5.5 The culture conditions modulated ASC gene and protein expression within the cell-assembled bead foams

An RT-qPCR array was performed to investigate the expression of genes associated with ECM synthesis and remodelling, angiogenesis and inflammation in the human ASCs within the cell-assembled bead foams after 8 days of culture (Figure 3.5). Consistent with the previous results, the majority of the markers for ECM synthesis and remodelling showed increased mRNA levels in the +GF condition as compared to the basal Prime-XV+A2P medium group. The levels of gene expression of the proteoglycans biglycan (*BGN*), decorin (*DCN*), and versican (*VCAN*) were significantly upregulated in the +GF samples, consistent with the enhanced total sulphated GAG content in this group (Figure 3.3). mRNA levels of the ECM synthesis and remodelling genes smooth muscle actin alpha 2 (*ACTA2*), collagen type I alpha 1 chain (*COL1A1*), collagen type III alpha 1 chain (*COL3A1*), connective tissue growth factor (*CTGF*), and matrix metalloproteinase 1 and 2 (*MMP1* and *MMP2*, respectively) were significantly increased in the +GF samples, consistent with the enhanced MMP activity, enhanced scaffold contraction, and ECM synthesis observed (Figures 3.3 and 3.4). The modulation of the angiogenic markers was more complex, with increased levels of *IGF1* and *VEGFA*, along with decreased levels of *FGF2* and *SERPINE1*, in the +GF group. Interestingly, a trend for enhanced expression of genes associated with the immunodulatory functionality of ASCs was observed in the +GF group, although the differences were only statistically significant for colony stimulating factor 2 (*CSF2*), which could potentially be due to cell donor variability.

Expression of a selected set of pro-angiogenic factors at the protein level was also investigated using a Luminex® magnetic bead assay to probe bead and bead foam lysates, at day 0 and day 8 respectively. (Figure 3.6). For the four pro-angiogenic factors

investigated, angiopoietin-1, CXCL12, HGF, and VEGF, the protein levels were increased in both groups at day 8 when compared to freshly-seeded beads at day 0. Consistent with the RT-qPCR array findings, varying patterns of expression were observed between the two experimental groups at day 8. More specifically, a significant decrease in CXCL12 levels and a significant increase in VEGF levels were observed in the +GF group relative to the basal media conditions, with no differences observed in the relative expression levels of angiopoietin-1 (ANGPT1) or HGF between the groups. Overall, the findings suggest that preconditioning with the growth factors did not substantially alter the expression of the investigated pro-angiogenic factors in the ASCs within the cell-assembled bead foams.

3.5.6 Human ASCs co-expressing Fluc2 and tdT maintain their trilineage differentiation capacity

To enable *in vivo* cell tracking, the scaffolds were prepared with human ASCs that had been transduced with lentiviral vectors to constitutively express Fluc2 and tdT prior to *in vivo* experimentation. To confirm that the transduction process did not alter the capacity of the ASCs to differentiate towards the chondrogenic, adipogenic, and osteogenic lineages, trilineage differentiation assays were performed. For all three lineages, the cells were confirmed to retain their capacity to differentiate based on characteristic marker expression (Supplementary Figure 3.2).

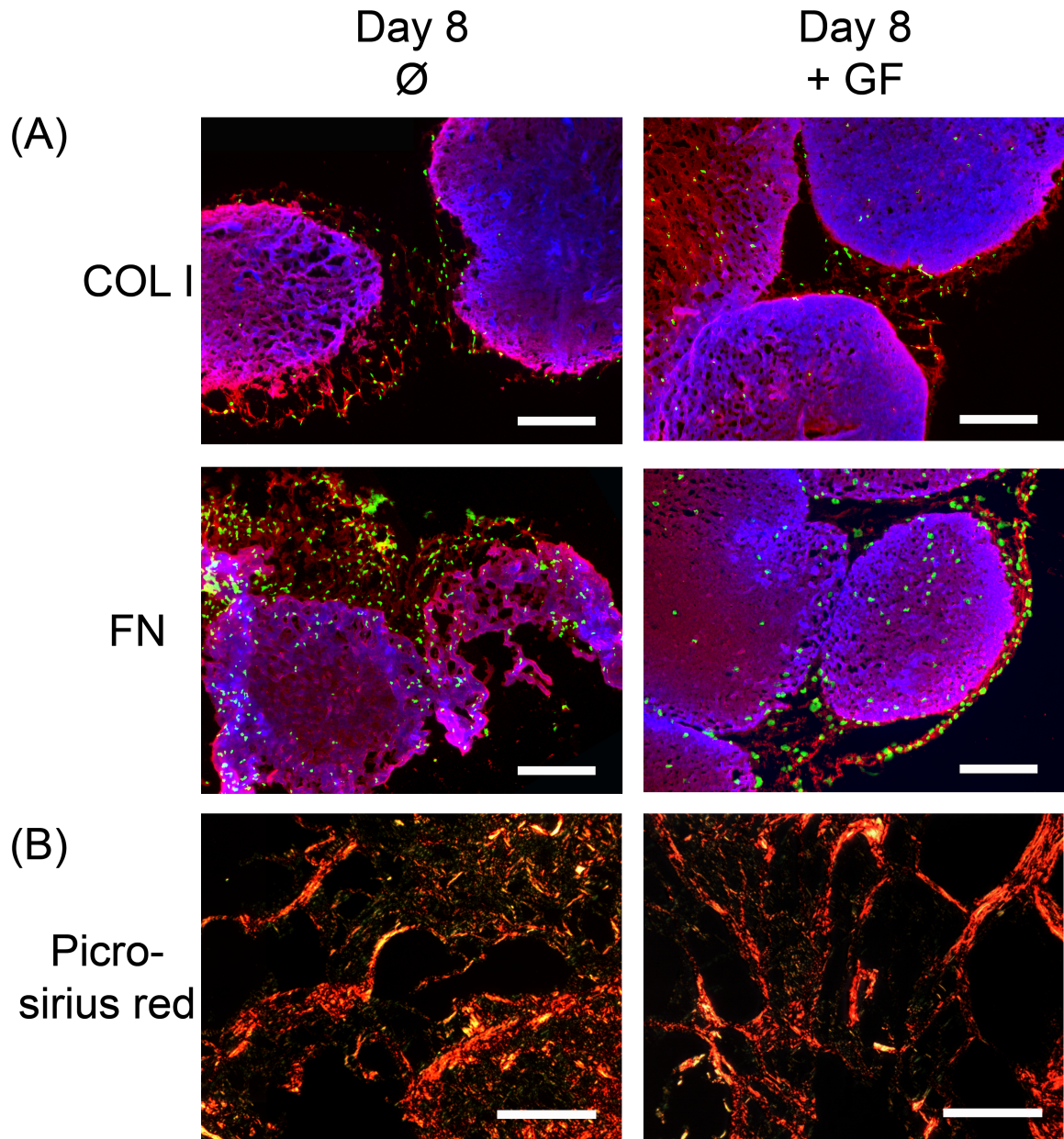


Figure 3.4: Cell-assembly was mediated through ECM synthesis. (A) Representative scaffold cross-section showed abundant expression of newly-synthesized collagen type I and fibronectin in the cell dense region (nuclei shown in green) between two DAT beads in the cell-assembled bead foams after 8 days of culture. The DAT beads were pre-labelled with an Alexa Fluor 350® succinimidyl ester, to distinguish the newly-synthesized COL I and FN (red) from the pre-existing ECM in the DAT (blue). (B) Picrosirius red staining showed interconnected networks of collagen fibers of varying sizes in both groups. Scale bar = 200 μ m. Abbreviation: COL I = collagen type 1, FN = fibronectin.

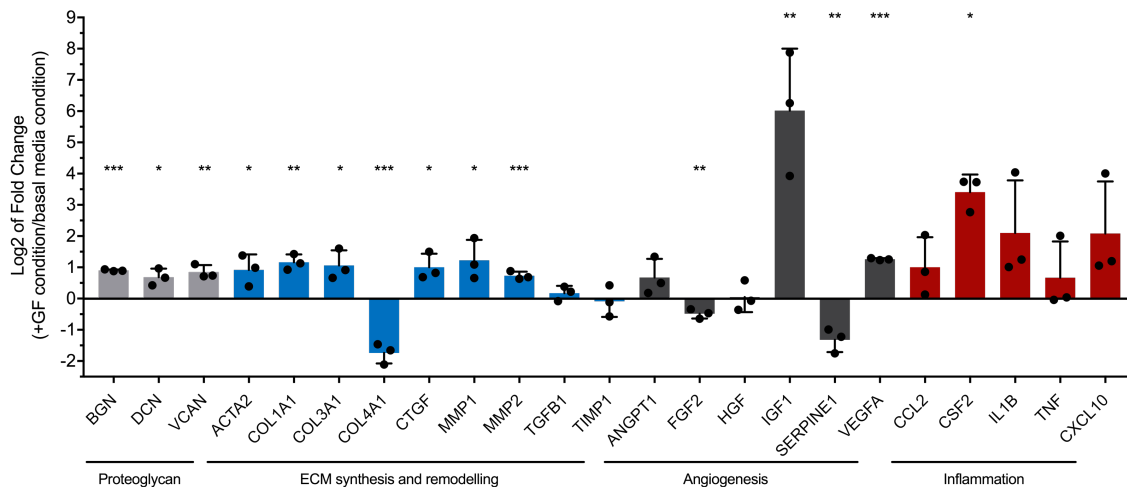


Figure 3.5: ECM-associated gene expression was modulated by growth factor preconditioning in ASCs within the cell-assembled bead foams. Gene array results represented as a Log2 of the fold change of +GF condition over the basal media condition, where positive values represent higher mRNA levels in the +GF group and negative values represent higher mRNA levels in the basal group. mRNA levels of most of the genes associated with ECM synthesis and remodelling, including proteoglycans, were significantly increased in the +GF condition. Four genes associated with angiogenesis were also significantly modulated, with varying patterns between the experimental groups. Globally, inflammatory gene markers appeared to increase in the +GF group, although the difference was only significant for *CSF2*. n=3 scaffolds pooled/trial, N=3 trials with different cell donors; multiple t-test analysis with a false discovery rate correction of 5%; * $P < 0.05$, ** $P < 0.01$, *** $P < 0.001$.

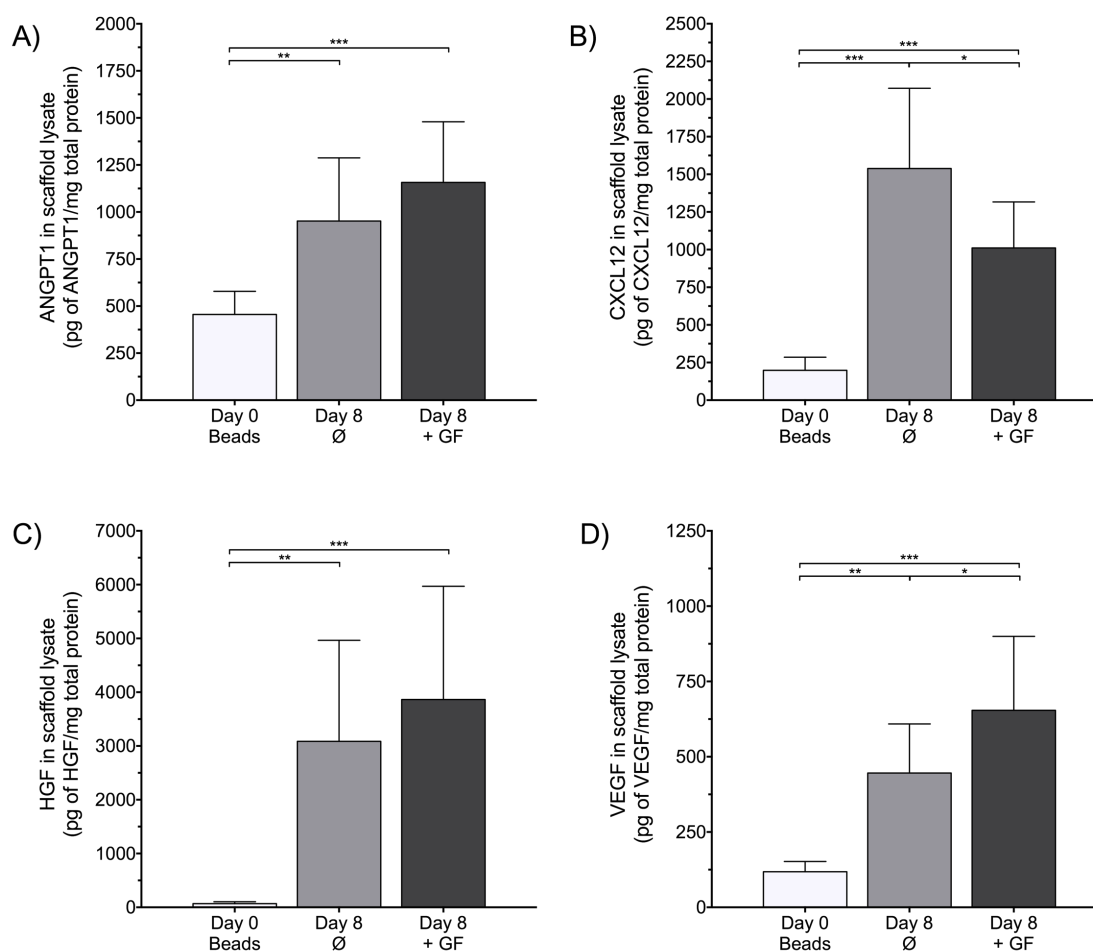


Figure 3.6: The cell-assembly fabrication process increased the expression of pro-angiogenic proteins by the ASCs, compared to freshly-seeded beads. Protein levels of (A) ANGPT1, (B) CXCL12, (C) HGF, and (D) VEGF were quantified in bead and bead foam lysates using a Luminex® magnetic bead assay at day 0 (24 hours after seeding) and day 8. Results are reported relative to the total protein content. Significantly lower levels of CXCL12 and higher levels of VEGF were observed in the day 8 +GF group compared to the basal media condition. Abbreviations: ANGPT1= angiopoietin-1, CXCL12= chemokine with C-X-C motif ligand 12, HGF= hepatocyte growth factor, VEGF= vascular endothelial growth factor. n=3 scaffolds/trial, N=3 trials with different cell donors; one-way ANOVA with Tukey's post-hoc test; * $P < 0.05$.

3.5.7 The cell-assembled bead foams show enhanced detection of viable ASCs at early timepoints and greater murine CD31⁺ cell recruitment at 28 days

The cell-assembled bead foams fabricated using the +GF condition were selected for further analysis *in vivo* due to their improved stability and handling properties, as well their enhanced cell density relative to the scaffolds fabricated in the basal Prime-XV+A2P media conditions. *In vivo* ASC retention and murine CD31⁺ cell recruitment were compared relative to ASCs statically seeded at the same density on our previously-established pre-assembled DAT bead foam platform [14, 264] in a subcutaneous implant model in athymic nude mice. Transduced ASCs were used in this study to enable long-term *in vivo* cell tracking through BLI imaging using a luciferase reporter, as well as ASC localization within tissue cross-sections using the tdT reporter. Based on analysis of tdT expression by flow cytometry, the average transduction efficiency was $\sim 74.7 \pm 5.2\%$ at passage 3 and $\sim 75.5 \pm 4.4\%$ at passage 4 when seeded on scaffolds. BLI measurements of both type of scaffold were performed *in vitro* and showed similar number of viable cells at day 0 prior to implantation (Supplementary Figure 3.3A and B).

The BLI results showed an increase in signal in the cell-assembled bead foams at day 2 compared to day 0, suggesting there may be enhanced delivery of the luciferin or potentially an increase in live cell numbers in this group in the early phase following implantation (Figure 3.7A). When comparing the two scaffold groups together, the BLI results indicated that the number of viable ASCs was significantly higher in the cell-assembled bead foam group at day 2. While the trend for enhanced detection of viable ASCs in the cell-assembled bead foams continued at days 4 and 7, variability was observed and the difference between the groups was not statistically significant. Data from the later timepoints suggested that both platforms contained similar numbers of viable ASCs, which was corroborated by tdT⁺ cell counts within tissue cross-sections from the implants collected at 28 days (Fig. 3.7B and C). Overall, both platforms were effective at supporting the localization of viable ASCs within the implant site over the 4-week study.

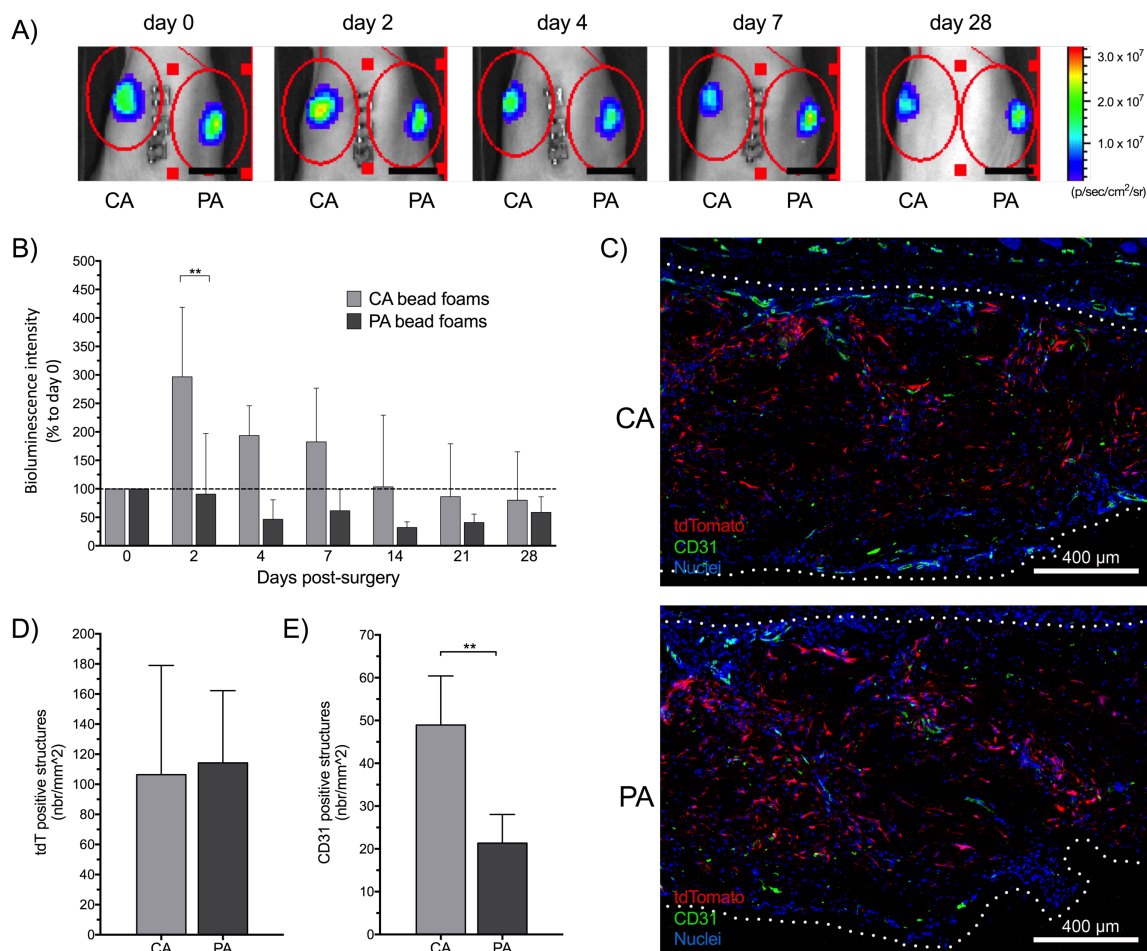


Figure 3.7: Early human ASC retention, as well as murine CD31⁺ cell recruitment at 28 days, was enhanced within the cell-assembled (CA) DAT bead foams as compared to ASCs seeded and delivered on pre-assembled (PA) DAT bead foams. (A) Representative macroscopic and bioluminescence images (superposed) from a mouse with cell-assembled (left) and pre-assembled (right) implants at day 0, 2, 4, 7, and 28. Scale bars = 1 cm. (B) Relative bioluminescence intensity levels, expressed as a percentage of the levels at day 0, suggesting that early cell retention was enhanced in the cell-assembled bead foams. (C) Representative CD31 immunostaining (green) and tdT endogenous signal (red) in explanted scaffolds at day 28, showing qualitatively enhanced CD31⁺ cell infiltration in the cell-assembled bead foams (top) compared to the pre-assembled bead foams (bottom) at 28 days post-implantation. Nuclei were counter-stained with DAPI (blue), and the white dotted lines denote the scaffold periphery. Scale bars = 400 μ m. (D) Quantification of tdT⁺ structures on cryo-sections indicating both that both groups show similar human ASC retention at day 28. (E) Quantification of CD31⁺ structures on cryo-sections suggesting that angiogenesis was enhanced in the cell-assembled bead foam group at day 28. Abbreviations: CA = cell-assembled bead foams, PA = pre-assembled bead foams. n=2-3 scaffolds/trial, N=2 trials with different cell donors; two-way ANOVA with Tukey's post-hoc test (B) or t-tests (D-E); ** $P < 0.01$.

Macroscopic observation of the explants showed that all scaffold integrated within the host tissues (Supplementary Figure 3.3C). Immunohistochemical analysis of the implants also revealed the presence of murine CD31⁺ cells distributed heterogeneously at the scaffold-tissue interface in both groups, with CD31⁺ structure counts indicating that there were more CD31⁺ cells in the cell-assembled bead foams (Figure 3.7B and D), suggesting there was enhanced angiogenesis within this implant group.

3.6 Discussion

While DAT can be applied in its intact form as a 3-D cell-instructive scaffold for adipose tissue engineering applications [104], DAT can also be further processed to incorporate the complex ECM composition within alternative formats that may offer greater flexibility in terms of other scaffold properties [13, 14, 119, 131, 134-136, 264]. Numerous studies have reported on the pro-adipogenic effects of a wide variety of DAT-based bioscaffolds both *in vitro* and *in vivo* [13, 14, 119, 131, 134-136, 264], which support the use of DAT as a platform for soft tissue regeneration in plastic and reconstructive surgery. Of note, our previous findings also indicate that our pre-assembled DAT bead foams promoted cell survival and angiogenic marker expression in human dermal fibroblasts, which would be favorable for enhancing implant integration and remodelling into host-derived soft tissues [264]. In the current study, we sought to harness these benefits in the design of novel scaffolds that were more structurally robust and compatible with maturation under dynamic culture conditions [135], in order to achieve a high density of viable cells with pro-angiogenic functionality that were well distributed throughout the scaffolds.

The soft and compliant DAT beads, which had an average Young's modulus in the range of human skin (0.1 kPa to 10 kPa [251]), readily supported ASC attachment and survival under the established seeding regime [135]. In developing the new cell-assembly process, the culture conditions were selected to promote ASC expansion, as well as ECM synthesis and remodelling. By using our novel approach, it was possible to fabricate robust ~3-mm thick cell-assembled DAT bead foams containing an average of 3×10^5 ASCs within a total culture period of 9 days. Despite the thickness of the scaffolds, ASC viability was high (>95%) in all conditions. Notably, ASCs have been shown to be highly tolerant of hypoxic and ischemic microenvironments *in vitro* and *in vivo* [175, 274], and have been reported to adopt a more pronounced pro-angiogenic [215, 216] and pro-immunomodulatory

phenotype [275] in environments with oxygen tension below 5%. This resilience and adaptability to hypoxia, along with their ability to secrete pro-angiogenic molecules [276, 277], makes ASCs a highly promising cell source for promoting the vascularization of biomaterial implants.

We selected the Prime-XV® MSC EXPANSION XSFM as our basal media, based on previous observations in our lab that it promoted both ASC expansion and matrix deposition. Further, the cell-assembly approach exploited the recognized ability of ASCs to synthesize ECM upon stimulation with A2P *in vitro* [271, 272], with the cells forming new ECM enriched in collagen type I [278], fibronectin [278], and sulphated glycosaminoglycans [279] that functioned to fuse the beads together to create the cell-assembled bead foams. Interestingly, supplementation with recombinant human EGF, FGF-2, and IGF-1 was shown to be advantageous, resulting in an increased cell number and improved scaffold cohesion. Results indicated that the modular assembly was mediated by the presence of newly synthesized ECM, along with ECM remodelling, within the cell-assembled bead foams. Overall, these findings are in line with previous studies investigating the effects of these three growth factors. For example, all three growth factors have been reported to have cytoprotective and proliferative effects on MSCs [218, 219, 224-226, 268]. In addition, EGF and IGF-1 treatments have both been previously shown to increase the secretion of MMPs by ASCs [226, 268]. Further, EGF treatments were also shown to stimulate the secretion of proteoglycans such as decorin and endocan, as well as other proteins associated with ECM synthesis and remodelling including connective tissue growth factor (CTGF) and tissue inhibitors of matrix metalloproteinases (TIMPs) [268]. Moreover, FGF-2 preconditioning has been indicated to stimulate a pro-fibrotic phenotype in MSCs, which is consistent with the increased ECM secretion and remodelling observed in the +GF group [218, 225].

The qualitatively enhanced integrity of the scaffolds fabricated in the +GF conditions was consistent with the increased contraction and decreased porosity observed in this group compared to the basal media conditions. These physical changes may have impeded the diffusion of nutrients into, as well as the removal of waste from, the central regions of the scaffolds, which could in turn explain the slightly reduced viability in the +GF condition. However, accounting for these differences in viability, a significantly higher number of

viable cells were present in the cell-assembled bead foams when the growth factor preconditioning strategy was applied (~1.8-fold increase). Further, the *in vivo* results support that the contracted scaffolds did not function as a barrier for cell migration, but integrated well into the host tissues and supported the infiltration of host endothelial cells required for implant vascularization.

The angiogenic gene and protein expression data supported that the ASCs secreted a range of pro-angiogenic growth factors on the cell-assembled bead foams, regardless of whether the scaffolds were fabricated in the +GF or basal media conditions. This data reveals that, while there is variation in expression between the groups, there is no clear evidence that the +GF preconditioning had a benefit in terms of modulating the expression of the pro-angiogenic factors that were assessed in the current study. Interestingly, there was a clear trend towards the enhanced expression of immunomodulatory genes in the +GF conditions, although the differences were only significant for the *CSF2* gene, which could potentially be due to cell donor variability. There is a growing body of evidence that immunomodulation is an important mechanism of regeneration in ASC-based therapies [126, 209, 275]. As such, it would be interesting to further probe these factors at both the gene and protein levels in future studies incorporating a larger number of donors.

To date, the vast majority of studies evaluating biomaterial-based cell delivery strategies in preclinical models have relied on endpoint histological evaluations to assess cell retention. Popular approaches include the use of human-specific markers [249, 264] or cell tracker dyes that necessitate pre-labelling prior to implantation [280]. Limitations of these approaches include their inability to specifically identify viable cells, they do not allow for longitudinal tracking, and they require a large number of animals to perform long-term assessments [249, 264]. Further, they require the analysis of several cross-sections, which can introduce substantial variability in the analysis due to variability of the cell distribution across the depth of the scaffolds [249, 264]. Lipophilic membrane stains have been widely used, but the signal diminishes as the cells divide and results can be confounded by macrophage-mediated phagocytosis of the cells, as well as dye release and uptake by other cell populations [280].

Addressing many of these limitations, non-invasive cell tracking technologies using engineered cells represent an exciting alternative approach to enable long-term *in vivo*

tracking of viable cell populations, and are therefore an extremely valuable tool in comparing the efficacy of various biomaterial delivery platforms. In the present study, human ASCs were transduced to co-express Fluc2 and tdT reporters in order to perform longitudinal *in vivo* cell tracking studies using BLI imaging, as well as endpoint ASC localization within tissue cross-sections [270]. Interestingly, data from the present study suggests that the seeded ASCs remained within the bioscaffold area throughout the duration of the study, based on both BLI cell tracking and endpoint histological analyses. These results are in contrast with a previous study in which transduced human ASCs were delivered subcutaneously within a fibrin gel, showing broad distribution after implantation and up to 19 days post-procedure, with signals coming from the liver and, to a lesser extent, the lungs [281]. Transduced human ASCs delivered intramuscularly in PBS into the hindlimbs in BALB/c nude mice were also shown to have a small subset of cells migrating out of the injection site and distributing throughout the body, with an estimated 10% of the cells remaining 4 weeks after injection and stabilizing up to 32 weeks [282]. Other studies where transduced human ASCs were delivered downstream of femoral artery excisions in a hindlimb ischemia model [283] and in the peri-infarct region of a murine model of myocardial infarction [284] revealed an estimated cell retention of 5% at day 28 and 40% at 2 weeks, respectively. While varying models have been explored, the findings in the current study suggest that the DAT-derived bead foams provide a cell-supportive platform for localized ASC delivery within the subcutaneous space.

While providing interesting insights on the biodistribution of the ASCs over the course of the study, it is important to note that there are challenges associated with the dependence of BLI imaging on the delivery of the substrate and local oxygen concentration for imaging [285]. Although these two variables can impact the BLI readings, it has been shown that BLI can be applied effectively as an imaging modality in poorly vascularized areas, such as downstream of a femoral artery ligation, where blood perfusion can be reduced to < 15% of that in control limbs [283]. In the present study, the dependence on substrate and oxygen delivery may have affected the cell numbers detected, particularly at the earlier time points, due to the challenges in delivering the luciferin to the innermost portions of the implants, particularly after the local vascular network may have been disrupted by the implantation surgery. Regardless, BLI provides a useful tool to monitor the relative number of cells detected within the implants over time and compare the values between our two platforms

[285]. Further, it would be expected that this modulation in signal intensity would decrease over time, as the implants became more vascularized and improved the delivery of the substrate and oxygen.

The *in vivo* data showed an enhanced detection of viable ASCs in the cell-assembled bead foams relative to the pre-assembled bead foams at early timepoints, but this difference diminished over time. In addition, the IHC analysis of CD31⁺ structures as a marker of murine endothelial cell infiltration within the implants suggested there was increased angiogenesis in the cell-assembled bead foams. Knowing that the starting cell numbers were similar in both groups, these findings suggest that differences in early cell retention or alternatively in the composition and/or structure of the platforms may have impacted the angiogenic response. For example, the high concentration of sulphated GAGs detected in the cell-assembled bead foams may have contributed to the pro-angiogenic properties of these scaffolds, as GAGs are known to bind and sequester growth factors, and can also interact directly with endothelial cells through α_5 and α_v integrin interactions to modulate cellular processes involved in blood vessel development [33, 256]. The differences between the groups may also be attributed in part to the extended culture protocol employed in synthesizing the cell-assembled bead foams, which may have modulated the ASC phenotype and/or promoted the accumulation of beneficial paracrine factors within the scaffolds. However, further studies comparing the cell-assembled versus pre-assembled bead foams would be required to more fully assess the potential influence of these factors.

Regardless of the mechanisms, the data suggests that both platforms are favorable for supporting the localized delivery and retention of viable ASCs over 28 days, with the cell-assembled bead foams showing advantages in term of implant vascularization. The development of a stable vascular network is particularly important in the context of soft tissue engineering applications, where the need for new strategies to augment angiogenesis is recognized [74, 79]. Research in this field aims to develop tissue-engineered constructs with an intrinsic potential for therapeutic angiogenesis, as a means to avoid the failure of constructs due to poor vascularization resulting in associated cell death [74, 79]. Overall, the novel cell-assembled bead foams represent a promising bioscaffold format for ASC delivery in strategies to promote localized angiogenesis and soft tissue regeneration.

3.7 Conclusions

The cell-assembled DAT bead foams developed in the current study are a promising cell delivery approach for applications in soft tissue regeneration. The scaffolds fabricated with our novel methods were structurally robust and easy to handle, which would be favorable for clinical applications. Detailed *in vitro* studies confirmed that the cell-assembly process was mediated by the production of new ECM by the ASCs, enriched in collagen type I, fibronectin, and sulphated GAGs, which functioned to fuse the DAT beads into a cohesive 3-D network that held the shape of the fabrication mould. Notably, despite the thickness (~3 mm) of the constructs, cell viability remained high (>95%) after 8 days in culture, and the cell-assembled bead foams were shown to contain a well-distributed population of ASCs that secreted pro-regenerative paracrine factors. *In vivo* analysis confirmed the capacity of the DAT bead foams to support long-term viable ASC retention following subcutaneous implantation in a nu/nu mouse model, with an enhanced angiogenic response observed within the implant region with the new cell-assembled bead foams relative to when the ASCs were seeded and delivered on pre-assembled DAT foams. Overall, the cell-assembled DAT bead foams represent a promising pro-angiogenic MSC delivery platform for applications in soft tissue-engineering and therapeutic angiogenesis. Future work could assess the pro-regenerative effects of the cell-assembled bead foams in preclinical models of impaired wound healing or further explore the potential of these scaffolds for adipose tissue engineering by analyzing the response at later time points. In addition, the novel cell-assembly methods could be extended to other MSC populations and/or co-culture models, and the effects of varying the ECM source could also be explored to generate a diverse range of engineered tissues.

Chapter 4

4 The effects of matrix composition on the adipogenic differentiation of human adipose-derived stromal cells in cell-assembled matrix-derived bead foams

4.1 Co-authorship statement

The work presented in Chapter 4 was conceptualized in collaboration with Dr. Lauren Flynn. I personally designed and performed all of the experimental studies described in the Chapter, with technical support from:

- Ms. Courtney Brooks who helped to optimize the qPCR conditions (Figure 4.4C).

I analyzed all the data in collaboration with Dr. Flynn. I made all the figures. The manuscript was written in collaboration with Dr. Lauren Flynn.

4.2 Abstract

The extracellular matrix (ECM) of connective tissues is a three-dimensional environment that plays critical roles in mediating cellular behavior and cell fate. As such, it has been postulated that tissue-specific scaffolds derived from the ECM can mediate cell growth and direct stem cell differentiation. However, many studies to date do not include derived from non-tissue-specific ECM sources, making it challenging to interpret whether any observed effects are in fact tissue-specific. Building from the work in the previous chapter, the novel cell-assembly methods established with decellularized adipose tissue (DAT) were extended to fabricate tissue-specific cell-assembled bead foams derived from other compositionally distinct ECM sources. More specifically, decellularized trabecular bone (DTB) and purified collagen type I (COL) were selected to show the versatility of the approach with other decellularized tissues and commercially-sourced alternatives. The DAT, DTB, and COL beads used to make the foams had similar structural and biomechanical properties. Preliminary cell culture studies with human adipose-derived stromal cells (ASCs) confirmed that stable foams could be generated with all ECM sources using the cell-assembly approach. Analysis of adipogenic differentiation showed increased glycerol-3-phosphate dehydrogenase enzyme activity and adipogenic gene expression in the DAT- and COL-derived bead foams compared to the DTB-derived bead foams and tissue culture polystyrene controls. In addition, visualization of intracellular lipid through Bodipy® staining revealed differentiating adipocytes in the DAT- and COL-derived bead foams, but not in the DTB-derived group, suggesting that the bone-derived ECM may have inhibitory effects on ASC adipogenesis. Overall, the current study established that the cell-assembly approach using human ASCs can be used to generate robust three-dimensional scaffolds from a variety of ECM sources that may be useful as platforms for exploring the effects of ECM composition on stem cell differentiation.

4.3 Introduction

Comprised of a complex three-dimensional (3-D) network of proteins, glycoproteins, and polysaccharides, the extracellular matrix (ECM) can mediate cell function through its structural, biomechanical, and biochemical properties [16]. These properties vary from one connective tissue to another, with physical properties ranging from soft and compliant tissues, such as adipose tissue [113], to hard and stiff tissues, such as bone [286]. The biochemical composition of the ECM is also specific to each tissue, with immunohistological analysis showing that adipose tissue is an abundant source of collagen types I, IV, V, and VI, fibronectin, and laminin [60, 61]. In contrast, similar analysis of the organic phase of osseous tissue demonstrated that it is primarily comprised of collagen types I, III, IV, V, and XII, as well as fibronectin, glycosaminoglycans (GAGs), and specialized matricellular proteins, including osteocalcin (also known as bone gamma-carboxyglutamic acid-containing protein; BGLAP), osteonectin (also known as secreted protein acidic and rich in cysteine; SPARC), osteopontin (also known as secreted phosphoprotein 1; SPP1), and bone sialoproteins [65, 68, 69].

Due to the critical role of the ECM in mediating cellular functions, there has been increasing interest in the development of ECM-derived bioscaffolds for applications in tissue engineering and regenerative medicine. By removing immunogenic components from tissues (e.g. cells, intracellular organelles, and DNA), while preserving the structure and composition of the native ECM as much as possible, decellularization techniques have emerged as promising methods to obtain tissue-specific ECM [93, 94]. In recent proteomic analyses using high throughput mass spectrometry-based approaches to compare the composition of human decellularized adipose tissue (DAT) and human decellularized trabecular bone (DTB), it was shown that DAT incorporated higher levels of factors associated with adipogenesis, including fibroblast growth factors, chemokine (C-X-C motif) ligand 14 (CXCL14), and Wnt-11 [62], while DTB was enriched in factors associated with osteogenesis, including BMPs, insulin-like growth factor 2 (IGF-2), and TGF- β [62].

Based on these compositional differences, it has been widely postulated that tissue-specific ECM can be harnessed to promote the lineage-specific differentiation of stem and progenitor cell populations. For example, decellularized adipose tissue was shown to have (i) “adipo-inductive” and (ii) “adipo-conductive” properties on human adipose-derived stromal cells (ASCs), in both intact and further processed bioscaffold formats [14, 71, 104, 135]. These properties can be respectively described as (i) promoting adipogenesis in a microenvironment not typically supportive of adipocyte differentiation, and (ii) enhancing adipogenesis under adipogenic differentiation conditions. Similarly, DTB and DTB-derived biomaterials have been shown to have “osteo-inductive” and “osteo-conductive” effects on ASCs and other mesenchymal stromal cell (MSC) populations, such as bone marrow-derived mesenchymal stromal cells (BMSCs) [287].

When studying the inductive and conductive effects of a novel biomaterial, it is often difficult to identify the specific biomaterial properties that mediate cell fate and function. Multiple characteristics of ECM-derived scaffolds can influence cellular responses, including their structural, biomechanical, and biochemical properties. In particular, biomechanical properties have frequently been reported to impact the adipogenic and osteogenic cell differentiation balance *in vitro* [89, 90]. In studies with human MSCs and dermal fibroblasts, stiffer substrates were shown to stimulate differentiation towards the osteogenic lineages, while softer ones promoted differentiation towards the adipogenic lineage [89, 90]. Studies exploring the role of ECM composition often rely on comparisons to cell monolayers cultured on two-dimensional (2-D) surface coatings to draw their conclusions. However, it is widely recognized that cell behavior varies substantially in 2-D and 3-D systems [288] and these simplified 2-D models typically have highly different characteristics as compared to the biomaterials under investigation, which can profoundly impact the cellular response [87, 289].

With the goal of establishing robust platforms for exploring the effects of tissue-specific ECM composition on ASC differentiation, the cell-assembly methods established with the DAT in the previous chapter were extended to synthesize structurally-similar 3-D cell-assembled bead foams from compositionally distinct ECM sources. Due to the inverse relationship between adipogenesis and osteogenesis in MSCs [89, 90], DAT and DTB were selected as the primary ECM sources of interest. An additional compositional control of

purified collagen type I (COL) was included in the study to show the versatility of the fabrication approach with a commercially-available matrix source, as well as to broaden the analysis of the effects of the tissue-specific ECM composition. Following the validation of the fabrication methods for the new ECM sources, preliminary studies were conducted to probe the effects of ECM composition on the adipogenic differentiation of human ASCs within the cell-assembled DAT-, DTB- and COL-derived bead foam platforms.

4.4 Materials and methods

4.4.1 Decellularization of human adipose tissue

Human subcutaneous adipose tissue was obtained and processed as described in section 3.4.1.

4.4.2 Decellularization of bovine trabecular bone

Decellularization of trabecular bone was conducted following a 3-day decellularization protocol previously developed in the Flynn lab [290]. First, bovine trabecular bone was obtained from fused intervertebral discs in the tail region of 30-month old cows obtained from the Mount Brydges Abattoir, using a chisel and mallet, and cut into pieces (~ 2 mm x 2 mm x 2 mm). All the subsequent steps were performed at a reagent versus tissue ratio of 25 mL/g of tissue and all the decellularization solutions were supplemented with 1% antibiotic-antimycotic solution (Gibco, Burlington, ON, Canada) and 1% PMSF, with the exception of the enzymatic treatment steps where the PMSF was excluded. The bone fragments were rinsed in PBS for 20 min to remove blood, and then transferred into a hypotonic cell lysing solution (Solution A) comprised of 10 mM Tris and 5 mM EDTA. The tissue was then subjected to 3 freeze-thaw cycles (from -80°C to 37°C), with replacement of Solution A between each cycle. During the thawing step, the samples were agitated at 200 rpm to facilitate perfusion of the solution within the tissue. Following the freeze-thaw steps, decalcification of the tissue was performed by incubation in Formical 2000 (StatLab, Texas) at room temperature, 300 rpm, for 8 h. The processed bone was then incubated in 100% isopropanol overnight (200 rpm, 37°C). The next day, tissues were rinsed in Sorensen's phosphate buffer rinse solution (SPB rinse solution; 8 g/L NaCl, 200 mg/L KCl, 1g/L Na₂HPO₄, and 200 mg/L KH₂PO₄ (pH 8.0)) three times, 30 min each, at room temperature. Sorensen's phosphate buffer digest solution (SPB digest solution;

55 mM Na₂HPO₄, 17 mM KH₂PO₄, 4.9 mM MgSO₄·7H₂O) supplemented with 12.5 mg RNase Type III (from bovine pancreas), 15,000 U DNase Type II (from bovine pancreas) and 2,000 U Lipase type VI-S (from porcine pancreas) was then used to enzymatically digest the tissues (200 rpm, 37°C, overnight). The last day, the DTB was obtained following 3 additional rinses in the SPB rinse solution (30 min each, room temperature, 200 rpm), followed by two 30 min rinses in distilled H₂O, freezing at -80°C, and lyophilization.

4.4.3 Electro spraying of ECM suspensions

Lyophilized ECM samples, including type I bovine collagen (cat#5164, Advanced Biomatrix, San Diego, CA, USA) were finely minced, suspended into 0.2 M acetic acid, and homogenized (PowerGen Model 125 homogenizer, Fisher Scientific, Ottawa, ON, Canada). The homogenized suspensions were diluted with deionized water to obtain a final ECM concentration of 20 mg ECM/mL (dry weight). To increase the stability of the DTB suspension, a small proportion of COL was added as a stabilizer, resulting in a final ECM concentration of 20 mg ECM/mL (comprised of 17 mg/mL of DTB and 3 mg/mL of COL; dry weight). Electro spraying was then conducted as described in section 3.3.1 for the DAT and DTB suspensions, using of a 21G needle in place of a 25G needle for the DTB suspension, to prevent clogging attributed to the presence of some larger ECM particles that were more difficult to homogenize in this group. For the pure COL suspension, the applied voltage used was increased to 18-19 kV (as compared to 16-18 kV), with a lower extrusion speed of 30 mL/h (rather than 35 mL/h) to account for increased solution viscosity.

Following synthesis, ECM-derived beads were decontaminated and rehydrated through an ethanol series (100%, 99%, 98%, 95%, 90%, 80%, 70%, 50, 25%, and 12.5% (v/v) diluted with sterile PBS), followed by three washes in sterile PBS. The rehydrated beads were stored at 4°C before being used in the characterization and cell culture studies.

4.4.4 Human ASC isolation, expansion, and characterization

Collected human adipose tissue was processed within 2 h for ASC isolation following published protocols [12]. Isolated ASCs were cultured on tissue culture polystyrene (TCPS; Corning, NY, USA) at 37°C, 5% CO₂ in proliferation medium comprised of

DMEM:Ham's F12 (Wisent Bio Products, Montreal, QC) supplemented with 10% fetal bovine serum (FBS; Wisent Bio Products), 100 U/mL penicillin and 0.1 mg/mL streptomycin (Wisent Bio Products). Media was changed every 2-3 days. Cells were frozen at passage 0, stored in liquid nitrogen, and thawed when needed.

4.4.5 Physical and biochemical characterization of the individual ECM-derived beads

4.4.5.1 Bead diameter

Hydrated DAT, COL, and DTB beads were imaged under a light microscope at low magnification. The Feret's diameter function on ImageJ (NIH, <http://imagej.nih.gov/>) was then used to measure the largest diameter of the beads (N= 2-3 batch per conditions, n= 25 to 35 biological replicates per batch).

4.4.5.2 Mechanical Testing

The mechanical properties of individual ECM-derived beads were assessed using a CellScale MicroTester system (Waterloo, ON, Canada). Testing of individual beads was performed in a PBS bath at 37°C, using a 203 µm diameter cantilever attached to a square platen (2 mm x 2 mm), and the beads were compressed to 50% deformation for 3 preconditioning cycles at a strain rate of 0.01 s⁻¹ (1 cycle = 45 s compression, 1 s hold, 45 s recovery). The data was collected from 3 consecutive cycles and the Young's moduli were calculated using nonlinear least squares curve fitting with a published extended mechanics model for large elastic deformations of spherical microparticles [245] (N=2-3 batches per condition; n=6 beads/batch).

4.4.5.1 Porosity measurement

Samples of the rehydrated beads were lyophilized and weighed. After recording their dry mass, the scaffolds were immersed in 100% isopropanol overnight under light vacuum with gentle agitation to minimize the formation of air bubbles. Excess isopropanol was then removed through gentle blotting and the wet mass of the scaffold was recorded. Porosity was calculated using a modified Archimedes' method [246].

4.4.5.2 Scanning electron microscopy (SEM)

The ultrastructure of the DAT, COL and DTB beads was visualized by scanning electron microscopy (SEM) using published protocols [135]. Briefly, hydrated scaffolds were lyophilized and coated with osmium prior to imaging with a LEO 1530 scanning electron microscope at an accelerating voltage of 1 kV and working distance of 4 to 5 mm.

4.4.5.3 Picosirius red staining

Following rehydration, the ECM-derived beads were embedded in OCT and sectioned into 7- μ m thick cryo-sections. Picosirius red staining was performed, and stained bead cross-sections were visualized under circularly polarized light using a Nikon Optiphot microscope (Nikon, Mississauga, ON, Canada). Images were captured with an Infinity 2-3 CCD camera (Lumenera, Ottawa, Canada).

4.4.6 Production of cell-assembled DAT, COL, and DTB bead foams

Rehydrated DAT, DTB or COL beads were seeded as described in section 3.4.3.1 and scaffold assembly was performed as described in section 3.4.3.2.

4.4.7 *In vitro* adipogenic assessment

4.4.7.1 Adipogenic differentiation

Induction towards the adipogenic lineage was conducted following the 8-day cell-assembly protocol using an adipogenic induction medium comprised of DMEM/F12 supplemented with 33 mM biotin, 17 mM pantothenate, 10 mg/mL transferrin, 100 nM hydrocortisone, 66 nM human insulin, 1 nM triiodothyronine, and 1% pen-strep, with 0.25 mM isobutylmethylxanthine (IBMX), and 1 mg/mL troglitazone supplemented for the first 3 days only. Characterization of ASC differentiation within each ECM-derived scaffold was performed after 14 days of induction. Induced TCPS controls cultured in the differentiation media for 14 days and non-induced TCPS controls cultured in proliferation media were included in the studies.

4.4.7.2 Adipogenic Gene Expression

Total cellular RNA was isolated from the various ECM-derived cell-assembled bead foams and TCPS results at 0 and 14 days post-induction, as described in section 3.3.6. cDNA was then synthesized from 1 μ g of input RNA using the iScript™ Reverse Transcription Supermix kit (Bio-Rad; Cat. # 1708840) according to the manufacturer's protocol.

Amplifications were carried out in a CFX384 Touch™ Real-Time PCR Detection System (Bio-Rad) using SsoAdvanced Universal SYBR Green Supermix (Bio-Rad; 10 ng of cDNA/well) as follows: initial incubation at 95°C for 2 min, followed by 40 cycles of 95°C for 5 s and 58.5°C for 30 s. Three scaffolds from each cell line and each experimental group was run in technical triplicates for all the targeted genes: peroxisome proliferator-activated receptor γ (*PPARG*) and CCAAT enhancer-binding protein α (*CEBPA*). No template controls and no RT controls were included in all trials. The data was analyzed using the comparative Ct method with normalization to the geometric mean of two stable housekeeping genes, GAPDH and IPO8.

4.4.7.3 Glycerol-3-phosphate dehydrogenase (GPDH) enzyme activity assay

Intracellular GPDH enzyme activity was measured using a GPDH activity measurement kit (Kamiya Biomedical Corporation, Cat. # KT-010, Seattle, WA, USA) at 14 days after adipogenic induction. The data was normalized to total protein content using the Pierce 660 nm protein assay (Thermo Fisher Scientific, Oakville, ON, Canada).

4.4.7.4 Intracellular lipid staining

Intracellular lipid staining was performed using the lipophilic triglyceride-binding Bodipy® 493/503 staining reagent (Thermo Fisher Scientific) at 14 days post-induction of differentiation. Samples from the various ECM-derived bead foams and TCPS controls were rinsed in PBS twice (5 min each, 25 rpm, 37°C), prior to incubation in the staining solution (1:500 dye dilution in PBS+5% FBS, 1 h, at 37°C). Samples were then rinsed twice in PBS (5 min each, 25 rpm, 37°C) before imaging using a Zeiss Multiphoton LSM 510 META confocal microscope.

4.4.8 Statistical Analyses

All data were expressed as the mean \pm standard deviation (SD) and analyzed by one-way ANOVA with a Tukey's post-hoc comparison of the means. Statistical analyses were performed using GraphPad Prism 7 (GraphPad, La Jolla, CA, USA) and differences were considered statistically significant at $p < 0.05$.

4.5 Results

4.5.1 Beads derived from the three ECM sources have similar physical characteristics

Previously-established techniques for the fabrication of DAT-derived beads were adapted for the fabrication of beads derived from DTB and COL. By refining the electrospraying parameters tailored for each ECM suspension through systematically varying the voltage, extrusion speed, and needle size, spherical subunits or beads were successfully fabricated using the three ECM sources. The beads produced were characterized to confirm that varying the ECM source did not substantially alter the physical properties of the subunits used to fabricate the larger cell-assembled scaffolds.

SEM images revealed that DAT-, COL-, and DTB-derived beads were comprised of a complex network of fibers with a rough and porous surface (Figure 4.1A, top panel). Varying in texture and shape, the fibers from each group formed interconnected channels and pores, both at the surface (Figure 4.1A, top panel) and interior (Figure 4.1A, bottom panel) of the beads. Picrosirius red staining showed the presence of various sizes of collagen fibers, heterogeneously distributed in all groups (Figure 4.1B). Overall, qualitative assessments of the SEM and picrosirius red images did not show any obvious differences between the groups.

Analysis of the hydrated bead diameter revealed similar average size ranges for the electrosprayed beads, with an observed average Feret's diameter of $820 \pm 265 \mu\text{m}$, $1163 \pm 499 \mu\text{m}$, and $955 \pm 486 \mu\text{m}$ for the DAT, COL, and DTB beads respectively (Figure 4.2A). However, the size distribution for the COL and DTB beads appeared to be qualitatively broader as compared to the DAT beads, which may be related to the greater

challenges that were encountered in electrospraying these suspensions due to their increased viscosity and somewhat less homogeneous nature respectively. All three bead types were highly porous, with average values $>97\%$, based on a modified Archimedes' test (Figure 4.2B). The three types of beads showed similar viscoelastic behaviour during the mechanical testing under physiological conditions (37°C , in PBS; Figure 4.2C). There was no significant difference in the Young's modulus (DAT = 0.30 ± 0.16 kPa, COL = 0.25 ± 0.09 kPa, DTB = 0.39 ± 0.16 kPa) between the three ECM sources (Figure 4.2D).

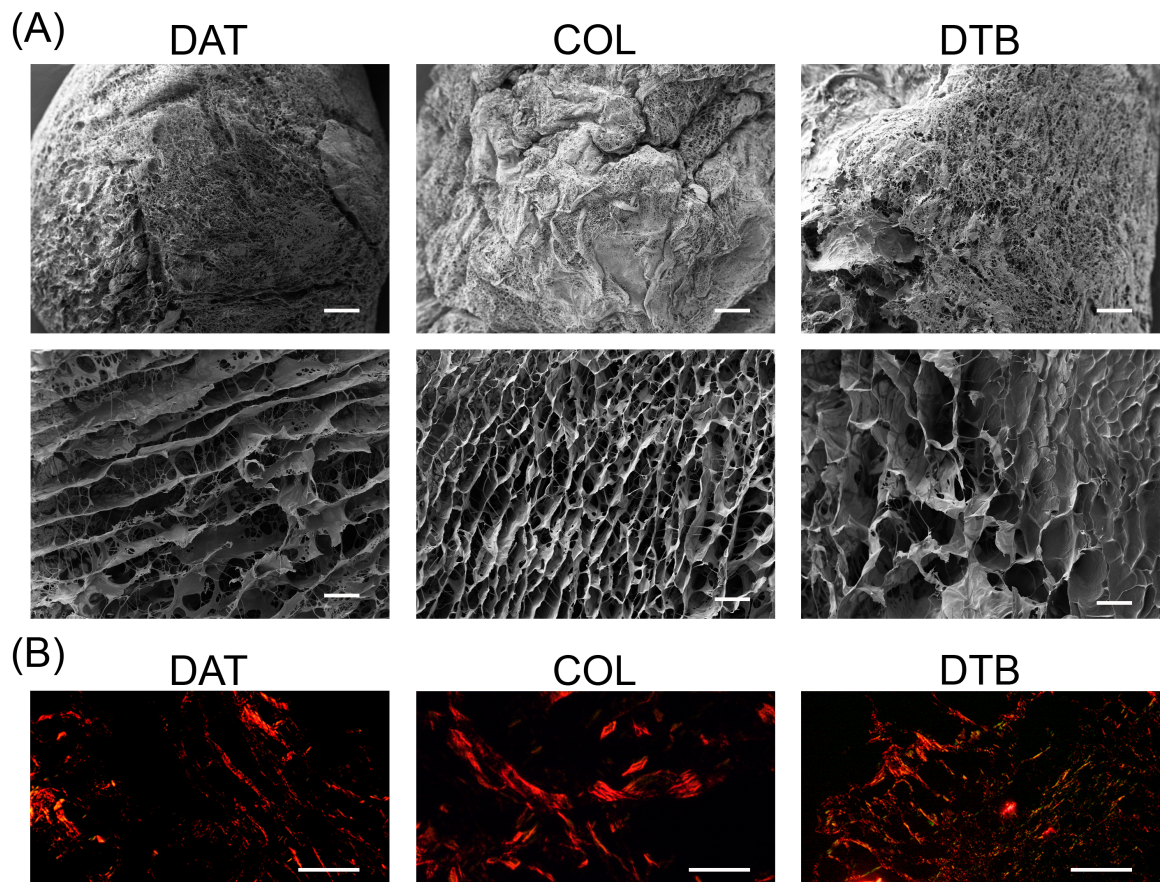


Figure 4.1: Qualitative microscopic analysis of DAT, COL, and DTB beads showed that the bead micro-architecture was similar across all ECM sources. (A). Representative SEM images of whole beads (top row) and cryo-fractured beads (bottom row), displaying the porous architecture of the ECM-derived beads. Scale bars: $100\ \mu\text{m}$ (Top row) and $10\ \mu\text{m}$ (bottom row). **(B)** Picosirius red staining showing the presence of varying sizes of collagen fibers present in all groups. Scale bar = $200\ \mu\text{m}$.

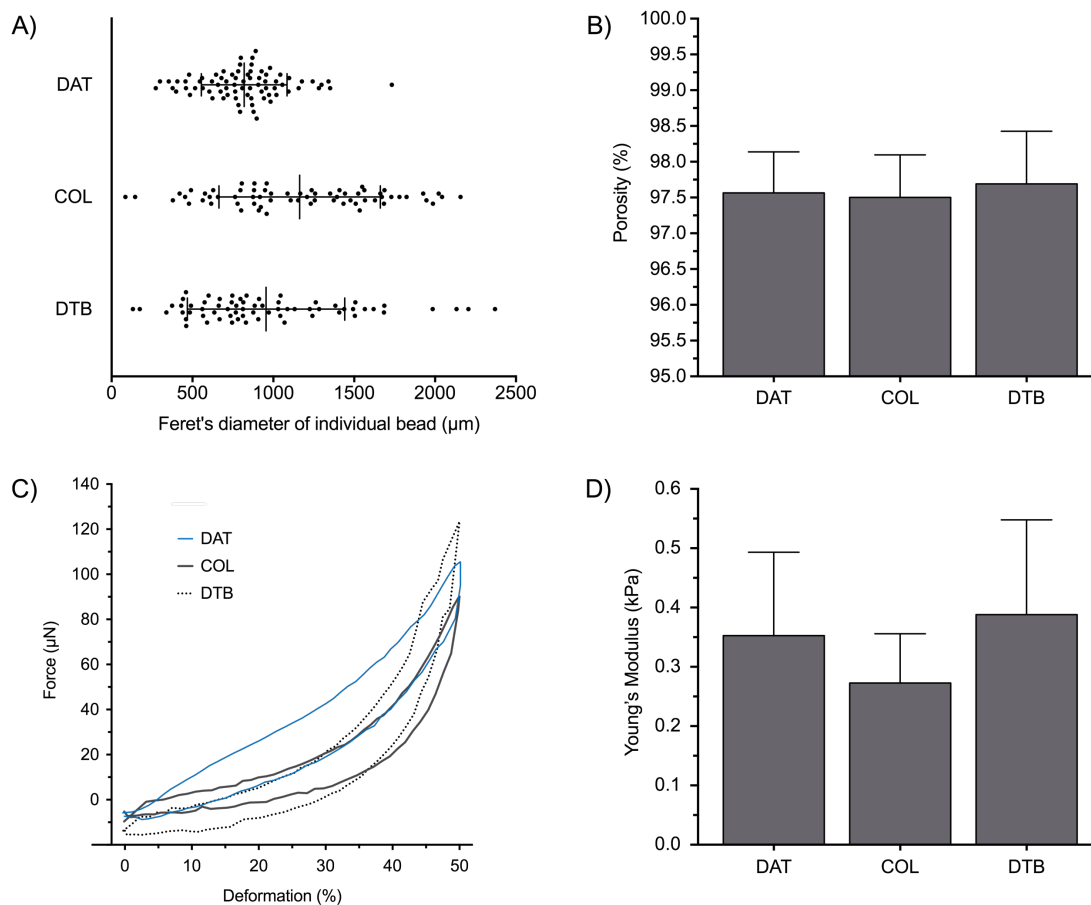


Figure 4.2: DAT, COL, and DTB beads had similar starting physical properties. (A) Feret's diameter of the individual beads used to fabricate the foams prior to cell-assembly (Pooled results: $n=20-30$ beads/trial, $N = 2-3$ trials with different ECM suspensions). (B) Porosity of the beads measured with a modified Archimedes' method. Percentage of porosity represented as mean \pm SD ($n = 3$ bead foams/trial, $N = 5$ trials with different ECM suspensions). (C) Representative force versus deformation curves for individual DAT, COL, and DTB beads prior to seeding. Data from the 4th compression cycle are shown for all beads, at a strain rate of 0.01 s^{-1} . (D) Young's modulus was calculated using nonlinear least squares curve fitting. Modulus represented as mean \pm SD ($n=6$ beads/trial, $N=2-3$ trials with different ECM suspensions).

4.5.2 DAT-, COL-, and DTB-derived beads similarly support ASC seeding and cell-assembled bead foam formation

Following the physical characterization, human ASCs were seeded on the DAT, COL, and DTB beads using the developed 24 h seeding regimen. Corresponding confocal Live/Dead® imaging of the ASC-seeded beads qualitatively showed comparable attachment of viable ASCs on all of the groups, with a homogeneous distribution of the cells across the surface of the beads derived from all three ECM sources (Figure 4.3A). Using the previously developed 8-day cell-assembly method developed in Chapter 3, robust cell-assembled bead foams were successfully produced from ASC-seeded DAT, COL, and DTB beads (Figure 4.3B).

4.5.3 DAT and COL scaffolds are adipo-conductive, while DTB scaffolds are adipo-repressive

Preliminary studies were then conducted to compare the adipogenic differentiation of the human ASCs within the DAT, COL, and DTB cell-assembled bead foams over 14 days in culture. To quantitatively assess the level of adipogenic differentiation, GPDH enzyme activity was measured and normalized to total protein content (Figure 4.4A). GPDH activity levels were increased in the DAT and COL bead foams relative to the DTB bead foams and the TCPS induced and non-induced controls. Consistent with the GPDH enzyme activity results, a qualitative increase in intracellular lipid accumulation was observed in the DAT and COL groups relative to the other experimental conditions (Figure 4.4B). These findings were also supported by RT-qPCR analysis of the early adipogenic markers, *PPARG* and *CEPBA*, which showed higher mRNA levels in the DAT and COL groups, compared to the DTB group and TCPS controls.

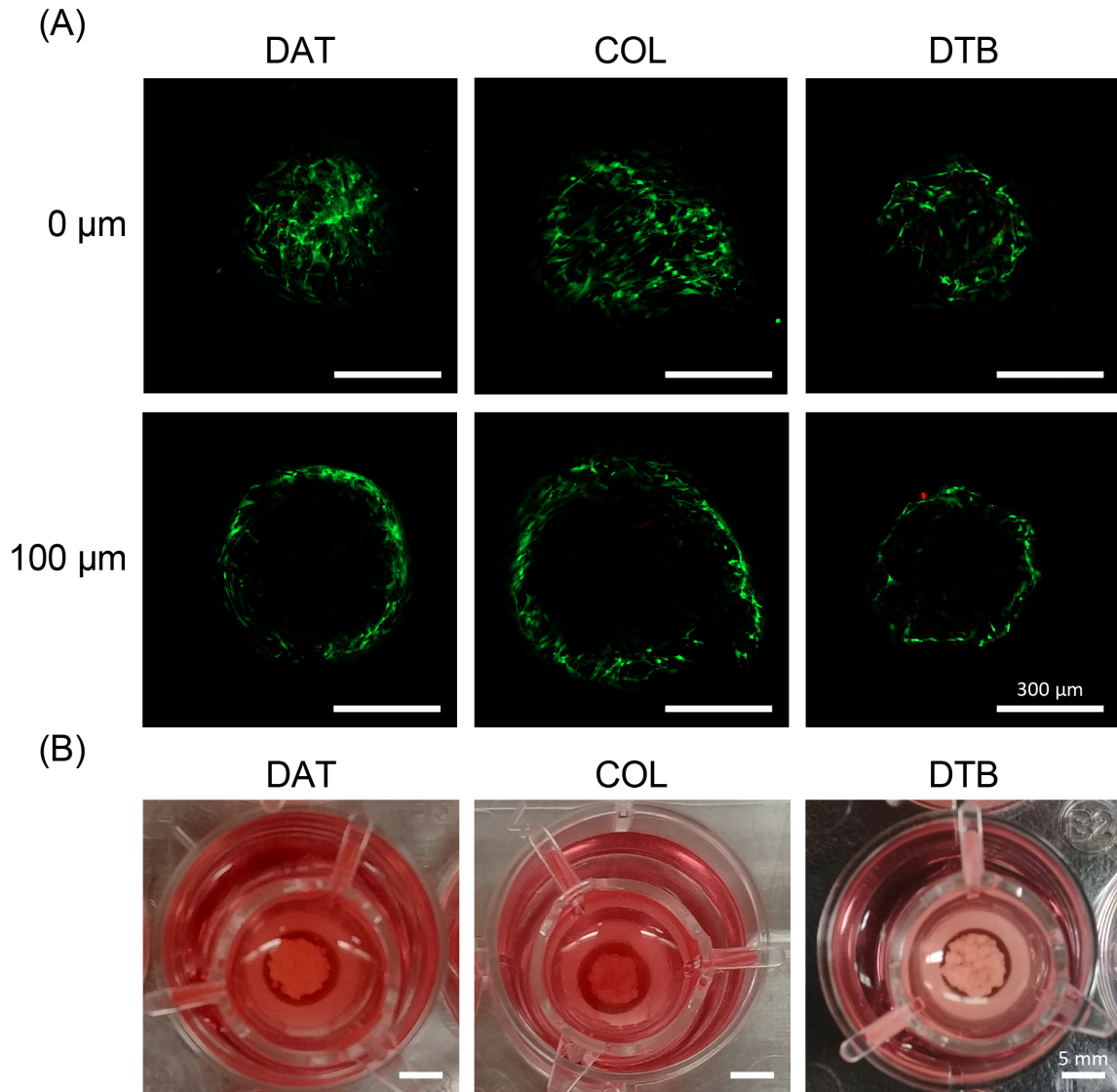


Figure 4.3: Representative microscopic and macroscopic images of ECM-derived beads and bead foams at 24 h post-seeding and 8-days post-moulding, respectively. (A) Representative live/dead[®] staining, labelling living cells in green and dead cells in red, showed that all ECM-derived sources promoted ASC attachment and survival 24 h after seeding. The surface (top row) and 100-μm deep cross-section (bottom row) were imaged using confocal microscopy. Scale bars: 300 μm. (B) Representative macroscopic images after 8 days of transwell culture demonstrated that the production of cell-assembled bead foams was possible with the three ECM sources. Scale bar: 5 mm.

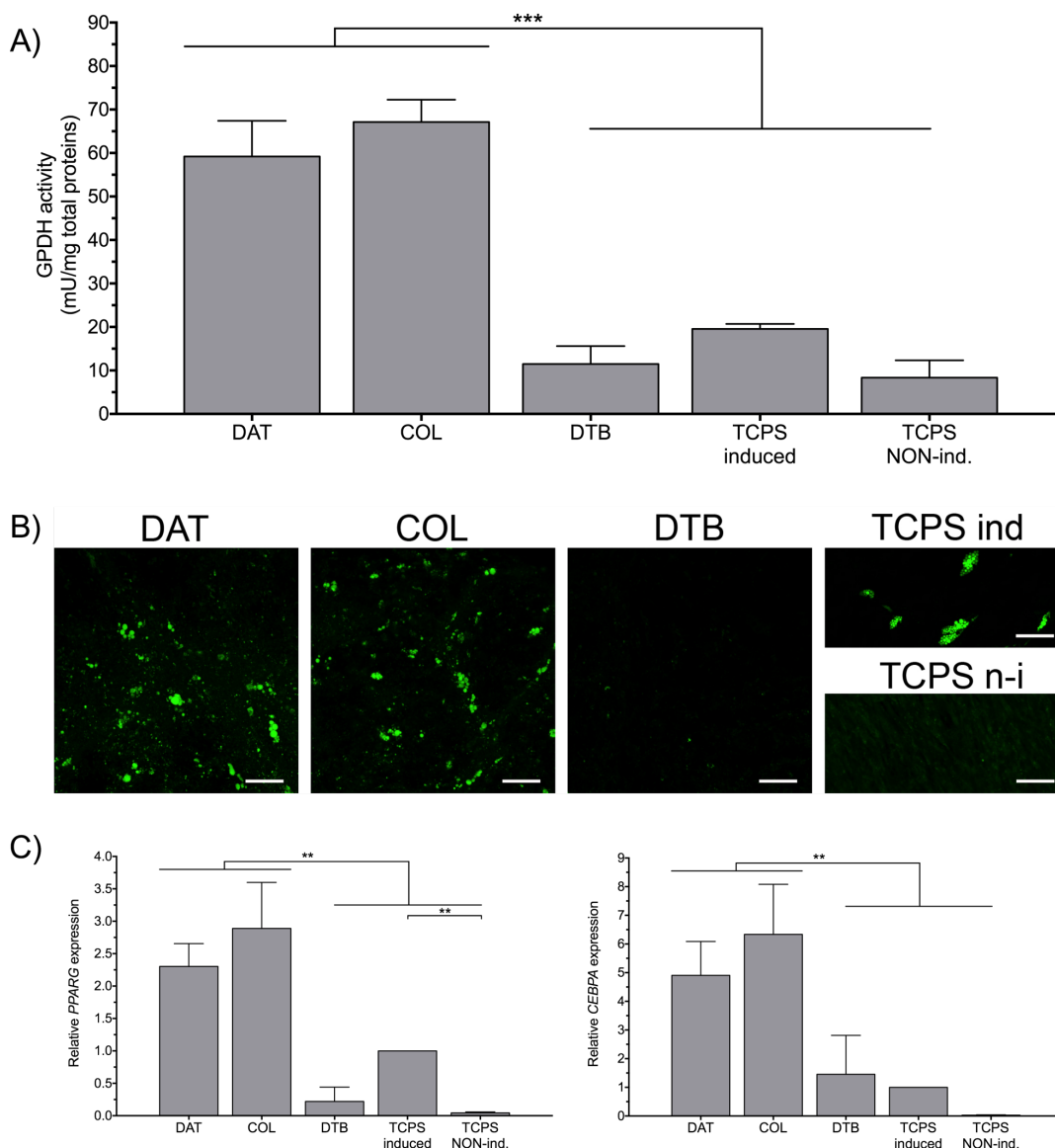


Figure 4.4: Preliminary results indicated that adipogenic differentiation appeared to be enhanced in the DAT and COL bead foams, compared to the DTB bead foams and TCPS controls, after 14 days of induction. (A) Normalized glycerol-3-phosphate dehydrogenase (GPDH) enzyme activity levels showed enhanced adipogenic activity in the DAT and COL bead foams, relative to the DTB bead foams and TCPS controls. (B) Representative BODIPY® staining of intracellular lipid accumulation showed a qualitatively increased presence of intracellular lipids in the DAT and COL bead foams, relative to the other groups. Scale bar = 100 μm. (C) RT-qPCR analysis of the adipogenic genes *PPARG* (left) and *CEBPA* (right) displayed increased expression in the DAT and COL groups compared to the other groups. Tissue culture polystyrene (TCPS) induced and non-induced (NON-ind.) were included for all assays. (A-C) n=3 bead foams/donor, N=1 donor; intra-donor variability measured using one-way ANOVA with Tukey's post-hoc test; ** $P < 0.01$.

4.6 Discussion

The microenvironment plays a critical role in mediating cell fate and a growing body of evidence has shown that tissue-specific ECM can direct cellular functions, including growth and differentiation [16]. Research focusing on 2-D *in vitro* cell culture models, such as coatings, has suggested that tissue-specific ECM derived from a range of decellularized tissues (dermis, liver, skeletal and cardiac muscles, lung, endometrium, brain, and adipose tissue) can direct stem and progenitor cell lineage commitment, when compared to non-tissue-specific coating controls or purified collagen coatings [136, 289, 291, 292, 293, 294, 295]. While convenient, these 2-D models fail to recapitulate the complex cell-ECM and cell-cell interactions that occur within 3-D microenvironments [288]. However, the use of bioscaffolds to study the effects of tissue-specific ECM in 3-D contexts isn't without challenges. For example, few studies include control scaffolds that have different biochemical composition but similar physical properties, due to the difficulty of producing tissue-specific and non-tissue-specific bioscaffolds with matching structural and biomechanical characteristics. This lack of proper controls makes it difficult to interpret the results of these studies, as confounding variables may interact together to modulate the effects mediated by the resulting scaffolds.

In the present study, we sought to produce physically similar cell-assembled bead foams from three ECM sources to study the effects of ECM biochemical composition on the adipogenic differentiation of human ASCs within 3-D bioscaffolds. As demonstrated through several *in vitro* studies, a variety of external cues contribute to the delicate balance of adipo-osteogenic differentiation in MSCs, including ECM-integrin interactions and soluble factor-receptor binding [296]. Interestingly, studies have shown that adipogenic induction factors inhibit osteogenesis, and conversely, osteogenic induction factors hinder adipogenesis [89, 296]. Signal integration is mediated through several signaling cascades, ultimately resulting in the activation or inhibition of the master adipogenic transcription factors, PPAR γ and C/EBP α [89, 296]. This inverse relationship between the adipogenic and osteogenic cell commitment led to the selection of DAT as a tissue-specific pro-adipogenic ECM source [104], along with DTB as a non-tissue-specific and potentially anti-adipogenic [297] ECM source. As collagen represents the main structural component of both decellularized tissues, COL was also included as an additional ECM source control.

Having different starting physical properties, DAT and DTB could not be used in their intact forms and had to be processed into other scaffold formats to allow for the production of scaffolds with matching physical properties. Due to the previous success in producing the DAT-derived cell-assembled bead foams, this bioscaffold format was selected for the present study. As a first step in the fabrication process, minced COL and DTB were homogenized in acetic acid and electrosprayed into liquid nitrogen. However, several challenges were encountered with the two new ECM suspensions having different characteristics in comparison to the DAT suspensions. The COL suspension was much more viscous than the DAT suspension and required fine-tuning of the electrospraying parameters. More specifically, the voltage was increased from 16-18 kV to 18-19 kV and the extrusion speed was reduced from 35 mL/h to 30 mL/h to compensate for the higher viscosity. An opposite issue was encountered with the pure DTB suspension: the suspension was thin and heterogenous, tending to separate into two phases. Small batches of this pure DTB suspension were electrosprayed, but the resulting pure DTB beads were found to be non-stable and disintegrated during the rehydration steps. Several strategies were explored to resolve the issues, such as increasing the ECM concentration in the suspension, greater homogenization and mixing time, and including an α -amylase digestion step [298], without any success. To overcome this challenge, the DTB suspension was supplemented with a small fraction of minced COL. Aiming to keep the total ECM concentration constant across all groups (20 mg/mL), supplementing 17 mg/mL DTB with 3 mg/mL COL was found to be the minimum required to synthesize beads that remained stable following rehydration (several DTB/COL ratios were tested; data not shown). Taken together, the characterization data demonstrated that DAT, COL, and DTB-derived beads with similar physical properties were produced, confirming the potential of the system for comparing compositionally distinct ECM sources.

Overall, the production of reproducible cell-assembled bead foams was possible across all conditions. It should be acknowledged that while the starting physical properties of the ECM-derived beads were similar across all groups, the physical properties of the cell-assembled bead foams were not characterized. It is therefore possible that the bead properties may have changed over the cell-assembly process, through remodeling by the cells; however, these potential differences between the groups could be attributed to the innate differences in ECM composition mediating subtle cell behaviour differences

between the groups. Motivated by technical considerations and tissue availability, COL and DTB were obtained from xenogenic sources. While this might have impacted the observed cell responses, the ECM is broadly conserved across species [253, 254], and bovine osseous tissue are considered to have the most similar physiochemical and structural resemblance to human osseous tissues compared to other sources [299]. In addition, differences between the adipo-conductive properties of the human-derived DAT and bovine-derived COL bead foams were not observed across all of the assays investigated, suggesting that the ASCs responded well on the bovine-sourced materials.

Interestingly, DAT and COL cell-assembled bead foams induced a similar strong adipogenic response that was greater compared to the DTB cell-assembled bead foam group and the TCPS controls. This is in line with previous literature that has shown that 3-D polycaprolactone (PCL) meshes coated with DAT, fibronectin, or laminin induced a similar high level of adipogenic differentiation in human BMSCs when cultured for 21 days in differentiation media, which was enhanced compared to uncoated PCL mesh controls [300]. These findings revealed that all ECM coatings had similar adipo-conductive properties compared to the uncoated PCL mesh. However, the DAT-coated mesh displayed the greatest adipo-inductive properties, as shown through a shorter two-day adipogenic induction protocol followed by a three-week culture period in maintenance medium including insulin but no other pro-adipogenic factors [300]. In this context, the highest adipogenic response was consistently observed on the DAT-coated mesh, relative to the other ECM-coated meshes [300]. As such, it would be interesting in future work to compare the ASC response in the DAT and COL bead foams under conditions that were less stimulatory towards the adipogenic pathway, to be able to discern more subtle inductive effects that may be present in the DAT.

Notably, the absence of adipocytes in the DTB group at day 14 of differentiation compared to the DAT and COL groups suggests that the DTB may have had inhibitory effects on adipogenesis. This difference in cell fate may be due to the unique ECM composition of the DTB bead foams. While little is known about the inhibitory effects of DTB on adipogenesis, these preliminary findings are in line with existing results from osteogenic-mimicking matrices [297, 301]. In this 2-D model, where matrices were derived from decellularized osteogenically- and adipogenically-induced BMSC-derived cell sheets,

PPARG gene expression was shown to be downregulated in BMSC-seeded osteogenic-mimicking matrices, compared to BMSC-seeded adipogenic-mimicking matrices [297, 301]. Building on this data, it would be interesting to study the effects of ECM composition on the osteogenic differentiation of ASCs using the cell-assembled DAT-, COL-, and DTB-derived platforms in future work.

4.7 Conclusions

The findings from the present study demonstrate the potential of the novel cell-assembled DAT and COL bead foams as a platform for adipose tissue engineering. In addition, we established a new DTB-derived platform that may hold utility for applications in bone regeneration. The approach generates robust 3-D scaffolds fabricated purely of cells and ECM, which could potentially be applied as tissue substitutes or as 3-D culture models for investigating the effects of ECM composition on the lineage-specific differentiation of the ASCs. Results from the proof-of-concept study comparing the adipogenic response of the ASCs within tissue-specific and non-tissue-specific cell-assembled bead foams, showed that the bead foams derived from DAT and COL supported a high level of adipogenic differentiation when induced in culture over 14 days. In contrast, the DTB bead foams were shown to have inhibitory effects on the adipogenic differentiation of the ASCs. Taken together, the study findings show that the newly developed cell-assembly platform is versatile and can be used for the controlled comparison of biochemical properties between various ECM sources. Future experiments could focus on further investigating the adipo-conductive properties of the three ECM sources with a greater number of cell donors, concomitant with studies focused on elucidating the temporal adipo-inductive properties of the ECM sources in conditions that do not stimulate adipocyte differentiation. Further experiments could also include a comparison of the osteo-inductive and osteo-conductive effects of the DAT, COL, and DTB derived cell-assembled bead foams, to explore their potential as cell delivery systems for bone regeneration.

Chapter 5

5 General discussion and conclusions

5.1 General discussion

A growing body of work has identified biomaterials derived from the extracellular matrix (ECM) as promising platforms that can be designed to mimic the biochemical, biophysical, and biomechanical properties of the soft tissue milieu and be applied in strategies to promote soft tissue regeneration [71]. These ECM-derived biomaterials can be versatile modeling systems for studying the effects of ECM composition on various cellular functions *in vitro*, such as survival and pro-angiogenic factor secretion, or can potentially be applied as rationally-designed delivery systems for pro-regenerative cell populations *in vivo*. Towards the development of tissue-specific strategies for soft tissue regeneration applications, the combined use of decellularized adipose tissue (DAT) and adipose-derived stromal cells (ASCs) has highlighted the cell-supportive effects of DAT-based biomaterials to: (i) enable attachment, proliferation, migration, and differentiation of ASC *in vitro* [13, 14, 104, 119, 131, 134-136], and (ii) to direct pro-regenerative cascades *in vivo*, mediated through cell infiltration, inflammation, angiogenesis, adipogenesis, and scaffold remodeling following implantation [13, 14, 119, 126, 302].

When directly comparing DAT-derived materials, DAT scaffolds applied in their intact form have shown great potential for volume retention and fat formation *in vivo*, while more processed and porous formats such as DAT-derived bead foams have shown more rapid scaffold remodeling and enhanced neo-vascularization [14]. As a result, these observations provide a strong rationale for using DAT bead foams as a pro-regenerative bioscaffold for soft tissue-engineering applications seeking to promote a pro-angiogenic response. Building from this knowledge, the present thesis sought to provide further insight into the design of modular DAT-derived bioscaffolds by studying the effects of ECM composition on cell function and fate within modular bioscaffolds (Chapters 2 and 4). Further, a novel method for fabricating robust, three-dimensional (3-D) cell-assembled ECM-derived foams that incorporated a high density of viable cells that were well-distributed throughout the scaffolds was developed and assessed for applications in soft tissue regeneration (Chapter 3).

Past research investigating the effects of ECM derived from decellularized tissues on cell function has been largely performed using *in vitro* two-dimensional (2-D) systems, such as ECM-derived coatings. When compared to non-tissue-specific decellularized tissue or collagen coating controls, decellularized dermal [289], hepatic [289, 293], skeletal muscle [289, 291], cardiac muscle [86, 291], pulmonary [292], brain [295], endometrial [294], and adipose [136] tissues have been found to promote the growth, survival and lineage-specific differentiation of tissue-matched cell types. While promising, these systems do not accurately reflect the spatial arrangement of cells in 3-D microenvironments, nor the complex nature of cell-ECM interactions [288]. To facilitate the investigation of tissue-specific effects between different ECM-derived biomaterials, studies from the present thesis directly compared the effects of different types of ECM in 3-D naturally-derived microenvironments. More specifically, the present studies are the first to compare the effects of complex 3-D bioscaffolds derived from DAT with similar bioscaffolds derived from purified collagen (Chapter 2 and 4) or non-tissue-specific sources, such as decellularized trabecular bone (Chapter 4).

Consequently, the present thesis sought to generate and apply 3-D control platforms that had similar structural and biomechanical properties to enable studies more specifically focused on exploring the effects of starting composition within ECM-derived bioscaffolds. In the first set of studies, pre-assembled DAT bead foams with similar physical characteristics to pre-assembled COL bead foams were developed and used to explore the effects of ECM composition on human wound edge dermal fibroblasts (weDFs). weDF survival and secretion of pro-angiogenic soluble factors, including angiopoietin-1, C-X-C motif chemokine 12 (CXCL12), hepatocyte growth factor (HGF), platelet-derived growth factor (PDGF), and vascular endothelial growth factor (VEGF) were shown to be significantly enhanced in the pre-assembled DAT bead foams, as compared to the pre-assembled COL bead foams. Consequently, it was found that the weDFs still possessed a pro-regenerative potential that could be better harnessed using DAT as an ECM source relative to COL. A study by Truong and collaborators compared different commercially-available bioengineered wound dressings including purified collagen-based sources (Dermagraft®, Integra®) and human decellularized dermis (Alloderm®, Dermalogen®, and in-lab produced decellularized dermal matrix) in an acute full-thickness excision

wound model in nude mice [303]. Although the wound dressings were fabricated using different processes, the human skin-derived products showed less wound contraction and a histologically thicker neo-dermis as compared to the collagen-based products [303]. Taken together, results from Truong *et al.* and the present study provide evidence supporting the use of complex ECM sources from soft decellularized connective tissues for the design of pro-regenerative bioengineered wound dressings, as an alternative to purified bovine collagen that is currently used in the clinical setting with mixed results [170, 171, 250].

Using histological analyses, the initial studies in the present work complemented previous work investigating DAT composition published by Flynn (2010) [104] and Kuljanin *et al.* (2017) [62]. Findings from the present work revealed that DAT-derived bead foams contained higher levels of known pro-angiogenic ECM macromolecules including sulphated glycosaminoglycans (GAGs), and collagen types IV, V, and VI, relative to purified COL. Interestingly, heparan sulphate, a subtype of sulphated GAG, has the innate ability to support angiogenesis through direct endothelial cell interactions mediated by α_5 and α_v integrin binding, as well as through pro-angiogenic factor sequestration, which can be released following tissue injury and ECM remodelling [256]. In addition, basement membrane collagens type IV [257] and VI [22] have been demonstrated to stimulate angiogenesis by recruiting endothelial cells. Collagen type IV has also been found to have dose-dependent effects on vessel elongation and stabilization [258], and collagen type VI-deficient mice have been found to have impaired endothelial cell survival and sprouting [22]. Additionally, collagen type V has also been implicated in promoting newly developed blood vessels in granulation tissue [259], and its haploinsufficiency has been associated with impaired wound healing outcomes in patients suffering from Ehlers–Danlos Syndrome [21].

Along with biochemical composition, scaffold stability and cell distribution are other important design considerations for ECM-derived cell delivery platforms [80, 81]. Even though the weDFs on our previous pre-assembled DAT bead foams showed enhanced survival and angiogenic marker expression (Chapter 2), the physical structure of the scaffolds only allowed for static cell seeding and culture methods. Known to result in limited cellular infiltration and distribution compared to dynamic approaches [304], these

static methods were seen as a limitation of the biomaterial format and resulted in heterogeneously distributed cells that were predominantly localized in proximity to the upper surface of the pre-assembled bead foams. As such, methods were developed to produce our next-generation cell-assembled DAT bead foams, which contained a higher density of viable ASCs that were more well distributed throughout the scaffolds. The resulting novel cell-assembly approach harnessed the ASC ability to synthesize new ECM, allowing for individual beads to fuse together to generate a stable construct without the use of synthetic additives or chemical cross-linking, which may allow for enhanced biocompatibility and bioactivity [85, 252]. Through the combined use of xenogenic-free chemically defined media (XFCD), dynamic cell culture, L-ascorbic acid 2-phosphate (A2P) stimulation, and growth factor preconditioning, the newly developed system allowed for the development of thick (~3 mm thick) constructs with high cell viability (>95%) after 8 days in culture. Preconditioning using epidermal growth factor (EGF), basic fibroblast growth factor (FGF-2), and insulin-like growth factor-1 (IGF-1) showed positive effects in our unique system that were similar to previous studies exploring the impact of these three growth factors on MSCs. In particular, EGF and IGF-1 treatments alone were found to promote the secretion of MMPs by ASCs [226, 268], and EGF alone has been demonstrated to promote the expression of ECM-related proteins, including proteoglycans, connective tissue growth factor (CTGF) and tissue inhibitors of matrix metalloproteinases (TIMPs) [268]. In addition, FGF-2 preconditioning induced a pro-fibrotic phenotype in MSCs, in accordance with the data obtained in our study [218, 225]. Taken together, the preconditioning treatments used in the fabrication process were beneficial for the production of cohesive cell-assembled bead foams with a high cellularity and remodelling potential.

For the second set of studies, human ASCs that were transduced to co-express firefly luciferase (Fluc2) and tdTomato (tdT) reporters were employed to enable longitudinal *in vivo* cell tracking studies using bioluminescence imaging (BLI), as well as endpoint analyses of ASC distribution within tissue cross-sections using endogenous fluorescence. This system was used to address limitations associated with classical cell identification techniques often employed to evaluate donor cell retention within ECM-derived biomaterials in pre-clinical models. For example, the use of immunohistological analyses of human-specific markers does not allow for longitudinal tracking, and requires a large

number of animals to perform long-term assessments [249, 264]. Further, there can be substantial variability across the depth of the scaffolds that can result in inaccuracies when trying to localize and quantify cell populations in thin sections taken from implants. The use of cell tracker dyes to pre-stain cell populations prior to implantation, such as lipophilic membrane dyes, has similar challenges associated with immunohistological analyses, in addition to limitations associated with the loss of signal through cell division, as well as dye release and uptake by other cell populations [280].

Measured using non-invasive BLI, the cell retention data from the current studies showed enhanced detection of viable ASCs in the cell-assembled bead foams relative to the pre-assembled bead foams at an early timepoint, as well as the localized ASC distribution within the implant region in both groups. The data obtained showed improved cell localization to the implant, as compared to a similar study from Wolbank and colleagues, which detected transduced human ASCs expressing luciferase throughout the body of nude mice 19 days after subcutaneous implantation within a fibrin gel [281]. Other studies have reported ASC retention to range from 5% to 10% of cells retained at the site of injection 4 weeks after intramuscular delivery into ischemic [283] or normal [282] hindlimbs, further suggesting that the cell-assembled DAT-derived bead foams provide a supportive platform for localized ASC delivery within the subcutaneous space.

In addition to the cell retention data, histological CD31⁺ structure counts indicated there were more murine endothelial cells within the cell-assembled bead foams, suggestive of augmented implant angiogenesis relative to the pre-assembled bead foams. Since the number of cells seeded onto the beads foams were similar in the cell-assembled and pre-assembled groups, results from the *in vivo* studies suggest that early cell retention or scaffold composition and/or structure may have increased the angiogenic response in the cell-assembled bead foams. These differences in composition and structure could be attributed to the distinct culture protocol utilized to produce the cell-assembled bead foams as compared to the pre-assembled bead foams. More specifically, the extended culture protocol in the cell-assembled bead foams may have modulated the ASC phenotype or promoted the accumulation of beneficial paracrine factors. Further studies comparing both scaffold platforms would be needed to more fully understand the specific mechanisms involved in the enhanced pro-regenerative potential of the cell-assembled foams.

In addition, it should be recognized that ASCs can exhibit donor-dependent behavior. This inter-donor variability can be attributed to several factors such as age [305, 306], donor health and disease status [305, 307], and the adipose depot used for sourcing [248]. More specifically, aging alone has been shown to negatively impact ASC proliferation [306, 307], and in combination with the presence of systemic diseases, such as diabetes, it has been attributed to impaired pro-angiogenic potential of the cells through decreased paracrine activity [305, 306]. Further, aging and body mass index has also been correlated with reduced ASC differentiation potential [307]. Consequently, matching ASCs for known donor variables, including age, adipose tissue depot, and body mass index as performed in Chapter 3 can help in minimizing inter-individual variability [248, 305-307]. However, donor-dependent behavior is inherent to the use of these primary cell population and other unknown donor factors could also be contributors to increase donor variability.

For the last set of experiments, the methods used to generate the cell-assembled DAT bead foams were extended to produce structurally-similar 3-D cell-assembled bead foams from compositionally distinct ECM sources. With a special interest in evaluating the tissue-specific contribution of ECM composition on adipogenesis within the new constructs, DAT and DTB were selected as the primary ECM sources due to the inverse relationship between adipogenesis and osteogenesis in MSCs [89, 90]. Purified collagen type I (COL) was included as an additional compositional control to highlight the versatility of the fabrication approach by using a commercially available matrix source, as well as to broaden the analysis of the effects of the tissue-specific ECM composition. When subjected to 14 days of *in vitro* culture in adipogenic differentiation media, both the cell-assembled DAT and COL bead foams induced an enhanced adipogenic response as compared to the DTB cell-assembled bead foams and the tissue culture polystyrene (TCPS) controls. These results were consistent with a study performed by Blum and collaborators in which 3-D polycaprolactone (PCL) meshes coated with ECM derived from DAT, fibronectin, or laminin showed similarly enhanced adipogenic differentiation in human bone marrow-derived stromal cells (BMSCs) as compared to uncoated PCL mesh controls [300]. Using a shorter two-day adipogenic induction protocol followed by a three-week culture period in proliferation media including insulin but no other pro-adipogenic factors, this study also showed that the BMSCs cultured on the DAT-coated meshes displayed enhanced adipogenic lineage commitment relative to those cultured on the fibronectin and laminin

coated groups [300]. These findings therefore demonstrated greater “adipo-inductive” properties of the DAT-coated mesh compared to the other ECM groups [300]. In this context, the highest adipogenic response was consistently observed on the DAT-coated mesh, relative to the other ECM-coated meshes [300].

While the “adipo-conductive” properties of DAT as an ECM source were confirmed by our preliminary study, our experimental design did not allow for the evaluation of the “adipo-inductive” properties of the cell-assembled bead foams. However, the *in vitro* study also revealed that the DTB group appeared to have inhibitory effects on adipogenesis, when compared to the DAT and COL groups. Although there has been very limited research on the effects of bone-derived ECM on adipogenesis, these findings are consistent with previous results from 2-D BMSC-derived osteogenic matrices that revealed a downregulation of *PPARG* gene expression in osteogenic matrices, compared to BMSC-derived adipogenic matrices [297, 301]. These differences could be explained by the distinct biochemical composition of the ECM specific to each tissue. Surrounding adipocytes, fat lobules, blood vessels, and nerves, adipose tissue is rich in basement membrane and its constituents including collagen type IV, type VI, laminin and nidogens [60, 61]. The organic phase of osseous tissue was shown to be comprised of high levels of collagen type I, but also contains smaller amounts of collagen type IX, X, and XII [308], along with specialized matricellular proteins that include osteocalcin (also known as bone gamma-carboxyglutamic acid-containing protein; BGLAP), osteonectin (also known as secreted protein acidic and rich in cysteine; SPARC), osteopontin (also known as secreted phosphoprotein 1; SPP1), and bone sialoproteins [65, 68, 69].

5.2 Future work

The body of work documented in my thesis provides strong evidence indicating that ECM composition can impact cell behaviour and cell fate, as shown by alterations in weDF phenotype on pre-assembled bead foams derived from DAT and COL and by adipogenic lineage commitment in ASCs within cell-assembled bead foams derived from DAT, COL, and DTB. Moreover, murine studies conducted with both pre-assembled and cell-assembled bead foams showed the pro-regenerative potential of both biomaterial formats.

More specifically, work presented in Chapter 2 showed that the survival and pro-angiogenic capacity of human weDFs were enhanced on the pre-assembled DAT bead foams both *in vitro* and *in vivo* when compared to bead foams fabricated from COL. While the pre-assembled foams have some limitations when applied as cell delivery vehicles, they represent a useful platform for *in vitro* studies. Their high tunability and ease of production supports future work focused on producing this bioscaffold format from other ECM sources. For example, based on previous work by our team and others to decellularize cardiac tissues [86, 128], pre-assembled cardiac-derived bead foams could be engineered to culture cardiac progenitor cells under pathophysiological oxygen tensions and inflammatory cytokines mimicking the infarct-heart microenvironment. Using this model, cardiac progenitor proliferation, survival and function, such as their secretory profile, could be investigated. Similar studies could be conducted with pro-regenerative cell populations, such as BMSCs or circulatory endothelial progenitor cells, to better assess their survival and functional capacities in conditions simulating stresses from the infarct-heart microenvironment. Additionally, studies could focus on studying the effects of cell-free pre-assembled DAT bead foams in an impaired wound healing model.

With regards to the work presented in Chapter 3, our findings revealed that the novel cell-assembled DAT bead foams are a promising pro-regenerative cell delivery platform that supports the localized *in vivo* retention of delivered ASCs with pro-angiogenic functionality. Upcoming studies could further assess angiogenesis within the scaffold using end-point 3-D x-ray micro-computed tomography angiography [309]. While these next-generation scaffolds showed great pro-angiogenic potential, the current study design did not probe extensively for the inflammatory cell response, nor adipose tissue formation *in vivo*. Consequently, further studies could aim to understand the leukocyte response to the material, through immunohistological and/or flow cytometry analyses of cell-assembled bead foams explanted at 1, 2, 4, and 8-weeks to assess for spatial distribution and quantification, respectively. Leukocytes of interests could include neutrophils (neutrophil elastase positive cells) [142] and macrophages (F4/80 positive cells; pan-macrophage marker), and include analysis of macrophage subpopulations, e.g. activated towards the more pro-inflammatory “M1” or pro-inflammatory “M2” axis of the M1-M2 spectrum [143]. In this context, it would be interesting to quantify the relative levels of expression of pro-inflammatory markers (e.g. CD80 and inducible nitric oxide synthase (iNOS)) and

pro-regenerative markers (e.g. CD163, CD206 and arginase-1) [143]. Using similar time points, investigation of adipogenesis within the scaffolds could also be performed by staining whole-mount explants for perilipin, and imaging the stained explants using 3-D confocal imaging combined with a previously published tissue clarification method [310]. In addition, suggested directions could also evaluate the pro-regenerative effects of the scaffolds in other preclinical models, which could include murine impaired wound healing or hindlimb ischemia models. Finally, next steps of this project could examine the feasibility of producing cell-assembled bead foams using other cell populations, such as BMSCs, or using co-culture methods that could include a combination of ASC-seeded DAT beads with microvascular endothelial cell-seeded DAT beads. It would then be interesting to assess the potential such pre-endothelialized cell-assembled bead foams to anastomose *in vivo* with the existing murine vasculature.

In line with the results from Chapter 2 that demonstrated that the ECM composition within the pre-assembled bead foams modulated the response of seeded cell populations in culture, the preliminary data from Chapter 4 suggested that adipogenic differentiation was enhanced in the cell-assembled bead foams fabricated from DAT and COL as compared to DTB, supporting that the ECM composition within the platforms can modulate ASC differentiation. Future experiments should focus on confirming the observed adipo-conductive properties of the three ECM sources with a greater number of cell donors, along with investigations aimed to elucidate the adipo-inductive properties of the ECM sources in conditions that do not promote adipogenesis. These studies could broaden the panel of genes used and include additional early-to-mid- (lipoprotein lipase, adiponectin, or leptin) and late-stage (adipocyte-specific fatty acid binding protein, or perilipin) adipogenic markers to more fully characterize the differentiation response [311]. Next directions could also include a comparison of the osteo-inductive and osteo-conductive properties of the cell-assembled bead foams derived from DAT, COL, and DTB, to explore their potential as cell delivery systems for bone regeneration. Assays for assessing osteogenic differentiation could include an enzymatic alkaline-phosphatase assay, a mineralization assay using the fluorescent dye osteoimage® from Lonza, and gene expression analysis of early (runt-related transcription factor 2 (*RUNX2*) and transcription factor Sp7, also called osterix (*OSX*)) and mid-to-late (*BGLAP*, *SPARC*, *SPPI*) osteogenic markers to probe the differentiation response over time [69, 312].

5.3 Summary and significance

The body of work reported in my thesis demonstrated the potential of modular naturally-derived DAT biomaterials for soft tissue-engineering applications. When inoculated with either weDFs or ASCs, DAT bioscaffolds promoted seeded cell survival, implant vascularization, and constructive remodelling compared to controls *in vivo*. Moreover, preliminary studies showed high levels of adipogenic differentiation in the ASCs cultured within the cell-assembled DAT and COL bead foams.

The pre-assembled and cell-assembled bead foams were shown to be robust platforms enabling the production of scaffolds with distinct tissue-specific ECM composition, while having similar initial structural and biomechanical characteristics. Within the pre-assembled format, DAT was shown to be a clinically-relevant human matrix source for the design of novel pro-angiogenic biomaterials for potential applications in wound healing. Building from these findings, innovative cell-assembled DAT bead foams were developed and were shown to have a greater pro-angiogenic potential than the previously-established pre-assembled bead foams. These findings confirmed the potential of our novel modular DAT-derived bead foam technology as an ASC delivery platform for applications in soft tissue engineering, wound healing and therapeutic angiogenesis. To further evaluate the effects of tissue-specific ECM composition on ASC differentiation, the cell-assembly method was adapted to produce cell-assembled bead foams from distinct ECM sources, namely DAT, COL, and DTB. Preliminary adipogenic differentiation data suggested the DAT and COL were both highly adipo-conductive, while the DTB had inhibitory effects on ASC adipogenesis. Overall, the work completed in this thesis supports the rationale that DAT-derived bioscaffolds are promising pro-regenerative biomaterials and cell delivery platforms for applications in soft connective tissue engineering, and that complex ECM composition is an important factor in the design of biomaterials.

References

- [1] R. Londono, S.F. Badylak, Biologic scaffolds for regenerative medicine: mechanisms of in vivo remodeling, *Ann Biomed Eng* 43(3) (2015) 577-92.
- [2] L. Labusca, D.D. Herea, K. Mashayekhi, Stem cells as delivery vehicles for regenerative medicine-challenges and perspectives, *World J Stem Cells* 10(5) (2018) 43-56.
- [3] G. Dragneva, P. Korpisalo, S. Yla-Herttuala, Promoting blood vessel growth in ischemic diseases: challenges in translating preclinical potential into clinical success, *Dis Model Mech* 6(2) (2013) 312-22.
- [4] T.R. Heathman, A.W. Nienow, M.J. McCall, K. Coopman, B. Kara, C.J. Hewitt, The translation of cell-based therapies: clinical landscape and manufacturing challenges, *Regen Med* 10(1) (2015) 49-64.
- [5] S.F. Badylak, D.O. Freytes, T.W. Gilbert, Extracellular matrix as a biological scaffold material: Structure and function, *Acta Biomater* 5(1) (2009) 1-13.
- [6] C.R. Nuttelman, M.C. Tripodi, K.S. Anseth, Synthetic hydrogel niches that promote hMSC viability, *Matrix biology : journal of the International Society for Matrix Biology* 24(3) (2005) 208-18.
- [7] M.P. Lutolf, J.A. Hubbell, Synthetic biomaterials as instructive extracellular microenvironments for morphogenesis in tissue engineering, *Nat Biotechnol* 23(1) (2005) 47-55.
- [8] A. Shridhar, E. Gillies, B.G. Amsden, L.E. Flynn, Composite Bioscaffolds Incorporating Decellularized ECM as a Cell-Instructive Component Within Hydrogels as In Vitro Models and Cell Delivery Systems, *Methods Mol Biol* 1577 (2018) 183-208.
- [9] D.J. Lee, S. Diachina, Y.T. Lee, L. Zhao, R. Zou, N. Tang, H. Han, X. Chen, C.C. Ko, Decellularized bone matrix grafts for calvaria regeneration, *J Tissue Eng* 7 (2016) 2041731416680306.
- [10] A.J. Sutherland, E.C. Beck, S.C. Dennis, G.L. Converse, R.A. Hopkins, C.J. Berkland, M.S. Detamore, Decellularized cartilage may be a chondroinductive material for osteochondral tissue engineering, *PLoS One* 10(5) (2015) e0121966.
- [11] Y.C. Choi, J.S. Choi, B.S. Kim, J.D. Kim, H.I. Yoon, Y.W. Cho, Decellularized extracellular matrix derived from porcine adipose tissue as a xenogeneic biomaterial for tissue engineering, *Tissue Eng Part C Methods* 18(11) (2012) 866-76.
- [12] L. Flynn, J.L. Semple, K.A. Woodhouse, Decellularized placental matrices for adipose tissue engineering, *J Biomed Mater Res A* 79(2) (2006) 359-69.
- [13] A.E. Turner, C. Yu, J. Bianco, J.F. Watkins, L.E. Flynn, The performance of decellularized adipose tissue microcarriers as an inductive substrate for human adipose-derived stem cells, *Biomaterials* 33(18) (2012) 4490-9.

- [14] C. Yu, J. Bianco, C. Brown, L. Fuetterer, J.F. Watkins, A. Samani, L.E. Flynn, Porous decellularized adipose tissue foams for soft tissue regeneration, *Biomaterials* 34(13) (2013) 3290-302.
- [15] M. Gingras, I. Paradis, F. Berthod, Nerve regeneration in a collagen-chitosan tissue-engineered skin transplanted on nude mice, *Biomaterials* 24(9) (2003) 1653-61.
- [16] J. Engel, M. Chiquet, An Overview of Extracellular Matrix Structure and Function, in: R.P. Mecham (Ed.), *The Extracellular Matrix: an Overview*, Springer Berlin Heidelberg 2011, p. 440 pages.
- [17] B. Alberts, A. Johnson, J. Lewis, M. Raff, K. Roberts, P. Walter, *The Extracellular Matrix of Animals*, 4th ed., Garland Science 2002.
- [18] J.C. Schittny, P.D. Yurchenco, Basement membranes: molecular organization and function in development and disease, *Current opinion in cell biology* 1(5) (1989) 983-8.
- [19] P. Bornstein, H. Sage, Structurally distinct collagen types, *Annu Rev Biochem* 49 (1980) 957-1003.
- [20] M. van der Rest, R. Garrone, Collagen family of proteins, *FASEB J* 5(13) (1991) 2814-23.
- [21] S. Viglio, N. Zoppi, A. Sangalli, A. Gallanti, S. Barlati, M. Mottes, M. Colombi, M. Valli, Rescue of migratory defects of Ehlers-Danlos syndrome fibroblasts in vitro by type V collagen but not insulin-like binding protein-1, *J Invest Dermatol* 128(8) (2008) 1915-9.
- [22] P. Chen, M. Cescon, P. Bonaldo, Collagen VI in cancer and its biological mechanisms, *Trends Mol Med* 19(7) (2013) 410-7.
- [23] W. Li, J. Fan, M. Chen, S. Guan, D. Sawcer, G.M. Bokoch, D.T. Woodley, Mechanism of human dermal fibroblast migration driven by type I collagen and platelet-derived growth factor-BB, *Mol Biol Cell* 15(1) (2004) 294-309.
- [24] X. Liu, H. Wu, M. Byrne, S. Krane, R. Jaenisch, Type III collagen is crucial for collagen I fibrillogenesis and for normal cardiovascular development, *Proc Natl Acad Sci U S A* 94(5) (1997) 1852-6.
- [25] S. Heinonen, M. Mannikko, J.F. Klement, D. Whitaker-Menezes, G.F. Murphy, J. Uitto, Targeted inactivation of the type VII collagen gene (*Col7a1*) in mice results in severe blistering phenotype: a model for recessive dystrophic epidermolysis bullosa, *Journal of cell science* 112 (Pt 21) (1999) 3641-8.
- [26] R.P. Mecham, Elastin biosynthesis: a look at the current scene, *Connect Tissue Res* 8(3-4) (1981) 155-60.
- [27] S. Seite, H. Zucchi, D. Septier, S. Igondjo-Tchen, K. Senni, G. Godeau, Elastin changes during chronological and photo-ageing: the important role of lysozyme, *Journal of the European Academy of Dermatology and Venereology : JEADV* 20(8) (2006) 980-7.
- [28] F. Grinnell, Fibronectin and wound healing, *J Cell Biochem* 26(2) (1984) 107-16.

- [29] V.B. Kumar, R.I. Viji, M.S. Kiran, P.R. Sudhakaran, Angiogenic response of endothelial cells to fibronectin, *Adv Exp Med Biol* 749 (2012) 131-51.
- [30] K.M. French, J.T. Maxwell, S. Bhutani, S. Ghosh-Choudhary, M.J. Fierro, T.D. Johnson, K.L. Christman, W.R. Taylor, M.E. Davis, Fibronectin and Cyclic Strain Improve Cardiac Progenitor Cell Regenerative Potential In Vitro, *Stem Cells Int* 2016 (2016) 8364382.
- [31] W.S. To, K.S. Midwood, Plasma and cellular fibronectin: distinct and independent functions during tissue repair, *Fibrogenesis Tissue Repair* 4 (2011) 21.
- [32] E. Klotzsch, M.L. Smith, K.E. Kubow, S. Muntwyler, W.C. Little, F. Beyeler, D. Gourdon, B.J. Nelson, V. Vogel, Fibronectin forms the most extensible biological fibers displaying switchable force-exposed cryptic binding sites, *Proc Natl Acad Sci U S A* 106(43) (2009) 18267-72.
- [33] A. Pozzi, P.D. Yurchenco, R.V. Iozzo, The nature and biology of basement membranes, *Matrix biology : journal of the International Society for Matrix Biology* 57-58 (2017) 1-11.
- [34] K. Kick, K. Nekolla, M. Rehberg, A.M. Vollmar, S. Zahler, New View on Endothelial Cell Migration: Switching Modes of Migration Based on Matrix Composition, *Arterioscler Thromb Vasc Biol* 36(12) (2016) 2346-2357.
- [35] M.M. Smith, J. Melrose, Proteoglycans in Normal and Healing Skin, *Adv Wound Care (New Rochelle)* 4(3) (2015) 152-173.
- [36] R.O. Hynes, A. Naba, Overview of the matrisome--an inventory of extracellular matrix constituents and functions, *Cold Spring Harb Perspect Biol* 4(1) (2012) a004903.
- [37] E.S. Wijelath, S. Rahman, M. Namekata, J. Murray, T. Nishimura, Z. Mostafavi-Pour, Y. Patel, Y. Suda, M.J. Humphries, M. Sobel, Heparin-II domain of fibronectin is a vascular endothelial growth factor-binding domain: enhancement of VEGF biological activity by a singular growth factor/matrix protein synergism, *Circ Res* 99(8) (2006) 853-60.
- [38] S. Rahman, Y. Patel, J. Murray, K.V. Patel, R. Sumathipala, M. Sobel, E.S. Wijelath, Novel hepatocyte growth factor (HGF) binding domains on fibronectin and vitronectin coordinate a distinct and amplified Met-integrin induced signalling pathway in endothelial cells, *BMC Cell Biol* 6(1) (2005) 8.
- [39] F. Lin, X.D. Ren, Z. Pan, L. Macri, W.X. Zong, M.G. Tonnesen, M. Rafailovich, D. Bar-Sagi, R.A. Clark, Fibronectin growth factor-binding domains are required for fibroblast survival, *J Invest Dermatol* 131(1) (2011) 84-98.
- [40] L. Banyai, P. Sonderegger, L. Patthy, Agrin binds BMP2, BMP4 and TGFbeta1, *PLoS One* 5(5) (2010) e10758.
- [41] J.S. Munger, D. Sheppard, Cross talk among TGF-beta signaling pathways, integrins, and the extracellular matrix, *Cold Spring Harb Perspect Biol* 3(11) (2011) a005017.
- [42] A.H. Morris, T.R. Kyriakides, Matricellular proteins and biomaterials, *Matrix biology : journal of the International Society for Matrix Biology* 37 (2014) 183-91.

- [43] J.T. Walker, S.S. Kim, S. Michelsons, K. Creber, C.G. Elliott, A. Leask, D.W. Hamilton, Cell-matrix interactions governing skin repair: matricellular proteins as diverse modulators of cell function, *Res Rep Biochem* 5 (2015) 73-88.
- [44] T.R. Kyriakides, P. Bornstein, Matricellular proteins as modulators of wound healing and the foreign body response, *Thrombosis and haemostasis* 90(6) (2003) 986-92.
- [45] H. Nagase, R. Visse, G. Murphy, Structure and function of matrix metalloproteinases and TIMPs, *Cardiovasc Res* 69(3) (2006) 562-73.
- [46] A. Jablonska-Trypuc, M. Matejczyk, S. Rosochacki, Matrix metalloproteinases (MMPs), the main extracellular matrix (ECM) enzymes in collagen degradation, as a target for anticancer drugs, *J Enzyme Inhib Med Chem* 31(sup1) (2016) 177-183.
- [47] J.D. Mott, Z. Werb, Regulation of matrix biology by matrix metalloproteinases, *Current opinion in cell biology* 16(5) (2004) 558-64.
- [48] J.Z. Kechagia, J. Ivaska, P. Roca-Cusachs, Integrins as biomechanical sensors of the microenvironment, *Nature reviews. Molecular cell biology* (2019).
- [49] L.A. Cary, D.C. Han, J.L. Guan, Integrin-mediated signal transduction pathways, *Histol Histopathol* 14(3) (1999) 1001-9.
- [50] D.S. Harburger, D.A. Calderwood, Integrin signalling at a glance, *Journal of cell science* 122(Pt 2) (2009) 159-63.
- [51] S.P. Alexander, A. Mathie, J.A. Peters, *Guide to Receptors and Channels (GRAC)*, 5th edition, *Br J Pharmacol* 164 Suppl 1 (2011) S1-324.
- [52] B. Alberts, A. Johnson, J. Lewis, M. Raff, K. Roberts, P. Walter, *Signaling through Enzyme-Linked Cell-Surface Receptors*, 4th ed., Garland Science 2002.
- [53] A. Reiner, J. Levitz, Glutamatergic Signaling in the Central Nervous System: Ionotropic and Metabotropic Receptors in Concert, *Neuron* 98(6) (2018) 1080-1098.
- [54] M.A. Garcia, W.J. Nelson, N. Chavez, Cell-Cell Junctions Organize Structural and Signaling Networks, *Cold Spring Harb Perspect Biol* 10(4) (2018).
- [55] V. Mohamed-Ali, J.H. Pinkney, S.W. Coppack, Adipose tissue as an endocrine and paracrine organ, *Int J Obes Relat Metab Disord* 22(12) (1998) 1145-58.
- [56] Y. Han, X. You, W. Xing, Z. Zhang, W. Zou, Paracrine and endocrine actions of bone-the functions of secretory proteins from osteoblasts, osteocytes, and osteoclasts, *Bone Res* 6 (2018) 16.
- [57] E.C. Mariman, P. Wang, Adipocyte extracellular matrix composition, dynamics and role in obesity, *Cell Mol Life Sci* 67(8) (2010) 1277-92.
- [58] A. Wronska, Z. Kmiec, Structural and biochemical characteristics of various white adipose tissue depots, *Acta Physiol (Oxf)* 205(2) (2012) 194-208.
- [59] I. Nakajima, T. Yamaguchi, K. Ozutsumi, H. Aso, Adipose tissue extracellular matrix: newly organized by adipocytes during differentiation, *Differentiation; research in biological diversity* 63(4) (1998) 193-200.
- [60] S. Kajimura, Adipose tissue in 2016: Advances in the understanding of adipose tissue biology, *Nat Rev Endocrinol* 13(2) (2017) 69-70.

- [61] J.H. Stern, P.E. Scherer, Adipose tissue biology in 2014: Advances in our understanding of adipose tissue homeostasis, *Nat Rev Endocrinol* 11(2) (2015) 71-2.
- [62] M. Kuljanin, C.F.C. Brown, M.J. Raleigh, G.A. Lajoie, L.E. Flynn, Collagenase treatment enhances proteomic coverage of low-abundance proteins in decellularized matrix bioscaffolds, *Biomaterials* 144 (2017) 130-143.
- [63] M. Spencer, R. Unal, B. Zhu, N. Rasouli, R.E. McGehee, Jr., C.A. Peterson, P.A. Kern, Adipose tissue extracellular matrix and vascular abnormalities in obesity and insulin resistance, *J Clin Endocrinol Metab* 96(12) (2011) E1990-8.
- [64] M. McKinley, V.D. O'Loughlin, Cartilage and Bone Connective Tissue, in: K.A. Perterson (Ed.), *Human Anatomy*, McGraw-Hill 2006, pp. 147-288.
- [65] B.Q. Le, V. Nurcombe, S.M. Cool, C.A. van Blitterswijk, J. de Boer, V.L.S. LaPointe, The Components of Bone and What They Can Teach Us about Regeneration, *Materials (Basel)* 11(1) (2017).
- [66] R.W. Norrdin, R.D. Phemister, R.S. Jaenke, C.A. Lo Presti, Density and composition of trabecular and cortical bone in perinatally irradiated beagles with chronic renal failure, *Calcif Tissue Res* 24(1) (1977) 99-104.
- [67] J.K. Gong, J.S. Arnold, S.H. Cohn, Composition of Trabecular and Cortical Bone, *Anat Rec* 149 (1964) 325-31.
- [68] A.R. Amini, C.T. Laurencin, S.P. Nukavarapu, Bone tissue engineering: recent advances and challenges, *Crit Rev Biomed Eng* 40(5) (2012) 363-408.
- [69] Y.D. Halvorsen, D. Franklin, A.L. Bond, D.C. Hitt, C. Auchter, A.L. Boskey, E.P. Paschalis, W.O. Wilkison, J.M. Gimble, Extracellular matrix mineralization and osteoblast gene expression by human adipose tissue-derived stromal cells, *Tissue Eng* 7(6) (2001) 729-41.
- [70] G. Tomoaia, R.D. Pasca, On the Collagen Mineralization. A Review, *Clujul Med* 88(1) (2015) 15-22.
- [71] T.T. Han, A. Shridhar, K.P. Robb, A. Kornmuller, C. Brown, L.E. Flynn, Natural Materials as Smart Scaffolds for Tissue Engineering, in: Q. Wang (Ed.), *Smart Materials for Tissue Engineering: Fundamental Principles*, The Royal Society of Chemistry 2017, pp. 124-162.
- [72] C.J. Flaim, D. Teng, S. Chien, S.N. Bhatia, Combinatorial signaling microenvironments for studying stem cell fate, *Stem Cells Dev* 17(1) (2008) 29-39.
- [73] F. Edalat, I. Sheu, S. Manoucheri, A. Khademhosseini, Material strategies for creating artificial cell-instructive niches, *Curr Opin Biotechnol* 23(5) (2012) 820-5.
- [74] K.P. Robb, A. Shridhar, L.E. Flynn, Decellularized Matrices As Cell-Instructive Scaffolds to Guide Tissue-Specific Regeneration, *ACS Biomaterials Science & Engineering* 4(11) (2017) 3627-3643.
- [75] J.M. Aamodt, D.W. Grainger, Extracellular matrix-based biomaterial scaffolds and the host response, *Biomaterials* 86 (2016) 68-82.

- [76] M.D. Swartzlander, A.K. Blakney, L.D. Amer, K.D. Hankenson, T.R. Kyriakides, S.J. Bryant, Immunomodulation by mesenchymal stem cells combats the foreign body response to cell-laden synthetic hydrogels, *Biomaterials* 41 (2015) 79-88.
- [77] C. Bergeret-Galley, Comparison of resorbable soft tissue fillers, *Aesthetic surgery journal / the American Society for Aesthetic Plastic surgery* 24(1) (2004) 33-46.
- [78] B.L. Eppley, B. Dadvand, Injectable soft-tissue fillers: clinical overview, *Plast Reconstr Surg* 118(4) (2006) 98e-106e.
- [79] A. Porzionato, E. Stocco, S. Barbon, F. Grandi, V. Macchi, R. De Caro, Tissue-Engineered Grafts from Human Decellularized Extracellular Matrices: A Systematic Review and Future Perspectives, *Int J Mol Sci* 19(12) (2018).
- [80] K. Coopman, N. Medcalf, From production to patient: challenges and approaches for delivering cell therapies, *StemBook*, Cambridge (MA), 2008.
- [81] Y. Ikada, Challenges in tissue engineering, *J R Soc Interface* 3(10) (2006) 589-601.
- [82] K.W. Wissemann, B.S. Jacobson, Pure gelatin microcarriers: synthesis and use in cell attachment and growth of fibroblast and endothelial cells, *In Vitro Cell Dev Biol* 21(7) (1985) 391-401.
- [83] K. Sisson, C. Zhang, M.C. Farach-Carson, D.B. Chase, J.F. Rabolt, Evaluation of cross-linking methods for electrospun gelatin on cell growth and viability, *Biomacromolecules* 10(7) (2009) 1675-80.
- [84] F. O'Brien, Biomaterials & scaffolds for tissue engineering, *Materials Today* 14(3) (2011) 88-95.
- [85] L.J. White, A.J. Taylor, D.M. Faulk, T.J. Keane, L.T. Saldin, J.E. Reing, I.T. Swinehart, N.J. Turner, B.D. Ratner, S.F. Badylak, The impact of detergents on the tissue decellularization process: A ToF-SIMS study, *Acta Biomater* 50 (2017) 207-219.
- [86] R. Gaetani, C. Yin, N. Srikumar, R. Braden, P.A. Doevendans, J.P. Sluijter, K.L. Christman, Cardiac-Derived Extracellular Matrix Enhances Cardiogenic Properties of Human Cardiac Progenitor Cells, *Cell Transplant* 25(9) (2016) 1653-1663.
- [87] L. Hou, J. Coller, V. Natsu, T.J. Hastie, N.F. Huang, Combinatorial extracellular matrix microenvironments promote survival and phenotype of human induced pluripotent stem cell-derived endothelial cells in hypoxia, *Acta Biomater* 44 (2016) 188-99.
- [88] C.J. Flaim, S. Chien, S.N. Bhatia, An extracellular matrix microarray for probing cellular differentiation, *Nat Methods* 2(2) (2005) 119-25.
- [89] M.J. Dalby, A.J. Garcia, M. Salmeron-Sanchez, Receptor control in mesenchymal stem cell engineering, *Nat Rev. Materials* (2018).
- [90] J.S. Park, J.S. Chu, A.D. Tsou, R. Diop, Z. Tang, A. Wang, S. Li, The effect of matrix stiffness on the differentiation of mesenchymal stem cells in response to TGF-beta, *Biomaterials* 32(16) (2011) 3921-30.
- [91] C. Branco da Cunha, D.D. Klumpers, W.A. Li, S.T. Koshy, J.C. Weaver, O. Chaudhuri, P.L. Granja, D.J. Mooney, Influence of the stiffness of three-

- dimensional alginate/collagen-I interpenetrating networks on fibroblast biology, *Biomaterials* 35(32) (2014) 8927-36.
- [92] H. El-Mohri, Y. Wu, S. Mohanty, G. Ghosh, Impact of matrix stiffness on fibroblast function, *Mater Sci Eng C Mater Biol Appl* 74 (2017) 146-151.
- [93] T.W. Gilbert, T.L. Sellaro, S.F. Badylak, Decellularization of tissues and organs, *Biomaterials* 27(19) (2006) 3675-83.
- [94] A. Gilpin, Y. Yang, Decellularization Strategies for Regenerative Medicine: From Processing Techniques to Applications, *Biomed Res Int* 2017 (2017) 9831534.
- [95] T.J. Keane, I.T. Swinehart, S.F. Badylak, Methods of tissue decellularization used for preparation of biologic scaffolds and in vivo relevance, *Methods* 84 (2015) 25-34.
- [96] J. Burk, I. Erbe, D. Berner, J. Kacza, C. Kasper, B. Pfeiffer, K. Winter, W. Brehm, Freeze-thaw cycles enhance decellularization of large tendons, *Tissue Eng Part C Methods* 20(4) (2014) 276-84.
- [97] S. Funamoto, K. Nam, T. Kimura, A. Murakoshi, Y. Hashimoto, K. Niwaya, S. Kitamura, T. Fujisato, A. Kishida, The use of high-hydrostatic pressure treatment to decellularize blood vessels, *Biomaterials* 31(13) (2010) 3590-5.
- [98] N. Poornejad, T.S. Frost, D.R. Scott, B.B. Elton, P.R. Reynolds, B.L. Roeder, A.D. Cook, Freezing/Thawing without Cryoprotectant Damages Native but not Decellularized Porcine Renal Tissue, *Organogenesis* 11(1) (2015) 30-45.
- [99] B. Cox, A. Emili, Tissue subcellular fractionation and protein extraction for use in mass-spectrometry-based proteomics, *Nat Protoc* 1(4) (2006) 1872-8.
- [100] C.C. Xu, R.W. Chan, N. Tirunagari, A biodegradable, acellular xenogeneic scaffold for regeneration of the vocal fold lamina propria, *Tissue Eng* 13(3) (2007) 551-66.
- [101] J. Hodde, A. Janis, D. Ernst, D. Zopf, D. Sherman, C. Johnson, Effects of sterilization on an extracellular matrix scaffold: part I. Composition and matrix architecture, *Journal of materials science. Materials in medicine* 18(4) (2007) 537-43.
- [102] C. Gardin, S. Ricci, L. Ferroni, R. Guazzo, L. Sbricoli, G. De Benedictis, L. Finotti, M. Isola, E. Bressan, B. Zavan, Decellularization and Delipidation Protocols of Bovine Bone and Pericardium for Bone Grafting and Guided Bone Regeneration Procedures, *PLoS One* 10(7) (2015) e0132344.
- [103] M.J. Sawkins, W. Bowen, P. Dhadha, H. Markides, L.E. Sidney, A.J. Taylor, F.R. Rose, S.F. Badylak, K.M. Shakesheff, L.J. White, Hydrogels derived from demineralized and decellularized bone extracellular matrix, *Acta Biomater* 9(8) (2013) 7865-73.
- [104] L.E. Flynn, The use of decellularized adipose tissue to provide an inductive microenvironment for the adipogenic differentiation of human adipose-derived stem cells, *Biomaterials* 31(17) (2010) 4715-24.
- [105] S.B. Lumpkins, N. Pierre, P.S. McFetridge, A mechanical evaluation of three decellularization methods in the design of a xenogeneic scaffold for tissue engineering the temporomandibular joint disc, *Acta Biomater* 4(4) (2008) 808-16.

- [106] N. Zhang, M. Zhou, Y. Zhang, X. Wang, S. Ma, L. Dong, T. Yang, L. Ma, B. Li, Porcine bone grafts defatted by lipase: efficacy of defatting and assessment of cytocompatibility, *Cell Tissue Bank* 15(3) (2014) 357-67.
- [107] J. Dunmore-Buyze, D.R. Boughner, N. Macris, I. Vesely, A comparison of macroscopic lipid content within porcine pulmonary and aortic valves. Implications for bioprosthetic valves, *J Thorac Cardiovasc Surg* 110(6) (1995) 1756-61.
- [108] R.J. Levy, N. Vyavahare, M. Ogle, P. Ashworth, R. Bianco, F.J. Schoen, Inhibition of cusp and aortic wall calcification in ethanol- and aluminum-treated bioprosthetic heart valves in sheep: background, mechanisms, and synergism, *J Heart Valve Dis* 12(2) (2003) 209-16; discussion 216.
- [109] J.S. Cartmell, M.G. Dunn, Effect of chemical treatments on tendon cellularity and mechanical properties, *J Biomed Mater Res* 49(1) (2000) 134-40.
- [110] T. Woods, P.F. Gratzner, Effectiveness of three extraction techniques in the development of a decellularized bone-anterior cruciate ligament-bone graft, *Biomaterials* 26(35) (2005) 7339-49.
- [111] S.L.M. Dahl, J. Koh, V. Prabhakar, L.E. Niklason, Decellularized Native and Engineered Arterial Scaffolds for Transplantation, *Cell Transplant* 12(6) (2003) 659-666.
- [112] P.M. Crapo, T.W. Gilbert, S.F. Badylak, An overview of tissue and whole organ decellularization processes, *Biomaterials* 32(12) (2011) 3233-43.
- [113] E. Omid, L. Fuetterer, S. Reza Mousavi, R.C. Armstrong, L.E. Flynn, A. Samani, Characterization and assessment of hyperelastic and elastic properties of decellularized human adipose tissues, *Journal of biomechanics* 47(15) (2014) 3657-63.
- [114] M.T. Kasimir, E. Rieder, G. Seebacher, G. Silberhumer, E. Wolner, G. Weigel, P. Simon, Comparison of different decellularization procedures of porcine heart valves, *Int J Artif Organs* 26(5) (2003) 421-7.
- [115] J.E. Reing, B.N. Brown, K.A. Daly, J.M. Freund, T.W. Gilbert, S.X. Hsiong, A. Huber, K.E. Kullas, S. Tottey, M.T. Wolf, S.F. Badylak, The effects of processing methods upon mechanical and biologic properties of porcine dermal extracellular matrix scaffolds, *Biomaterials* 31(33) (2010) 8626-33.
- [116] E. Rieder, M.T. Kasimir, G. Silberhumer, G. Seebacher, E. Wolner, P. Simon, G. Weigel, Decellularization protocols of porcine heart valves differ importantly in efficiency of cell removal and susceptibility of the matrix to recellularization with human vascular cells, *J Thorac Cardiovasc Surg* 127(2) (2004) 399-405.
- [117] H. Xu, B. Xu, Q. Yang, X. Li, X. Ma, Q. Xia, Y. Zhang, C. Zhang, Y. Wu, Y. Zhang, Comparison of decellularization protocols for preparing a decellularized porcine annulus fibrosus scaffold, *PLoS One* 9(1) (2014) e86723.
- [118] B.N. Brown, J.M. Freund, L. Han, J.P. Rubin, J.E. Reing, E.M. Jeffries, M.T. Wolf, S. Tottey, C.A. Barnes, B.D. Ratner, S.F. Badylak, Comparison of three methods for the derivation of a biologic scaffold composed of adipose tissue extracellular matrix, *Tissue Eng Part C Methods* 17(4) (2011) 411-21.

- [119] D.A. Young, D.O. Ibrahim, D. Hu, K.L. Christman, Injectable hydrogel scaffold from decellularized human lipoaspirate, *Acta Biomater* 7(3) (2011) 1040-9.
- [120] Q. Zhang, J.A. Johnson, L.W. Dunne, Y. Chen, T. Iyyanki, Y. Wu, E.I. Chang, C.D. Branch-Brooks, G.L. Robb, C.E. Butler, Decellularized skin/adipose tissue flap matrix for engineering vascularized composite soft tissue flaps, *Acta Biomater* 35 (2016) 166-84.
- [121] Q.W. Tan, Y. Zhang, J.C. Luo, D. Zhang, B.J. Xiong, J.Q. Yang, H.Q. Xie, Q. Lv, Hydrogel derived from decellularized porcine adipose tissue as a promising biomaterial for soft tissue augmentation, *J Biomed Mater Res A* (2017).
- [122] S. Zhang, Q. Lu, T. Cao, W.S. Toh, Adipose Tissue and Extracellular Matrix Development by Injectable Decellularized Adipose Matrix Loaded with Basic Fibroblast Growth Factor, *Plast Reconstr Surg* 137(4) (2016) 1171-80.
- [123] J.S. Choi, B.S. Kim, J.Y. Kim, J.D. Kim, Y.C. Choi, H.J. Yang, K. Park, H.Y. Lee, Y.W. Cho, Decellularized extracellular matrix derived from human adipose tissue as a potential scaffold for allograft tissue engineering, *J Biomed Mater Res A* 97(3) (2011) 292-9.
- [124] C. Thomas-Porch, J. Li, F. Zanata, E.C. Martin, N. Pashos, K. Genemaras, J.N. Poche, N.P. Totaro, M.R. Bratton, D. Gaupp, T. Frazier, X. Wu, L.M. Ferreira, W. Tian, G. Wang, B.A. Bunnell, L. Flynn, D. Hayes, J.M. Gimble, Comparative proteomic analyses of human adipose extracellular matrices decellularized using alternative procedures, *J Biomed Mater Res A* 106(9) (2018) 2481-2493.
- [125] L. Wang, J.A. Johnson, Q. Zhang, E.K. Beahm, Combining decellularized human adipose tissue extracellular matrix and adipose-derived stem cells for adipose tissue engineering, *Acta Biomater* 9(11) (2013) 8921-31.
- [126] T.T. Han, S. Toutounji, B.G. Amsden, L.E. Flynn, Adipose-derived stromal cells mediate in vivo adipogenesis, angiogenesis and inflammation in decellularized adipose tissue bioscaffolds, *Biomaterials* 72 (2015) 125-37.
- [127] H.K. Kleinman, Preparation of basement membrane components from EHS tumors, *Curr Protoc Cell Biol Chapter 10* (2001) Unit 10 2.
- [128] V. Russo, E. Omid, A. Samani, A. Hamilton, L.E. Flynn, Porous, Ventricular Extracellular Matrix-Derived Foams as a Platform for Cardiac Cell Culture, *Biores Open Access* 4(1) (2015) 374-88.
- [129] A. Kornmuller, C.F.C. Brown, C. Yu, L.E. Flynn, Fabrication of Extracellular Matrix-derived Foams and Microcarriers as Tissue-specific Cell Culture and Delivery Platforms, *J Vis Exp* (122) (2017).
- [130] P. Morissette Martin, A. Shridhar, C. Yu, C. Brown, L.E. Flynn, Decellularized Adipose Tissue Scaffolds for Soft Tissue Regeneration and Adipose-Derived Stem/Stromal Cell Delivery, *Methods Mol Biol* 1773 (2018) 53-71.
- [131] M.P. Francis, P.C. Sachs, P.A. Madurantakam, S.A. Sell, L.W. Elmore, G.L. Bowlin, S.E. Holt, Electrospinning adipose tissue-derived extracellular matrix for adipose stem cell culture, *J Biomed Mater Res A* 100(7) (2012) 1716-24.

- [132] A.E. Turner, L.E. Flynn, Design and characterization of tissue-specific extracellular matrix-derived microcarriers, *Tissue Eng Part C Methods* 18(3) (2012) 186-97.
- [133] D. Adam Young, V. Bajaj, K.L. Christman, Award winner for outstanding research in the PhD category, 2014 Society for Biomaterials annual meeting and exposition, Denver, Colorado, April 16-19, 2014: Decellularized adipose matrix hydrogels stimulate in vivo neovascularization and adipose formation, *J Biomed Mater Res A* 102(6) (2014) 1641-51.
- [134] F. Pati, J. Jang, D.H. Ha, S. Won Kim, J.W. Rhie, J.H. Shim, D.H. Kim, D.W. Cho, Printing three-dimensional tissue analogues with decellularized extracellular matrix bioink, *Nat Commun* 5 (2014) 3935.
- [135] C. Yu, A. Kornmuller, C. Brown, T. Hoare, L.E. Flynn, Decellularized adipose tissue microcarriers as a dynamic culture platform for human adipose-derived stem/stromal cell expansion, *Biomaterials* 120 (2017) 66-80.
- [136] A. Shridhar, A.Y.L. Lam, Y. Sun, C.A. Simmons, E.R. Gillies, L.E. Flynn, Culture on tissue-specific Coatings Derived from alpha-amylase-digested Decellularized Adipose Tissue Enhances the Proliferation and Adipogenic Differentiation of Human adipose-derived Stromal Cells, *Biotechnol J* (2019) e1900118.
- [137] A.H. Morris, D.K. Stamer, T.R. Kyriakides, The host response to naturally-derived extracellular matrix biomaterials, *Semin Immunol* 29 (2017) 72-91.
- [138] S. Guo, L.A. Dipietro, Factors affecting wound healing, *Journal of dental research* 89(3) (2010) 219-29.
- [139] M. Cherubino, J.P. Rubin, N. Miljkovic, A. Kelmendi-Doko, K.G. Marra, Adipose-derived stem cells for wound healing applications, *Ann Plast Surg* 66(2) (2011) 210-5.
- [140] P. Morissette Martin, K. Kreber, D.W. Hamilton, Measuring gene expression changes on biomaterial surfaces, in: R.J. Narayan (Ed.), *Monitoring and Evaluation of Biomaterials and their Performance In Vivo*, Woodhouse publishing 2016, pp. 111-132.
- [141] A.J. Singer, R.A. Clark, Cutaneous wound healing, *The New England journal of medicine* 341(10) (1999) 738-46.
- [142] N. Borregaard, Neutrophils, from marrow to microbes, *Immunity* 33(5) (2010) 657-70.
- [143] C.J. Ferrante, S.J. Leibovich, Regulation of Macrophage Polarization and Wound Healing, *Adv Wound Care (New Rochelle)* 1(1) (2012) 10-16.
- [144] A. Desmouliere, C. Chaponnier, G. Gabbiani, Tissue repair, contraction, and the myofibroblast, *Wound Repair Regen* 13(1) (2005) 7-12.
- [145] K.S. Midwood, L.V. Williams, J.E. Schwarzbauer, Tissue repair and the dynamics of the extracellular matrix, *Int J Biochem Cell Biol* 36(6) (2004) 1031-7.
- [146] L. Micallef, N. Vedrenne, F. Billet, B. Coulomb, I.A. Darby, A. Desmouliere, The myofibroblast, multiple origins for major roles in normal and pathological tissue repair, *Fibrogenesis Tissue Repair* 5(Suppl 1) (2012) S5.

- [147] C.G. Elliott, J. Wang, X. Guo, S.W. Xu, M. Eastwood, J. Guan, A. Leask, S.J. Conway, D.W. Hamilton, Periostin modulates myofibroblast differentiation during full-thickness cutaneous wound repair, *Journal of cell science* 125(1) (2012) 121-32.
- [148] R.H. Adams, K. Alitalo, Molecular regulation of angiogenesis and lymphangiogenesis, *Nature reviews. Molecular cell biology* 8(6) (2007) 464-78.
- [149] D. Ribatti, V. Djonov, Intussusceptive microvascular growth in tumors, *Cancer Lett* 316(2) (2012) 126-31.
- [150] J.H. Distler, A. Hirth, M. Kurowska-Stolarska, R.E. Gay, S. Gay, O. Distler, Angiogenic and angiostatic factors in the molecular control of angiogenesis, *Q J Nucl Med* 47(3) (2003) 149-61.
- [151] R. Goldman, Growth factors and chronic wound healing: past, present, and future, *Advances in skin & wound care* 17(1) (2004) 24-35.
- [152] G. Bazzoni, E. Dejana, Endothelial cell-to-cell junctions: molecular organization and role in vascular homeostasis, *Physiol Rev* 84(3) (2004) 869-901.
- [153] L. Eklund, B.R. Olsen, Tie receptors and their angiopoietin ligands are context-dependent regulators of vascular remodeling, *Exp Cell Res* 312(5) (2006) 630-41.
- [154] T.A. Mustoe, K. O'Shaughnessy, O. Kloeters, Chronic wound pathogenesis and current treatment strategies: a unifying hypothesis, *Plast Reconstr Surg* 117(7 Suppl) (2006) 35S-41S.
- [155] M.A. Fonder, G.S. Lazarus, D.A. Cowan, B. Aronson-Cook, A.R. Kohli, A.J. Mamelak, Treating the chronic wound: A practical approach to the care of nonhealing wounds and wound care dressings, *Journal of the American Academy of Dermatology* 58(2) (2008) 185-206.
- [156] T.R. Einarson, A. Acs, C. Ludwig, U.H. Pantou, Prevalence of cardiovascular disease in type 2 diabetes: a systematic literature review of scientific evidence from across the world in 2007-2017, *Cardiovasc Diabetol* 17(1) (2018) 83.
- [157] W.J. Jeffcoate, K.G. Harding, Diabetic foot ulcers, *Lancet* 361(9368) (2003) 1545-51.
- [158] C.K. Sen, G.M. Gordillo, S. Roy, R. Kirsner, L. Lambert, T.K. Hunt, F. Gottrup, G.C. Gurtner, M.T. Longaker, Human skin wounds: a major and snowballing threat to public health and the economy, *Wound repair and regeneration : official publication of the Wound Healing Society [and] the European Tissue Repair Society* 17(6) (2009) 763-71.
- [159] N. Spravchikov, G. Sizyakov, M. Gartsbein, D. Accili, T. Tennenbaum, E. Wertheimer, Glucose effects on skin keratinocytes: implications for diabetes skin complications, *Diabetes* 50(7) (2001) 1627-35.
- [160] P.J. Hennessey, E.G. Ford, C.T. Black, R.J. Andrassy, Wound collagenase activity correlates directly with collagen glycosylation in diabetic rats, *J Pediatr Surg* 25(1) (1990) 75-8.
- [161] P. Dandona, A. Aljada, A. Bandyopadhyay, Inflammation: the link between insulin resistance, obesity and diabetes, *Trends in immunology* 25(1) (2004) 4-7.

- [162] H. Cucak, L.G. Grunnet, A. Rosendahl, Accumulation of M1-like macrophages in type 2 diabetic islets is followed by a systemic shift in macrophage polarization, *Journal of leukocyte biology* 95(1) (2014) 149-60.
- [163] F.G. Fowkes, D. Rudan, I. Rudan, V. Aboyans, J.O. Denenberg, M.M. McDermott, P.E. Norman, U.K. Sampson, L.J. Williams, G.A. Mensah, M.H. Criqui, Comparison of global estimates of prevalence and risk factors for peripheral artery disease in 2000 and 2010: a systematic review and analysis, *Lancet* 382(9901) (2013) 1329-40.
- [164] E. Faglia, G. Clerici, J. Clerissi, L. Gabrielli, S. Losa, M. Mantero, M. Caminiti, V. Curci, T. Lupattelli, A. Morabito, Early and five-year amputation and survival rate of diabetic patients with critical limb ischemia: data of a cohort study of 564 patients, *Eur J Vasc Endovasc Surg* 32(5) (2006) 484-90.
- [165] F. Gottrup, J. Apelqvist, T. Bjansholt, R. Cooper, Z. Moore, E.J. Peters, S. Probst, EWMA document: Antimicrobials and non-healing wounds. Evidence, controversies and suggestions, *J Wound Care* 22(5 Suppl) (2013) S1-89.
- [166] C. Ruangsetakit, K. Chinsakchai, P. Mahawongkajit, C. Wongwanit, P. Mutirangura, Transcutaneous oxygen tension: a useful predictor of ulcer healing in critical limb ischaemia, *J Wound Care* 19(5) (2010) 202-6.
- [167] A. Carreau, B. El Hafny-Rahbi, A. Matejuk, C. Grillon, C. Kieda, Why is the partial oxygen pressure of human tissues a crucial parameter? Small molecules and hypoxia, *J Cell Mol Med* 15(6) (2011) 1239-53.
- [168] S.H. Ko, D.F. Bandyk, Therapeutic angiogenesis for critical limb ischemia, *Semin Vasc Surg* 27(1) (2014) 23-31.
- [169] R.V. Shevchenko, S.L. James, S.E. James, A review of tissue-engineered skin bioconstructs available for skin reconstruction, *J R Soc Interface* 7(43) (2010) 229-58.
- [170] S. Saim, A.B. Heintzelman, R.A. Bryan, Cellular- and/or Tissue-Based products for wounds, in: R.A. Bryant, D. Nix (Eds.), *Acute and Chronic Wounds*, 5th Edition, Elsevier Health Sciences 2016, p. 648.
- [171] Integra LifeSciences Corporation, A Safety and Efficacy Study of INTEGRA® Dermal Regeneration Template for the Treatment of Diabetic Foot Ulcers, 2016. <https://clinicaltrials.gov/ct2/show/results/NCT01060670>. (Accessed February 7th 2017).
- [172] D.M. Wise, Histologic proof that acellular dermal matrices (ADM)--Enduragen, DermaMatrix, and DuraMatrix--are not repopulated or nonviable and that AlloDerm may be repopulated but degraded synchronously, *Aesthetic surgery journal / the American Society for Aesthetic Plastic surgery* 32(3) (2012) 355-8.
- [173] C.E. Hart, A. Loewen-Rodriguez, J. Lessem, Dermagraft: Use in the Treatment of Chronic Wounds, *Adv Wound Care (New Rochelle)* 1(3) (2012) 138-141.
- [174] C.M. Botham, W.L. Bennett, J.P. Cooke, Clinical trials of adult stem cell therapy for peripheral artery disease, *Methodist DeBakey Cardiovasc J* 9(4) (2013) 201-5.

- [175] M.H. Moon, S.Y. Kim, Y.J. Kim, S.J. Kim, J.B. Lee, Y.C. Bae, S.M. Sung, J.S. Jung, Human adipose tissue-derived mesenchymal stem cells improve postnatal neovascularization in a mouse model of hindlimb ischemia, *Cell Physiol Biochem* 17(5-6) (2006) 279-90.
- [176] V.W. Wong, K.C. Rustad, J.P. Glotzbach, M. Sorkin, M. Inayathullah, M.R. Major, M.T. Longaker, J. Rajadas, G.C. Gurtner, Pullulan hydrogels improve mesenchymal stem cell delivery into high-oxidative-stress wounds, *Macromol Biosci* 11(11) (2011) 1458-66.
- [177] Y. Zhang, H. Hao, J. Liu, X. Fu, W. Han, Repair and regeneration of skin injury by transplanting microparticles mixed with Wharton's jelly and MSCs from the human umbilical cord, *Int J Low Extrem Wounds* 11(4) (2012) 264-70.
- [178] J.L. Ungerleider, T.D. Johnson, M.J. Hernandez, D.I. Elhag, R.L. Braden, M. Dzieciatkowska, K.G. Osborn, K.C. Hansen, E. Mahmud, K.L. Christman, Extracellular Matrix Hydrogel Promotes Tissue Remodeling, Arteriogenesis, and Perfusion in a Rat Hindlimb Ischemia Model, *JACC Basic Transl Sci* 1(1-2) (2016) 32-44.
- [179] G.J. Jeong, S.Y. Song, M. Kang, S. Go, H.S. Sohn, B.S. Kim, An Injectable Decellularized Matrix That Improves Mesenchymal Stem Cell Engraftment for Therapeutic Angiogenesis, *Acs Biomaterials Science & Engineering* 4(7) (2018) 2571-2581.
- [180] J.M. Davidson, Animal models for wound repair, *Arch Dermatol Res* 290 Suppl (1998) S1-11.
- [181] A.A. Hellingman, A.J. Bastiaansen, M.R. de Vries, L. Seghers, M.A. Lijkwan, C.W. Lowik, J.F. Hamming, P.H. Quax, Variations in surgical procedures for hind limb ischaemia mouse models result in differences in collateral formation, *Eur J Vasc Endovasc Surg* 40(6) (2010) 796-803.
- [182] J. Frey-Vasconcells, K.J. Whittlesey, E. Baum, E.G. Feigl, Translation of stem cell research: points to consider in designing preclinical animal studies, *Stem Cells Transl Med* 1(5) (2012) 353-8.
- [183] C.W. Patrick, R. Uthamanthil, E. Beahm, C. Frye, Animal models for adipose tissue engineering, *Tissue engineering. Part B, Reviews* 14(2) (2008) 167-78.
- [184] M. Proulx, K. Aubin, J. Lagueux, P. Audet, M. Auger, M.A. Fortin, J. Fradette, Magnetic Resonance Imaging of Human Tissue-Engineered Adipose Substitutes, *Tissue Eng Part C Methods* (2015).
- [185] R. Khorramirouz, J.L. Go, C. Noble, S. Jana, E. Maxson, A. Lerman, M.D. Young, A novel surgical technique for a rat subcutaneous implantation of a tissue engineered scaffold, *Acta Histochem* 120(3) (2018) 282-291.
- [186] C.G. Elliott, T.L. Forbes, A. Leask, D.W. Hamilton, Inflammatory microenvironment and tumor necrosis factor alpha as modulators of periostin and CCN2 expression in human non-healing skin wounds and dermal fibroblasts, *Matrix biology : journal of the International Society for Matrix Biology* (2015).

- [187] K. Hehenberger, G. Kratz, A. Hansson, K. Brismar, Fibroblasts derived from human chronic diabetic wounds have a decreased proliferation rate, which is recovered by the addition of heparin, *Journal of dermatological science* 16(2) (1998) 144-51.
- [188] M.A. Loots, E.N. Lamme, J.R. Mekkes, J.D. Bos, E. Middelkoop, Cultured fibroblasts from chronic diabetic wounds on the lower extremity (non-insulin-dependent diabetes mellitus) show disturbed proliferation, *Arch Dermatol Res* 291(2-3) (1999) 93-9.
- [189] M.A. Loot, S.B. Kenter, F.L. Au, W.J. van Galen, E. Middelkoop, J.D. Bos, J.R. Mekkes, Fibroblasts derived from chronic diabetic ulcers differ in their response to stimulation with EGF, IGF-I, bFGF and PDGF-AB compared to controls, *Eur J Cell Biol* 81(3) (2002) 153-60.
- [190] L.K. Park, A.G. Maione, A. Smith, B. Gerami-Naini, L.K. Iyer, D.J. Mooney, A. Veves, J.A. Garlick, Genome-wide DNA methylation analysis identifies a metabolic memory profile in patient-derived diabetic foot ulcer fibroblasts, *Epigenetics* 9(10) (2014) 1339-49.
- [191] A.I. Caplan, Mesenchymal Stem Cells: Time to Change the Name!, *Stem Cells Transl Med* 6(6) (2017) 1445-1451.
- [192] R. Hass, C. Kasper, S. Bohm, R. Jacobs, Different populations and sources of human mesenchymal stem cells (MSC): A comparison of adult and neonatal tissue-derived MSC, *Cell Commun Signal* 9 (2011) 12.
- [193] M. Dominici, K. Le Blanc, I. Mueller, I. Slaper-Cortenbach, F. Marini, D. Krause, R. Deans, A. Keating, D. Prockop, E. Horwitz, Minimal criteria for defining multipotent mesenchymal stromal cells. The International Society for Cellular Therapy position statement, *Cytotherapy* 8(4) (2006) 315-7.
- [194] B.M. Strem, M.H. Hedrick, The growing importance of fat in regenerative medicine, *Trends Biotechnol* 23(2) (2005) 64-6.
- [195] K.M. Safford, K.C. Hicok, S.D. Safford, Y.D. Halvorsen, W.O. Wilkison, J.M. Gimble, H.E. Rice, Neurogenic differentiation of murine and human adipose-derived stromal cells, *Biochemical and biophysical research communications* 294(2) (2002) 371-9.
- [196] P.A. Zuk, M. Zhu, P. Ashjian, D.A. De Ugarte, J.I. Huang, H. Mizuno, Z.C. Alfonso, J.K. Fraser, P. Benhaim, M.H. Hedrick, Human adipose tissue is a source of multipotent stem cells, *Mol Biol Cell* 13(12) (2002) 4279-95.
- [197] P.A. Zuk, M. Zhu, H. Mizuno, J. Huang, J.W. Futrell, A.J. Katz, P. Benhaim, H.P. Lorenz, M.H. Hedrick, Multilineage cells from human adipose tissue: implications for cell-based therapies, *Tissue Eng* 7(2) (2001) 211-28.
- [198] V. Planat-Benard, C. Menard, M. Andre, M. Puceat, A. Perez, J.M. Garcia-Verdugo, L. Penicaud, L. Casteilla, Spontaneous cardiomyocyte differentiation from adipose tissue stroma cells, *Circ Res* 94(2) (2004) 223-9.
- [199] P. Bourin, B.A. Bunnell, L. Casteilla, M. Dominici, A.J. Katz, K.L. March, H. Redl, J.P. Rubin, K. Yoshimura, J.M. Gimble, Stromal cells from the adipose tissue-derived stromal vascular fraction and culture expanded adipose tissue-derived stromal/stem cells: a joint statement of the International Federation for Adipose

- Therapeutics and Science (IFATS) and the International Society for Cellular Therapy (ISCT), *Cytotherapy* 15(6) (2013) 641-8.
- [200] N. Bertozzi, F. Simonacci, M.P. Grieco, E. Grignaffini, E. Raposio, The biological and clinical basis for the use of adipose-derived stem cells in the field of wound healing, *Ann Med Surg (Lond)* 20 (2017) 41-48.
- [201] J. Rehman, D. Traktuev, J. Li, S. Merfeld-Clauss, C.J. Temm-Grove, J.E. Bovenkerk, C.L. Pell, B.H. Johnstone, R.V. Considine, K.L. March, Secretion of angiogenic and antiapoptotic factors by human adipose stromal cells, *Circulation* 109(10) (2004) 1292-8.
- [202] S.M. Dallabrida, D. Zurakowski, S.C. Shih, L.E. Smith, J. Folkman, K.S. Moulton, M.A. Rupnick, Adipose tissue growth and regression are regulated by angiopoietin-1, *Biochem Biophys Res Commun* 311(3) (2003) 563-71.
- [203] A. Blasi, C. Martino, L. Balducci, M. Saldarelli, A. Soleti, S.E. Navone, L. Canzi, S. Cristini, G. Invernici, E.A. Parati, G. Alessandri, Dermal fibroblasts display similar phenotypic and differentiation capacity to fat-derived mesenchymal stem cells, but differ in anti-inflammatory and angiogenic potential, *Vascular cell* 3(1) (2011) 1-14.
- [204] W.S. Kim, B.S. Park, J.H. Sung, J.M. Yang, S.B. Park, S.J. Kwak, J.S. Park, Wound healing effect of adipose-derived stem cells: a critical role of secretory factors on human dermal fibroblasts, *Journal of dermatological science* 48(1) (2007) 15-24.
- [205] T. Skurk, V. van Harmelen, H. Hauner, Angiotensin II stimulates the release of interleukin-6 and interleukin-8 from cultured human adipocytes by activation of NF-kappaB, *Arterioscler Thromb Vasc Biol* 24(7) (2004) 1199-203.
- [206] K. Takahashi, S. Mizuarai, H. Araki, S. Mashiko, A. Ishihara, A. Kanatani, H. Itadani, H. Kotani, Adiposity elevates plasma MCP-1 levels leading to the increased CD11b-positive monocytes in mice, *The Journal of biological chemistry* 278(47) (2003) 46654-60.
- [207] S.T. Hsiao, Z. Lokmic, H. Peshavariya, K.M. Abberton, G.J. Dusting, S.Y. Lim, R.J. Dilley, Hypoxic conditioning enhances the angiogenic paracrine activity of human adipose-derived stem cells, *Stem Cells Dev* 22(10) (2013) 1614-23.
- [208] D. Bastelica, P. Morange, B. Berthet, H. Borghi, O. Lacroix, M. Grino, I. Juhan-Vague, M.C. Alessi, Stromal cells are the main plasminogen activator inhibitor-1-producing cells in human fat: evidence of differences between visceral and subcutaneous deposits, *Arterioscler Thromb Vasc Biol* 22(1) (2002) 173-8.
- [209] S.T. Hsiao, A. Asgari, Z. Lokmic, R. Sinclair, G.J. Dusting, S.Y. Lim, R.J. Dilley, Comparative analysis of paracrine factor expression in human adult mesenchymal stem cells derived from bone marrow, adipose, and dermal tissue, *Stem Cells Dev* 21(12) (2012) 2189-203.
- [210] M.B. Murphy, K. Moncivais, A.I. Caplan, Mesenchymal stem cells: environmentally responsive therapeutics for regenerative medicine, *Experimental & molecular medicine* 45 (2013) e54.
- [211] L.K. Kolaparthi, S. Sanivarapu, S. Moogla, R.S. Kutchem, Adipose Tissue - Adequate, Accessible Regenerative Material, *Int J Stem Cells* 8(2) (2015) 121-7.

- [212] W. Wagner, F. Wein, A. Seckinger, M. Frankhauser, U. Wirkner, U. Krause, J. Blake, C. Schwager, V. Eckstein, W. Ansorge, A.D. Ho, Comparative characteristics of mesenchymal stem cells from human bone marrow, adipose tissue, and umbilical cord blood, *Exp Hematol* 33(11) (2005) 1402-16.
- [213] A. Shabbir, D. Zisa, G. Suzuki, T. Lee, Heart failure therapy mediated by the trophic activities of bone marrow mesenchymal stem cells: a noninvasive therapeutic regimen, *Am J Physiol Heart Circ Physiol* 296(6) (2009) H1888-97.
- [214] M. Mastro, H. Lin, T. Lee, Enhancing the efficacy of mesenchymal stem cell therapy, *World J Stem Cells* 6(2) (2014) 82-93.
- [215] C.P. Chang, C.C. Chio, C.U. Cheong, C.M. Chao, B.C. Cheng, M.T. Lin, Hypoxic preconditioning enhances the therapeutic potential of the secretome from cultured human mesenchymal stem cells in experimental traumatic brain injury, *Clin Sci (Lond)* 124(3) (2013) 165-76.
- [216] H. Thangarajah, I.N. Vial, E. Chang, S. El-Ftesi, M. Januszyk, E.I. Chang, J. Paterno, E. Neofytou, M.T. Longaker, G.C. Gurtner, IFATS collection: Adipose stromal cells adopt a proangiogenic phenotype under the influence of hypoxia, *Stem Cells* 27(1) (2009) 266-74.
- [217] P.C. Baer, J.M. Overath, A. Urbschat, R. Schubert, B. Koch, A.A. Bohn, H. Geiger, Effect of Different Preconditioning Regimens on the Expression Profile of Murine Adipose-Derived Stromal/Stem Cells, *Int J Mol Sci* 19(6) (2018).
- [218] D. Nawrocka, K. Kornicka, J. Szydlarska, K. Marycz, Basic Fibroblast Growth Factor Inhibits Apoptosis and Promotes Proliferation of Adipose-Derived Mesenchymal Stromal Cells Isolated from Patients with Type 2 Diabetes by Reducing Cellular Oxidative Stress, *Oxid Med Cell Longev* 2017 (2017) 3027109.
- [219] G. Lu, M. Ashraf, K.H. Haider, Insulin-like growth factor-1 preconditioning accentuates intrinsic survival mechanism in stem cells to resist ischemic injury by orchestrating protein kinase calpha-erk1/2 activation, *Antioxid Redox Signal* 16(3) (2012) 217-27.
- [220] J.E. Frith, B. Thomson, P.G. Genever, Dynamic three-dimensional culture methods enhance mesenchymal stem cell properties and increase therapeutic potential, *Tissue Eng Part C Methods* 16(4) (2010) 735-49.
- [221] G.M. Fortier, R. Gauvin, M. Proulx, M. Vallee, J. Fradette, Dynamic culture induces a cell type-dependent response impacting on the thickness of engineered connective tissues, *J Tissue Eng Regen Med* 7(4) (2013) 292-301.
- [222] X. Wei, Z. Du, L. Zhao, D. Feng, G. Wei, Y. He, J. Tan, W.H. Lee, H. Hampel, R. Dodel, B.H. Johnstone, K.L. March, M.R. Farlow, Y. Du, IFATS collection: The conditioned media of adipose stromal cells protect against hypoxia-ischemia-induced brain damage in neonatal rats, *Stem Cells* 27(2) (2009) 478-88.
- [223] H. Liu, W. Xue, G. Ge, X. Luo, Y. Li, H. Xiang, X. Ding, P. Tian, X. Tian, Hypoxic preconditioning advances CXCR4 and CXCR7 expression by activating HIF-1alpha in MSCs, *Biochem Biophys Res Commun* 401(4) (2010) 509-15.

- [224] K. Tamama, H. Kawasaki, A. Wells, Epidermal growth factor (EGF) treatment on multipotential stromal cells (MSCs). Possible enhancement of therapeutic potential of MSC, *Journal of biomedicine & biotechnology* 2010 (2010) 795385.
- [225] J. Park, J.H. Lee, B.S. Yoon, E.K. Jun, G. Lee, I.Y. Kim, S. You, Additive effect of bFGF and selenium on expansion and paracrine action of human amniotic fluid-derived mesenchymal stem cells, *Stem Cell Res Ther* 9(1) (2018) 293.
- [226] S. Lin, Q. Zhang, X. Shao, T. Zhang, C. Xue, S. Shi, D. Zhao, Y. Lin, IGF-1 promotes angiogenesis in endothelial cells/adipose-derived stem cells co-culture system with activation of PI3K/Akt signal pathway, *Cell Prolif* 50(6) (2017).
- [227] B.A. Golomb, T.T. Dang, M.H. Criqui, Peripheral arterial disease: morbidity and mortality implications, *Circulation* 114(7) (2006) 688-99.
- [228] M. Lovell, K. Harris, T. Forbes, G. Twillman, B. Abramson, M.H. Criqui, P. Schroeder, E.R. Mohler, 3rd, A.T. Hirsch, C. Peripheral Arterial Disease, Peripheral arterial disease: lack of awareness in Canada, *Can J Cardiol* 25(1) (2009) 39-45.
- [229] D.J. Margolis, J. Kantor, J.A. Berlin, Healing of diabetic neuropathic foot ulcers receiving standard treatment. A meta-analysis, *Diabetes Care* 22(5) (1999) 692-5.
- [230] J. Apelqvist, J. Larsson, What is the most effective way to reduce incidence of amputation in the diabetic foot?, *Diabetes Metab Res Rev* 16(Suppl 1) (2000) S75-83.
- [231] E. Black, J. Vibe-Petersen, L.N. Jorgensen, S.M. Madsen, M.S. Agren, P.E. Holstein, H. Perrild, F. Gottrup, Decrease of collagen deposition in wound repair in type 1 diabetes independent of glycemic control, *Archives of surgery* 138(1) (2003) 34-40.
- [232] A.B. Wysocki, L. Staiano-Coico, F. Grinnell, Wound fluid from chronic leg ulcers contains elevated levels of metalloproteinases MMP-2 and MMP-9, *J Invest Dermatol* 101(1) (1993) 64-8.
- [233] F. Xu, C. Zhang, D.T. Graves, Abnormal cell responses and role of TNF-alpha in impaired diabetic wound healing, *Biomed Res Int* 2013 (2013) 754802.
- [234] F.X. Maquart, G. Bellon, S. Pasco, J.C. Monboisse, Matrikines in the regulation of extracellular matrix degradation, *Biochimie* 87(3-4) (2005) 353-60.
- [235] I. Vlodaysky, H.Q. Miao, B. Medalion, P. Danagher, D. Ron, Involvement of heparan sulfate and related molecules in sequestration and growth promoting activity of fibroblast growth factor, *Cancer metastasis reviews* 15(2) (1996) 177-86.
- [236] K.P. Robb, A. Shridhar, L.E. Flynn, Decellularized Matrices As Cell-Instructive Scaffolds to Guide Tissue-Specific Regeneration, *ACS Biomaterials Science & Engineering* (2017) A-Q.
- [237] T.J. Keane, S.F. Badylak, The host response to allogeneic and xenogeneic biological scaffold materials, *J Tissue Eng Regen Med* 9(5) (2015) 504-11.
- [238] G. Agmon, K.L. Christman, Controlling stem cell behavior with decellularized extracellular matrix scaffolds, *Curr Opin Solid State Mater Sci* 20(4) (2016) 193-201.

- [239] C.G. Elliott, T.L. Forbes, A. Leask, D.W. Hamilton, Inflammatory microenvironment and tumor necrosis factor alpha as modulators of periostin and CCN2 expression in human non-healing skin wounds and dermal fibroblasts, *Matrix biology : journal of the International Society for Matrix Biology* 43 (2015) 71-84.
- [240] C. Quan, M.K. Cho, Y. Shao, L.E. Miannecki, E. Liao, D. Perry, T. Quan, Dermal fibroblast expression of stromal cell-derived factor-1 (SDF-1) promotes epidermal keratinocyte proliferation in normal and diseased skin, *Protein Cell* 6(12) (2015) 890-903.
- [241] I.B. Wall, R. Moseley, D.M. Baird, D. Kipling, P. Giles, I. Laffafian, P.E. Price, D.W. Thomas, P. Stephens, Fibroblast dysfunction is a key factor in the non-healing of chronic venous leg ulcers, *J Invest Dermatol* 128(10) (2008) 2526-40.
- [242] A.G. Maione, Y. Brudno, O. Stojadinovic, L.K. Park, A. Smith, A. Tellechea, E.C. Leal, C.J. Kearney, A. Veves, M. Tomic-Canic, D.J. Mooney, J.A. Garlick, Three-dimensional human tissue models that incorporate diabetic foot ulcer-derived fibroblasts mimic in vivo features of chronic wounds, *Tissue Eng Part C Methods* 21(5) (2015) 499-508.
- [243] H.J. Wallace, M.C. Stacey, Levels of tumor necrosis factor-alpha (TNF-alpha) and soluble TNF receptors in chronic venous leg ulcers--correlations to healing status, *J Invest Dermatol* 110(3) (1998) 292-6.
- [244] M.T. Goldberg, Y.P. Han, C. Yan, M.C. Shaw, W.L. Garner, TNF-alpha suppresses alpha-smooth muscle actin expression in human dermal fibroblasts: an implication for abnormal wound healing, *J Invest Dermatol* 127(11) (2007) 2645-55.
- [245] K. Kim, J. Cheng, Q. Liu, X.Y. Wu, Y. Sun, Investigation of mechanical properties of soft hydrogel microcapsules in relation to protein delivery using a MEMS force sensor, *J Biomed Mater Res A* 92(1) (2010) 103-13.
- [246] B.G. Ilagan, B.G. Amsden, Macroporous photocrosslinked elastomer scaffolds containing microposity: preparation and in vitro degradation properties, *J Biomed Mater Res A* 93(1) (2010) 211-8.
- [247] I.G. Fels, Hydration and density of collagen and gelatin, *J. Appl. Polym. Sci.* 8(4) (1964) 1813-1824.
- [248] V. Russo, C. Yu, P. Belliveau, A. Hamilton, L.E. Flynn, Comparison of human adipose-derived stem cells isolated from subcutaneous, omental, and intrathoracic adipose tissue depots for regenerative applications, *Stem Cells Transl Med* 3(2) (2014) 206-17.
- [249] J. Allard, K. Li, X.M. Lopez, S. Blanchard, P. Barbot, S. Rorive, C. Decaestecker, R. Pochet, D. Bohl, A.C. Lepore, I. Salmon, C. Nicaise, Immunohistochemical toolkit for tracking and quantifying xenotransplanted human stem cells, *Regen Med* 9(4) (2014) 437-52.
- [250] Shire Regenerative Medicine Inc, Pivotal Trial of Dermagraft(R) to Treat Venous Leg Ulcers (DEVO), 2013. <https://clinicaltrials.gov/ct2/show/results/NCT00909870>. (Accessed February 7th 2017).

- [251] V.F. Achterberg, L. Buscemi, H. Diekmann, J. Smith-Clerc, H. Schwengler, J.J. Meister, H. Wenck, S. Gallinat, B. Hinz, The nano-scale mechanical properties of the extracellular matrix regulate dermal fibroblast function, *J Invest Dermatol* 134(7) (2014) 1862-1872.
- [252] B. Ma, X. Wang, C. Wu, J. Chang, Crosslinking strategies for preparation of extracellular matrix-derived cardiovascular scaffolds, *Regen Biomater* 1(1) (2014) 81-9.
- [253] D.A. Stover, B.C. Verrelli, Comparative vertebrate evolutionary analyses of type I collagen: potential of COL1a1 gene structure and intron variation for common bone-related diseases, *Mol Biol Evol* 28(1) (2011) 533-42.
- [254] F. Rodriguez-Pascual, D.A. Slatter, Collagen cross-linking: insights on the evolution of metazoan extracellular matrix, *Sci Rep* 6 (2016) 37374.
- [255] R. Parenteau-Bareil, R. Gauvin, S. Cliche, C. Gariépy, L. Germain, F. Berthod, Comparative study of bovine, porcine and avian collagens for the production of a tissue engineered dermis, *Acta Biomater* 7(10) (2011) 3757-65.
- [256] R.V. Iozzo, J.D. San Antonio, Heparan sulfate proteoglycans: heavy hitters in the angiogenesis arena, *J Clin Invest* 108(3) (2001) 349-55.
- [257] R. Kalluri, Basement membranes: structure, assembly and role in tumour angiogenesis, *Nat Rev Cancer* 3(6) (2003) 422-33.
- [258] E. Bonanno, M. Iurlaro, J.A. Madri, R.F. Nicosia, Type IV collagen modulates angiogenesis and neovessel survival in the rat aorta model, *In Vitro Cell Dev Biol Anim* 36(5) (2000) 336-40.
- [259] K. Inkinen, H. Wolff, K. Von Boguslawski, J. Ahonen, Type V collagen in experimental granulation tissue, *Connect Tissue Res* 39(4) (1998) 281-94.
- [260] G. Biondani, K. Zeeberg, M.R. Greco, S. Cannone, I. Dando, E. Dalla Pozza, M. Mastrodonato, S. Forciniti, V. Casavola, M. Palmieri, S.J. Reshkin, R.A. Cardone, Extracellular matrix composition modulates PDAC parenchymal and stem cell plasticity and behavior through the secretome, *FEBS J* 285(11) (2018) 2104-2124.
- [261] A. De Boeck, A. Hendrix, D. Maynard, M. Van Bockstal, A. Daniels, P. Pauwels, C. Gespach, M. Bracke, O. De Wever, Differential secretome analysis of cancer-associated fibroblasts and bone marrow-derived precursors to identify microenvironmental regulators of colon cancer progression, *Proteomics* 13(2) (2013) 379-88.
- [262] L. Chen, Y. Xu, J. Zhao, Z. Zhang, R. Yang, J. Xie, X. Liu, S. Qi, Conditioned medium from hypoxic bone marrow-derived mesenchymal stem cells enhances wound healing in mice, *PLoS One* 9(4) (2014) e96161.
- [263] S.W. Kim, H.Z. Zhang, L. Guo, J.M. Kim, M.H. Kim, Amniotic Mesenchymal Stem Cells Enhance Wound Healing in Diabetic NOD/SCID Mice through High Angiogenic and Engraftment Capabilities, *PLoS One* 7(7) (2012) e41105.
- [264] P. Morissette Martin, A. Grant, D.W. Hamilton, L.E. Flynn, Matrix composition in 3-D collagenous bioscaffolds modulates the survival and angiogenic phenotype of human chronic wound dermal fibroblasts, *Acta Biomater* 83 (2019) 199-210.

- [265] L.E. Flynn, C. Yu, Collagenous foam materials, U.S. Patent Application No. 14/403,396; Filing date Nov. 24, 2014, 2014.
- [266] K. Hyldig, S. Riis, C.P. Pennisi, V. Zachar, T. Fink, Implications of Extracellular Matrix Production by Adipose Tissue-Derived Stem Cells for Development of Wound Healing Therapies, *Int J Mol Sci* 18(6) (2017).
- [267] A.J. Salgado, R.L. Reis, N.J. Sousa, J.M. Gimble, Adipose tissue derived stem cells secretome: soluble factors and their roles in regenerative medicine, *Current stem cell research & therapy* 5(2) (2010) 103-10.
- [268] P.C. Baer, J.M. Overath, A. Urbschat, R. Schubert, H.m. Geiger, Preconditioning of Human Adipose-derived Stromal/Stem Cells: Evaluation of Short-term Preincubation Regimens to Enhance their Regenerative Potential, *Journal of Stem Cell Research & Therapy* 6 (2016) 331.
- [269] W. Klockner, J. Buchs, Advances in shaking technologies, *Trends Biotechnol* 30(6) (2012) 307-14.
- [270] A.M. Hamilton, P.J. Foster, J.A. Ronald, Evaluating Nonintegrating Lentiviruses as Safe Vectors for Noninvasive Reporter-Based Molecular Imaging of Multipotent Mesenchymal Stem Cells, *Hum Gene Ther* 29(10) (2018) 1213-1225.
- [271] R. Hata, H. Senoo, L-ascorbic acid 2-phosphate stimulates collagen accumulation, cell proliferation, and formation of a three-dimensional tissuelike substance by skin fibroblasts, *J Cell Physiol* 138(1) (1989) 8-16.
- [272] J. Yu, Y.K. Tu, Y.B. Tang, N.C. Cheng, Stemness and transdifferentiation of adipose-derived stem cells using L-ascorbic acid 2-phosphate-induced cell sheet formation, *Biomaterials* 35(11) (2014) 3516-26.
- [273] Y. Farhat, Preparing an Active MMP-2 Standard for Gelatin Zymography, 2014. <http://protocol-place.com/>. (Accessed 08/21/2019 2019).
- [274] S.L. Stubbs, S.T. Hsiao, H.M. Peshavariya, S.Y. Lim, G.J. Disting, R.J. Dille, Hypoxic preconditioning enhances survival of human adipose-derived stem cells and conditions endothelial cells in vitro, *Stem Cells Dev* 21(11) (2012) 1887-96.
- [275] M. Roemeling-van Rhijn, F.K. Mensah, S.S. Korevaar, M.J. Leijts, G.J. van Osch, J.N. Ijzermans, M.G. Betjes, C.C. Baan, W. Weimar, M.J. Hoogduijn, Effects of Hypoxia on the Immunomodulatory Properties of Adipose Tissue-Derived Mesenchymal Stem cells, *Front Immunol* 4 (2013) 203.
- [276] S.A. Young, S.E. Sherman, T.T. Cooper, C. Brown, F. Anjum, D.A. Hess, L.E. Flynn, B.G. Amsden, Mechanically resilient injectable scaffolds for intramuscular stem cell delivery and cytokine release, *Biomaterials* 159 (2018) 146-160.
- [277] K. Aubin, M. Safoine, M. Proulx, M.A. Audet-Casgrain, J.F. Cote, F.A. Tetu, A. Roy, J. Fradette, Characterization of In Vitro Engineered Human Adipose Tissues: Relevant Adipokine Secretion and Impact of TNF-alpha, *PLoS One* 10(9) (2015) e0137612.
- [278] F. Wei, C. Qu, T. Song, G. Ding, Z. Fan, D. Liu, Y. Liu, C. Zhang, S. Shi, S. Wang, Vitamin C treatment promotes mesenchymal stem cell sheet formation and tissue

- regeneration by elevating telomerase activity, *J Cell Physiol* 227(9) (2012) 3216-24.
- [279] J. Kao, G. Huey, R. Kao, R. Stern, Ascorbic acid stimulates production of glycosaminoglycans in cultured fibroblasts, *Exp Mol Pathol* 53(1) (1990) 1-10.
- [280] H. Agrawal, H. Shang, A.P. Sattah, N. Yang, S.M. Peirce, A.J. Katz, Human adipose-derived stromal/stem cells demonstrate short-lived persistence after implantation in both an immunocompetent and an immunocompromised murine model, *Stem Cell Res Ther* 5(6) (2014) 142.
- [281] S. Wolbank, A. Peterbauer, E. Wassermann, S. Hennerbichler, R. Voglauer, M. van Griensven, H.C. Duba, C. Gabriel, H. Redl, Labelling of human adipose-derived stem cells for non-invasive in vivo cell tracking, *Cell Tissue Bank* 8(3) (2007) 163-77.
- [282] M. Vilalta, I.R. Degano, J. Bago, D. Gould, M. Santos, M. Garcia-Arranz, R. Ayats, C. Fuster, Y. Chernajovsky, D. Garcia-Olmo, N. Rubio, J. Blanco, Biodistribution, long-term survival, and safety of human adipose tissue-derived mesenchymal stem cells transplanted in nude mice by high sensitivity non-invasive bioluminescence imaging, *Stem Cells Dev* 17(5) (2008) 993-1003.
- [283] W. Fan, D. Sun, J. Liu, D. Liang, Y. Wang, K.H. Narsinh, Y. Li, X. Qin, J. Liang, J. Tian, F. Cao, Adipose stromal cells amplify angiogenic signaling via the VEGF/mTOR/Akt pathway in a murine hindlimb ischemia model: a 3D multimodality imaging study, *PLoS One* 7(9) (2012) e45621.
- [284] X. Bai, Y. Yan, M. Coleman, G. Wu, B. Rabinovich, M. Seidensticker, E. Alt, Tracking long-term survival of intramyocardially delivered human adipose tissue-derived stem cells using bioluminescence imaging, *Mol Imaging Biol* 13(4) (2011) 633-45.
- [285] K.M. Parkins, V.P. Dubois, A.M. Hamilton, A.V. Makela, J.A. Ronald, P.J. Foster, Multimodality cellular and molecular imaging of concomitant tumour enhancement in a syngeneic mouse model of breast cancer metastasis, *Sci Rep* 8(1) (2018) 8930.
- [286] R. Oftadeh, M. Perez-Viloria, J.C. Villa-Camacho, A. Vaziri, A. Nazarian, Biomechanics and mechanobiology of trabecular bone: a review, *J Biomech Eng* 137(1) (2015).
- [287] A. Mansour, M.A. Mezour, Z. Badran, F. Tamimi, (*) Extracellular Matrices for Bone Regeneration: A Literature Review, *Tissue Eng Part A* 23(23-24) (2017) 1436-1451.
- [288] M.G. Rubashkin, G. Ou, V.M. Weaver, Deconstructing signaling in three dimensions, *Biochemistry* 53(13) (2014) 2078-90.
- [289] Y. Zhang, Y. He, S. Bharadwaj, N. Hammam, K. Carnagey, R. Myers, A. Atala, M. Van Dyke, Tissue-specific extracellular matrix coatings for the promotion of cell proliferation and maintenance of cell phenotype, *Biomaterials* 30(23-24) (2009) 4021-8.
- [290] A. Shridhar, Design of tissue-specific cellular microenvironments for adipose-derived stromal cell culture and delivery, Chemical Engineering, The University of Western Ontario, Electronic Thesis and Dissertation Repository. 6088, 2019.

- [291] J.A. DeQuach, V. Mezzano, A. Miglani, S. Lange, G.M. Keller, F. Sheikh, K.L. Christman, Simple and high yielding method for preparing tissue specific extracellular matrix coatings for cell culture, *PLoS One* 5(9) (2010) e13039.
- [292] A.J. Booth, R. Hadley, A.M. Cornett, A.A. Dreffs, S.A. Matthes, J.L. Tsui, K. Weiss, J.C. Horowitz, V.F. Fiore, T.H. Barker, B.B. Moore, F.J. Martinez, L.E. Niklason, E.S. White, Acellular normal and fibrotic human lung matrices as a culture system for in vitro investigation, *Am J Respir Crit Care Med* 186(9) (2012) 866-76.
- [293] J.S. Lee, J. Shin, H.M. Park, Y.G. Kim, B.G. Kim, J.W. Oh, S.W. Cho, Liver extracellular matrix providing dual functions of two-dimensional substrate coating and three-dimensional injectable hydrogel platform for liver tissue engineering, *Biomacromolecules* 15(1) (2014) 206-18.
- [294] H. Campo, X. Garcia-Dominguez, S. Lopez-Martinez, A. Faus, J.S. Vicente Anton, F. Marco-Jimenez, I. Cervello, Tissue-specific decellularized endometrial substratum mimicking different physiological conditions influences in vitro embryo development in a rabbit model, *Acta Biomater* 89 (2019) 126-138.
- [295] D. Lam, H.A. Enright, J. Cadena, S.K.G. Peters, A.P. Sales, J.J. Osburn, D.A. Soccia, K.S. Kulp, E.K. Wheeler, N.O. Fischer, Tissue-specific extracellular matrix accelerates the formation of neural networks and communities in a neuron-glia co-culture on a multi-electrode array, *Sci Rep* 9(1) (2019) 4159.
- [296] Q. Chen, P. Shou, C. Zheng, M. Jiang, G. Cao, Q. Yang, J. Cao, N. Xie, T. Velletri, X. Zhang, C. Xu, L. Zhang, H. Yang, J. Hou, Y. Wang, Y. Shi, Fate decision of mesenchymal stem cells: adipocytes or osteoblasts?, *Cell Death Differ* 23(7) (2016) 1128-39.
- [297] T. Hoshiba, N. Kawazoe, G. Chen, The balance of osteogenic and adipogenic differentiation in human mesenchymal stem cells by matrices that mimic stepwise tissue development, *Biomaterials* 33(7) (2012) 2025-31.
- [298] F.S. Steven, The Nishihara Technique for the Solubilization of Collagen. Application to the Preparation of Soluble Collagens from Normal and Rheumatoid Connective Tissue, *Ann Rheum Dis* 23 (1964) 300-1.
- [299] N.H. Brown, Extracellular matrix in development: insights from mechanisms conserved between invertebrates and vertebrates, *Cold Spring Harb Perspect Biol* 3(12) (2011).
- [300] C. Blum, K. Schlegelmilch, T. Schilling, A. Shridhar, M. Rudert, F. Jakob, P.D. Dalton, T. Blunk, L.E. Flynn, J. Groll, Extracellular Matrix-Modified Fiber Scaffolds as a Proadipogenic Mesenchymal Stromal Cell Delivery Platform, *ACS Biomater Sci Eng Epub ahead of print* (2019).
- [301] T. Hoshiba, G. Chen, C. Endo, H. Maruyama, M. Wakui, E. Nemoto, N. Kawazoe, M. Tanaka, Decellularized Extracellular Matrix as an In Vitro Model to Study the Comprehensive Roles of the ECM in Stem Cell Differentiation, *Stem Cells Int* 2016 (2016) 6397820.
- [302] A. Kayabolen, D. Keskin, A. Aykan, Y. Karslioglu, F. Zor, A. Tezcaner, Native extracellular matrix/fibroin hydrogels for adipose tissue engineering with enhanced vascularization, *Biomed Mater* 12(3) (2017) 035007.

- [303] A.T. Truong, A. Kowal-Vern, B.A. Latenser, D.E. Wiley, R.J. Walter, Comparison of dermal substitutes in wound healing utilizing a nude mouse model, *J Burns Wounds* 4 (2005) e4.
- [304] G.A. Villalona, B. Udelsman, D.R. Duncan, E. McGillicuddy, R.F. Sawh-Martinez, N. Hibino, C. Painter, T. Mirensky, B. Erickson, T. Shinoka, C.K. Breuer, Cell-seeding techniques in vascular tissue engineering, *Tissue engineering. Part B, Reviews* 16(3) (2010) 341-50.
- [305] S. El-Ftesi, E.I. Chang, M.T. Longaker, G.C. Gurtner, Aging and diabetes impair the neovascular potential of adipose-derived stromal cells, *Plast Reconstr Surg* 123(2) (2009) 475-85.
- [306] M.S. Choudhery, M. Badowski, A. Muise, J. Pierce, D.T. Harris, Donor age negatively impacts adipose tissue-derived mesenchymal stem cell expansion and differentiation, *J Transl Med* 12 (2014) 8.
- [307] T.P. Frazier, J.M. Gimble, J.W. Devay, H.A. Tucker, E.S. Chiu, B.G. Rowan, Body mass index affects proliferation and osteogenic differentiation of human subcutaneous adipose tissue-derived stem cells, *BMC Cell Biol* 14 (2013) 34.
- [308] M. Tzaphlidou, The role of collagen in bone structure: an image processing approach, *Micron* 36(7-8) (2005) 593-601.
- [309] P.V. Granton, C.J. Norley, J. Umoh, E.A. Turley, B.C. Frier, E.G. Noble, D.W. Holdsworth, Rapid in vivo whole body composition of rats using cone beam muCT, *J Appl Physiol* (1985) 109(4) (2010) 1162-9.
- [310] K. Aubin, C. Vincent, M. Proulx, D. Mayrand, J. Fradette, Creating capillary networks within human engineered tissues: Impact of adipocytes and their secretory products, *Acta Biomater* 11C (2014) 333-345.
- [311] S. Niemelä, S. Miettinen, J. Sarkanen, N. Ashammakhi, Adipose Tissue and Adipocyte Differentiation: Molecular and Cellular Aspects and Tissue Engineering Applications in: N. Ashammakhi, R.L. Reis, F. Chiellini (Eds.), *Topics in Tissue Engineering* 2008.
- [312] E. Arrigoni, S. Lopa, L. de Girolamo, D. Stanco, A.T. Brini, Isolation, characterization and osteogenic differentiation of adipose-derived stem cells: from small to large animal models, *Cell Tissue Res* 338(3) (2009) 401-11.

Appendix A: Supplementary data

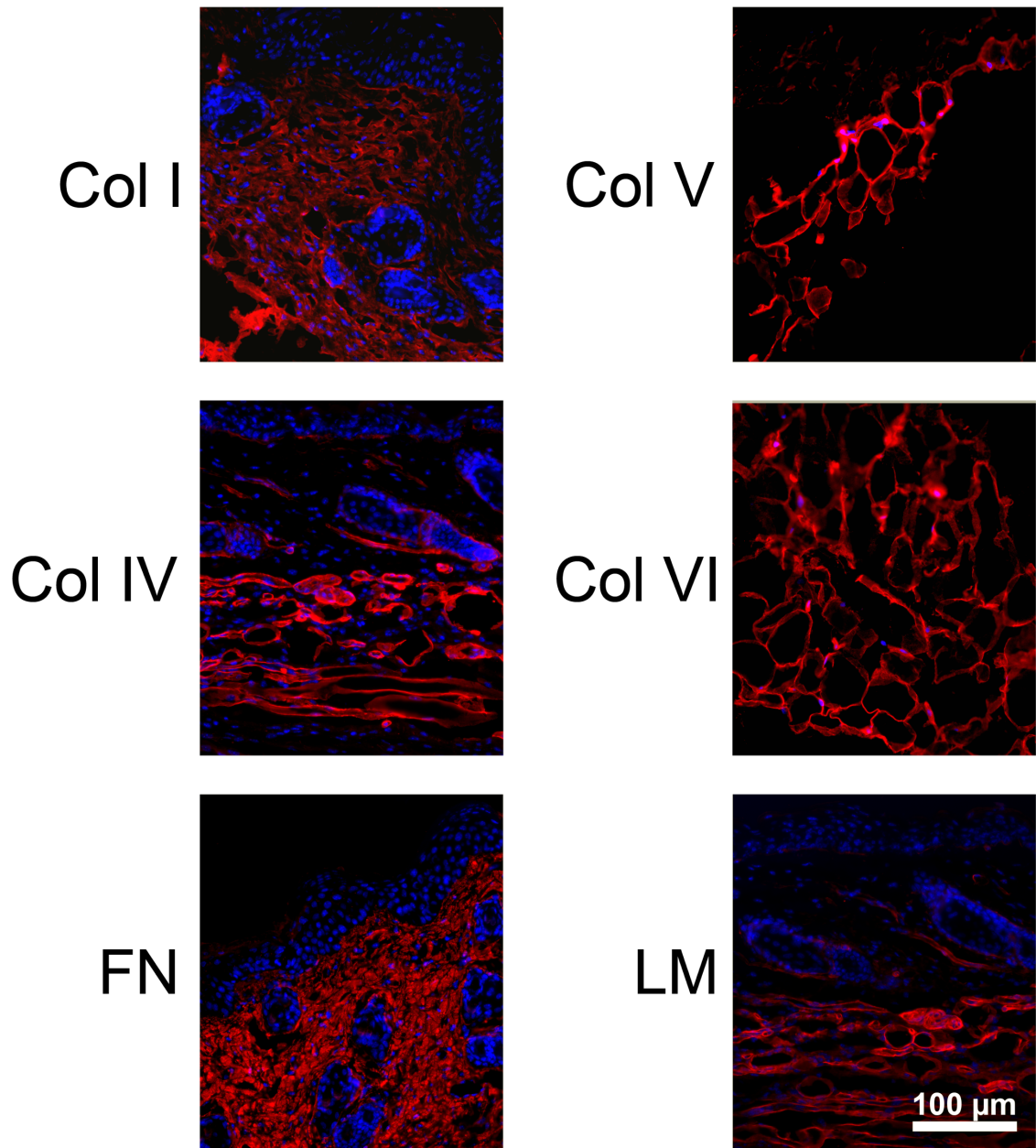
A.1 Supplementary data of Chapter 2

Supplementary Table 2.1: Cell donor information

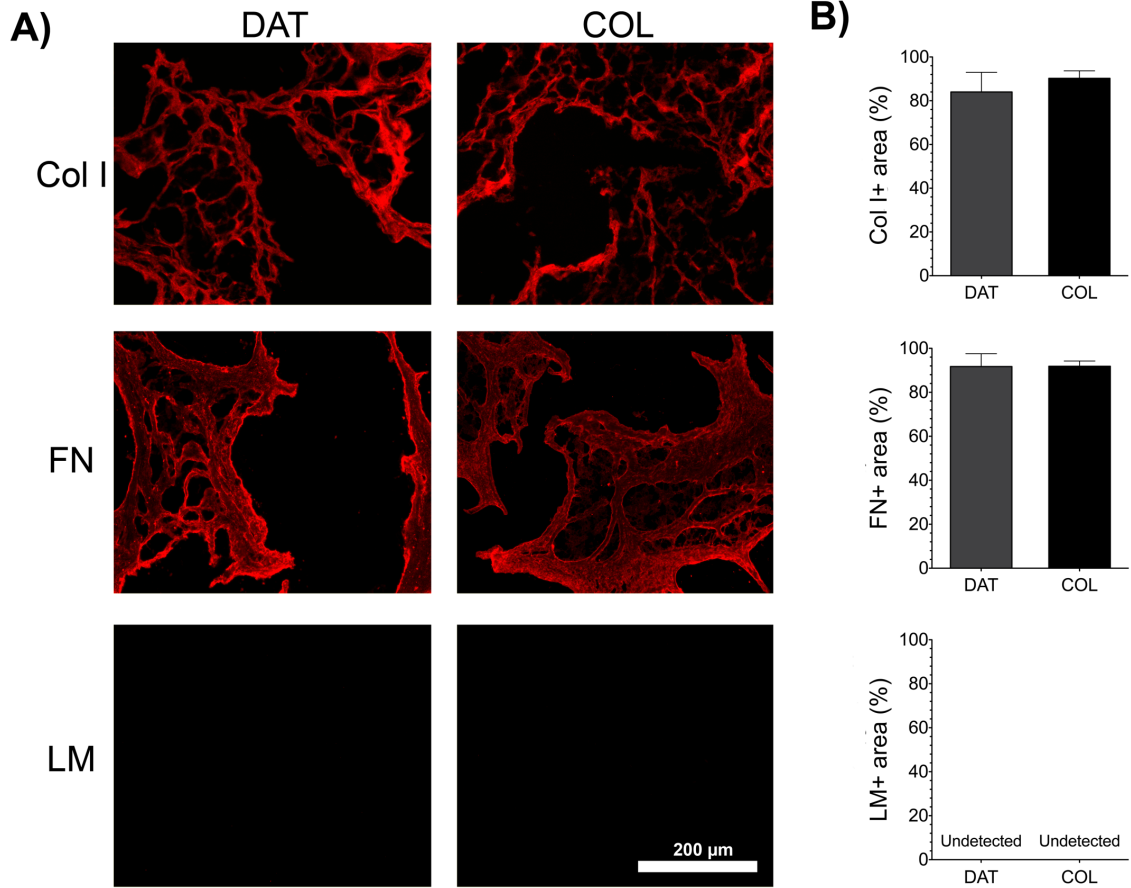
Donor	Gender	Age	Amputation site	Wound site	Diagnosed risk factors (etiology)
1	Male	60	Below the knee	Toe	Perivascular disease (non-diabetic patient)
2	Female	87	Below the knee	Toe	Perivascular disease and Type II diabetes
3	Female	64	Below the knee	Toe	Perivascular disease (non-diabetic patient)

Supplementary Table 2.2: Immunophenotype of wound edge dermal fibroblasts

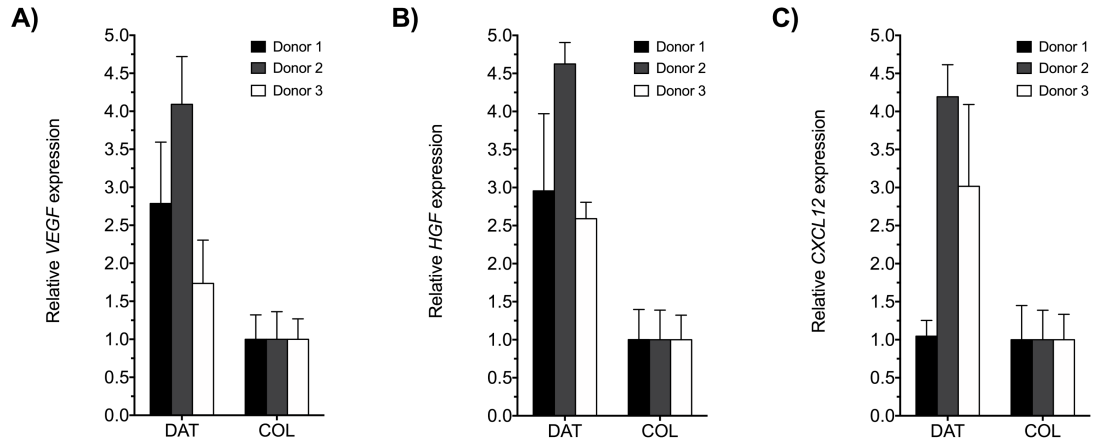
Marker	Mean \pm Standard deviation (%) (n=3, N=3)
CD90	99.2 \pm 0.8
CD105	99.1 \pm 0.8
CD73	96.2 \pm 4.2
CD44	99.6 \pm 0.4
CD29	99.0 \pm 0.7
CD34	3.5 \pm 1.0
CD45	1.5 \pm 1.0
CD146	1.5 \pm 1.0
CD31	1.4 \pm 1.5



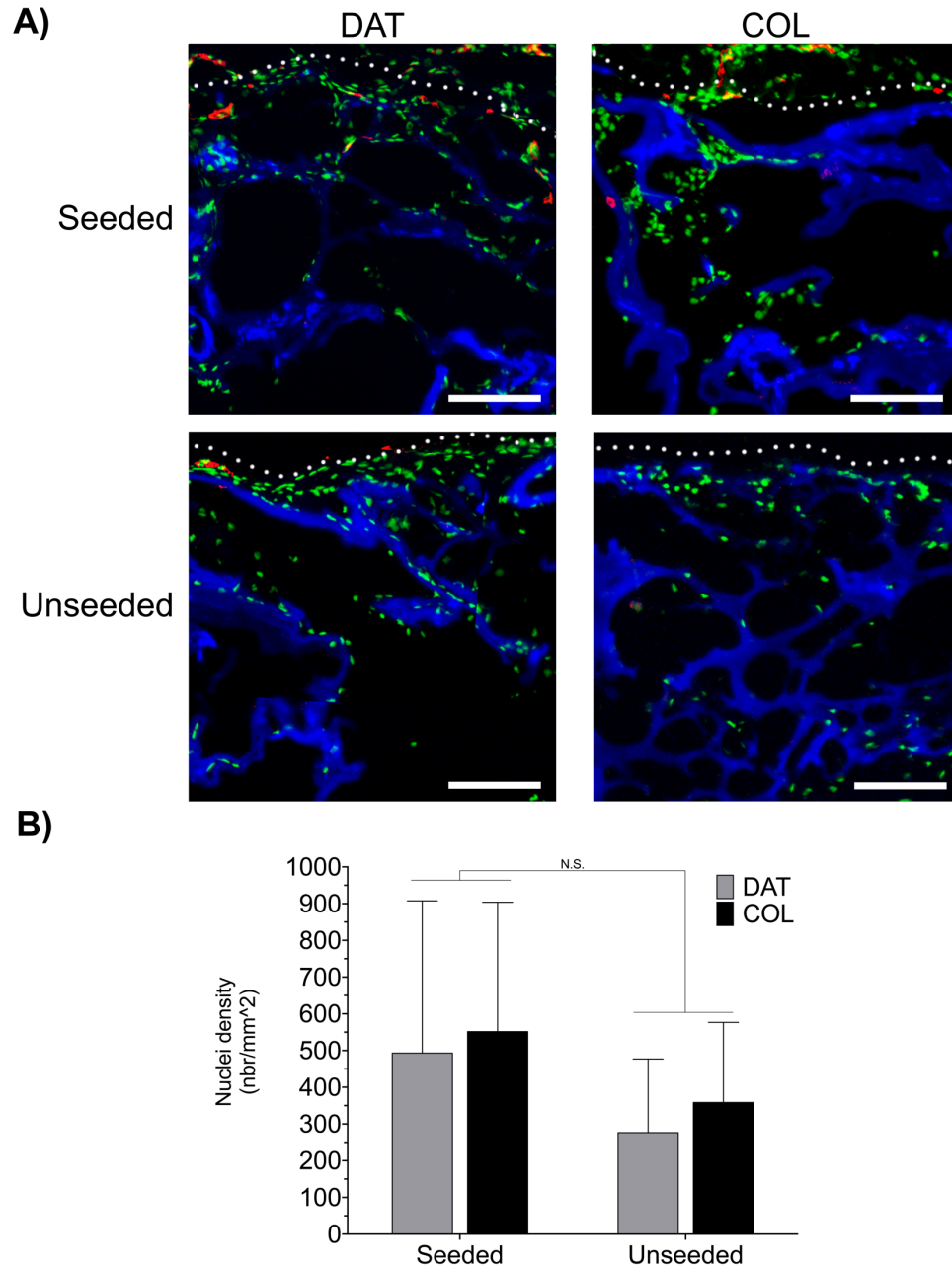
Supplementary Figure 2.1: Positive controls for the immunofluorescence staining of the ECM components. Mouse skin was used as a positive control for collagen type I (COL I), collagen type IV (COL IV), fibronectin (FN), and laminin (LM) staining, while human adipose tissue was used as a positive control for collagen type V (COL V) and VI (COL VI) staining.



Supplementary Figure 2.2: DAT and COL bead foams contain similar relative levels of collagen type I and fibronectin, with no detectable laminin expression. (A) Representative immunohistochemical staining for collagen type I, fibronectin (FN), and laminin (LN) in cryo-sections of the DAT and COL bead foams. (B) Quantification of relative collagen type I, fibronectin and laminin levels, with no statistical difference between the groups (n=2-6 scaffolds/trial, N=3 trials with different ECM suspensions).



Supplementary Figure 2.3: Pro-angiogenic gene expression for the individual cell donors. Relative mRNA levels of the pro-angiogenic markers (A) *VEGFA*, (B) *HGF*, and (C) *CXCL12* at 9 days post-seeding showing the same trend for increased expression of *VEGFA* and *HGF* in the weDF cultured on the DAT bead foams for all 3 cell donors, as well as enhanced *CXCL12* expression for donors 2 and 3. Gene expression levels were normalized to the COL bead foam group for each cell donor, with 18S as the housekeeping gene. (n=3 scaffolds/trial, N=3 cell donors).



Supplementary Figure 2.4: Representative CD31 immunostaining (red) of seeded and unseeded experimental groups showing qualitatively enhanced blood vessel infiltration in the seeded DAT bead foams relative to the seeded COL bead foams and unseeded controls at 14 days post-implantation. (A) Nuclei were counter-stained with PicoGreen Reagent® (green) and the scaffolds were pre-labeled with an Alexa Fluor 350 succinimidyl ester (blue). White dotted lines denote the scaffold periphery. Scale bars = 100 μm . **(B)** Quantitative analysis of nuclear density within the bead foam implants, showing no significant differences in total cell infiltration between the groups.

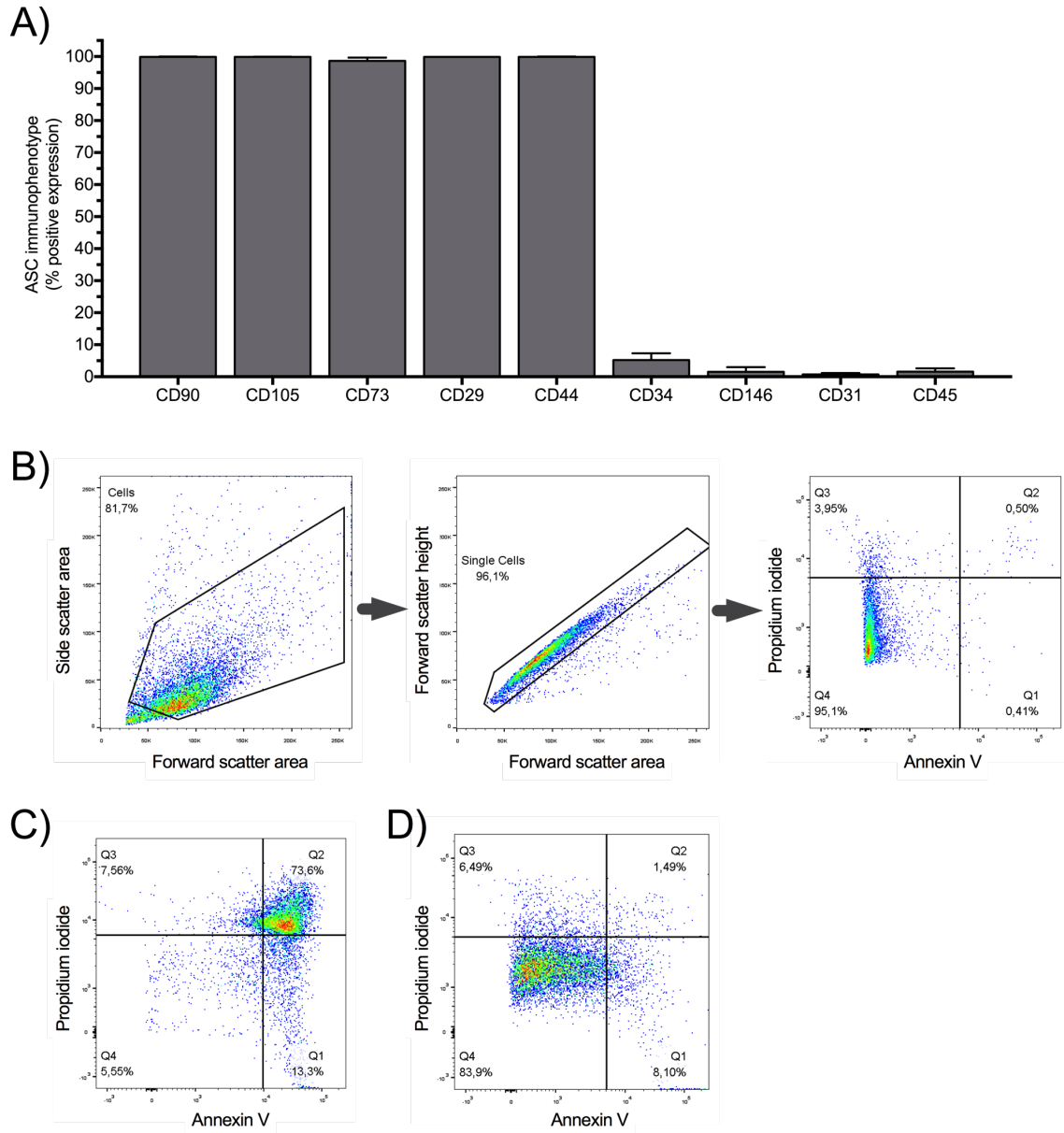
A.2 Supplementary data of Chapter 3

Supplementary Table 3.1: Cell donor information

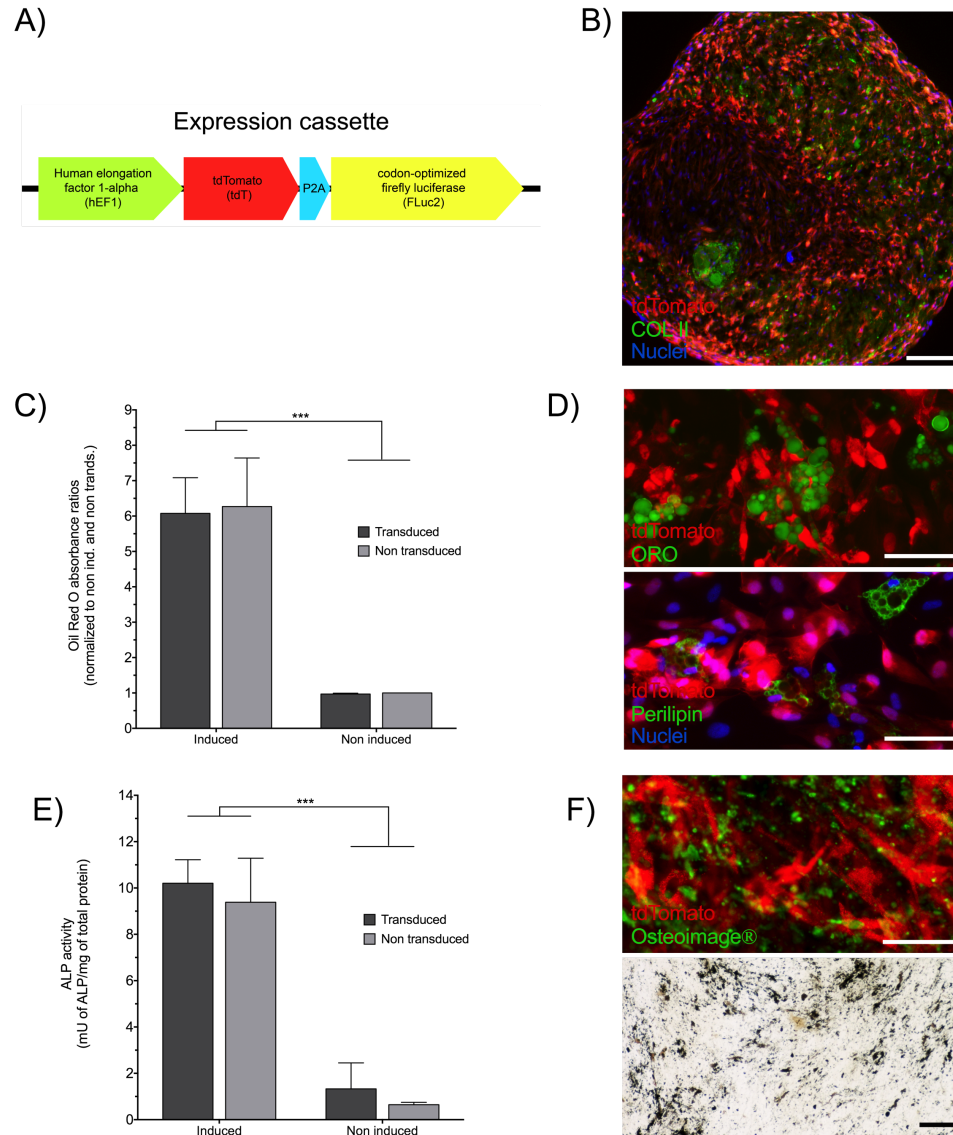
Donor	Gender	Age	Anatomical localization	Body mass index
1	Female	51	Subcutaneous abdominal adipose tissue	25.9
2	Female	53	Subcutaneous abdominal adipose tissue	32.8
3	Female	66	Subcutaneous breast adipose tissue	25.3

Supplementary Table 3.2: Genes from the custom-made qPCR arrays (Bio-Rad; PrimePCR™ arrays)

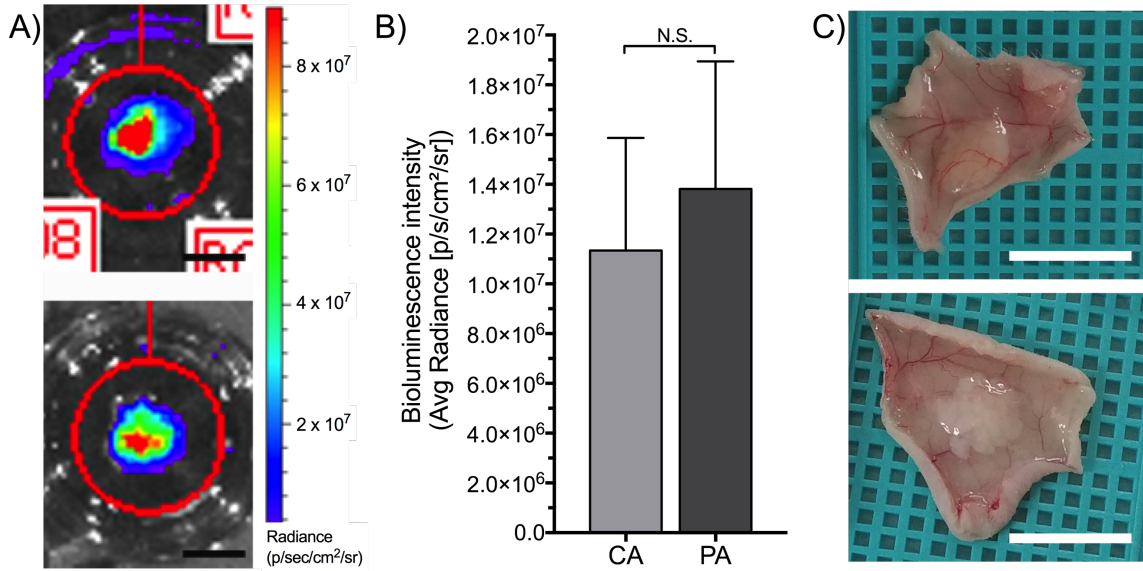
Gene associated with	Gene symbol	Gene name
Proteoglycans	BGN	Biglycan
	DCN	Decorin
	VCAN	Versican
ECM synthesis and remodelling	ACTA2	Smooth muscle actin alpha 2
	COL1A1	Collagen type I alpha 1 chain
	COL3A1	Collagen type III alpha 1 chain
	COL4A1	Collagen type IV alpha 1 chain
	CTGF	Connective tissue growth factor
	MMP1	Matrix metalloproteinase 1
	MMP2	Matrix metalloproteinase 1
	TGFB1	Transforming growth factor beta 1
	TIMP1	Tissue inhibitor of metalloproteinases 1
Angiogenesis	ANGPT1	Angiopoietin 1
	FGF2	Fibroblast growth factor 2
	HGF	Hepatocyte growth factor
	IGF1	Insulin like growth factor 1
	SERPINE1	Serpin Family E Member 1
	VEGFA	Vascular endothelial growth factor A
Inflammation	CCL2	C-C motif chemokine ligand 2
	CSF2	Colony stimulating factor 2
	IL1B	Interleukin 1 Beta
	TNF	Tumor Necrosis Factor
	CXCL10	C-X-C motif chemokine ligand 10
Housekeeping genes	RPS18	Ribosomal Protein S18
	UBC	Ubiquitin C



Supplementary Figure 3.1: Immunophenotype of human ASCs and flow cytometry controls for the viability studies. (A) The P4 ASCs used in the studies showed high expression of mesenchymal markers (>98%; CD105, CD90, CD73, CD44, and CD29), low expression of the progenitor cell marker CD34 (<5%), and negligible expression of leukocyte, pericyte and endothelial markers (CD45, CD146, and CD31) (n = 3 samples/donors, N = 3 different donors). (B) Examples of the cell (left graph) and single cell (middle graph) gating applied prior to the propidium iodide and annexin V double-staining analyses (right graph; also presented in Figure 3.2D). (C-D) Propidium iodide and annexin V double-stained ASCs cultured on tissue culture plastic (TCPS) used for the gating. (C) TCPS cultured apoptotic control (treated with 1 μ M staurosporine, 18 hours). (D) TCPS viable control (non-treated).



Supplementary Figure 3.2: The transduced ASCs co-expressing codon optimized luciferase (Fluc2) and tdTomato (tdT) maintained their tri-lineage differentiation capacity. (A) Expression cassette used in transduction of human ASCs. (B) Transduced cells were qualitatively confirmed to differentiate towards the chondrogenic lineage, as shown by the co-localization of the endogenous tdT signal (red) with staining for the chondrogenic ECM marker collagen type II (green) in aggregate cultures at day 28. (C-D) Transduced cells differentiated towards the adipogenic lineage, as shown by (C) quantification of extracted Oil red O (ORO) dye at day 14, and confirmed by colocalization of tdT⁺ cells (red) with (D; top panel) ORO-stained lipids (green) and (D; bottom panel) perilipin (green). (E-F) Transduced cells differentiated towards the osteogenic lineage, as shown by the (E) ALP enzyme activity assay, and (F; top panel) co-localization of the tdT signal (red) with mineralized matrix identified with osteoimage® staining (green), and confirmed by (F; bottom panel) von Kossa staining. Scale bars = 100 μ m. (A-E) n=3 scaffolds/trial, N=3 trials with different cell donors; two-way ANOVA with Tukey's post-hoc test; *** P <0.001.



Supplementary Figure 3.3: Cell-assembled (CA) and pre-assembled (PA) bead foams had similar cell numbers at day 0, while explanted scaffolds at day 28 were shown to be well integrated within the host tissues. (A) Representative macroscopic and bioluminescence images (superposed) from a cell-assembled (top) and pre-assembled (bottom) bead foam *in vitro* at day 0 (day of implantation in mice). The circle red area represents the area quantified for each scaffold. Scale bars = 5 mm. (B) Relative bioluminescence intensity levels showing similar cell numbers in both scaffold at day 0 (day of implantation in mice). (A-B) n=3-4 scaffolds/trial, N=2 trials with different cell donors; t-test; N.S. = non-significant. (C) Representative macroscopic image of explanted scaffold at day 28, showing integration within the host tissues. Scale bars = 1 cm. n=2-3 scaffolds/trial, N=2 trials with different cell donors.

Appendix B: Research ethics board approval



Western
Research

Research Ethics

Western University Health Science Research Ethics Board HSREB Delegated Initial Approval Notice

Principal Investigator: Dr. Lauren Flynn

Department & Institution: Schulich School of Medicine and Dentistry\Anatomy & Cell Biology, Western University

HSREB File Number: 105426

Study Title: Tissue Engineering with Adipose-derived Stem Cells

Sponsor: Canadian Institutes of Health Research

HSREB Initial Approval Date: August 13, 2014

HSREB Expiry Date: August 31, 2019

Documents Approved and/or Received for Information:

Document Name	Comments	Version Date
Other	Letter for OR and Clinic Staff to Introduce the Study (received June 2/14)	
Western University Protocol		2014/07/23
Letter of Information & Consent		2014/07/23

The Western University Health Science Research Ethics Board (HSREB) has reviewed and approved the above named study, as of the HSREB Initial Approval Date noted above.

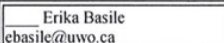
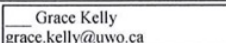
HSREB approval for this study remains valid until the HSREB Expiry Date noted above, conditional to timely submission and acceptance of HSREB Continuing Ethics Review. If an Updated Approval Notice is required prior to the HSREB Expiry Date, the Principal Investigator is responsible for completing and submitting an HSREB Updated Approval Form in a timely fashion.

The Western University HSREB operates in compliance with the Tri-Council Policy Statement Ethical Conduct for Research Involving Humans (TCPS2), the International Conference on Harmonization of Technical Requirements for Registration of Pharmaceuticals for Human Use Guideline for Good Clinical Practice Practices (ICH E6 R1), the Ontario Personal Health Information Protection Act (PHIPA, 2004), Part 4 of the Natural Health Product Regulations, Health Canada Medical Device Regulations and Part C, Division 5, of the Food and Drug Regulations of Health Canada.

Members of the HSREB who are named as Investigators in research studies do not participate in discussions related to, nor vote on such studies when they are presented to the REB.

The HSREB is registered with the U.S. Department of Health & Human Services under the IRB registration number IRB 00000940.

Ethics Officer to Contact for Further Information

 Erika Basile ebasile@uwo.ca	 Grace Kelly grace.kelly@uwo.ca	 Mina Mekhail mmekhail@uwo.ca	 Vikki Tran vikki.tran@uwo.ca
--	---	--	---

This is an official document. Please retain the original in your files.

Appendix C: Animal protocol approval



2015-049:5:

AUP Number: 2015-049

AUP Title: Characterization of Soft Tissue Regeneration with Bioscaffolds and Adipose-derived Stem/Stromal Cells (ASCs)

Yearly Renewal Date: 11/01/2019

The YEARLY RENEWAL to Animal Use Protocol (AUP) 2015-049 has been approved by the Animal Care Committee (ACC), and will be approved through to the above review date.

Please at this time review your AUP with your research team to ensure full understanding by everyone listed within this AUP.

As per your declaration within this approved AUP, you are obligated to ensure that:

- 1) Animals used in this research project will be cared for in alignment with:
 - a) Western's Senate MAPPs 7.12, 7.10, and 7.15
http://www.uwo.ca/univsec/policies_procedures/research.html
 - b) University Council on Animal Care Policies and related Animal Care Committee procedures
http://uwo.ca/research/services/animalethics/animal_care_and_use_policies.html
- 2) As per UCAC's Animal Use Protocols Policy,
 - a) this AUP accurately represents intended animal use;
 - b) external approvals associated with this AUP, including permits and scientific/departmental peer approvals, are complete and accurate;
 - c) any divergence from this AUP will not be undertaken until the related Protocol Modification is approved by the ACC; and
 - d) AUP form submissions - Annual Protocol Renewals and Full AUP Renewals - will be submitted and attended to within timeframes outlined by the ACC. http://uwo.ca/research/services/animalethics/animal_use_protocols.html
- 3) As per MAPP 7.10 all individuals listed within this AUP as having any hands-on animal contact will
 - a) be made familiar with and have direct access to this AUP;
 - b) complete all required CCAC mandatory training (_training@uwo.ca); and
 - c) be overseen by me to ensure appropriate care and use of animals.
- 4) As per MAPP 7.15,
 - a) Practice will align with approved AUP elements;
 - b) Unrestricted access to all animal areas will be given to ACVS Veterinarians and ACC Leaders;
 - c) UCAC policies and related ACC procedures will be followed, including but not limited to:

- i) Research Animal Procurement
- ii) Animal Care and Use Records
- iii) Sick Animal Response
- iv) Continuing Care Visits

5) As per institutional OH&S policies, all individuals listed within this AUP who will be using or potentially

exposed to hazardous materials will have completed in advance the appropriate institutional OH&S training, facility-level training, and reviewed related (M)SDS Sheets, <http://www.uwo.ca/hr/learning/required/index.html>

Submitted by: Copeman, Laura
on behalf of the Animal Care Committee
University Council on Animal Care

The University of Western Ontario
Animal Care Committee / University Council on Animal
Care

London, Ontario Canada N6A 5C1
519-661-2111 x 88792 Fax 519-661-2028
auspc@uwo.ca http://www.uwo.ca/research/services/animal_ethics/index.html

*** THIS IS AN EMAIL NOTIFICATION ONLY. PLEASE DO NOT REPLY ***

Curriculum Vitae

Name: Pascal Morissette Martin

Post-secondary Education and Degrees:

Université Laval
 Québec City, Québec, Canada
 2009-2012, B.Sc. in Biochemistry

Université Laval
 Québec City, Québec, Canada
 2012-2015, M.Sc. in Cell and Molecular Biology

The University of Western Ontario
 London, Ontario, Canada
 2015-present, Ph.D. in Anatomy and Cell Biology

Honours and Awards:

Alexander Graham Bell Canada Graduate Scholarship (CGS D)
 Natural Sciences and Engineering Research Council of Canada
 2017-2019

Suzanne M. Bernier Memorial Award (SSHRC)
 2018

Invitation to present research at the CIHR Canadian Student
 Health Research Forum
 2017

Doctoral Graduate Scholarship
 Fonds de recherche du Québec en Santé (FRQS)
 2015-2018 (3rd year declined)

Ontario Graduate Scholarship (OGS)
 2015 (declined, 2015)

Western Graduate Research Scholarship (WGRS)
 2015-2017

Frederick Banting and Charles Best Canada Graduate Scholarship,
 Canadian Institutes of Health Research
 2012-2013 (during M.Sc.)

Master's Graduate Scholarship
 Fonds de recherche du Québec en Santé (FRQS)
 2013-2014 (during M.Sc.)

Related Work Teaching Assistant, MEDSCI 4900G

Experience The University of Western Ontario
2015-2019

Teaching Assistant, BCM-1902/1002
2013-2014 (during M.Sc.)

Publications:

1. **Morissette Martin P**, Grant A, Hamilton DW, Flynn LE, “Matrix composition in 3-D collagenous bioscaffolds modulates the survival and angiogenic phenotype of human chronic wound dermal fibroblasts”, *Acta Biomaterialia*, 83(2019): 199-210.
2. (Book chapter) **Morissette Martin P**, Shridhar A., Yu C., Brown C, and Flynn LE, “Decellularized Adipose Tissue Scaffolds for Soft Tissue Regeneration and Adipose-derived Stem/Stromal Cell Delivery”; in *Adipose-Derived Stem Cells: Methods and Protocols - Second Edition*; Editors: Bunnell B & Gimble J; *Methods in Molecular Biology: Springer Protocols*, Humana Press, 2018: 53-71
3. (Book chapter) **Morissette Martin P**, Creber K, and Hamilton DW, “Measuring gene expression changes on biomaterial surfaces”; in *Monitoring and Evaluation of Biomaterials and their Performance in vivo*, Editor: Narayan R, Woodhead Publishing, 2017: 111-132.
4. (during M.Sc.) **Morissette Martin P**, Maux A, Laterreur V, Mayrand D, Gagné VL, Moulin VJ, Fradette J, “Enhancing repair of full-thickness excisional wounds in a murine model: impact of tissue-engineered biological dressings featuring human differentiated adipocytes”, *Acta Biomaterialia*, 22(2015): 39-49.
5. (during M.Sc.) Hayward CJ, Fradette J, **Morissette Martin P**, Guignard R, Germain L, Auger F, “Using Umbilical Cord Cells for Tissue Engineering: A Comparison With Skin-derived Cells”, *Differentiation*, 87, 3-4(2014): 172-181.